

ulm university universität ulm

Polypeptide Hybrid Biomaterials Developed from Protein Precursors – A Novel Strategy and Biomedical Applications

Dissertation zur Erlangung des Doktorgrades Dr. rer. nat.

der Fakultät für Naturwissenschaften der Universität Ulm

vorgelegt von

Yuzhou WU

aus Henan, China,

2013



ulm university universität ulm

Polypeptide Hybrid Biomaterials Developed from Protein Precursors – A Novel Strategy and Biomedical Applications

A dissertation submitted in partial satisfaction of the

requirements for the degree Doctor of Philosophy

by

Yuzhou WU

in

Faculty of Natural Science

Ulm University

2013

Dissertation der Universität Ulm:

Amtierender Dekan: Prof. Dr. Joachim Ankerhold

1. Gutachter: Prof. Dr. Tanja Weil

2. Gutachter: Prof. Dr. Mika Lindén

Tag der Promotion: 13.05.2013

Universität Ulm, Fakultät für Naturwissenschaften, 2013

DEDICATION

This dissertation is dedicated to my husband and my parents.

ABSTRACT OF THE DISSERTATION

Peptide based materials are highly attractive for biomedical applications due to their biocompatibility, biodegradability and their potential to achieve unique macromolecular architectures with tailored properties. However, the preparation of polypeptides with controlled molecular weight distribution, ordered polymer architecture and a large variety of functional groups at defined locations remains a major challenge. Polypeptides are mainly prepared by ring-opening polymerization, solid-phase peptide synthesis or genetically engineered protein expression. Polymerization reactions are only able to prepare polypeptides with repeated amino acid sequences, whereas solid-phase peptide synthesis and protein engineering techniques are limited by sophisticated procedures, low yields and high costs. Therefore, it is highly desirable to develop other efficient approaches for the synthesis of defined polypeptides with tunable properties.

In this thesis, a convenient approach for the synthesis of narrowly dispersed protein based polypeptide copolymers (PbPs) of defined compositions is presented. The controlled denaturation of the native proteins followed by an *in situ* stabilization with polyethylene(oxide) chains yielded polypeptide side chain copolymers with precisely defined backbone lengths as well as secondary structure elements. Supramolecular architectures were formed in solution due to the presence of hydrophobic and hydrophilic amino acids along the polypeptide main chain. PbPs reported herein exhibited excellent solubility and stability in aqueous media, insignificant cytotoxicity at

relevant concentrations. They could be degraded *via* proteolysis, which was very attractive for biomedical applications. Diverse native functional groups presented at precise positions along protein backbone allowed further orthogonal modifications. *Via a priori* and *a posteriori* modification strategies, functionalized PbPs could be prepared with highly tunable properties, such as variable net charges, distinct hydrophobicity as well as varied self-assemble possibilities. Moreover, PbPs could further incorporate other functional moieties, such as chromophores, anti-cancer drugs or MRI contrast agents, serving as a highly versatile platform for broad applications.

This thesis further describes our investigation on various biomedical applications of PbPs, such as fluorescent bioimaging and anti-cancer drug delivery. Water soluble and biocompatible quantum dots (QDs) were prepared by coating the hydrophobic QDs with PbPs. These PbP-QDs were non-cytotoxic and notably stable in live cells. They have attractive pH responsive optical properties, which were attributed to conformational rearrangements of the peptide backbone on QDs surface. In addition, QDs coated with a cationic albumin (cBSA) derived PbP shell exhibited significant photo-responsiveness to DNA loading and were able to transfect plasmid DNA into mammalian cells. Thus, they have great potential for investigating gene delivery processes. For anti-cancer drug delivery, drug molecules were loaded into PbPs micelles *via* hydrophobic interaction or covalent conjugation onto PbPs backbone. The hydrophobic loading strategy provided high loading capacity and flexibility, whereas the covalent loading approach could minimize non-specific leakage. A highly defined multi-stimuli responsive core-shell system was also achieved by conjugating doxorubicin with PbP backbone *via* hydrazone linker. *In vitro*

and preliminary *in vivo* studies demonstrated the efficient drug delivery, controlled drug release, potent toxicity as well as beneficial passive targeting effect. MRI contrast agents were further introduced into this system to enable simultaneous imaging and therapy.

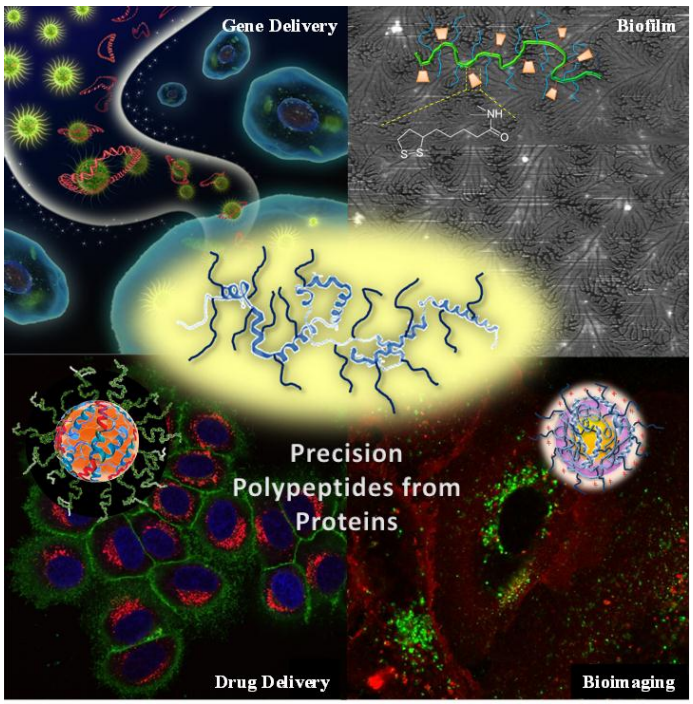

Adapted with permission*. Copyright 2012, Wiley-VCH.

* The picture is partially adapted from (1). Wu, Y.; Ihme, S.; Feuring-Buske, M.; Kuan, S. L.; Eisele, K.; Lamla, M.; Wang, Y.; Buske, C.; Weil, T., Adv. Healthcare Mater. 2013, DOI: 10.1002/adhm.201200296. (2). Wu, Y.; Eisele, K.; Doroshenko, M.; Algara-Siller, G.; Kaiser, U.; Koynov, K.; Weil, T., Small 2012, 8 (22), 3465-3475. The dissertation author is the first author of these papers.

Table of Contents

Abstract of the Dissertation..... iii
Table of Contents..... vi
List of Tables..... xi
List of Figures..... xii
List of Schemes..... xix
List of Abbreviations..... xx

Chapter 1

Polypeptide Based Biomaterials – the Preparation Methods and Biomedical Applications..... 1
1.1 Introduction..... 2
1.2 Chemical synthesis of polypeptides..... 6
1.2.1 NCR ring opening polymerization..... 7
1.2.2 Solid phase peptide synthesis..... 10
1.2.3 Preparation of long polypeptides *via* chemical ligation..... 14
1.3 Preparation of polypeptides by genetic engineering..... 17
1.3.1 Protein engineering techniques..... 18
1.3.2 Examples of synthetic polypeptides produced by genetic engineering..... 22
1.4 Protein-polymer hybrid biomaterials..... 25
1.4.1 Statistical conjugation of polymers onto native proteins..... 27
1.4.2 Site-directed polymer conjugation..... 29
1.4.3 Non-covalent assemblies..... 33
1.5 Polypeptide/protein based biomaterials for biomedical applications..... 35
1.5.1 Criteria for designing delivery systems for biomedical applications..... 36
1.5.2 Polypeptide based polymeric micelles as delivery carriers.. 41
1.5.3 Chemically modified proteins as nanocarriers..... 46

1.5.4 Decoration of multiple functional moieties on polypeptide based nanocarriers…… 49
1.6 Scope of the dissertation…… 53
1.6.1 Motivation and objective…… 53
1.6.2 Overview of the dissertation…… 56
1.7 References…… 59

Chapter 2

Rational Design and Synthesis of Protein Based Polypeptide Copolymers…… 76
2.1 Introduction…… 78
2.2 Preparation of PbPs from different protein precursors…… 79
2.2.1 Preparation of long polypeptide copolymers from albumins…… 80
2.2.2 Preparation of short polypeptide copolymers from lysozyme…… 84
2.2.3 Preparation of giant polypeptide copolymers from dimeric BSA…… 86
2.2.4 Polypeptide copolymers with highly defined structures and secondary elements …… 89
2.2.5 Alternating hydrophilic and lipophilic amino acids and induced formation of nanoscopic micelles…… 93
2.2.6 Non-cytotoxic and biodegradable polypeptide copolymers…… 94
2.3 Synthesis of polypeptide polyelectrolytes *via a priori* modification of precursor proteins…… 96
2.3.1 Preparation of polycationic and polyanionic polypeptide copolymers by *a priori* modification of serum albumin…… 96
2.3.2 Polypeptide copolymers containing multiple positive and negative charges along their backbones…… 99
2.3.3 Self-assembly of polyelectrolytes in aqueous solution…… 101

2.3.4 Modified polypeptide copolymers with non-cytotoxicity and biodegradability…….…... 103
2.3.5 Tunable cell uptake efficiency…….……..…… 105
2.4 *A posteriori* modification to introduce tunable copolymer properties…… 106
2.4.1 *A posteriori* modification tuning the hydrophobicity of the polypeptides…… 107
2.4.2 *A posteriori* modification tuning the surface partterning of the polypeptides…….. 113
2.4.3 Introduction of functional moieties *via a posteriori* modification…….…. 119
2.5 Summary…… 132
2.6 Materials and methods…… 133
2.7 References…… 152

Chapter 3

Protein Based Polypeptide Copolymers Coated Biocompatible QDs for Imaging, Biosensoring and Gene Delivery……..... 160
3.1 Introduction……. 161
3.2 Preparation and characterization of PbPs coated biocompatible QDs…… 165
3.2.1 Preparation of water soluble QDs with serum albumin copolymer coatings……..…… 166
3.2.2 Size distribution and composition of PbP-QDs……..…. 168
3.2.3 The stability of PbP-QDs under biological conditions……..…. 173
3.2.4 Test of biocompatibility of PbP-QDs …..……..…. 176
3.2.5 Tuning of cell uptake efficiency of PbP-QDs……..…. 177
3.3 PbPs coated QDs as biosensors..……..…. 180
3.3.1 Quantum yield of HSA-QDs responsive to pH change……. 180
3.3.2 Discussion of the mechanism of pH responsiveness…… 182
3.3.3 cBSA-QDs as DNA sensor…… 186
3.4 cBSA-QDs as photoswitch for DNA detection, gene transfection and live-cell imaging……..……..…… 191

3.4.1 cBSA-QD form stable complexes with DNA..... 192
3.4.2 cBSA-QD/DNA complexes efficiently transfect mammalian cells..... 194
3.4.3 Investigation of cBSA-QDs and cBSA-QD/DNA complexes in live cells using confocal imaging and FCS..... 196
3.5 Summary..... 205
3.6 Materials and methods..... 207
3.7 References..... 220

Chapter 4

Protein Based Polypeptide Copolymers Derived Drug Delivery Systems..... 227
4.1 Introduction..... 228
4.2 Nano-sized PbP micelles encapsulate doxorubicin by hydrophobic interactions for efficient drug delivery..... 234
4.2.1 Preparation and characterization of PbP DOX micelles..... 235
4.2.2 Characterization of dcBSA-PEO(5000)$_{27}$-DOX micelles..... 237
4.2.3 *In vitro* assessment of micelle stability..... 240
4.2.4 Enhanced cellular uptake..... 242
4.2.5 *In vitro* cytotoxicity of dcBSA-PEO(5000)$_{27}$-DOX micelle..... 244
4.3 Defined PbP based drug carrier for high capacity loading and two-step release of doxorubicin with enhanced anti-leukemia activity 246
4.3.1 Preparation of DOX covalently loaded to cationic and pegylated albumin..... 246
4.3.2 cHSA-PEO(2000)$_{16}$-DOX$_{27}$ micelles (**2-24**) exhibit positive net charge..... 250
4.3.3 Size distribution and morphology of DOX loaded cHSA-PEO(2000)$_{16}$-DOX$_{27}$ (**2-24**)..... 251
4.3.4 Efficient two-step DOX release with reduced undesirable drug leakage..... 254
4.3.5 Cellular uptake and intracellular localization of cHSA-PEO(2000)$_{16}$-DOX$_{27}$ (**2-24**)..... 259

4.3.6 Cytotoxicity and apoptosis in HeLa cells……..…….. 262
4.3.7 cHSA-$(PEO2000)_{16}$-DOX_{27} (**2-24**) micelles with reduced immunogenicity…….…… 264
4.3.8 *In vitro* anti-leukemia activity……..…... 265
4.3.9 Therapeutic efficacy on leukemic engraftment……..…… 267
4.4 PbPs based carriers for anticancer drug delivery and simultaneous ultrasensitive MR imaging……..……..…..... 269
4.4.1 Preparation of PbP micelles with high loading of DOX and DOTA-Gd……..…… 270
4.4.2 Characterization of the relaxivity of DOTA-Gd loaded PbP (**2-26**)……..…… 272
4.4.3 *In vitro* test of cHSA-$PEG(2000)_{16}$-Gd-DOX_{27} (**4-2**) in mammalian cells……..…… 274
4.5 Summary……..…….. 276
4.6 Materials and Methods……..…… 279
4.7 References…… 292

Chapter 5

Conclusion and Perspectives…..……..……..……. 301
5.1 Conclusions…..……..……..…… 302
5.2 Perspectives……..…… 304

Erklärung / Declaration of Originality…….…… 307
Acknowledgments……..…… 308
Curriculum Vitae……..…… 310
List of Publications……..…. 312

List of Tables

Table 2-1. Summary of molecular weight (M.W.), zeta potential, size distribution in aqueous solution and complete proteolysis digestion time of various polypeptide copolymers and their precursor proteins……..…... 94

Table 2-2. Summary of molecular weight (M.W.), zeta potential, size distribution in aqueous solution, complete proteolysis digestion time and cell uptake efficiency of various polypeptide copolymers and their precursor proteins…… 103

Table 2-3. Summary of hydrodynamic radii and PDI determined by DLS (n=5, standard deviation presented as error)……..... 112

Table 3-1. Summary of the fluorescence quantum yields (QY) and total emission intensities (EI) and diameters (d) of HSA-QDs as well as the respective conformational changes of PbP (**2-16**) at different pH values. 185

Table 3-2. Summary of size and optical properties of cBSA-QDs and cBSA-QD/DNA complexes (8:1)…… 190

Table 4-1. Summary of the loading efficiencies of DOX molecules into dcBSA-PEO(5000)$_{27}$ micelles (**4-1**)…….. 239

Table 4-2. Summary of the IC_{50} of DOX loaded cHSA-PEO(2000)$_{16}$-DOX_{27} (**2-24**) in different cell lines…….. 267

Table 4-3. Summary of the IC_{50} of free DOX, DOX loaded cHSA-PEO(2000)$_{16}$-DOX_{27} (**2-24**) and DOX and DOTA-Gd co-loaded cHSA-PEO(2000)$_{16}$-Gd-DOX_{27} (**4-2**)…… 276

List of Figures

Figure 1-1. From amino acids to proteins: Depiction of the primary, secondary, tertiary and quaternary structure of proteins…..…… 4

Figure 1-2. (a) Structure of Fmoc protected amino acids with acid labile side-chain protection groups. (b) Examples of amide coupling reagents used for solid phase peptide synthesis……..……. 13

Figure 1-3. Preparation of polypeptide by protein engineering……... 19

Figure 1-4. Illustration of (a) silk-like peptide (SLP), (b) coiled-coil peptide, (c) elastin-like peptide (ELP) and (d) leucine zipper finger domain……. 23

Figure 1-5. Methods to prepare protein-polymer hybrids……. 27

Figure 1-6. Illustration of polyNIPAAm conjugated proteins responsive to temperature changes……. 29

Figure 1-7. Site-directed mutagenesis by genetic engineering…….. 30

Figure 1-8. Photo-switchable endoglucanase prepared by site-directed polymer conjugation…… 31

Figure 1-9. Incorporation of unnatural amino acids in protein expression by (a) engineering the genetic codon and (b) treating the native amino acid analogs in auxotrophic bacterials……..……..... 33

Figure 1-10. Non-covalent polymer-protein hybrids prepared by (a) streptavidin-biotin interaction which formed bioactive self-assemble monolayer and (b) heme-horseradish peroxidase binding which formed nanoscope architectures…..…….. 35

Figure 1-11. Tumor targeting strategies used in nanomedicine……. 38

Figure 1-12. Strategies toward stimuli responsive carriers……. 40

Figure 1-13. Self-assemble of amphiphilic polypeptides in aqueous solution…….. 42

Figure 1-14. Amphiphilic PEG-polypeptide block copolymers forming core-shell micelles for gene delivery and drug delivery……..... 45

Figure 1-15. Illustration of protein cage and streptavidin based delivery carriers…….. 48

Figure 1-16. Examples of polypeptide/protein based multifunctional carriers…….. 52

Figure 1-17. Illustration of the motivations for preparing PbPs……... 56

Figure 1-18. Summary of the structure of the dissertation……. 57

Figure 2-1. Characterization of dHSA-PEO(5000)$_{27}$ (**2-2**)…….. 82

Figure 2-2. Amino acid sequence of HSA……..…… 84

Figure 2-3. Characterization of dLY-PEO(5000)$_8$ (**2-4**)..……... 85

Figure 2-4. Amino acid sequence of lysozyme..……... 86

Figure 2-5. Characterization of BSA-derived polypeptide block copolymer architectures……. 89

Figure 2-6. Secondary structure analysis of (a) (**2-2**), (b) (**2-4**) and (c) (**2-8**) compared with their corresponding protein precursors…..……..….. 92

Figure 2-7. Cell viability assays showing no significant cytotoxicity of polypeptide copolymer (**2-2**) and (**2-4**)……. 95

Figure 2-8. Trypsin digestion of polypeptide copolymer (**2-2**), (**2-4**) and (**2-8**) analyzed by 4%-10% SDS-PAGE…….. 96

Figure 2-9. a) MALDI-ToF MS spectra of native BSA and cBSA (**2-9**); Matrix: Sinapinic acid. b). SDS-PAGE of cBSA and the corresponding PbPs (**2-11**). c). MALDI-TOF MS spectrum of aHSA (**2-12**) compared to native HSA. b). SDS-PAGE of aHSA and the corresponding polypeptide copolymers (**2-14**)…….. 99

Figure 2-10. Characterization of charge properties of polypeptide copolymers…….. 101

Figure 2-11. Cell viability assay showing no significant cytotoxicity of polypeptide copolymer (**2-11**) and (**2-14**)…… 104

Figure 2-12. Trypsin digestion of polypeptide copolymer (**2-11**) and (**2-14**) analyzed by 4%-10% SDS-PAGE……..... 104

Figure 2-13. LSCM imaging of rhodamine labeled (**2-2**) (B1-B5) and (**2-11**) (A1-A5) incubated with A549 cells for 24 hr……. 106

Figure 2-14. Illustration of *a posteriori* modification of PbPs for different applications…….. 107

Figure 2-15. (a) TEM imaging after uranyl acetate staining (90 nm scale bar) of dcBSA-PEO(5000)$_{27}$ (**2-11**) and dcBSA-PEO(5000)$_{27}$-alkyne (**2-15**). (b) Extraction of 3-azidocoumarin with water (blue line), 1 μM copolymer (**2-11**) solution (green line) and 1 μM copolymer (**2-11**) solution (red line)……. 111

Figure 2-16. SDS-PAGE analysis of thioctic acid functionalized PbPs…. 114

Figure 2-17. CD spectra of a) dHSA-PEO(5000)$_{27}$ (**2-2**, blue line) and dHSA-PEO(5000)$_{27}$-TA$_{22}$ (**2-16**, green line); b) dcBSA-PEO(5000)$_{27}$ (**2-11**, blue line) and dcBSA-PEO(5000)$_{27}$-TA$_{26}$ (**2-17**, green line) and c) dLY-PEO(5000)$_8$ (**2-4**, blue line) and dLY-PEO(5000)$_8$-TA$_8$ (**2-18**, green line)……..…… 115

Figure 2-18. (a) AFM image of Protein-derived copolymers deposited on mica *via* drop casting. Left panel: Pegylated copolymers (**2-2**), (**2-11**) and (**2-4**), Right panels: Thiolated copolymers (**2-16**), (**2-17**) and (**2-18**). Scale bars are 2 μm. (b) Relative amounts of secondary structure elements of all copolymers as measured by circular dichroism (dark color: Pegylated copolymers, light color: Thiolated copolymers)…….. 118

Figure 2-19. (a). SDS-PAGE characterization of coumarin conjugated polypeptide (**2-20**). Fluorescent image of (i) protein makers and (ii) (**2-20**) and the Coomassie stained image of (iii) protein makers and (iv) (**2-20**) are compared. Protein bands are indicated with arrow. (b). Absorbance spectrum and (c) emission spectrum (λ_{ex} = 254 nm) of the conjugate coumarin-polypeptide (**2-20**). (d) Cell imaging of using coumarin-polypeptide (**2-20**) by fluorescence microscopy (λ_{ex} = 405 nm). 122

Figure 2-20. Size distribution of functionalized PbPs in solution according to DLS……. 123

Figure 2-21. (a) Cytotoxicity of 1 μM of polypeptide (**2-11**), (**2-15**) and coumarin-conjugated copolymer (**2-20**). (b) Cytotoxicity of DOX loaded copolymer (**2-22**) compared with free DOX HCl……... 124

Figure 2-22. Characterization of cHSA-PEO(2000)$_{16}$ (**2-23**) and cHSA-PEO(2000)$_{16}$-DOX$_{27}$ micelles (**2-24**)……..……. 128

Figure 2-23. MALDI-ToF mass spectra of (A) cHSA-PEG(2000)$_{16}$-DOTA (**2-25**) and (B) cHSA-PEG(2000)$_{16}$-Gd (**2-26**)…….…… 130

Figure 2-24. Calibration of thioctic acid concentration……. 147

Figure 3-1. Representative absorbance and emission spectra of QDs…. 162

Figure 3-2. Ligand exchange to make water soluble QDs…….. 163

Figure 3-3. Absorption (black) and PL (red) spectra of (a) 561nm quantum dots and (b) 599nm quantum dots……... 166

Figure 3-4. An illustration of a QD coated with PbPs……..…… 167

Figure 3-5. Emission spectra of HSA-QDs, cBSA-QDs and LY-QDs compared with as-synthesized QDs…….…….. 168

Figure 3-6. TEM micrograph of (a) HSA-QDs and (b) cBSA-QDs…...…. 170

Figure 3-7. Hydrodynamic diameter distributions of (a) HSA-QDs and (b) cBSA-QDs measured by DLS……. 171

Figure 3-8. Hydrodynamic diameter distributions of (a) HSA-QDs and (b) cBSA-QDs measured by FCS…….……... 172

Figure 3-9. Scratch of quantum dots diameter…….. 173

Figure 3-10. cBSA-QDs emission spectra under different condition……. 174

Figure 3-11. Proteolytic stability of cBSA-QDs…….. 175

Figure 3-12. Cytotoxicity of cBSA-QDs and HSA-QDs comparing with gene transfection standard polyethyleneimine (PEI)…… 177

Figure 3-13. (a). Isoelectric focusing (IEF) experiment of native BSA and cBSA: A – IEF Standards, pI range 4.45 – 9.6; B: Native BSA; C: cBSA; (b). Agarose gel electrophoresis showing different net charges of QDs coated by three PbPs at pH7.4; (c). Confocal micrograph of HSA-QDs in A549 cells after a 24-hr incubation. No cell uptake was observed; (d). Confocal micrograph of cBSA-QDs in A549 cells after a 24-hr incubation. cBSA-QDs revealed fast cell uptake as well as enrichment in the perinuclear region showing by the white arrow……. 179

Figure 3-14. Endocytosis mechanism study of cBSA-QDs in A549 cells using confocal microscope……..… 180

Figure 3-15. (a) Emission intensities of HSA-QDs at different pH (λ_{ex} = 254 nm); (b) Integrated emission intensities *versus* pH based on four consecutive measurements……... 181

Figure 3-16. Reversibility of the pH responsiveness between pH 5 and pH 9 based on three independent measurements. The emission intensity was recovered after increasing the pH from 5 to 9 as well as decreasing the pH from 9 to 5……... 182

Figure 3-17. Changes in the secondary structure of dHSA-PEO(5000)$_{27}$–TA$_{22}$ (**2-16**) at different pH values…….. 184

Figure 3-18. Number size distributions of coated HSA-QDs by DLS. At pH 3, 5 and 9, average hydrodynamic radii of 23.5±5.0 nm, 30.2±3.1 nm and 37.0±7.7 nm, respectively, were obtained after two independent measurements……..... 185

Figure 3-19. Characterization of cBSA-QD/DNA complexes and gene transfection. (a). Relative PL efficiency of complexes with different ratios (cBSA-QD/DNA). pUC19 and pGL4.73 were tested as model DNAs. Data were obtained in triplicate, and standard deviations were shown as error bars. (b). Emission spectra of different complex ratios (cBSA-QD/pUC19-DNA). (λ_{ex} = 254 nm)……. 187

Figure 3-20. TEM images of (a) 8:1 cBSA-QD/DNA complexes and (b) 1:1 cBSA-QD/DNA complexes. (c). FCS autocorrelation curves measured for cBSA-QDs and pUC19 plasmid complexes in aqueous solution at approximately 10 nM concentration. The solid lines represent the corresponding best-fit lines with single component equations. (d). Hydrodynamic diameter distribution measured by DLS. Average diameter was calculated based on three independent measurements and the standard deviation was presented as error……..…. 189

Figure 3-21. SDS-PAGE characterization of cBSA-QDs and cBSA-QDs/DNA complex……..... 194

Figure 3-22. Gene transfection efficiencies of cBSA-QDs measured using the Renilla-Glo® Luciferase Assay. Data were obtained in triplicate, and standard deviations were shown as error bars. Experiments were repeated three times independently…….. 195

Figure 3-23. Confocal imaging of cBSA-QDs and 8:1 cBSA-QD/DNA complexes…… 198

Figure 3-24. Live cell confocal imaging and FCS measurement of cBSA-QDs and 8:1 cBSA-QD/DNA complexes.…… 201

Figure 3-25. Investigation of location of QDs with ER tracker…… 202

Figure 3-26. Statistical quantification of the emission intensities of QDs in individual cells based on a number of 25 to 30 cells……. 204

Figure 3-27. pH reversibility test protocol…….. 215

Figure 4-1. Different strategies for DOX delivery…….. 232

Figure 4-2. Illustration of covalent and non-covalent drug loading into PbPs drug delivery systems……..… 234

Figure 4-3. Preparation of dcBSA-PEO$(5000)_{27}$-DOX micelles…….. 235

Figure 4-4. Characterization of dcBSA-PEO$(5000)_{27}$-DOX micelles (**4-1**)…… 237

Figure 4-5. Loading of different ratios of DOX into dcBSA-PEO$(5000)_{27}$-DOX micelles (**4-1**)……..……... 238

Figure 4-6. (a). Negative staining TEM imaging of (**4-1**); (b) size distribution of (**4-1**) calculated by the NIH ImageJ program with default settings. (c). Size distribution of (**4-1**) measured by DLS……..…….... 240

Figure 4-7. (a) Absorbance spectra of dcBSA-PEO$(5000)_{27}$-DOX micelles (**4-1**) before and after dialysis in different physiological buffers; (b) Absorbance spectra of (**4-1**) before and after dialysis in different pH buffer solutions…….. 242

Figure 4-8. Live confocal images of DOX in A549 cells. A. DOX in dcBSA-PEO$(5000)_{27}$-DOX is delivered into the A549 cells, top panel – cells incubated with free DOX, bottom panel – A549 cells incubated with dcBSA-PEO$(5000)_{27}$-DOX. B. Enlarged view of a field (marked by a square) from panel A. Cell membrane (red color), DOX (green color)……..…….. 243

Figure 4-9. Quantification of intracellular DOX in A549 cells after 1 hr incubation time…… 244

Figure 4-10. Cytotoxicity of free DOX and dcBSA-PEO$(5000)_{27}$-DOX micelles (**4-1**) after 12 hr, 24 hr and 48 hr incubation times……. 245

Figure 4-11. (a). Preparation of DOX loaded cHSA-PEO(2000)$_{16}$-DOX$_{27}$ micelles (**2-24**); (b). Illustration of two-step DOX release from cHSA-PEO(2000)$_{16}$-DOX$_{27}$ micelles (**2-24**) in tumor cells…… 248

Figure 4-12. Agarose gel electrophoresis characterization of net charge. Lane 1: cHSA-PEO(2000)$_{16}$ (**2-23**), lane 2: cHSA-PEO(2000)$_{16}$-DOX$_{27}$ (**2-24**), lane 3: free DOX hydrochloride…….…… 251

Figure 4-13. Size distribution and morphology of DOX loaded cHSA-PEO(2000)$_{16}$-DOX$_{27}$ (**2-24**) characterized by (A) TEM and (B) DLS…….. 253

Figure 4-14. Size distribution of cHSA-PEO(2000)$_{16}$-DOX$_{27}$ (**2-24**) under different buffer conditions…….. 253

Figure 4-15. Commassie stained SDS-PAGE of cHSA-PEO(2000)$_{16}$-DOX$_{27}$ (**2-24**) digested by Cathepsin B and Trypsin…….. 255

Figure 4-16. *In vitro* DOX release from cHSA-PEO(2000)$_{16}$-DOX$_{27}$ (**2-24**)…… 256

Figure 4-17. Representative ESI-MS spectrum of (a) free DOX and (b) peptide fragments after cathepsin B digestion analyzed by LC-MS…….. 257

Figure 4-18. HPLC chromatogram of cHSA-PEO(2000)$_{16}$-DOX$_{27}$ (**2-24**) digestion metabolites recorded at 480 nm and 554 nm…… 258

Figure 4-19. HPLC chromatogram of cHSA-PEO(2000)$_{16}$-DOX$_{27}$ (**2-24**) incubated at pH 5 buffer without enzyme for 48 hr…… 259

Figure 4-20. Confocal microscope imaging of HeLa cells incubated with (a) DOX loaded cHSA-PEO(2000)$_{16}$-DOX$_{27}$ (**2-24**) and (a) DOX hydrochloride for 24 hr…… 260

Figure 4-21. Quantification of DOX uptake based on Confocal imaging. p<0.05…….. 261

Figure 4-22. Confocal microscope image of cHSA-PEG2000$_{16}$-DOX$_{27}$ (**2-24**) uptake by HeLa cells after 6 hr…….... 261

Figure 4-23. Cytotoxicity of (a) cHSA-PEO(2000)$_{16}$-DOX$_{27}$ (**2-24**) in HeLa cells (24 hr incubation) in comparison to DOX hydrochloride and (b) the free carrier cHSA-PEO(2000)$_{16}$ (**2-23**)……..…… 262

Figure 4-24. Caspase-3/7 activity of DOX loaded cHSA-PEO(2000)$_{16}$-DOX$_{27}$ (**2-24**) in comparison to DOX hydrochloride. *** p <= 0.0001..…... 263

Figure 4-25. Human albumin ELISA immunoassay evaluating immunogenicity of cHSA-PEO(2000)$_{16}$ (**2-23**)…… 264

Figure 4-26. Cytotoxicity of cHSA-PEO(2000)$_{16}$-DOX$_{27}$ (**2-24**) in (a) MV4-11 cells, (b) Kasumi-1 cells and (c) Oci-AML3 cells after different incubation times……. 266

Figure 4-27. Survival curve of NSG mice injected with MV4-11 cells pre-treated by drugs for 72 hr…….. 268

Figure 4-28. Preparation of Gd and DOX loaded PbP micelles cHSA-PEO(2000)$_{16}$-Gd-DOX$_{27}$ (**4-2**)…….....……. 271

Figure 4-29. Relaxivity test of cHSA-PEG(2000)$_{16}$-Gd (**2-26**) comparing with gadoteric acid…….. 273

Figure 4-30. Confocal micrographs of cHSA-PEG(2000)$_{16}$-Gd-DOX$_{27}$ (**4-2**) (1 μM) incubated with HeLa cells for 24 hr……..…….. 275

Figure 4-31. Cytotoxicity of cHSA-PEO(2000)$_{16}$-Gd-DOX$_{27}$ (**4-2**) in HeLa cells after 24 hr, 48 hr and 72 hr incubation……..…….. 276

List of Schemes

Scheme 1-1. NCA ring opening polymerization initiated by (a) primary amine and (b) other nucleophiles and bases…….. 8

Scheme 1-2. NCA ring opening polymerization initiated by metal complexes…… 9

Scheme 1-3. Solid phase peptide synthesis…….. 11

Scheme 1-4. (a). General scheme of native chemical ligation. (b). Native chemical ligation with auxiliary……. 15

Scheme 1-5. Traceless Staudinger ligation for polypeptide synthesis….. 17

Scheme 2-1. Preparation of albumin and LY derived polypeptide copolymers……... 80

Scheme 2-2. Preparation of polycationic (**2-11**) and polyanionic (**2-14**) PbPs by *a priori* modification of serum albumin……..... 97

Scheme 2-3. Tuning the hydrophobicity of polypeptide copolymer *via* ethynyl decoration……... 109

Scheme 2-4. Preparation of thioctic acid functionalized PbPs…… 113

Scheme 2-5. Conjugation of 3-azidocoumarin and azido-DOX with dcBSA-PEO(5000)$_{27}$-alkyne (**2-15**) *via* click reactions…….. 120

Scheme 2-6. Preparation of cHSA-PEO(2000)$_{16}$-DOX$_{27}$ (**2-24**)……. 125

Scheme 2-7. Preparation of biopolymers containing MRI contrast agents…… 129

Scheme 2-8. Synthesis of azido-coumarin……. 142

Scheme 2-9. Synthesis of azido-doxorubicin……. 143

Scheme 2-10. DPS test reaction…….. 147

List of Abbreviations

3D	Three dimension
AFM	Atomic force microscopy
AML	Acute myeloid leukemia
aHSA	Anionic human serum albumin
BSA	Bovin serum albumin
cBSA	Cationic bovin serum albumin
cHSA	Cationic human serum albumin
CAME	Caveolae mediated endocytosis
CD	Circular dichroism
CHLP	Chlorpromazine hydrochloride
CLME	Clathrin mediated endocytosis
DCM	Dichloromethane
d_H	Hydrodynamic diameters
DHLA	Dihydrolipoic acid
DIPEA	Diisopropylethylamine
DLS	Dynamic light scattering
DMEM	Dulbecco's modified eagle medium
DMF:	Dimethylformamide
DMSO:	Dimethylsulfoxide
DNA	Deoxyribonucleic acid
DOTA	1,4,7,10-tetraazacyclododecane-1,4,7,10-tetraacetic acid
DOX	Doxorubicin
DPS	4,4'-dithiodipyridine
DTT	Dithiothreitol
E. coli	Escherichia coli
EDTA	Ethylenediamine tetraacetic acid
EGFRs	Epidermal growth factor receptors
ELP	Elastin-like protein/peptide
EMCH	Doxorubicin-6-maleimidocaproyl hydrazone
EPR	Enhanced permeability and retention
ER	Endoplasmic reticulum
ESI	Electron spray ionization
EtOAc	Ethyl acetate
FBS	Fetal bovine serum
FCS	Fluorescence correlation spectroscopy
FDA	Food and drug administration (USA)

FIA	Flow injection analysis
FIL	Filipin
FPLC	Fast protein liquid chromatography
FRET	Förster (Fluorescence) resonance energy transfer
GPC	Gel permeation chromatography
HPLC	High performance liquid chromotography
hr	Hour
HRP	Horseradish peroxidase
HSA	Human serum albumin
IEF	Isoelectric focusing
kDa	Kilo dalton
Kd	Dissociation constant
LC-MS	Liquid chromatography–mass spectrometry
LCST	Lower critical solution temperature
LSCM	Laser scanning confocal microscopy
LY	Lysozyme
MALDI-ToF MS	Matrix assisted laser desorption ionisation time-of-flight mass spectrometry
MRI	Magnetic resonance imaging
mRNA	Messenger RNA
MI	Maleimide
min	Minute
M_n	Number average molecular weight
MS	Mass spectrometry
M.W.	Molecular weight
MWCO	Molecular weight cut-off
NCS	N-carboxyanhydrides
NHS	N-hydroxysuccinimide
NIPAAm	N-isopropyl acrylamide
NIR	Near-infrared
NMR	Nuclear magnetic resonance
PAMAM	Poly(amido amine)
PAsp	Polyaspartate
PbPs	Protein based polypeptide copolymers
PBS	Phosphate buffered saline
PDI	Polydispersity index
pDNA	Plasmid DNA
PEG	Polyethylene glycol

PEO	Polyethylene(oxide)
PGA	Poly(l-glutamic acid)
PGlu	Poly(glutamate)
PL	Photoluminescence
PLGA	Poly(lactic-co-glycolic acid)
PLL	Poly(l-lysine)
PMSF	Phenylmethanesulfonyl fluoride
QD	Quantum dot
QY	Quantum yield
RDL	Recursive directional ligation
RES	Reticuloendothelial system
RNA	Ribonucleic acid
SA	Streptavidin
SDS-PAGE	Sodium dodecyl sulfate polyacrylamide gel electrophoresis
SDV	Standard deviation
SEC	Size exclusion chromatography
SELEX	Systematic evolution of ligands by exponential enrichment
SELP	Silk-elastin-like protein
SIM	Selective ion monitoring
siRNA	Small interfering RNA
SLP	Silk-like protein/peptide
SPPS	Solid phase peptide synthesis
TA	Thioctic acid
TCEP	Tris(2-carboxyethyl)phosphine
TEA buffer	Tris-acetate-EDTA buffer
TEM	Transmission electron microscopy
THF	Tetrahydrofuran
TMRh	Tetramethylrhodamine
TMS	Trimethylsilyl
TOP	Trioctyl phosphine
TOPO	Trioctyl phosphine oxide
Tt	Transition temperature
tRNA	Transfer RNA
UV	Ultraviolet-visible spectroscopy

Chapter 1

Polypeptide Based Biomaterials – the Preparation Methods and Biomedical Applications

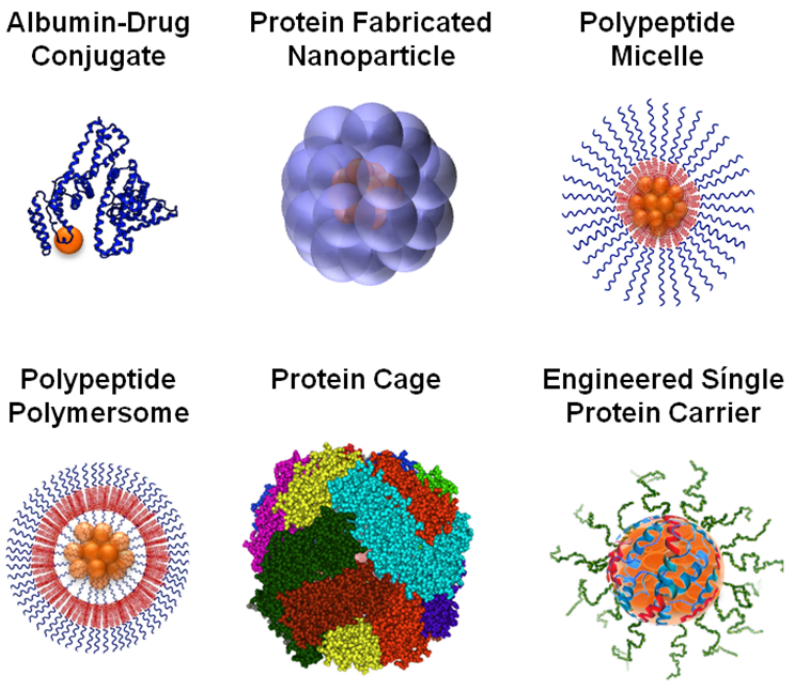

Partially adapted with permission*. Copyright 2013, Wiley-VCH.

* The picture is partially adapted from Wu, Y.; Ihme, S.; Feuring-Buske, M.; Kuan, S. L.; Eisele, K.; Lamla, M.; Wang, Y.; Buske, C.; Weil, T., Adv. Healthcare Mater. 2013, DOI: 10.1002/adhm.201200296. The dissertation author is the first author of this publication.

1.1 Introduction

Modern science and technology have led to an unprecedented evolution of the anthropic world in complement to nature. For instance, internet and computational science grants people an amazing virtual life. More incredibly, sophisticated giant spaceflight apparatus equipments like artificial satellite can be precisely controlled from a few hundreds of kilometers away in the earth. However, digging into the basis of all these exceptionally talented inventions, their sophisticated functions are fundamentally realized just through the most simple logic calculations between “1 and 0”, which is named bit. Therefore, it follows that with precision control over elementary units, man realized the existing complex world in our life in a designed fashion. Such a principle is actually also the case in the natural world. For instance, the human body is one of the most sophisticated organisms. However, all the fancy functions of the human body are eventually controlled by the simplest biomolecules such as amino acids which stepwise build up proteins, tissue, organs and ultimately the complete organism. In this sense, the life system is exactly another precisely designed and operated world. Re-examining the advanced, man-made, “synthetic ” world created by human beings in a very similar manner as nature creates complex life systems, we come up with an inspirational question: how man can envision and lead to another evolutional world if we can precisely design and operate the elementary units of nature? Despite such a sophisticated ethical question, numerous scientists have been excited on creating hybrid systems to bridge biological and synthetic matter. Given the fact that proteins (polypeptides) represent an utmost important basis of

natural materials, integration of proteins and synthetic materials paves the way to unique hybrids for the next generation of material science.

Peptides and proteins are natural biopolymers consisting of amino acid monomers. Normally, the peptides containing more than 50 amino acids are considered as proteins, whereas those less than 50 amino acids are referred as polypeptides [1]. (To simplify subsequent discussions, in this thesis, the term “protein” specifically refers to peptides > 50 amino acids and “polypeptide” refers to peptides of varying lengths). Proteins and polypeptides are considered as nature’s “work horses” fulfilling a broad range of tasks from enzymatic catalysis to structural scaffolding. Therefore, utilization of natural polypeptides also is an ideal starting point for the design of novel artificial biomaterials. Polypeptides could be synthesized from 20 proteinogenic amino acids and more than 500 non-proteinogenic amino acids [2]. By controlling the sequence of the amino acid building blocks (the primary structure), polypeptides could be formed with highly ordered secondary, tertiary and quaternary structures (**Figure 1-1**) that provide sophisticated functions and properties. For medicinal applications, it is particularly attractive that the polyamide backbone could be enzymatically degraded into non-toxic fragments *in vivo*, which makes it an attractive biocompatible material. From these aspects, polypeptides have been involved into a variety of biomedical applications, such as tissue engineering scaffolds [3], drug delivery matrices [4], and as detectors and transducers in biosensors [5].

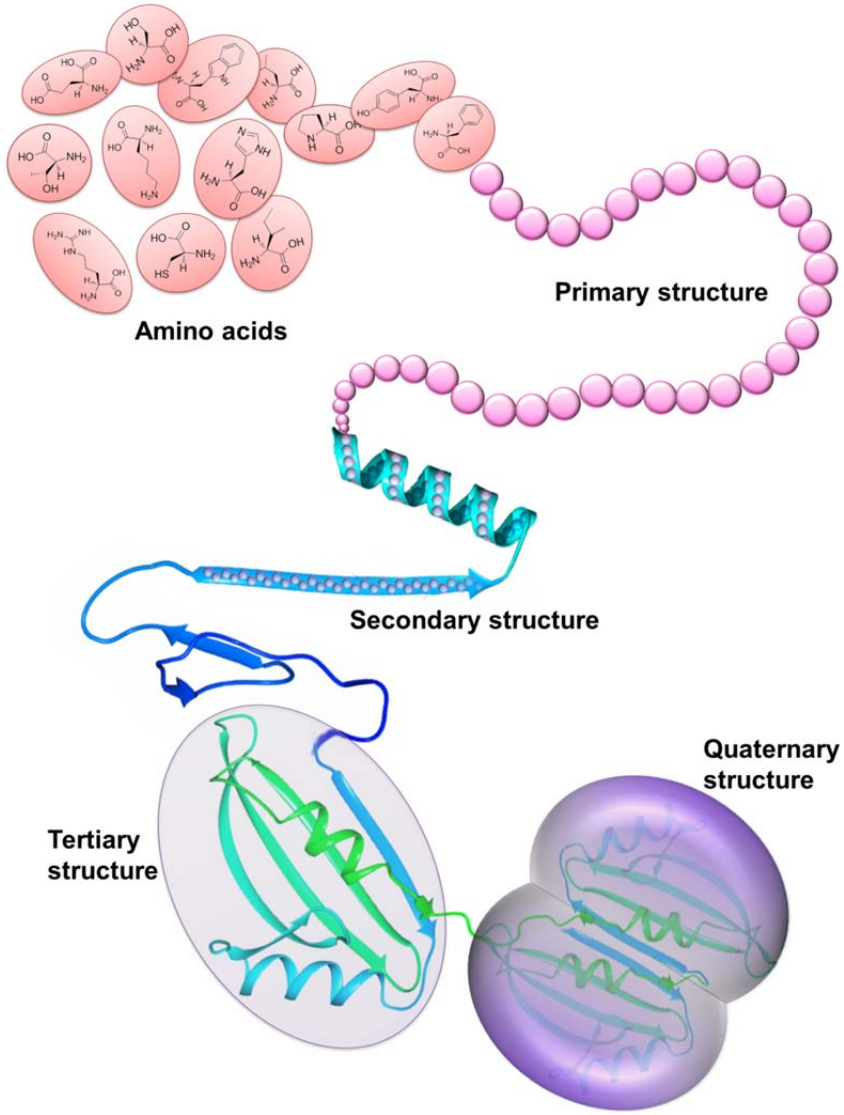

Figure 1-1. From amino acids to proteins: Depiction of the primary, secondary, tertiary and quaternary structure of proteins.

Using polypeptide based materials as biological transporters for e.g. drug delivery, gene delivery and imaging regent delivery is especially attractive and promising. Native proteins, such as albumin [6], casein [7], gelatin [8] and collagen [9], have been fabricated into microspheres and substantial amount of drug molecules or imaging regents could be encapsulated inside and delivered into target tissues. In this way, several nanomedicinal protein-drug

formulations have already been approved in clinic [10]. In contrast to these naturally occurring polypeptide materials, ‘‘engineered’’ peptide based biopolymers have recently attracted considerable attention as a new class of versatile and tunable materials. The emerge of bioengineered polypeptides is driven by two factors: (i) the increasing understanding towards structure–function relationship in proteins, which provides peptide motifs that are useful for the design of repetitive, polypeptide based materials; (ii) the maturation of recombinant DNA technologies, which allows preparation of the designed polypeptides with precise control over the chain length, stereochemistry, and monodispersity [11]. These materials not only retain the biocompatibility and biodegradability originated from natural polypeptides and proteins, but also provide access to unique chemical and physical properties, such as stimuli responsiveness [12] and sophisticated three dimensional architectures [13]. In addition to the progress of bioengineering techniques, from a synthetic point of view, new methods have been developed to synthesize polypeptides in large scales with high yields and improved sequence control [14, 15]. Although the synthesis and modification of polypeptides still holds several limitations compared to oligopeptide synthesis, there have been great achievements in recent years allowing producing peptides with significantly reduced costs thus promoting their applications in many different areas. However, the preparation of polypeptides with complex and precise structures as well as functions like native proteins is still challenging to achieve by either bioengineering or synthetic methods. Therefore, new avenues for the modification of native protein scaffolds have recently been recognized as a powerful strategy to access new classes of biomaterials of high potential for biomedical

applications with well-defined structures as well as multiple functional entities [4].

In this chapter, the major strategies to prepare polypeptides, including chemical synthesis, bioengineering as well as protein modification, will be introduced. In addition, recent achievements of using polypeptide based materials for drug delivery and bioimaging will be further summarized.

1.2 Chemical synthesis of polypeptides

The chemical state of the art methods to synthesize polypeptides include ring opening polymerization, solution phase and solid phase peptide synthesis. The most economical approach for the synthesis of long polypeptide chains is the ring opening polymerization of α-amino acid N-carboxyanhydrides (NCAs) (**Scheme 1-1**) [14, 16]. This method opens access to high molecular weight polypeptides from simple reagents in both good yields and large quantities. However, the polypeptides prepared from this method normally have repeating sequence, and it is very challenging to achieve complicated peptide sequences as found in natural proteins. The preparation of polypeptides from different amino acids with tailored sequences could only be achieved following a step-wise amide coupling sequence. Such reactions may proceed in solution or on solid phase. Solution phase peptide synthesis is useful for the preparation of short sequences of up to 10 residues in length. Non-quantitative yields of the amide coupling and the often problematic solubility of oligopeptides remain major difficulties that limit the

application of this technique. Therefore, it has been replaced by solid phase peptide synthesis in most cases. Solid phase peptide synthesis allows the preparation of the desired polypeptides sequences in a relatively fast and convenient manner, and especially allows the straight forward preparation of polypeptides *via* an automatic peptide synthesizer. This method has been widely used in both laboratory and industry. However, notably, it is not practical for the direct preparation of large polypeptides (> 100 residues) due to unavoidable deletions and truncations that result from incomplete deprotection and coupling steps.

1.2.1 NCA ring opening polymerization

Since the late 1940s, NCA based ring opening polymerizations have been the most common technique used for large scale preparation of high molecular weight polypeptides [17]. A considerable variety of NCAs has been synthesized (>200) allowing the preparation of a large diversity of polypeptides [16, 18]. The conventionally used NCA polymerizations are initiated by many different nucleophiles and bases, such as primary amines, tertiary amines and alkoxides (**Scheme 1-1**). After polymerization, the initiator becomes the C-terminal polypeptide end-group. Therefore, it is especially useful to prepare chain-end functionalized polypeptides and hybrid block copolymers. However, several challenges still exist with these initiators. First of all, the reactivity of the growing polymer chain-end during polymerization reaction lacks proper control and undergoes a variety of undesired side reactions (chain termination and chain transfer). In addition, the traces of

impurities in the reaction system, such as acid left from NCA synthesis and water from solvent, can quench the propagating chains or catalyze side reactions. Therefore, recent developments have been focused on overcoming the side reactions in these systems to produce narrowly dispersed polypeptides, e.g. by using of amine hydrochloride salts or trimethylsilyl-amine (TMS-amine) as initiators [19, 20]. Although significant improvements have been achieved, the level of control in NCA polymerizations is still not comparable with other synthetic polymerizations (e.g., vinyl addition polymerizations) and sophisticated polymer architectures are still challenging to obtain (e.g., stereospecific polymers and block copolymers).

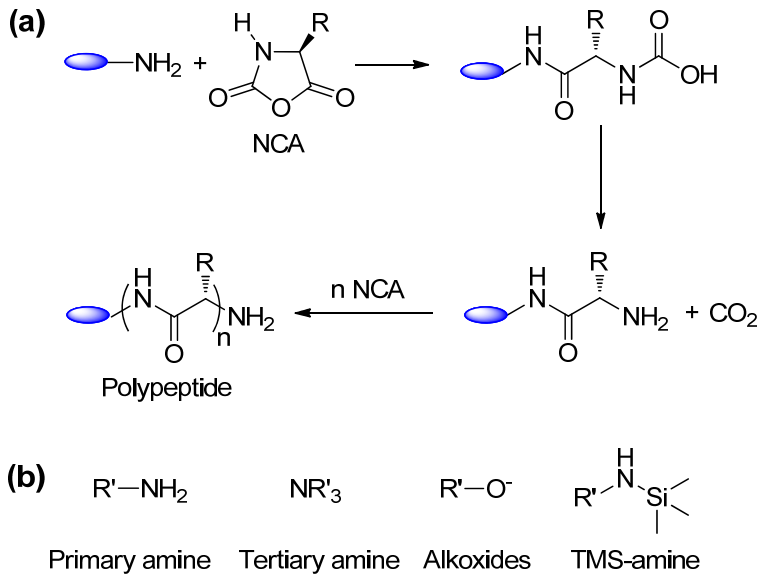

Scheme 1-1. NCA ring opening polymerization initiated by (a) primary amine and (b) other nucleophiles and bases.

To eliminate side reactions in NCA polymerizations, another strategy focuses on transition metal complexes as active species to control the addition of NCA monomers to polymer chain-ends. Nickel and cobalt

containing initiators (i.e., $(PMe_3)_4Co$ [21] and bpyNi(COD) [15]) were developed by Deming that allow an unprecedented activation of the NCAs into covalent propagating species. The metal ions can be conveniently removed from the polymers by precipitation or dialysis after polymerization. These cobalt and nickel complexes are generally applicable for a wide range of NCA monomers, and are able to produce polypeptides with different molecular weight (500 < Mn < 500,000 g/mol) and narrow chain length distributions (polydispersivity index (PI) < 1.2) [21, 22]. However, this method does not allow the attachment of functionalities to the carboxyl chain-end of the polypeptides, since the active propagating species are generated *in situ* (**Scheme 1-2**). Therefore, in case of preparing C-terminal functionalized polypeptides, amine based initiators are still preferred.

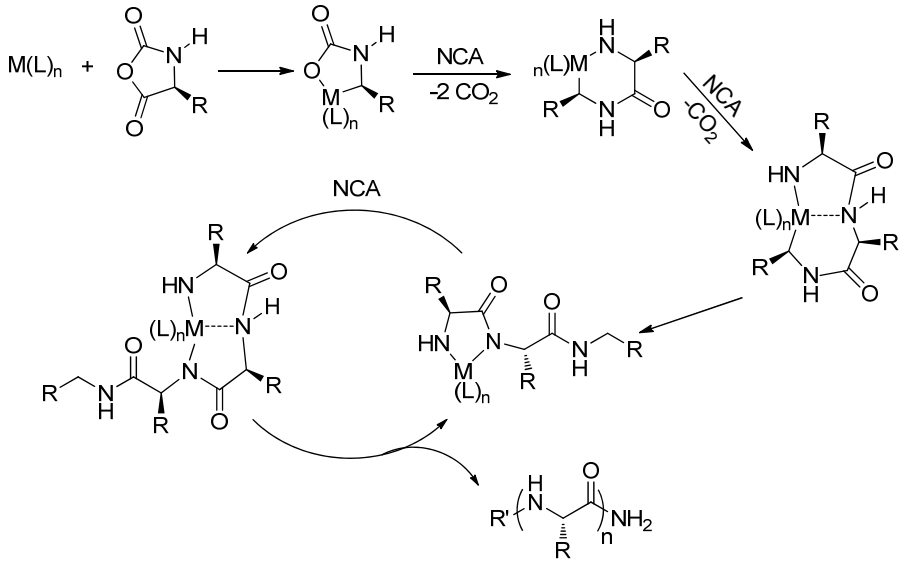

Scheme 1-2. NCA ring opening polymerization initiated by metal complexes.

Optimal polymerization conditions often differ for each NCA due to the different properties of individual NCAs and their polymers (e.g., solubility and reactivity). To date, there are no universal initiators or conditions applicable

for the preparation of high molecular weight polymers from any monomer. Moreover, regardless of the initiation methods, the polypeptides obtained by NCA polymerization have primarily been homopolymers, random copolymers, or graft copolymers that lack the sequence specificity and monodispersity of natural proteins. Therefore, to obtain polypeptides with specially designed sequences, step by step peptide synthesis is the method of choice.

1.2.2 Solid phase peptide synthesis

For the synthesis of medium-sized peptides with desired sequence, solid phase peptide synthesis (SPPS) has proven to be the most efficient approach. This method was firstly invented by R.B. Merrifield (Nobel Prize 1984), which had an enormous impact on the further development of peptide synthesis. The synthesis involves stepwise coupling reactions between a single N-terminal protected amino acid and a solid phase supported peptide fixed *via* the C-terminus. The reacted peptide is then deprotected to obtain a new free N-terminus to which a further amino acid could be attached (**Scheme 1-3**). By repeating such circles, the elongation of polypeptide chains could proceed. The immobilization of peptides allows the use of reagents in excess for high reaction yields and enables convenient wash cycles after each step for completely removing excess reagent. Based on this technique, automated peptide synthesis using a peptide synthesizer has already been widely used in both laboratory and industry.

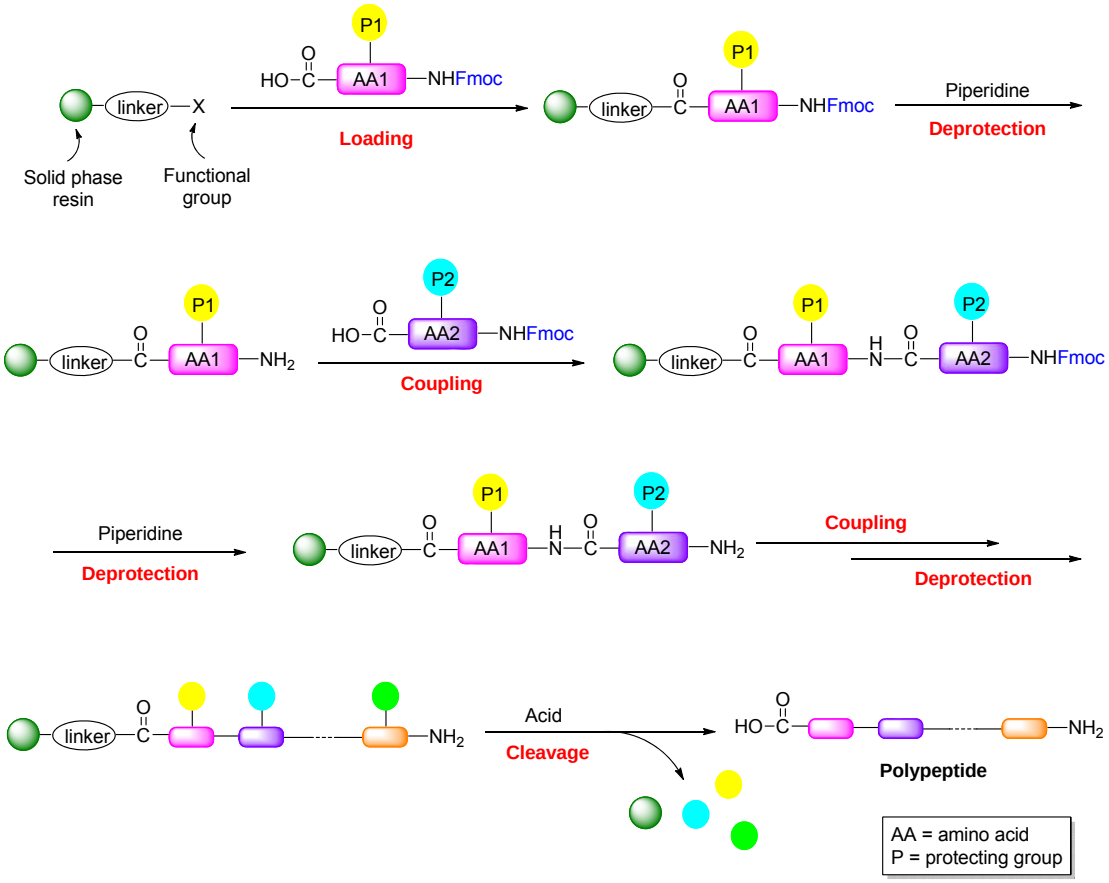

Scheme 1-3. Solid phase peptide synthesis.

Several criteria are critical for achieving an efficient SPPS, including stable solid support, appropriate protection-deprotection strategies as well as high yield and enantioselective coupling reagents. The solid support used for SPPS is expected to be chemically inert and should have high mechanical stability and solvation behaviour. The cross-linked poly(styrene-divinylbenzene) was the first resin developed by Merrifield, which is still in use [23]. However, more polar resins have been shown to give better results, such as cross-linked poly(dimethylacrylamide) resins [24] as well as combinations of polyamides or polyethylene oxide with highly cross-linked polystyrene [25, 26]. These resins are nowadays commercially available with appropriate handles

for anchoring the protected C-terminal amino acid residue by the formation of ester or amide bonds.

To ensure a clean coupling reaction at the desired position only, efficient protecting/deprotection steps are essential in SPPS. The Fmoc strategy – developed by Carpino in 1970 [27] – is still the most commonly used approach in SPPS. It makes use of the base-labile Fmoc group for protection of the N-terminal and acid-labile protecting groups for side-chain protection, which allows the entire process of SPPS to be carried out using mild reaction conditions. The deprotection of N-terminal Fmoc is normally achieved by piperidine and TFA is generally sufficient to remove all side-chain protections and also cleaves the polypeptide from the solid support. Different acid labile side-chain protecting groups are available, such as Cys(Trt), His(Trt), Trp(Boc), Lys(Dde), Lys(Aloc), Arg(Pbf) [27] (**Figure 1-2a**).

Remarkable achievements have also been made to improve the amide bond coupling efficiency in SPPS. The strategy is to *in situ* activate the carboxylic acid group on the N-protected amino acid monomers which increases the coupling efficiency. Although the traditional coupling methods, such as diimide-based activation [28], anhydride-mediated couplings [29] and preactivated esters [30] could be successfully used for SPPS as well, recently developed phosphonium- or uronium/guanidinium (aminium)- based structures are the most widely used activators today, especially in automated SPPS. These novel carboxylic activation reagents include PyBOP, TBTU, HBTU, HATU and PyAOP et al [31] (**Figure 1-2b**). They convert N-protected amino acids into their corresponding OBt/OAt esters, which undergo amide

coupling with reduced side reactions and also avoid epimerization of the amino acid chiral centre. A tertiary amine (generally diisopropylethylamine (DIPEA)) is also required to assist the coupling reaction.

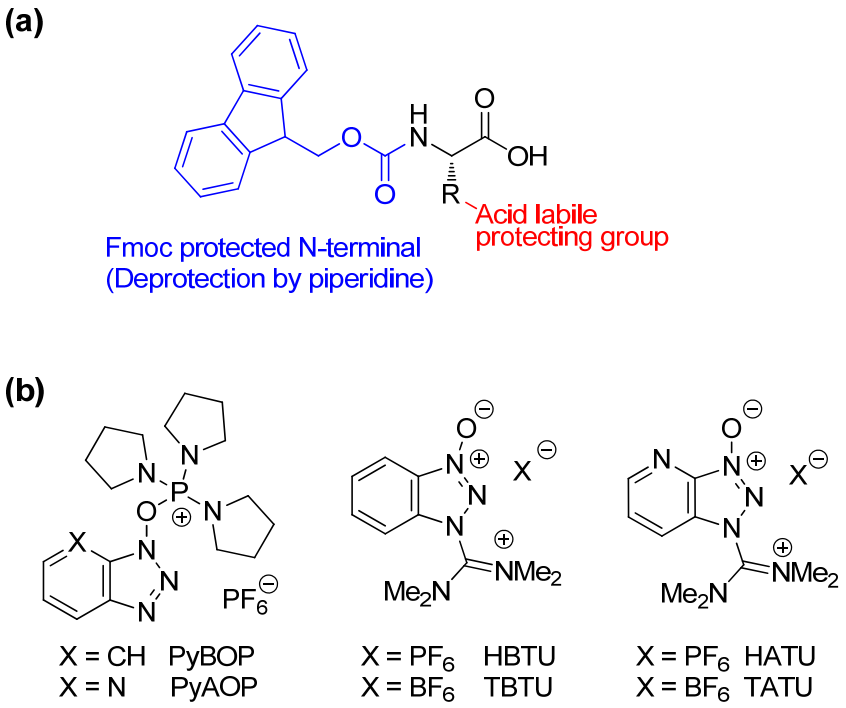

Figure 1-2. (a) Structure of Fmoc protected amino acids with acid labile side-chain protection groups. (b) Examples of amide coupling reagents used for solid phase peptide synthesis.

As a result of the fruitful research in this field, nowadays many medium-sized 30-50-mer peptides can be smoothly synthesized by manual or automated SPPS. This technique has also been successfully applied to large-scale production of peptides in pharmaceutical industry [32]. However, with increasing the length of polypeptides, the reaction yield dramatically decreases and a HPLC purification of the crude products after SPPS are normally required. Longer protein-like polypeptides are practically not achieved by direct SPPS. Therefore, alternative strategies such as connecting

small peptide segments *via* amide coupling [33] or chemical ligation [34] are developed.

1.2.3 Preparation of long polypeptides *via* chemical ligation

The SPPS is limited by the length of the peptide which can be made without defects [23, 35]. To overcome this limitation, chemical ligation methods have been developed to build up long polypeptides from shorter peptide segments. The most successful example is the native chemical ligation. This method is based on the reaction of a peptide-α-thioester with an N-terminal cysteine (Cys) on the other peptide segment (**Scheme 1-4a**). The formed thioester intermediate spontaneously rearranges to form an amide bond between two peptide segments. This approach allows a traceless ligation of two unprotected peptide segments with excellent reaction yield, specific chemoselectivity and high stereocontrol. Since native chemical ligation was developed, it has been used to make hundreds of proteins ranging in size up to more than 200 amino acids [36]. However, the most important limitation of native chemical ligation is the requirement of a Cys at the ligation site. Numerous attempts have been made to extend native chemical ligation of unprotected peptides to non-Cys sites. One strategy is using of thiol-containing auxiliaries that mimic the presence of a Cys residue at the N-terminal, which can be selectively removed after the ligation reaction (**Scheme 1-4b**). But in practice, the reaction efficiency remains still much lower than for the native chemical ligation at Cys [37].

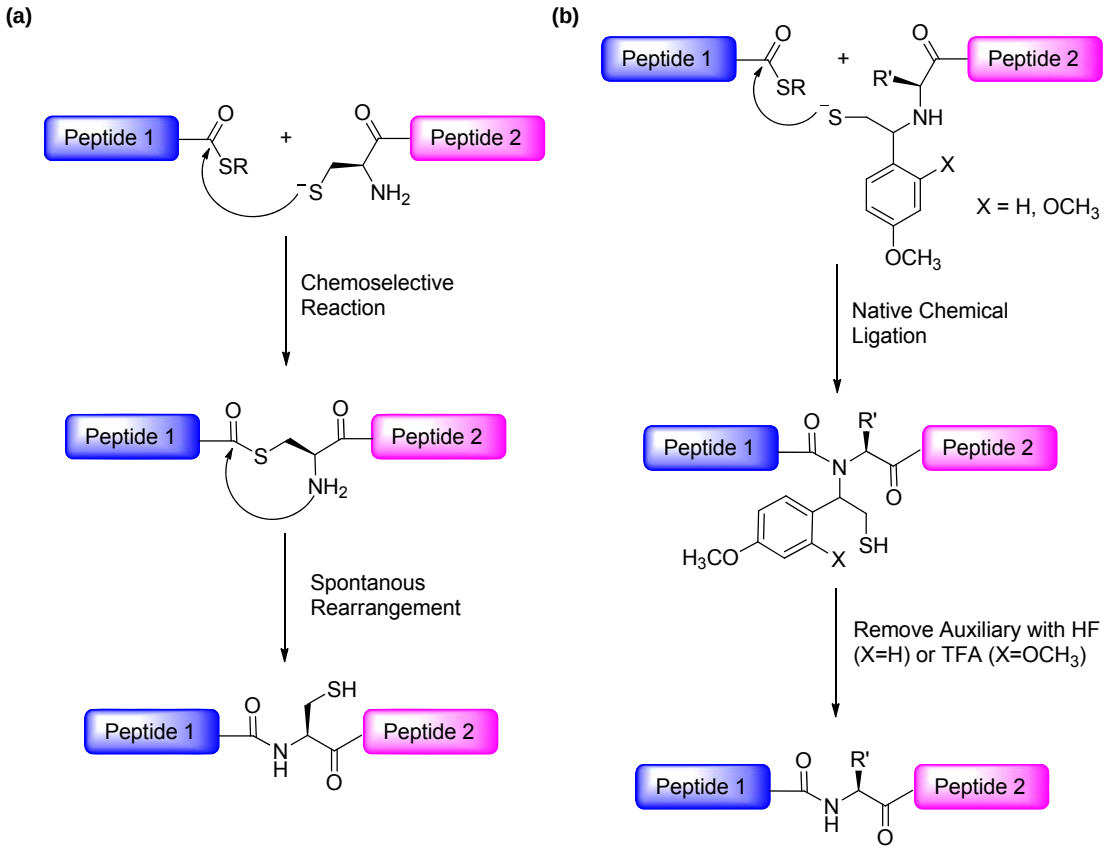

Scheme 1-4. (a). General scheme of native chemical ligation. (b). Native chemical ligation with an auxiliary.

Another useful method for peptide ligation represents the azide-phosphane based Staudinger ligation. This reaction has been discovered more than 80 years ago. But its potential for peptide ligation has only been investigated since recently [38]. Ideally, the traceless Staudinger ligation allows forming an amide bond between one polypeptide with a phosphane modified C-terminus and the other peptide with an azide modified N-terminus without depending on specific amino acid residues (**Scheme 1-5**). As an demonstration of the power of the Staudinger ligation for polypeptide synthesis, Raines and co-workers completed the total synthesis of ribonuclease A (31, RNAse A, 124 amino acids) by linking three peptide

fragments *via* Staudinger ligation and native chemical ligation [39]. The resulting protein proved to be fully functional RNAse A. However, this impressive result should not detract from the fact that peptide ligation using Staudinger reaction has just started and the potential and limitations of this method have not yet been fully explored. For instance, although several reactions are available to obtain phosphane and azide modifications, including C-terminal phosphane thioesterification [40] and N-terminal diazo transfer [41, 42, 43] (**Scheme 1-5**), they often lack of chemoselectivity when carboxyl- and amino-side chains are present on the target peptide. In addition, the reaction efficiency and side reactions still need to be further investigated with ligation of more-complex peptide fragments.

Therefore, even though the chemical ligation strategy has opened many opportunities for the chemical synthesis of large protein-like long polypeptide chains, there are still significant limitations associated with this method. In particular, the preparation of long polypeptide chains remains a rather challenging and sophisticated task in most cases.

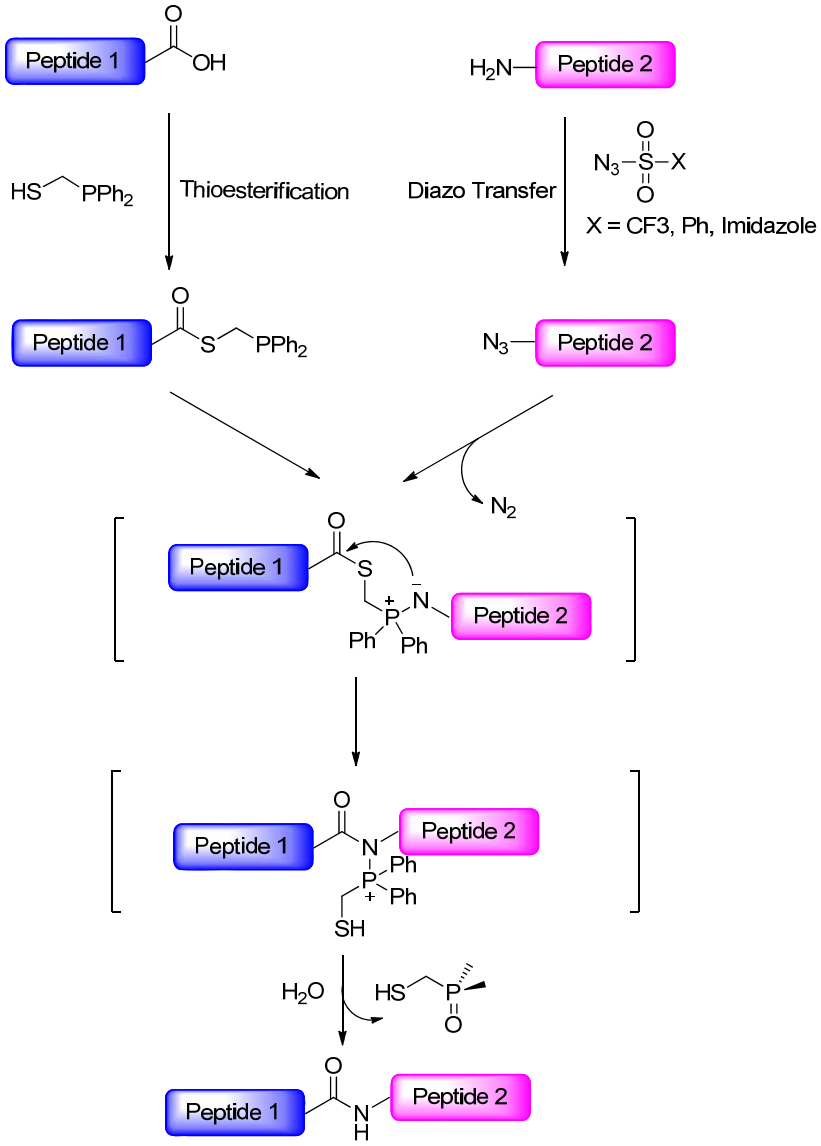

Scheme 1-5. Traceless Staudinger ligation for polypeptide synthesis.

1.3 Preparation of polypeptides by genetic engineering

Complementary to chemical synthesis, microbial technologies also provide powerful tools for polypeptide preparation. Protein engineering

techniques established from DNA recombination and protein expression have been developing rapidly as versatile techniques to access tailored large molecular weight polypeptides and proteins. Cloning and expression of genes represents an established tool in molecular biology [44], but only during the past decade, it has been recognized as a powerful tool for materials science. Based on this technique, monodispersed, high molecular weight polypeptides and recombinant proteins [45] have been prepared with complete sequence control. They have been used successfully to introduce site-specific mutations or bioorthoganol functional groups for subsequent chemical conjugation.

1.3.1 Protein engineering techniques

Protein engineering is a microbiology technique that allows the manipulation of DNA sequences encoding the peptide or protein of interest, as well as the subsequent biological expression of the translated protein products. Conceptually, the synthesis of polypeptides by applying protein engineering techniques is based on three steps: (i) the design and construction of a recombinant gene segment that codes for the peptide of interest; (ii) insertion of this segment into a DNA vector, typically a plasmid, and transformation of this recombinant DNA molecule into host cells, (iii) cultivation of the genetically modified cells to express the desired polypeptides and harvest them from host cells (**Figure 1-3**).

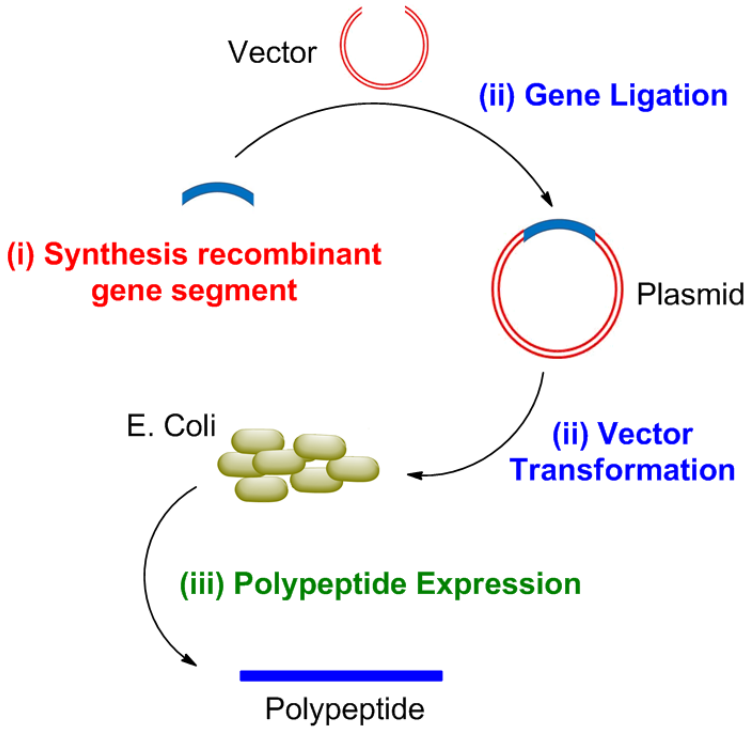

Figure 1-3. Preparation of polypeptides by protein engineering.

Due to the degeneracy of the genetic code, there are multiple choices of DNA sequences for expressing a particular polypeptide. Therefore, the careful design of a recombinant gene sequence is the first and critical step for successful production of the desired polypeptides. Although the genetic code is in principle the same for almost all organisms, the specific codons used for particular amino acid could differ greatly from organism to organism [46]. In addition, in case the desired polypeptides have repetitive amino acid sequences, a diversity of codons would also be needed to avoid DNA recombination [47]. Moreover, to construct appropriate DNA structures, the mRNA sequence after transcription should also be considered, including the proximity and similarity of the mRNA codons to any neighbouring translational sites, and the presence of the appropriate ribosome-binding sites on the mRNA [48, 49]. Furthermore, codon bias, tRNA availability, mRNA stability, and

mRNA structure also play an important role in the gene expression process [49, 50, 51, 52], which are unpredictable in most cases and not yet fully understood. Therefore, codon optimization is essential and could be highly challenging for a particular polypeptide sequence and expression system.

After designing the appropriate DNA template, the short DNA sequences of up to 100 nucleotides can be directly synthesized chemically on an automated solid phase DNA synthesizer [53]. The larger DNA sequences are normally assembled from short chemically synthesized DNA segments by different DNA ligation strategies using restriction enzymes and DNA ligases [54]. There are several methods available for the construction of large repetitive DNA sequences from short segments, including concatenation of oligonucleotides, recursive directional ligation (RDL), and mutagenesis or amplification of existing gene segments using polymerase chain reaction (PCR) [55]. On the other hand, if the desired polypeptides or polypeptide analogous are naturally occurring, it is also possible to obtain the corresponding DNA fragment from the original genomic DNA pool by enzymatic reactions, instead of using chemical strategies [56].

The obtained DNA sequence then needs to be inserted into a proper vector and introduced into an appropriate organism for expression. The vectors are generally plasmids, however there are diverse choices of plasmids with different sequences and functional regions [57]. To select a proper vector, the organisms chosen for expression, the required expression conditions (e.g. temperature, initiation condition), the multiple cloning site suitable for insertion of the prepared DNA segment need to be considered [58].

After construction of the vectors, they need to be transfected into the expression organism. E. coli is the most commonly used expression system since it is relatively inexpensive, easy to be cultured and grows fast. There are a number of genetically modified E. coli strains to enhance protein expression and even allow the incorporation of nonnatural amino acids [59]. However, over expression of the foreign polypeptides in E. coli can lead to aggregates, known as inclusion bodies, which are one of the most common problems faced in most labs [46]. In addition to E. coli, yeasts are also widely used as a eukaryotic system for recombinant protein expression. It is especially preferred if the engineered proteins requires posttranslational modifications [60]. However, it is still challenging to engineer proteins of high complexity in E.coli and even yeast, especially to correctly fold the engineered proteins into desired secondary and tertiary structures. Although the higher organisms may also be used for protein expression, transfection and cell/organism culture conditions are more complicated and more expensive.

Thus, the design and synthesis of polypeptides by bioengineering technologies is emerging but also comprises a number of challenges compared with chemical synthesis. A recombinant gene must be designed and synthesized to achieve high translational efficiency and the expression system and conditions should be optimized to produce the engineered proteins in high yield [61]. Therefore, establishing a recombinant protein engineering protocol for any newly designed polypeptide sequence is time consuming and labor intensive.

1.3.2 Examples of synthetic polypeptides produced by genetic engineering

Genetically engineered polypeptides generally consist of repeating sequences of modular peptide motifs that are derived from wild-type [62, 63] or engineered sequences [64, 65]. The most prominent studies were based on structural motifs produced by genetic engineering including β-sheets structures in silk-like peptides [66], β-spirals domains in elastin-like peptides [67], leucine zipper motifs in DNA-binding proteins [68], coiled-coil motives [69] and animal cell adhesion sequences in fibronectin [70], et. al (**Figure 1-4**). Silk-like peptides comprise highly repetitive amino acid sequences consisting of alanine rich β-sheets, which mimic the crystalline domain in native silk proteins [71]. They are highly hydrophobic and able to crystallize into films and fibers with high mechanical strength, which is attractive for numerous material-related applications (**Figure 1-4a**). Elastin-like polypeptides are derived from mammalian tropoelastin which has repeated extensibility followed by elastic recoil (**Figure 1-4c**) [67]. The most common elastin-like motif has the sequence $(VPGXG)_m$, where X can be any amino acid other than proline, and m is the number of repeats [72]. They undergo temperature dependent phase transition: they are highly soluble in an aqueous solution below their transition temperature (Tt), but aggregate rapidly above their Tt [72]. Therefore, they are important components for many temperature responsive biomaterials. In addition, coiled-coil motifs, as another class of engineered polypeptides, are present in a large variety of proteins, like DNA binding proteins, keratins and muscle proteins [69]. They consist of two individual coil

motifs tightly interacting with each other below pH 7.4 and defolding at pH 5-6.5 [73] (**Figure 1-4b**). This biocompatible interaction has been used to prepare pH-dependent reversible hydrogels [74] and controlled release peptide linkers [73].

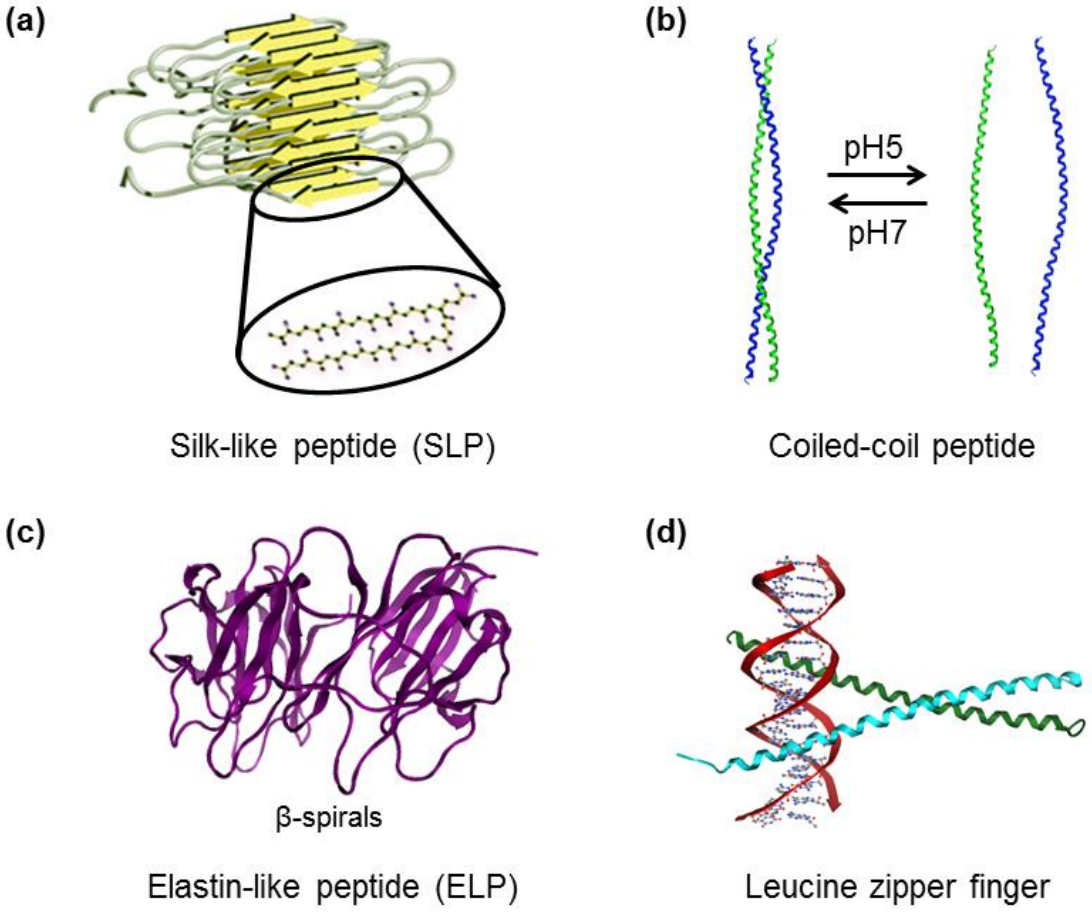

Figure 1-4. Illustration of (a) silk-like peptide (SLP) [75], (b) coiled-coil peptide, (c) elastin-like peptide (ELP) [76] and (d) leucine zipper finger domain [77].

Similar as the chemical ligation strategies, bioengineering techniques also allow connecting different polypeptide segments into a large multi-block polypeptide using the general method discussed above. These multi-block polypeptides are normally combining different structure motifs into one polymer chain and therefore display synergistic physical and chemical

properties. Combining silk-like peptides and elastin-like peptides, yielding so called silk-elastin-like proteins (SELP), is one of the most common genetically engineered block copolymers. They are made of silk-like blocks (Gly-Ala-Gly-Ala-Gly-Ser) from *Bombyx mori* (silkworm) and elastin-like blocks (Gly-Val-Gly-Val-Pro) from mammalian elastin. The ratio of silk-to-elastin blocks determines the self-assembling properties of these polypeptides [78]. At body temperature, the SELP undergo irreversible solution-to-gel transition, which has been investigated for drug delivery and tissue engineering applications [79].

In summary, protein engineering is an elegant method with which attractive polypeptide materials can be created with a high degree of structural definition. There are several advantages for using protein engineering, such as complete control over the desired sequence and molecular weight, no polydispersity as generally observed for polymers, and the possibility to synthesize large molecular weight polypeptides and proteins with no deletions or mistakes in their sequence. However, there are also several drawbacks which limit the use of protein engineering techniques for material science applications. Protein engineering is a complex and still difficult technique, which often requires long optimization cycles for the production of one peptide sequence, and for every new sequence, a new DNA construct needs to be synthesized. In addition, it is also challenging to upscale polypeptides using protein engineering. Therefore, there is still considerable interested in alternative techniques that allow straight forward preparation of polypeptides of natural diversity.

1.4 Protein-polymer hybrid biomaterials

Synthetic polymers and biopolymers represent two major classes of macromolecules bearing their own distinct features. The composition and architecture of synthetic polymers is versatile due to the availability of a large number of monomer building blocks and the availability of various controlled polymerization methods. They can be prepared with a wide variety of topologies, including block copolymers and hyperbranched structures [80, 81, 82]. Therefore, synthetic polymers could be fine-tuned to adapt to broad range of applications. However, although substantial efforts have been made to improve the structural control of synthetic polymers, it still remains a great challenge to achieve polymers with absolute control over molecular weight and monomer sequence. These features that are difficult to implement into synthetic polymers are, however, predominantly present in biopolymers such as proteins. Nature programs the perfect synthesis of nucleotides or amino acid sequences to store essential information of life in biopolymers. The lengths, monomer sequences, and even three dimensional structures of these biomacromolecules are precisely defined so that even minor mutations or structure misfolding could lead to undesirable functions or complete loss of function. Biomacromolecules, however, have the disadvantages that they are often unstable under *in vitro* conditions, e.g., because of thermal or enzymatic degradation or precipitation. In addition, the material properties and functions of biological polymers are difficult to be fine-tuned to adapt to special application requirements.

Therefore, there has been an emerging interest in the identification of novel classes of polymers that combine the benefits of both chemically and biologically synthesized polymers [83, 84, 85, 86]. The protein engineering techniques enabled producing proteins or peptides with designed sequences [87], which greatly expended the resources of proteins/polypeptides for materials scientists. Together with the evolution of different bio-orthogonal coupling methods, e.g. native chemical ligation or Staudinger ligation [36, 40], the field of protein/peptide and polymer hybrid materials has been developing rapidly in the past decade. Through these techniques, novel approaches have been established that enable the conjugation of synthetic polymers with native proteins and tailor-made polypeptides thus yielding well defined constructs termed “biohybrid materials” with characteristic properties.

The identification of biohybrid materials offers a number of distinct advantageous for various applications. For instance, biomaterials consisting of protein and polymer segments combine attractive physical properties as well as biocompatibility [84]. Conjugation of synthetic polymers with therapeutic proteins, e.g. proteins that have a beneficial effect in the human body, also helps to improve the stability of proteins for long term storage and prolonged blood circulation time [88]. In the next section, the general strategies to prepare protein-polymer hybrid materials will be discussed, including statistical protein modification, site-directed conjugation and non-covalent assembly (**Figure 1-5**).

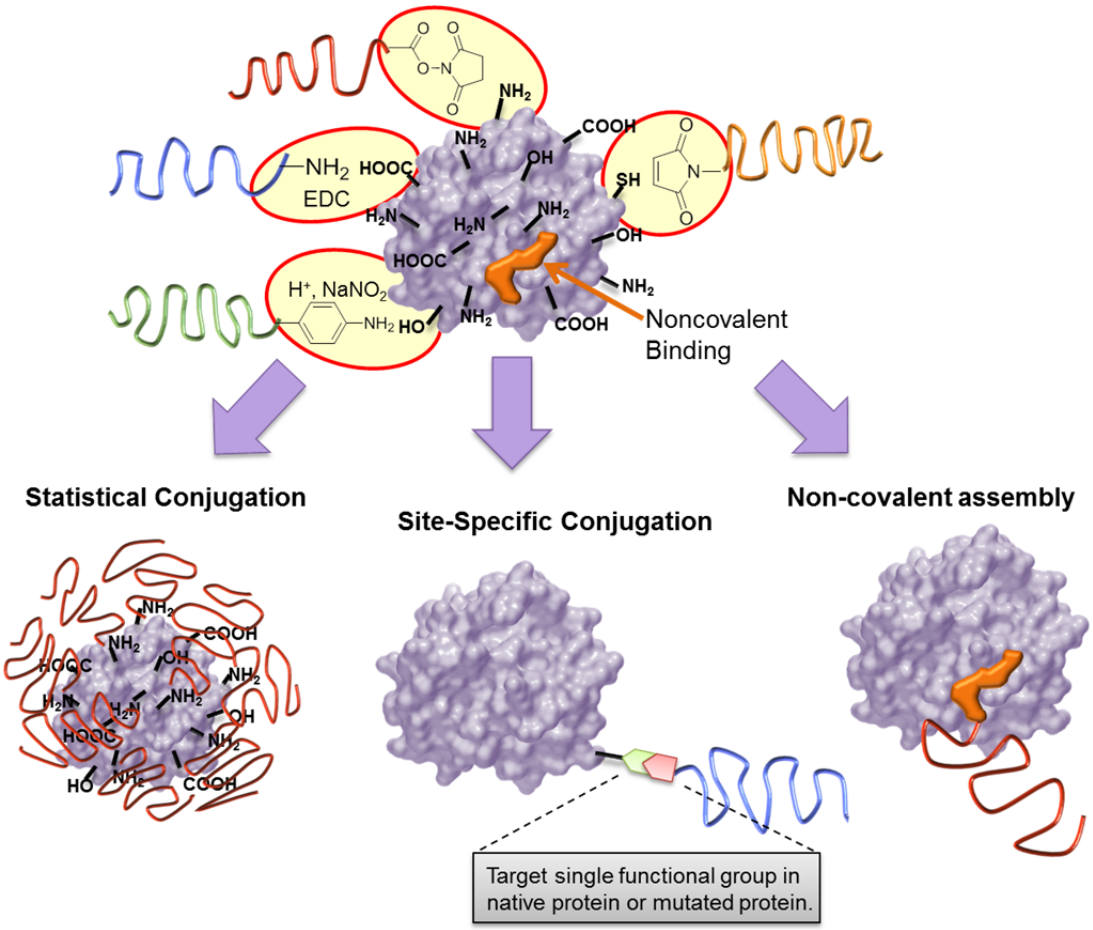

Figure 1-5. Methods to prepare protein-polymer hybrids.

1.4.1 Statistical conjugation of polymers onto native proteins

Native proteins have multiple copies of functional groups on their surface which are available for chemical reactions with synthetic polymers. The lysine amino groups are the most preferred reactive sites on proteins, since they exist in most proteins and they are often located well accessible on the protein surface [89, 90]. Other possible reactive sites include –COOH groups of aspartic or glutamic acid [91, 92], –OH groups of serine or tyrosine [93, 94] (**Figure 1-5**). Reactions on these abundant amino acids often lead to a statistical

modification of a protein surface with several polymer chains. These polymer chains could form a shell surrounding the protein, which protects the protein from degradation or alter the proteins' activity.

The most established class of such protein-polymer hybrids are the so-called PEGylated therapeutic proteins [90]. A number of proteins have been identified with important therapeutic effects. However, to use them as therapeutics, difficulties were encountered since they are often immunogenic and undergo fast degradation and excretion in the body [90]. It has been shown that by attaching polyethylene glycol (PEG, which is also called polyethylene oxide and PEO) chains on therapeutic proteins, favourable *in vivo* physicochemical properties could be achieved [95, 96]. For instance, the PEG chains shield the protein from the body's immune response and increase the circulation time of the protein in the body by preventing the excretion and degradation of proteins [97, 98].

Based on the methods developed for PEG conjugation, recent research demonstrated the conjugation of stimuli-responsive polymers and proteins to modulate their functional properties [99]. For instance, Hoffman´s group has invented a temperature sensitive protein system by statistical connection of several temperature-sensitive poly(N-isopropyl acrylamide) (poly(NIPAAm)) chains with proteins (**Figure 1-6**) [100, 101, 102]. Heating the protein-poly(NIPAAm) hybrid above the lower critical solution temperature (LCST) could induce precipitation of the proteins, whereas cooling down enables re-dissolving the proteins. The functional activity of the respective protein hybrid is often retained and even increased in some cases [101]. If poly(NIPAAm) was

conjugated on enzymes, such as trypsin, they could be used for easy separation of the enzymes from the reaction mixture after the enzymatic reactions [102]. If the protein is an antibody, this approach allows to selectively precipitating and purifying the target substrates, which is like affinity chromatography carried out without the packing (also called ‘‘affinity precipitation’’) [100].

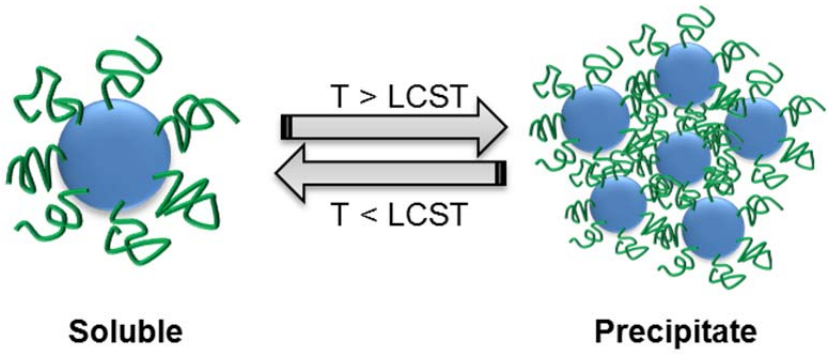

Figure 1-6. Illustration of poly(NIPAAm) conjugated proteins responsive to temperature changes [100].

1.4.2 Site-directed polymer conjugation

Although statistical functionalization of native proteins offers several useful applications especially in view of therapy, this strategy is still limited by their less defined structure and reproducibility. Thus, site-directed conjugation of polymers on native proteins is highly desirable. Today, it is still a big challenge to achieve site-directed modifications on proteins. One strategy for site-directed protein modification could be achieved *via* organic chemistry targeting non-abundant functionalities of amino acids, such as cysteine, tyrosine and disulfide bridges [103, 104]. But these methods are not generally

applicable and only work for certain proteins bearing one group more accessible than the others. In most cases, the specific functional group needs to be introduced by point mutation using bioengineering techniques.

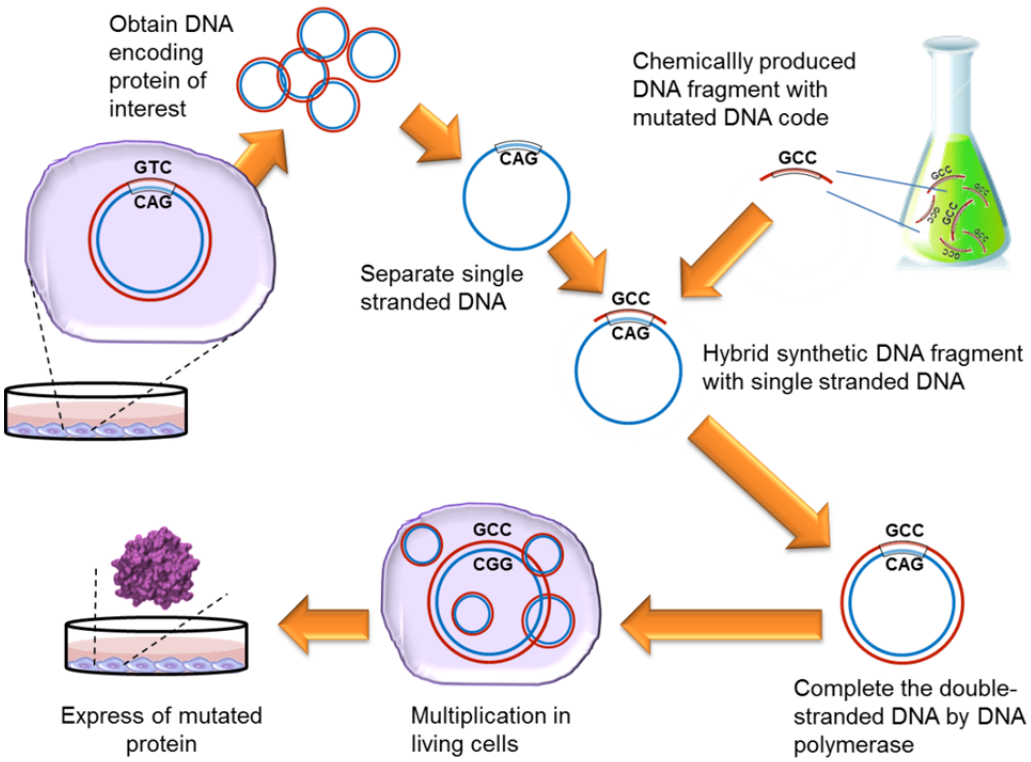

Figure 1-7. Site-directed mutagenesis by genetic engineering.

Site-directed mutagenesis is an established method to introduce rationally designed mutations into the plasmid DNA encoding for the protein of interest (**Figure 1-7**). Expression of such mutated plasmids in a bacterial host could produce structural proteins with specific functional groups at desired amino acid positions. *Via* this approach, polymers could be conjugated to a specific position on the protein which allows manipulating the proteins' function and properties in the desired fashion. Several interesting systems have been developed by Hoffman, Stayton and co-workers based on the direct attachment of a stimulus responsive polymer close to an active site of a

functional protein [105, 106]. For instance, they have introduced a cysteine mutation at the active site of endoglucanase, which was conjugated with a photoresponsive ((N,N´-dimethylacrylamide)-co-4-phenylazophenyl acrylate) polymer, thus a photoswitchable endoglucanase could be prepared which could be active for glycoside hydrolysis by UV irradiation at 350 nm but inactive under 420 nm light [105] (**Figure 1-8**). Similarly, the thermal responsive polymer could also be conjugated to streptavidin at a mutated cysteine residue close to the biotin recognition site. The high affinity between biotin and streptavidin was maintained below 32 °C, but no binding was observed above this LCST since the collapse of the polymer blocked the recognition site. The switching behaviour was reversible for several cycles [106].

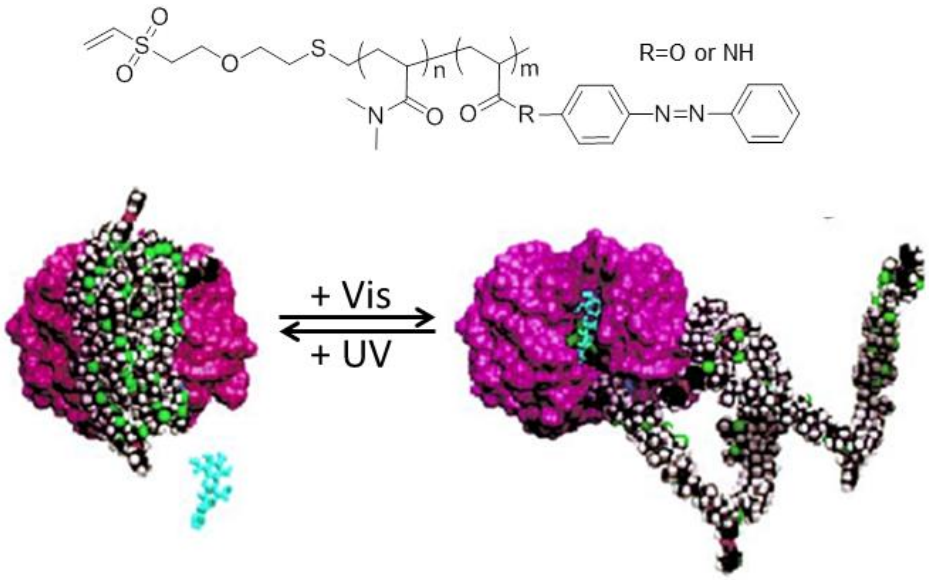

Figure 1-8. Photo-switchable endoglucanase prepared by site-directed polymer conjugation [105].

In addition to mutate native amino acids of proteins, there is also a broad interest in incorporating non-canonical amino acids into proteins to increase

the chemical space of the functionalities for bioconjugation, especially in view of bioorthoganol functional groups, for polymer conjugation. Several methods were investigated for this purpose. One approach is based on mutagenesis of a target gene with a non-sense codon at the site of interest and the synthesis of a chemically modified transfer RNA (tRNA) carrying the non-natural amino acid with the complementary codon (**Figure 1-9**). This strategy has been extensively explored by Schultz´s group [107, 108]. They showed that a variety of unnatural amino acids, including amino acids with alkenyl, azido, iodo, and keto functional groups can be genetically incorporated into proteins with good efficiencies and high selectivities, and these bioorthogonal groups were used to couple sugars, biotin, PEG and fluorescent probes to proteins [109, 110, 111]. The alternative method involves the substitution of a natural amino acid with a close structural analogue [112, 113]. This method uses bacterial auxotrophs, which are bacteria that have lost the ability to produce one of the natural amino acids. These bacteria are dependent on the medium for their supply of this amino acid and, therefore, if a close analogue is added to the medium it can be incorporated instead (**Figure 1-9**). The introduction of azido and acetylene analogues of methionine has also led to the presence of bio-orthogonal functional handles that allow further modification of the proteins. However, this methodology has not yet been extended to the incorporation of synthetic polymers.

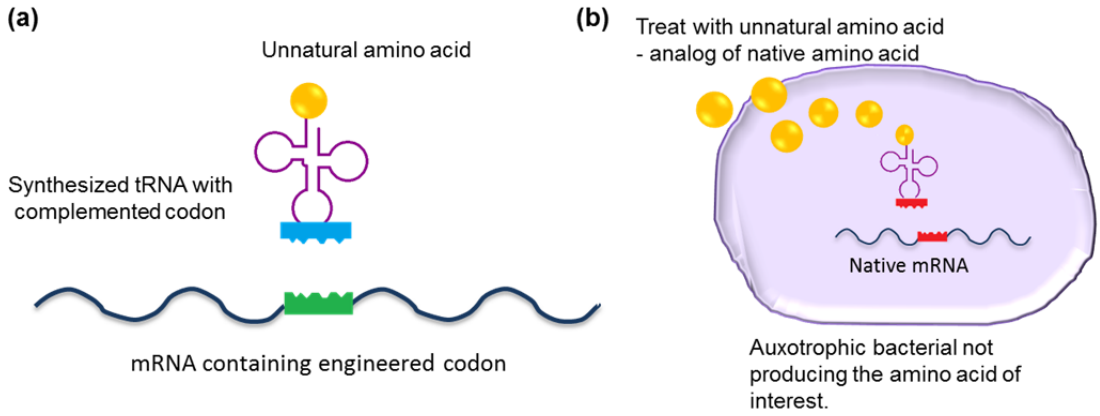

Figure 1-9. Incooperation of unnatural amino acid in protein expression by (a) engineer the genetic codon and (b) treating the native amino acid analogs in auxotrophic bacterials.

1.4.3 Non-covalent assemblies

Interestingly, it is not always necessary to conjugate the protein and polymer *via* a covalent bond. Non-covalent methods have also been demonstrated to allow the construction of protein-polymer hybrids. A few examples were reported by using the streptavin-biotin interaction, which is one of the strongest non-covalent interactions known in nature, with a dissociation constant (K_d) in the order of $\approx 10^{-14}$ mol/L [114]. Nolte and coworkers have prepared biotin-functionalized polystyrene and combined it with streptavidin to form giant amphiphiles [115]. Such constructs could self-assemble into a monolayer at the air–water interface. Due to the fact that streptavidin has four binding sites for biotin, further functionalization of the monolayer with other biotinylated entities offered the possibility to create biologically active monolayers (**Figure 1-10**). Alternatively, Bontempo and

Maynard [116] showed that a polymerization initiator modified with biotin assembled with streptavidin and enabled the *in situ* polymerization of NIPAAm. They claimed that the streptavidin was quantitatively modified with poly(NIPAAm) and specifically conjugated at the biotin binding sites only. In addition to streptavidin-biotin interactions, hemes are prosthetic groups for many hemeproteins, such as haemoglobin, myoglobin and horseradish peroxidase (HRP), which could also be used to construct protein-polymer hybrids [117, 118]. For instance, Nolte´s group has synthesized ferriprotoporphyrin XI coupled to amine-terminated polystyrene and then reconstituted with HRP to form a giant amphiphile [117]. Such giant amphiphile formed catalytically active vesicles that were characterized with electron microscopy. They also demonstrated that other heme proteins such as myoglobin could be modified *via* this approach. By using the amphiphilic block copolymer polystyrene-b-polyethylene glycol combined with different heme proteins, a large variation of self-assembled structures, such as micellar rods, vesicles, rotoids and octopus structures, were prepared [118] (**Figure 1-10**).

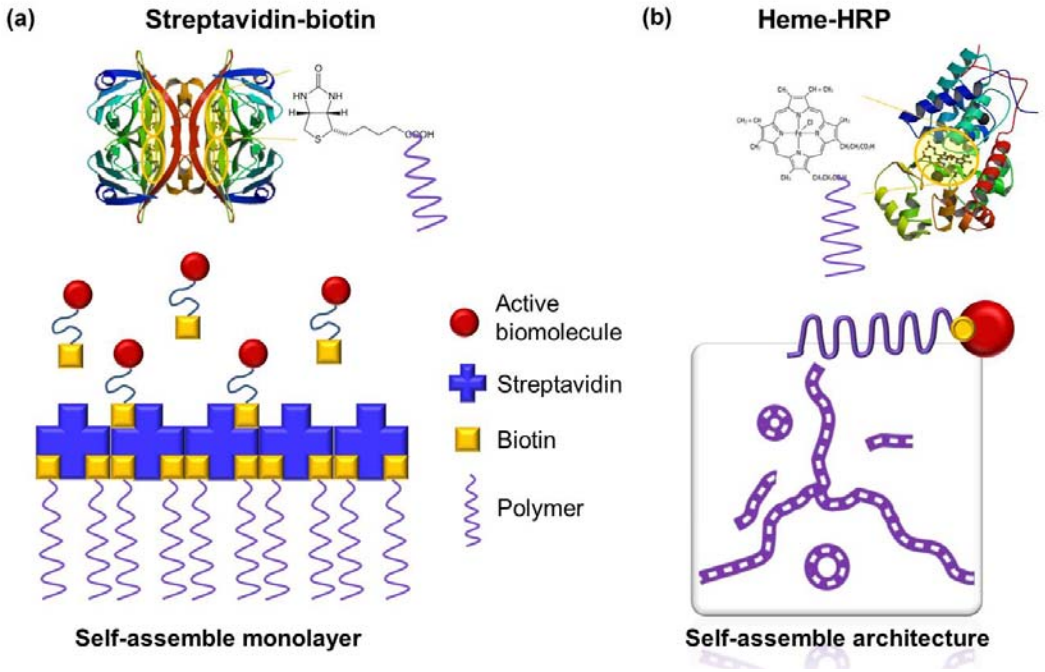

Figure 1-10. Non-covalent polymer-protein hybrids prepared by (a) streptavidin-biotin interaction which formed bioactive self-assemble monolayer and (b) heme-horseradish peroxidase binding which formed nanoscope architectures [118].

1.5 Polypeptide/protein based biomaterials for biomedical applications

Peptides and proteins are particularly attractive for biomedical applications since they are highly specific and they could be enzymatic degraded into non-toxic fragments. In addition, by controlling the sequence of the amino acid building blocks, polypeptides open access to a large number of architectures with tunable characteristics and functions. Therefore, a large

number of biomedical materials have been made from polypeptides and proteins, including tissue engineering scaffolds, drug delivery matrices as well as detectors and transducers in biosensors [3, 11]. In this thesis, the delivery of bioactive guest molecules using polypeptides/proteins based carriers, such as drug delivery, gene delivery and bioimaging nanocapsules will be a main concern.

1.5.1 Criteria for designing delivery systems for biomedical applications

In the practice of directly using active drugs and bioimaging molecules, unfavorable pharmacological properties are often recognized as a major challenge. For instance, hydrophobic molecules often have low water solubility and they tend to aggregate on plasma membranes. However, hydrophilic molecules usually have inefficient membrane permeability therefore reducing the ratio of effective molecules that reach their intracellular targets [119]. Moreover, small molecular drugs are anywhere distributed in the body and fast eliminated by renal excretion [120]. In addition, protein based drugs are often immunogenic and unstable in the blood circulation [121]. Loading biological active molecules into a delivery carrier represents a strategy offering great potential to solve many of the pharmacological problems. The carriers could protect the guest molecules from precipitation, aggregation and degradation in a physiological environment, [122] and even prevent their recognition by the immune system. If one envisions tailored carriers that are able to deliver the guest molecules exactly to their destination, drug efficiency would be greatly enhanced and side effects would

be reduced. However, to achieve all these desired features, a perfect delivery carrier would need to fulfill plenty of criteria which make it extremely challenging.

The basic criterion for ideal delivery vesicles encompasses the physical properties suitable for a given physiological environment of the target tissue, the non-toxicity and biocompatibility, low immunogenicity, the stability in blood circulation, and efficient release of the guest molecules at the targeted location [123]. Another important consideration is the number of drug molecules that a carrier could deliver. High loading of active molecules would allow using less delivery carriers and therefore reducing the risk of side effects from over-dosing the carrier [4]. The advanced delivery vesicles are also expected to target a specific organ, tissue and even intracellular compartments. The targeting function could be achieved by either passive targeting mechanism or active targeting mechanism.

The passive targeting concept, also called the ‘‘enhanced permeability and retention effect’’ (EPR effect), was first described by Maeda et al [124]. They have found that macromolecules, such as proteins, injected into blood vessels could accumulate at tumor tissue after a period of time. This phenomenon has been later found true for all nanometer sized particles. It is believed that the enhanced tumor accumulation is due to the decreased systemic elimination of macromolecular drugs through renal excretion which results in the prolonged blood circulation time, and together with the high vessel permeability at the tumor tissue which allows higher leaking of macromolecules than at the normal tissue (**Figure 1-11**). However, the EPR

effect only determines the accumulation at the tumor tissue, but does not guarantee efficient intracellular delivery. Therefore, in addition to passive targeting *via* the EPR effect, an active targeting concept was also developed.

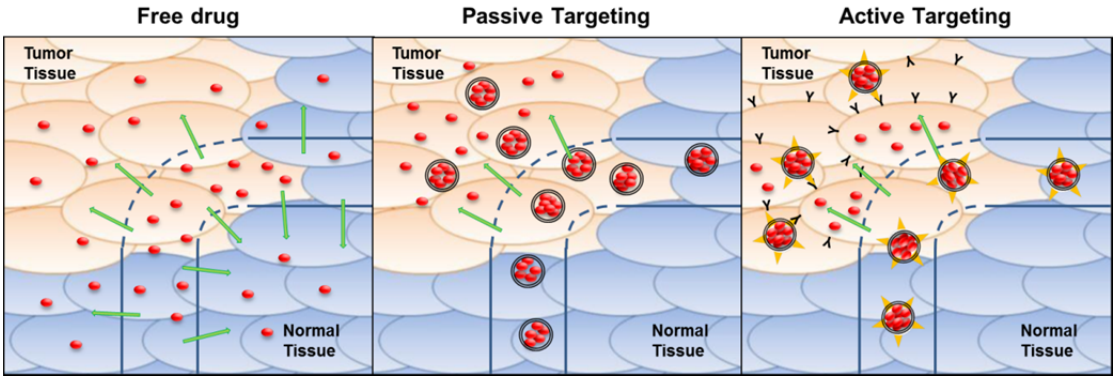

Figure 1-11. Tumor targeting strategies used in nanomedicine.

The active-targeting concept utilizes the ligands with specific binding affinity to cellular membrane receptors. Carriers conjugated with these targeting ligands would firstly reach the interstitial fluid of the tumor *via* the EPR effect, and subsequently, the ligands facilitate a much faster uptake into the cells possessing specific cell surface receptors compared with other cells (**Figure 1-11**). Several small molecules, short peptides and small proteins have been demonstrated as efficient targeting ligands for this approach. For instance, folic acid is a small molecular ligand interacting with the folate receptors that are up regulated in numerous cancer cells [125]; cyclic RGD is a short peptide sequence that has been used to interact with $\alpha v\beta 3$ and $\alpha v\beta 5$ integrins that overexpressed on the tumor vasculature [126, 127]; and the epidermal growth factor is one of the most commonly used protein ligands that recognizes epidermal growth factor receptors (EGFRs) [128] – the marker of various tumors. In addition, modern techniques also allow the development

of personal cancer therapy to target a specific type of cancer cells. Antibodies are one important representative of these techniques [129]. Antibodies are large Y shape proteins (~150 kDa) which could be generated toward a certain antigen with high specificity. Due to the size effect, they displayed both the passive and active targeting effect, and have been used for the delivery of several small molecular anticancer drugs, including vinblastin, methotrexate, and doxorubicin [130, 131, 132]. However, antibodies are expensive and efficient chemistry methods to conjugate cargoes to antibodies are also very limited. Alternatively, recently developed technologies, such as aptamer SELEX [133] and phage display [134], provided the possibilities to generate specific targeting nucleic acid sequences and short peptide sequences. But they are still at the early stage of biomedical applications [135].

Besides specific targeting, the cargo release kinetic is another essential factor for the design of efficient delivery carriers. The cargoes are normally expected to be stable in blood circulation, but to efficiently release from the carriers once they reach the targeted cells. This could be achieved by using stimuli responsive linkers between carriers and cargoes, or a smart delivery carrier which degrades only at the desired location (**Figure 1-12**). The commonly used stimuli responsive linkers including chemical linkers such as hydrazone [136, 137] which is stable under neutral but hydrolyzed under acidic pH, and peptide linkers such as enzyme cleavable peptide sequence [138]. In addition, stimuli responsive polypeptide materials allow the preparation of smart carriers that desintegrate inside the target cells and release their cargoes. For instance, PLGA (poly(lactic-co-glycolic acid)) is a synthetic

polypeptide segment which possesses a conformation transformation between coil and helix depending on environmental pH, which has been widely used to construct pH responsive carriers [139]. Poly(cysteines) forming redox sensitive disulfide crosslinks has been used to prepare redox responsive carriers [140]. Moreover, the thermal responsive ELP proteins have been intensively studies for thermal responsive drug delivery [141], which will also be discussed in section 1.5.2.

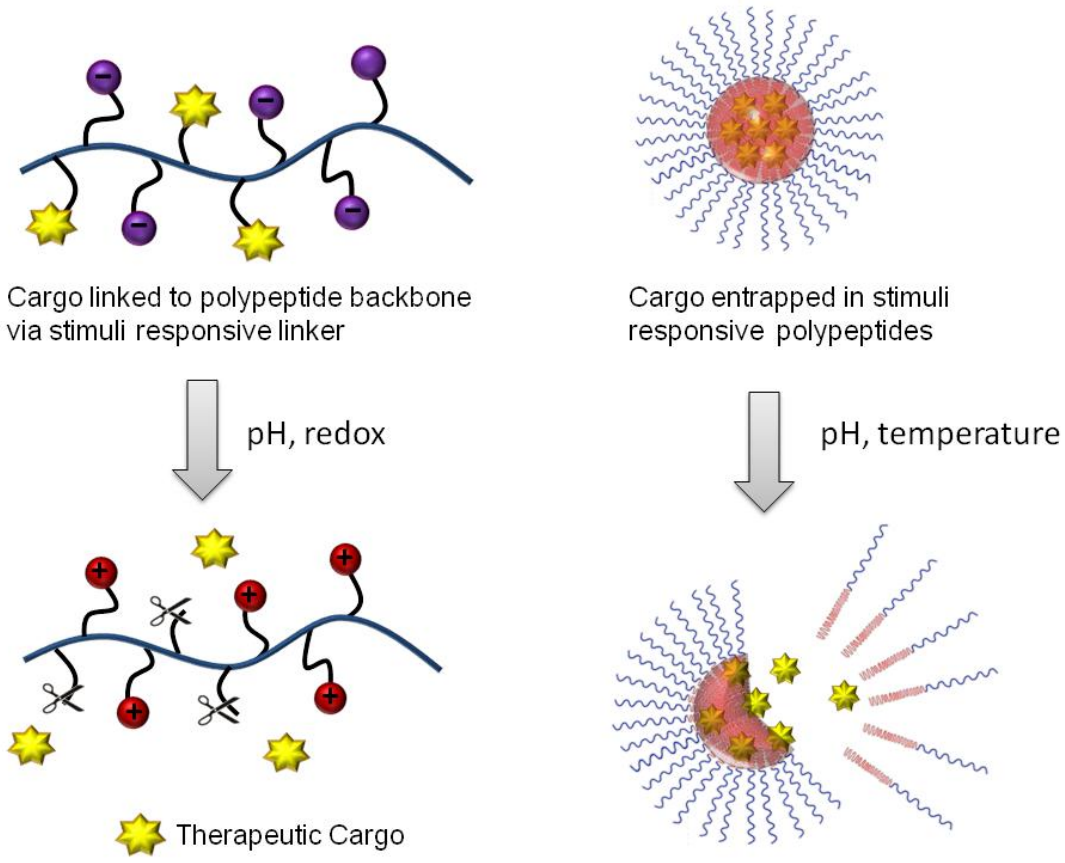

Figure 1-12. Strategies toward stimuli responsive carriers.

1.5.2 Polypeptide based polymeric micelles as delivery carriers

Amphiphilic block copolymers bear hydrophilic and hydrophobic segments that display different solubilities, which is the major driving force for their spontaneous self-assembly into three dimensional architectures in aqueous media. By adjusting the type of hydrophobic and hydrophilic blocks and the ratio of block lengths, different structures could form including micelles [142], hollow polymersomes [143] and wormlike micelles [12] (**Figure 1-13**). The geometry is dictated by the molecular packing parameter $p = v/al_c$, in which v is the volume of the densely packed hydrophobic segment, l_c is the chain length of the hydrophobic block normal to the interface, and a is the effective cross-sectional area of the hydrophilic group [144]. Based on this calculation, the morphology of amphiphilic self-assemblies would be predicted to be either spherical ($p < 1/3$), or cylindrical ($1/3 < p < 1/2$) or vesicle bilayer ($1/2 < p < 1$). Each of these architectures is known to possess its specific advantages. For instance, polymersomes reveal high and multiple drug loading capability [145], and cylindrical wormlike micelles have an improved long-term blood circulation [12].

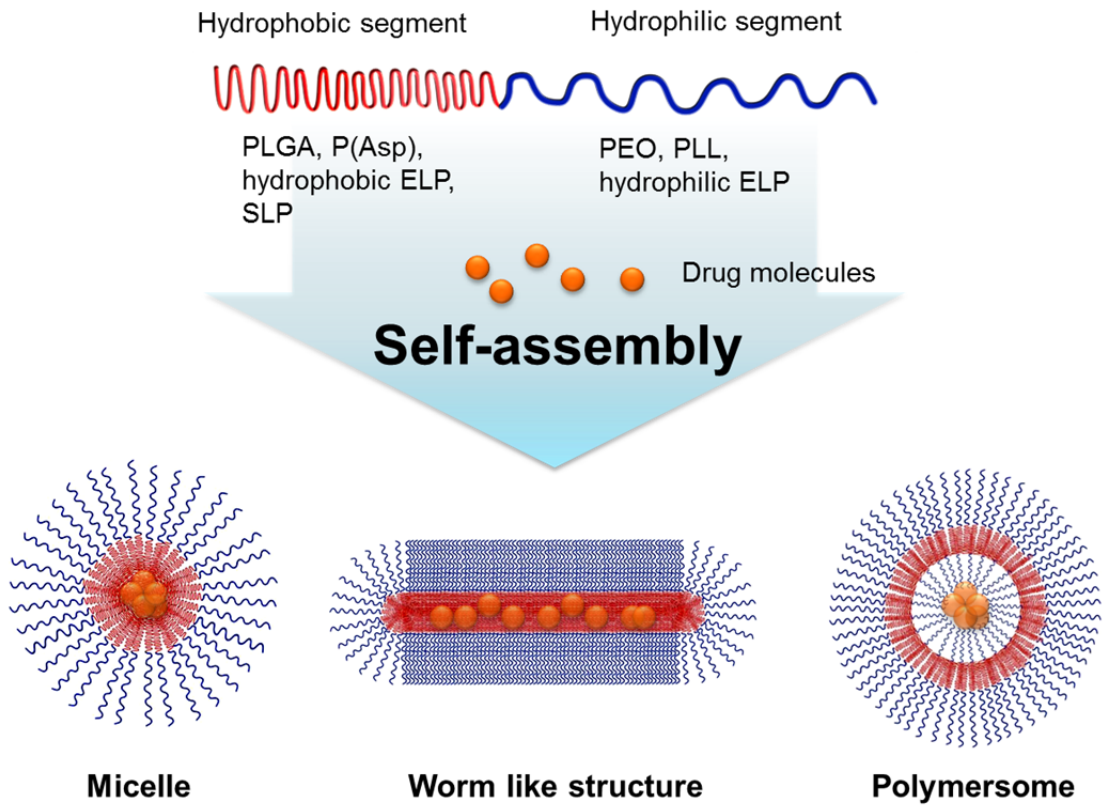

Figure 1-13. Self-assembly of amphiphilic polypeptides in aqueous solution.

The most common structural motif of self-assembled delivery systems is still the spherical micelle. Such micelles usually contain a hydrophobic inner core surrounded by a hydrophilic shell and form a distinct core–shell structure. Cargo molecules could be loaded into the hydrophobic core *via* either hydrophobic interactions or covalent conjugation. Several synthetic polypeptides have been used for this purpose, such as polyaspartate (PAsp), poly(l-glutamic acid) (PGA) and poly(l-lysine) (PLL). The polypeptides in such architectures normally serve as hydrophobic segments and represent a platform for the conjugation of drug molecules and other functional moieties, whereas PEG is often used as the hydrophilic segment because of its biocompatibility [146]. Surface functionalities, such as targeting ligands, could be further modified at the end of the PEG segment to introduce multiple

functionalities into the system (**Figure 1-16**), which will be discussed in detail in Section 1.5.4. For instance, the groups of Kataoka has developed doxorubicin-conjugated PEGb-poly(aspartate), (PEG–PAsp) block copolymers that spontaneously form polymeric micelles in aqueous media [142] (**Figure 1-14**). The hydrophobic anticancer drug doxorubicin is covalently conjugated at the side chains of the poly(aspartate) (PAsp) segment *via* a pH sensitive hydrazone linker to enhance the micelle stability. Additional doxorubicin molecules could be further entrapped inside the hydrophobic core of the micelles to enhance the toxic effect. This system exhibited a 7.4-fold higher tumour accumulation than free DOX at 24 hours due to the EPR effect. The optimal composition of PEG–PAsp(DOX) micelle is already in phase II clinical trials in Japan. Similarly, poly(glutamate)-PEG copolymers could be also used to form drug delivery micelles. The poly(glutamate) (PGlu) segment is more hydrophobic than PAsp due to the additional CH_2 in the side chain. Therefore, it has been used to increase the micelle stability, especially for more hydrophilic cargoes [147].

Synthetic polypeptides have also been used for gene therapy. With the increasing understanding of the biological mechanisms driving life processes at the molecular level, novel nucleic acid-based therapies, such as plasmid DNA and siRNA, have been developed as innovative therapeutics. However, due to their large molecular weight and anionic nature, their clinical applications are still limited due to their instability under physiological conditions and low cellular uptake efficiencies. DNA or RNA would be rapidly eliminated by DNase and RNase if they are directly administered into the

blood stream. Therefore, appropriate nanocarriers are necessary to incorporate DNA or RNA for the practical application of nucleic acid-based therapies. To prepare the carriers for gene therapy, polycationic peptides are normally used to complex nucleic acids, such as PLL, poly(arginine) [148] and poly{N-[N-(2-aminoethyl)-2-aminoethyl]aspartamide} P[Asp(DET)] [149]. For instance, Kataoka et al. [150] has recently reported nanosized polymeric micelles that deliver siRNA to solid tumors using functionalized poly(ethylene glycol)-block-poly(L-lysine) (PEG-*b*-PLL) (**Figure 1-14**). The amine group of lysine was modified with 2-iminothiolane (2IT) to improve control of micelle formation and also increase stability in the blood compartment, and the PEG terminus was decorated with the cyclo-Arg-Gly-Asp (cRGD) peptide to improve the active targeting and biological activities. Such stable and targeted micelle structures reveal improved siRNA accumulation within tumor tissue after intravenous injection, and effective tumor treatment was realized by knocking-down angiogenic proteins.

In addition to chemically prepared, synthetic polypeptides, bioengineered polypeptides have also been developed as delivery systems. Prototype examples of engineered peptide based biomaterials demonstrated for such applications include ELPs, SLPs and coiled-coil peptides (the preparation of these peptides was described in section 1.3.) ELPs are highly attractive for drug and gene delivery due to their thermodynamic inverse phase transition in aqueous solution at a specific temperature (Tt). ELPs are hydrophilic below Tt, but hydrophobic above Tt [141]. They are comprised of a repeating

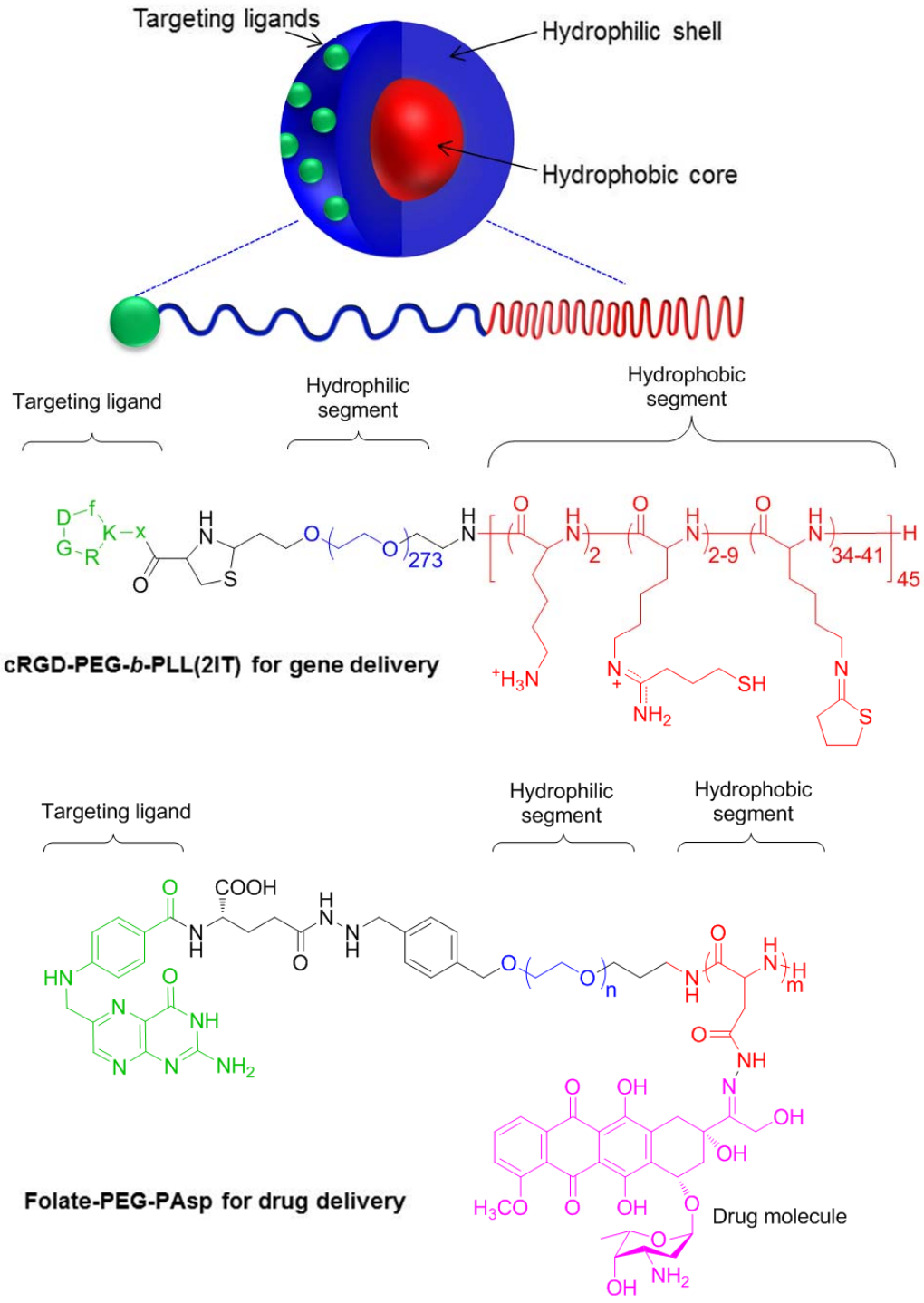

Figure 1-14. Amphiphilic PEG-polypeptide block copolymers forming core-shell micelles for gene and drug delivery.

pentapeptide sequence $(VPGXG)_n$ (X is any amino acid except proline). They could function both as hydrophobic segment and hydrophilic segment for polymeric micelles by varying the X amino acid to tune their hydrophobic properties or hydrophilic properties. By special fabrication techniques, ELPs could also be prepared as hollow spheres with high loading of drugs and therapeutic genes [151]. Silk like peptides are hydrophobic and easily self-assemble to defined nanostructures [152]. Therefore, they are normally fused to hydrophilic polypeptide sequences, such as ELP and polylysine, to gain water solubility and allow micelle formation. For instance, the silk-polylysine block copolymers formed ion complexes with pDNA and they are applied for targeted gene delivery by recombination with another target peptide like RGD or TAT peptides [152, 153]. Coiled coil peptides are used as a pH responsive, reversible non-covalent linker in durg delivery systems, which is formed by heterodimerization of two complementary peptide sequences that are linked to the polymer carrier and the cargo [154].

1.5.3 Chemically modified proteins as nanocarriers

Although substantial efforts have been made to develop synthetic polypeptides as delivery carriers, some functions and unique structures present in native proteins are still difficult to achieve. Chemical modification on native proteins paves another way of using native proteins with more flexibility to adapt to different requirements of delivery carriers. For instance, protein cages are perfect examples of natural nanocarrier platforms built from a process of hierarchical assembly [155]. They usually compose of a limited

number of subunits which assemble into chains, ribbons, and finally become ‘‘porous’’ nanospheres (**Figure 1-15**). Protein cages possess several significant advantages as delivery carriers [4]. Firstly, their uniform cage sizes make it possible to deliver drug with relatively even amounts of loading and avoid random macromolecular aggregation of nanoparticles. The diverse shapes of protein cages also provide different surfaces and various chemical and biological structures for drug delivery. Their intrinsic high stability in most physiological environments could effectively prevent drugs from enzymatic degradation. Moreover, protein cages can be genetically modified with bioorthogonal groups and they are robust to various chemical reactions, therefore, various functions could be introduced into protein cages, such as crosslinking drugs, imaging agents, and labeling fluorophores (**Figure 1-15**). They also can be further decorated with additional functionalities *via* chemical modification due to their robustness to different chemical environments. Furthermore, protein cages would assembly or disassemble at different conditions, allowing for loading drugs dynamically and plastically. With these attractive advantages, numerous application have been demonstrated including delivery of imaging molecules [156, 157], drugs [158, 159], antibodies [160] and therapeutic proteins [161].

Another class of protein based delivery carriers is the streptavidin/ avidin system [162]. Streptavidin serves as a molecular adapter between e.g. an antibody as the targeting component, and a biotinylated therapeutic or imaging agent (**Figure 1-15**). It has also been used to deliver drugs / toxins / imaging agents to targeted cells *in vitro* and *in vivo* [163, 164, 165]. For instance, a

TAT–streptavidin (TAT-SA) fusion protein, which retains the ability to bind biotinylated cargos while directing their efficient cellular uptake, was reported by Stayton group [166]. TAT-SA is internalized by Jurkat T-cells and NIH 3T3 cells whereas the native streptavidin is not. Biotinylated alkaline phosphatase was complexed to TAT-SA and was successfully delivered into Jurkat T-cells where it retained its activity. However the exceptionally slow biotin dissociation kinetics with native streptavidin prevents efficient cargo release and the binding between streptavidin and endogenous biotin also represents a concern. Protein engineering approaches allow the modification of individual subunits to impart a variety of special features, which are recombined in various combinations to create chimeric tetramers with multiple functionalities.

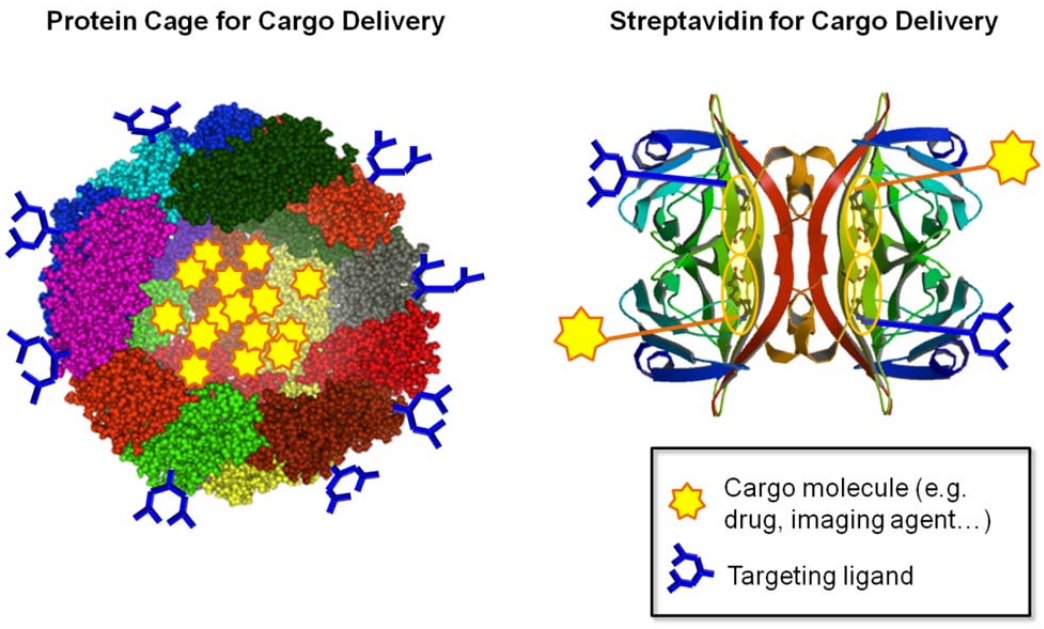

Figure 1-15. Illustration of protein cage and streptavidin based delivery carriers.

Although the examples of protein based drug delivery have shown numerous advantages, most of these systems are still in their early phase of *in vitro* studies and haven't been advanced to *in vivo* tests yet. In addition, the types of proteins that can be used and the preparation/modification strategies are still very limited, which significantly slows down the development of such systems. In order to allow more diversity of natural proteins to be used for biomedical applications, novel strategies are urgently required in this area.

1.5.4 Decoration of multiple functional moieties on polypeptide based nanocarriers

The ideal drug delivery carriers, which were nicknamed the "magic bullets", are expected to combine multiple functionalities into one particle, such as drug conjugation, membrane penetration, cell recognition, stimuli responsiveness and even co-delivery of imaging molecules for theranostics [167, 168]†. From this aspect, polypeptides made from different amino acid monomers could provide different orthogonal functional groups in one polymer, therefore enable the modification of multiple functionalities.

To form multifunctional delivery carriers, the functional moieties are normally introduced into the polypeptides before carrier formation. Synthetic

† Theranostics (a portmanteau of therapeutics and diagnostics) is an emerging strategy of combining both therapeutic and diagnostic capabilities in one dose. It is essential for optimization of drug efficacy and safety and will assist in development of individualized therapy targeting to an individual's' specific disease subtype and genetic profile [168].

polypeptides with functional moieties are often achieved by polymerization of pre-functionalized amino acid monomers. For instance, Heise et.al. [169] have prepared polypeptide based polymersomes functionalized with glycans for specific interactions with cells (**Figure 1-16a**). The glycan functionalized polypeptides are prepared by sequential ring-opening polymerization of benzyl-L-glutamate and propargylglycine (PG) N-carboxyanhydrides, and further glycosylation on the poly(PG) block by Huisgens cyclo-addition "click" reaction using azide-functionalized galactose. These structures display bioactive galactose units in the polymersome shell, as proven by selective lectin binding experiments. In addition, by mixing of amino acid monomers with different funcitonalities at a desired ratio, Kataoka's group has prepared PEG-*b*-PLL block copolymers which have hydrophilic PEG segment decorated with cyclic RGD peptide for targeting and a hydrophobic polylysine segment that was randomly polymerized from three functional moieties: (i) free lysine with cationic charges, (ii) 2-iminothiolane capped lysine providing sufficient hydrophobicity and (iii) modified lysine containing free thiol end groups to enhance micelle stability by forming disulfide bridges (structure see **Figure 1-14**). Such multifunctional polypeptides forming stable gene delivery vesicles have been shown to efficiently deliver siRNA into cancer cells [170].

In genetic engineered polypeptides, multiple functionalities could be directly designed and incorporated during expression. For instance, Chikoti et. al. [171] reported a ELP based nanoscale delivery system consisting of multivalent NGR-tripeptides to target the CD13 receptors that are preferentially up regulated in the tumor vasculature and perivascular cells.

They expressed multifunctional block polypeptides with four blocks: a hydrophilic ligand (NGR), a flexible GGS peptide linker, a hydrophilic ELP segment and a hydrophobic ELP segment followed by a trailer peptide (WPC) for conjugation of fluorophores or drugs to the Cys (C) residue (**Figure 1-16b**). These amphiphilic block copolymers could self-assemble into monodisperse spherical micelles, and display multivalent NGR targeting ligands on the surface. *In vivo* tumor targeting was studied and greater extravascular accumulation of nanoparticles in tumor tissue compared to normal tissue was observed.

Functionalization of native protein based carriers is normally achieved by chemical modification reactions at the reactive amino acid side chains or mutated amino acids. Ahn et. al [138] have prepared small heat shock protein (Hsp) cages that genetically modified with a GGDEVDGGCGGRGD peptide at the C-terminal of each Hsp subunit (**Figure 1-16c**). This peptide sequence contains cancer cell-binding peptides (RGD) and caspase cleavable substrates (DEVD). The cysteine in the middle of this peptide sequence provides a chemical modification side for conjugation with a fluorophore, demonstrated by cyanine 5.5 (Cy5.5). The fluorescent quencher BHQ3 was further conjugated on the protein cage's exterior *via* amide coupling on the amines of lysine side chains to quench the Cy5.5 fluorescence *via* FRET. Thus, multiple functionalities are integrated within a single protein cage, including drug loading capacibility inside the protein cage, tumor-specific targeting due to RGD peptides and caspase activity detection due to the cleavage of Cy5.5 fron DEVD linker.

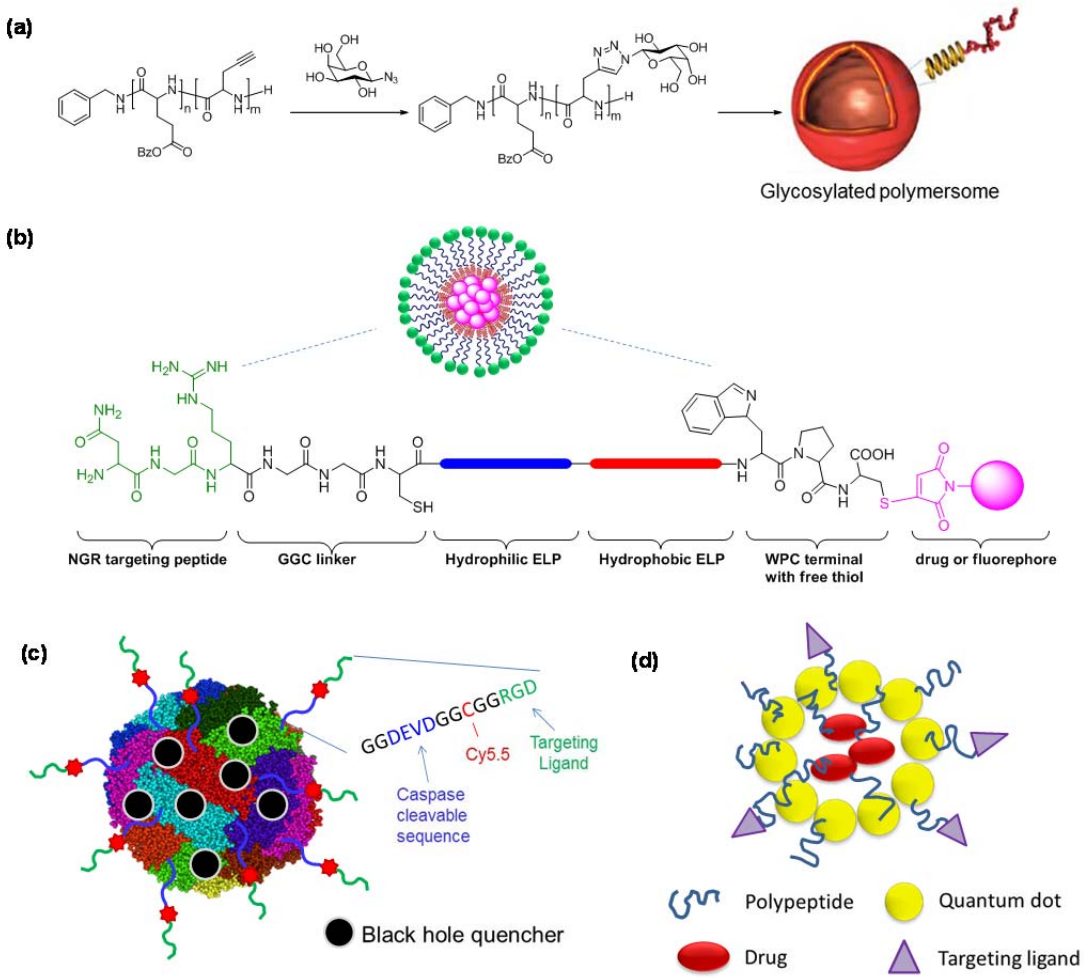

Figure 1-16. Examples of polypeptide/protein based multifunctional carriers. (a). Polypeptide based polymersomes functionalized with glycans for specific interactions with cells. (b). Multifucntional ELP micelles. (c). Small heat shock protein cage for tumor-specific drug delivery and caspase activity detection. (d) Polypeptide-QDs hybrids for targeted drug delivery and imaging.

Inorganic nanoparticles could also be integrated with polypeptide based drug carriers. They are preferred for many imaging techniques, such as long term fluorescence imaging using quantum dots (QDs) [172] and high contrast TEM imaging using gold nanoparticles [173]. Incorporation of such nanoparticles into drug delivery systems could enable simultaneous disease

detection and therapy, so call “theranostic”. For instance, a highly tunable QD–polypeptide hybrid assembly system was prepared (**Figure 1-16d**) through the self-assembly of carboxyl-functionalized QDs and poly(diethylene glycol- L-lysine)-poly(L-lysine) (PEGLL-PLL) diblock copolypeptides [174]. The surface of the assemblies is modified with a cyclic arginine-glycine-aspartate [c(RGD)] motif to target the integrins overexpressed on the tumor vasculature. Cargo molecules can be absorbed or encapsulated into these complexes, thus allowing cancer imaging and drug treatment in parallel (theranostics).

1.6 Scope of the dissertation

1.6.1 Motivation and objective

Polypeptide based materials are of emerging interest for biomedical applications due to their biocompatibility, biodegradability and their potential to achieve unique macromolecular architectures with tailored properties [175, 176, 177]. Biomedical applications require tailor-made polypeptide scaffolds of high structural definition as well as multiple functionalities that allow the attachment of drug molecules or imaging groups [178]. However, using currently available methods, the preparation of polypeptides with controlled molecular weight distributions, ordered polymer architectures and large variety of functional groups at defined locations still remain a major challenge. Therefore, it is highly desirable to develop alternative efficient approaches for the synthesis of defined polypeptides with tunable properties.

Natural proteins are produced in biological systems by a stepwise and complete controlled synthesis from amino acids, according to a predetermined sequence encoded in DNA. The information stored in the primary sequence of proteins results in a three-dimensional folded structure, which further determines the physical properties and biological function of proteins. It is conspicuous that, depending on generally only 20 amino acid building blocks, such diverse products can be constructed, including functional proteins such as enzymes as well as structural proteins such as collagen. Inspiring from the extraordinarily defined molecules and materials in nature, using of natural proteins as resources of polypeptide based materials might pave the way to next generation of biopolymers with a higher level of structural precision. Thus, the potential of preparing functional polymer materials from natural protein precursors has been a major goal.

Using proteins as polymer materials is not a flight of fancy since natural protein based materials, such as silk and leather, have been intensively used since ancient. However, only recently there has been research centered on proteins from a materials science perspective. The developing of this multidisciplinary area is boosted by the protein engineering technologies and the emerging of chemistry method for protein modification. Based on these technical advances, a large variation of engineered proteins have been produced and harnessed as a new class of versatile macromolecular building blocks for functional materials in various applications ranging from medicine, nanotechnology and catalysis to bioengineering.

However, unlike the synthetic polypeptide materials with their linear structure and exposed functionalities, proteins often have globular

architectures with most functional groups and structural elements buried at the interior. Thus the direct application of protein materials is not as flexible as polymers and mainly limited on their natural properties and activities. Whitesides and coworkers have discussed earlier a novel approach for the preparation of polymers from proteins by denaturation [179]. Functional groups hidden inside the tightly folded polypeptide backbone of proteins may become accessible upon prefunctionalization thus opening up the opportunity to achieve a new class of precision biopolymers, i.e., monodisperse polypeptides, from proteins. However, in most cases, denaturing the 3D structure of proteins usually causes precipitation and destabilization of the polypeptide backbone [180, 181], thus preventing the use of proteins as polypeptide resources.

In this thesis, a comprehensive and highly versatile approach has been developed to prepare protein based polypeptide copolymers (PbPs) from natural proteins with distinct molecular weights, chain lengths, ordered secondary structural elements and high numbers of functional groups. To achieve such copolymers, a novel method has been established to unfold the globular structure of native proteins under controlled condition and *in situ* stabilize the polypeptide backbone by grafting polyethylene(oxide) (PEO) chains to avoid precipitation. Such PbPs possess the benefits of protein based materials, such as monodisperse chain length, ordered secondary structures, biocompatibility and biodegradability. In addition, their unfolded backbone enables more flexible modifications and opens up further possibilities to re-assemble the backbone under desired conditions. Therefore,

these copolymers represent a highly versatile platform to build up unique hybrid materials for a broad range of applications, such as nano-patterning, drug delivery, gene delivery as well as bioimaging. This “semi-synthetic” chemistry approach to prepare polypeptide materials could be considered a valuable alternative to conventional polypeptide synthesis and expression providing fast and efficient access to numerous polypeptides of natural diversity.

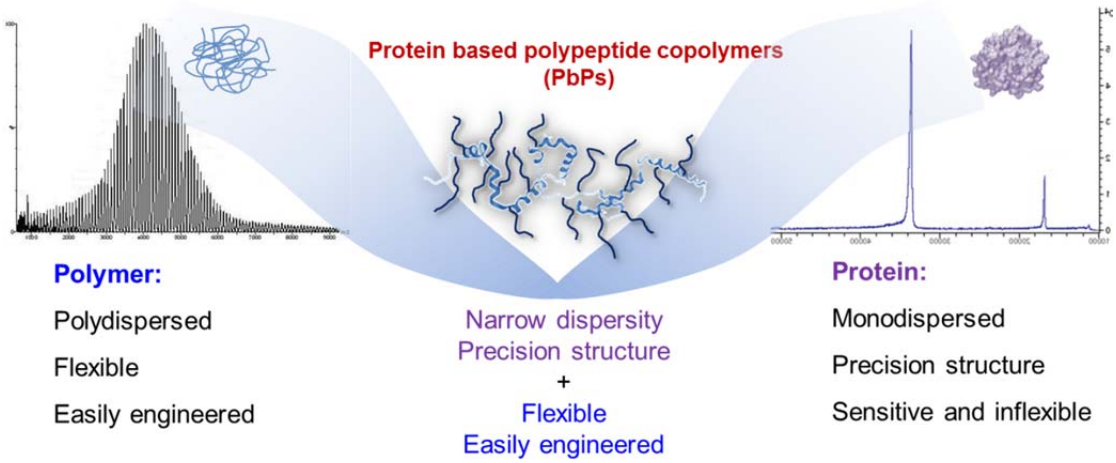

Figure 1-17. Illustration of the motivations for preparing PbPs.

1.6.2 Overview of the dissertation

This dissertation demonstrates a novel method to prepare PbPs from different proteins, the modification strategies to achieve versatile materials as well as the application of these copolymers for bioimaging and drug delivery. The discussion is divided into four chapters.

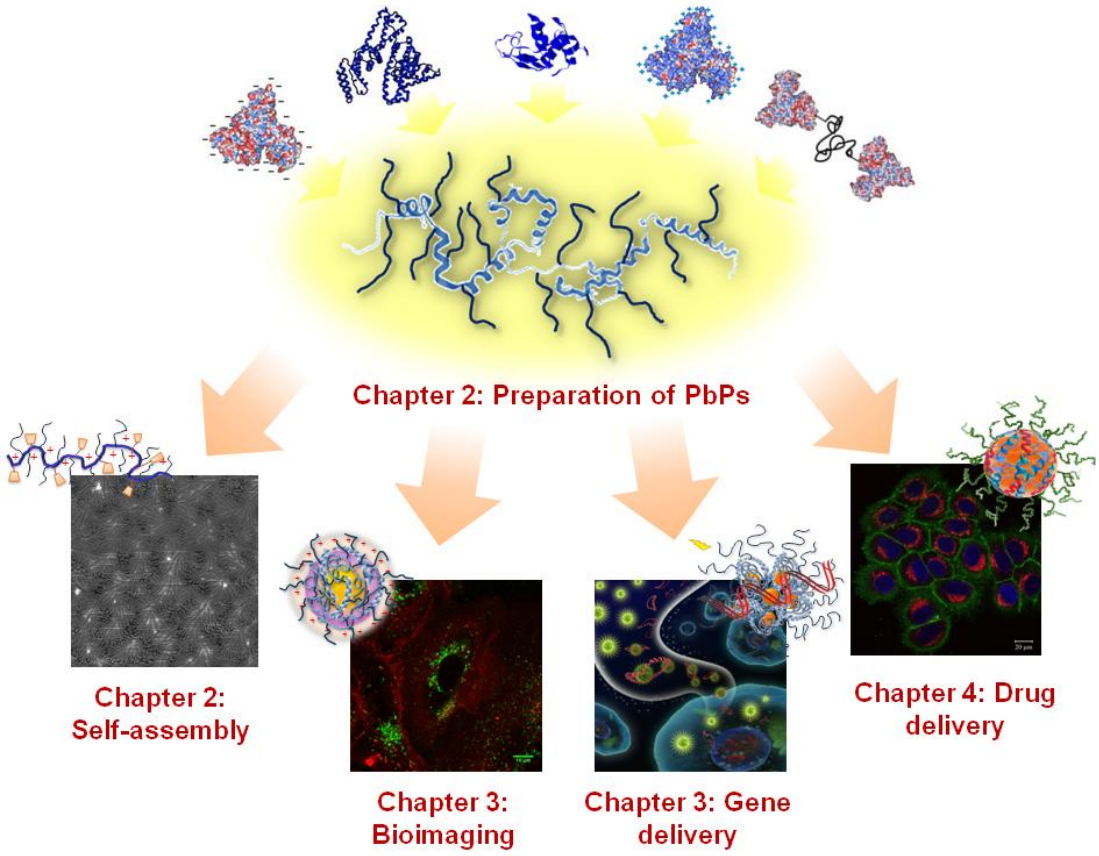

Figure 1-18. Summary of the structure of the dissertation. Partially adapted with permission[‡]. Copyright 2012, American Chemical Society and Copyright 2012, Wiley-VCH.

Chapter 1: the introduction of the background information for the dissertation, including conventional polypeptide preparation methods, protein based hybrid materials and the biomedical application of polypeptide/protein based materials.

Chapter 2: the general scheme to access PbPs with different properties. This chapter firstly discusses the preparation of PbPs from different proteins with different chain lengths, different charge properties and varying

[‡] The picture is partially adapted from (1). Wu, Y.; Pramanik, G.; Eisele, K.; Weil, T Biomacromolecules 2012, 13 (6), 1890-1898; (2). Wu, Y.; Eisele, K.; Doroshenko, M.; Algara-Siller, G.; Kaiser, U.; Koynov, K.; Weil, T., Small 2012, 8 (22), 3465-3475. The dissertation author is the first author of these papers.

hydrophobicities. In addition, further functionalities are also able to be introduced into PbPs by both *a priori* and *a posteriori* modification strategies, which are also discussed in detail.

Chapter 3: the application of PbPs as smart materials for bioimaging. This chapter demonstrates a method to functionalize inorganic fluorescent nanoparticles, quantum dots (QDs), with PbPs. The QDs coated with PbPs are highly water soluble, non-cytotoxic and notably stable in live cells. In addition, their optical properties are significantly responsive to environmental pH changes. Furthermore, the surface charges of these QDs can be tuned to facilitate efficient cell uptake as well as gene delivery. The cationic QDs exhibit significant photo-responsiveness to DNA loading and have great potential for investigating gene delivery processes in live-cells.

Chapter 4: the application of PbPs as versatile carriers for drug delivery. This chapter discusses several methods to achieve controlled anti-cancer drug delivery using PbPs. Drug molecules could be loaded into PbPs micelles *via* hydrophobic interaction or covalently conjugated onto PbPs backbone. The hydrophobic loading strategy provides high loading capacity and flexibility, whereas the covalent loading approach could minimize non-specific leakage. A highly defined multi-stimuli responsive core-shell system is also demonstrated by conjugate doxorubicin with PbP backbone *via* hydrazone linker. *In vitro* and preliminary *in vivo* studies demonstrated the efficient drug delivery, controlled drug release, potent toxicity as well as beneficial passive targeting effect.

1.7 References

[1]. Berg, J. M.; Tymoczko, J. L.; Stryer, L., *Section 3.2, Primary structure: amino acids are linked by peptide bonds to form polypeptide chains.* 5th ed.; W H Freeman: New York, 2002.

[2]. Wagner, I.; Musso, H., New naturally occurring amino acids. *Angew. Chem. Int. Ed.* **1983,** *22* (11), 816-828.

[3]. Hirano, Y.; Mooney, D. J., Peptide and protein presenting materials for tissue engineering. *Adv. Mater.* **2004,** *16* (1), 17-25.

[4]. MaHam, A.; Tang, Z.; Wu, H.; Wang, J.; Lin, Y., Protein-based nanomedicine platforms for drug delivery. *Small* **2009,** *5* (15), 1706-1721.

[5]. Giuliano, K. A.; Taylor, D. L., Fluorescent-protein biosensors: New tools for drug discovery. *Trends Biotechnol.* **1998,** *16* (3), 135-140.

[6]. Kratz, F., Albumin as a drug carrier: design of prodrugs, drug conjugates and nanoparticles. *J. Control. Release* **2008,** *132* (3), 171-183.

[7]. Latha, M. S.; Lal, A. V.; Kumary, T. V.; Sreekumar, R.; Jayakrishnan, A., Progesterone release from glutaraldehyde cross-linked casein microspheres: *in vitro* studies and *in vivo* response in rabbits. *Contraception* **2000,** *61* (5), 329-334.

[8]. Kuijpers, A. J.; van Wachem, P. B.; van Luyn, M. J.; Brouwer, L. A.; Engbers, G. H.; Krijgsveld, J.; Zaat, S. A.; Dankert, J.; Feijen, J., *In vitro* and *in vivo* evaluation of gelatin-chondroitin sulphate hydrogels for controlled release of antibacterial proteins. *Biomaterials* **2000,** *21* (17), 1763-1772.

[9]. Metzmacher, I.; Radu, F.; Bause, M.; Knabner, P.; Friess, W., A model describing the effect of enzymatic degradation on drug release from collagen minirods. *Eur. J. Pharm. Biopharm.* **2007,** *67* (2), 349-360.

[10]. Montana, M.; Ducros, C.; Verhaeghe, P.; Terme, T.; Vanelle, P.; Rathelot, P., Albumin-bound paclitaxel: the benefit of this new formulation in the treatment of various cancers. *J. Chemother.* **2011,** *23* (2), 59-66.

[11]. Chow, D.; Nunalee, M. L.; Lim, D. W.; Simnick, A. J.; Chilkoti, A., Peptide-based biopolymers in biomedicine and biotechnology. *Mater. Sci. Eng. R Rep.* **2008,** *62* (4), 125-155.

[12]. Gabrielson, N. P.; Lu, H.; Yin, L.; Li, D.; Wang, F.; Cheng, J., Reactive and bioactive cationic α-Helical polypeptide template for nonviral gene delivery. *Angew. Chem. Int. Ed.* **2012,** *51* (5), 1143-1147.

[13]. Li, H.; Cao, Y., Protein mechanics: from single molecules to functional biomaterials. *Acc. Chem. Res.* **2010,** *43* (10), 1331-1341.

[14]. Cheng, J.; Deming, T. J., Synthesis of polypeptides by ring-opening polymerization of alpha-amino acid N-carboxyanhydrides. *Top Curr Chem* **2012,** *310*, 1-26.

[15]. Deming, T. J., Facile synthesis of block copolypeptides of defined architecture. *Nature* **1997,** *390* (6658), 386-389.

[16]. Kricheldorf, H. R., *Amino acid-N-carboxyanhydrides and related materials*. Springer: New York, 1987.

[17]. Woodward, R. B.; Schramm, C. H., Synthesis of protein analogs. *J. Am. Chem. Soc.* **1947,** *69* (6), 1551-1552.

[18]. Penczek, S. S.; Kricheldorf, H. R., *Models of biopolymers by ring-opening polymerization*. CRC Press: Boca Raton, 1990.

[19]. Lu, H.; Wang, J.; Lin, Y.; Cheng, J., One-pot synthesis of brush-like polymers *via* integrated ring-opening metathesis polymerization and polymerization of amino acid N-carboxyanhydrides. *J. Am. Chem. Soc.* **2009,** *131* (38), 13582-13583.

[20]. Dimitrov, I.; Schlaad, H., Synthesis of nearly monodisperse polystyrene-polypeptide block copolymers *via* polymerisation of N-carboxyanhydrides. *Chem. Commun.* **2003,** (23), 2944-5.

[21]. Deming, T. J., Cobalt and iron initiators for the controlled polymerization of alpha-amino acid-*N*-carboxyanhydrides. *Macromolecules* **1999,** *32*, 4500-4502.

[22]. Deming, T. J.; Curtin, S. A., Chain initiation efficiency in cobalt- and nickel-mediated polypeptide synthesis. *J. Am. Chem. Soc.* **2000,** *122* (24), 5710-5717.

[23]. Merrifield, R. B., *Solid-phase peptide synthesis (methods in enzymology)*. Elsevier: Amsterdam, 1997; Vol. 289.

[24]. Atherton, E.; Clive, D. L. J.; Sheppard, R. C., Polyamide supports for polypeptide synthesis. *J. Am. Chem. Soc.* **1975,** *97* (22), 6584-6585.

[25]. Atherton, E.; Woolley, V.; Sheppard, R. C., Internal association in solid phase peptide synthesis. Synthesis of cytochrome C residues 66-104 on polyamide supports. *Chem. comm.* **1980,** (20), 970-971.

[26]. Bayer, E., Towards the chemical synthesis of proteins. *Angew. Chem. Int. Ed.* **1991,** *30* (2), 113-129.

[27]. Carpino, L. A.; Han, G. Y., 9-Fluorenylmethoxycarbonyl function, a new base-sensitive amino-protecting group. *J. Am. Chem. Soc.* **1970,** *92* (19), 5748-5749.

[28]. Sheehan, J. C.; Hess, G. P., A new method of forming peptide bonds. *J. Am. Chem. Soc.* **1955,** *77* (4), 1067-1068.

[29]. Wieland, T.; Kern, W.; Sehring, R., Über Anhydride von acylierten Aminosäuren. *Justus Liebigs Annalen der Chemie* **1950,** *569* (2), 117-121.

[30]. Schwyzer, R.; Iselin, B.; Feurer, M., Über aktivierte ester. I. aktivierte ester der hippursäure und ihre umsetzungen mit benzylamin. *HeIv. Chim. Acta* **1955,** *38* (1), 69-79.

[31]. Han, S.-Y.; Kim, Y.-A., Recent development of peptide coupling reagents in organic synthesis. *Tetrahedron* **2004,** *60* (11), 2447-2467.

[32]. Bray, B. L., Large-scale manufacture of peptide therapeutics by chemical synthesis. *Nat. Rev. Drug Discov.* **2003,** *2* (7), 587-593.

[33]. Amblard, M.; Fehrentz, J. A.; Martinez, J.; Subra, G., Methods and protocols of modern solid phase Peptide synthesis. *Mol. Biotechnol.* **2006,** *33* (3), 239-54.

[34]. Dawson, P. E.; Kent, S. B., Synthesis of native proteins by chemical ligation. *Annu. Rev. Biochem.* **2000,** *69*, 923-960.

[35]. Plaue, S.; Muller, S.; Briand, J. P.; Van Regenmortel, M. H. V., Recent advances in solid-phase peptide synthesis and preparation of antibodies to synthetic peptides. *Biologicals* **1990,** *18* (3), 147-157.

[36]. Kochendoerfer, G. G.; Chen, S.-Y.; Mao, F.; Cressman, S.; Traviglia, S.; Shao, H.; Hunter, C. L.; Low, D. W.; Cagle, E. N.; Carnevali, M.; Gueriguian, V.; Keogh, P. J.; Porter, H.; Stratton, S. M.; Wiedeke, M. C.; Wilken, J.; Tang, J.; Levy, J. J.; Miranda, L. P.; Crnogorac, M. M.; Kalbag, S.; Botti, P.; Schindler-Horvat, J.; Savatski, L.; Adamson, J. W.; Kung, A.; Kent, S. B. H.; Bradburne, J. A., Design and Chemical Synthesis of a

Homogeneous Polymer-Modified Erythropoiesis Protein. *Science* **2003,** *299* (5608), 884-887.

[37]. Kent, S. B. H., Total chemical synthesis of proteins. *Chem. Soc. Rev.* **2009,** *38* (2), 338-351.

[38]. Kohn, M.; Breinbauer, R., The Staudinger ligation-a gift to chemical biology. *Angew. Chem. Int. Ed.* **2004,** *43* (24), 3106-3116.

[39]. Nilsson, B. L.; Hondal, R. J.; Soellner, M. B.; Raines, R. T., Protein assembly by orthogonal chemical ligation methods. *J. Am. Chem. Soc.* **2003,** *125* (18), 5268-5269.

[40]. Nilsson, B. L.; Kiessling, L. L.; Raines, R. T., High-yielding staudinger Ligation of a phosphinothioester and azide to form a peptide. *Org. Lett.* **2001,** *3* (1), 9-12.

[41]. Scriven, E. F. V.; Turnbull, K., Azides: their preparation and synthetic uses. *Chem. Rev.* **1988,** *88* (2), 297-368.

[42]. Zaloom, J.; Roberts, D. C., Preparation of azido derivatives from amino acids and peptides by diazo transfer. *J. Org. Chem.* **1981,** *46* (25), 5173-5176.

[43]. Goddard-Borger, E. D.; Stick, R. V., An efficient, inexpensive, and shelf-stable diazotransfer reagent: imidazole-1-sulfonyl azide hydrochloride. *Org. Lett.* **2007,** *9* (19), 3797-3800.

[44]. Sambrook, J.; Fritsch, E. F.; Maniatis, T., *Molecular cloning: a laboratory manual.* Cold Spring Laboratory Press: Cold Spring, 1989.

[45]. van Hest, J. C. M.; Tirrell, D. A., Protein-based materials, toward a new level of structural control. *Chem. Commun.* **2001,** (19), 1897-1904.

[46]. Sengupta, D.; Heilshorn, S. C., Protein-engineered biomaterials: highly tunable tissue engineering scaffolds. *Tissue Eng. Part B Rev.* **2010,** *16* (3), 285-93.

[47]. Bzymek, M.; Lovett, S. T., Instability of repetitive DNA sequences: The role of replication in multiple mechanisms. *Proc. Natl. Acad. Sci. U.S.A.* **2001,** *98* (15), 8319-8325.

[48]. Eyre-Walker, A., The close proximity of Escherichia coli genes: consequences for stop codon and synonymous codon use. *J. Mol. Evol.* **1996,** *42* (2), 73-78.

[49]. Kudla, G.; Murray, A. W.; Tollervey, D.; Plotkin, J. B., Coding-sequence determinants of gene expression in Escherichia coli. *Science* **2009,** *324* (5924), 255-258.

[50]. Kim, C. H.; Oh, Y.; Lee, T. H., Codon optimization for high-level expression of human erythropoietin (EPO) in mammalian cells. *Gene* **1997,** *199* (1-2), 293-301.

[51]. Landrain, T. E.; Carrera, J.; Kirov, B.; Rodrigo, G.; Jaramillo, A., Modular model-based design for heterologous bioproduction in bacteria. *Curr. Opin. Biotechnol.* **2009,** *20* (3), 272-9.

[52]. Welch, M.; Govindarajan, S.; Ness, J. E.; Villalobos, A.; Gurney, A.; Minshull, J.; Gustafsson, C., Design Parameters to Control Synthetic Gene Expression in Escherichia coli. *PLoS ONE* **2009,** *4* (9), e7002.

[53]. Caruthers, M., Gene synthesis machines: DNA chemistry and its uses. *Science* **1985,** *230* (4723), 281-285.

[54]. Verma, S.; Eckstein, F., Modified oligonucleotides: synthesis and strategy for users. *Annu. Rev. Biochem.* **1998,** *67* (1), 99-134.

[55]. Chow, D.; Nunalee, M. L.; Lim, D. W.; Simnick, A. J.; Chilkoti, A., Peptide-based biopolymers in biomedicine and biotechnology. *Materials Science and Engineering: R: Reports* **2008,** *62* (4), 125-155.

[56]. Miyake, S.; Makimura, M.; Kanegae, Y.; Harada, S.; Sato, Y.; Takamori, K.; Tokuda, C.; Saito, I., Efficient generation of recombinant adenoviruses using adenovirus DNA-terminal protein complex and a cosmid bearing the full-length virus genome. *Proc. Natl. Acad. Sci. U.S.A.* **1996,** *93* (3), 1320-1324.

[57]. Meagher, R. B.; Tait, R. C.; Betlach, M.; Boyer, H. W., Protein expression in E. coli minicells by recombinant plasmids. *Cell* **1977,** *10* (3), 521-536.

[58]. Sengupta, D.; Heilshorn, S. C., Protein-engineered biomaterials: highly tunable tissue engineering scaffolds. *Tissue Eng. Part B Rev.* **2010,** *16* (3), 285-293.

[59]. Kwon, I.; Kirshenbaum, K.; Tirrell, D. A., Breaking the degeneracy of the genetic code. *J. Am. Chem. Soc.* **2003,** *125* (25), 7512-7513.

[60]. Hitzeman, R. A.; Hagie, F. E.; Levine, H. L.; Goeddel, D. V.; Ammerer, G.; Hall, B. D., Expression of a human gene for interferon in yeast. *Nature* **1981,** *293* (5835), 717-722.

[61]. Chow, D. C.; Dreher, M. R.; Trabbic-Carlson, K.; Chilkoti, A., Ultra-high expression of a thermally responsive recombinant fusion protein in E. coli. *Biotechnol. Prog.* **2006,** *22* (3), 638-646.

[62]. Pierschbacher, M. D.; Ruoslahti, E., Cell attachment activity of fibronectin can be duplicated by small synthetic fragments of the molecule. *Nature* **1984,** *309* (5963), 30-33.

[63]. Nicol, A.; Gowda, D. C.; Urry, D. W., Cell adhesion and growth on synthetic elastomeric matrices containing Arg-Gly-Asp-Ser-3. *J. Biomed. Mater. Res.* **1992,** *26* (3), 393-413.

[64]. Tong, A. H.; Drees, B.; Nardelli, G.; Bader, G. D.; Brannetti, B.; Castagnoli, L.; Evangelista, M.; Ferracuti, S.; Nelson, B.; Paoluzi, S.; Quondam, M.; Zucconi, A.; Hogue, C. W.; Fields, S.; Boone, C.; Cesareni, G., A combined experimental and computational strategy to define protein interaction networks for peptide recognition modules. *Science* **2002,** *295* (5553), 321-324.

[65]. Sidhu, S. S.; Bader, G. D.; Boone, C., Functional genomics of intracellular peptide recognition domains with combinatorial biology methods. *Curr. Opin. Chem. Biol.* **2003,** *7* (1), 97-102.

[66]. Vepari, C.; Kaplan, D. L., Silk as a biomaterial. *Prog. Polym. Sci.* **2007,** *32* (8-9), 991-1007.

[67]. MacEwan, S. R.; Chilkoti, A., Elastin-like polypeptides: Biomedical applications of tunable biopolymers. *Pept. Sci.* **2010,** *94* (1), 60-77.

[68]. Landschulz, W. H.; Johnson, P. F.; McKnight, S. L., The leucine zipper: a hypothetical structure common to a new class of DNA binding proteins. *Science* **1988,** *240* (4860), 1759-1764.

[69]. Mason, J. M.; Arndt, K. M., Coiled coil somains: stability, specificity, and biological implications. *ChemBioChem* **2004,** *5* (2), 170-176.

[70]. Pierschbacher, M.; Hayman, E. G.; Ruoslahti, E., Synthetic peptide with cell attachment activity of fibronectin. *Proc. Natl. Acad. Sci. U.S.A.* **1983,** *80* (5), 1224-1227.

[71]. Vepari, C.; Kaplan, D. L., Silk as a biomaterial. *Prog. Polym. Sci.* **2007,** *32* (8 鈥?), 991-1007.

[72]. Urry, D. W., Physical chemistry of biological free energy transduction as demonstrated by elastic protein-based polymers. *J. Phys. Chem. B* **1997,** *101* (51), 11007-11028.

[73]. Apostolovic, B.; Deacon, S. P. E.; Duncan, R.; Klok, H.-A., Hybrid polymer therapeutics incorporating bioresponsive, coiled coil peptide linkers. *Biomacromolecules* **2010,** *11* (5), 1187-1195.

[74]. Wang, C.; Stewart, R. J.; KopeCek, J., Hybrid hydrogels assembled from synthetic polymers and coiled-coil protein domains. *Nature* **1999,** *397* (6718), 417-420.

[75]. van Hest, J. C. M.; Tirrell, D. A., Protein-based materials, toward a new level of structural control. *Chemical Communications* **2001,** (19), 1897-1904.

[76]. Becker, N.; Oroudjev, E.; Mutz, S.; Cleveland, J. P.; Hansma, P. K.; Hayashi, C. Y.; Makarov, D. E.; Hansma, H. G., Molecular nanosprings in spider capture-silk threads. *Nat. Mater.* **2003,** *2* (4), 278-283.

[77]. Splettstoesser, T. http://en.wikipedia.org/wiki/File:Leucine_zipper.png. (accessed 2013. Feb. 12).

[78]. Xia, X.-X.; Xu, Q.; Hu, X.; Qin, G.; Kaplan, D. L., Tunable self-assembly of genetically engineered silk-elastin-like protein polymers. *Biomacromolecules* **2011,** *12* (11), 3844-3850.

[79]. Haider, M.; Cappello, J.; Ghandehari, H.; Leong, K., *In vitro* chondrogenesis of mesenchymal stem cells in recombinant silk-elastinlike hydrogels. *Pharmaceut. Res.* **2008,** *25* (3), 692-699.

[80]. Matyjaszewski, K.; Xia, J., Atom transfer radical polymerization. *Chem. Rev.* **2001,** *101* (9), 2921-2990.

[81]. Hawker, C. J.; Bosman, A. W.; Harth, E., New polymer synthesis by nitroxide mediated living radical polymerizations. *Chem. Rev.* **2001,** *101* (12), 3661-3688.

[82]. Moad, G.; Rizzardo, E.; Thang, S. H., Living radical polymerization by the RAFT process. *Aust. J. Chem.* **2005,** *58* (6), 379-410.

[83]. Cunliffe, D.; Pennadam, S.; Alexander, C., Synthetic and biological polymers-merging the interface. *Eur. Polym. J.* **2004,** *40* (1), 5-25.

[84]. Vandermeulen, G. W. M.; Klok, H.-A., Peptide/protein hybrid materials: enhanced control of structure and improved performance through conjugation of biological and synthetic polymers. *Macromol. Biosci.* **2004,** *4* (4), 383-398.

[85]. de Las Heras Alarcon, C.; Pennadam, S.; Alexander, C., Stimuli responsive polymers for biomedical applications. *Chem. Soc. Rev.* **2005,** *34* (3), 276-85.

[86]. Klok, H.-A.; Schlaad, H.; Löwik, D. P. M.; Ayres, L.; Smeenk, J.; Hest, J. M., Synthesis of bio-inspired hybrid polymers using peptide synthesis and protein engineering. In *Peptide Hybrid Polymers*, Springer Berlin Heidelberg: 2006; Vol. 202, pp 19-52.

[87]. van Hest, J. C. M.; Tirrell, D. A., Protein-based materials, toward a new level of structural control. *Chemical Communications* **2001,** (19), 1897-1904.

[88]. Jevsevar, S.; Kunstelj, M.; Porekar, V. G., PEGylation of therapeutic proteins. *Biotechnol. J.* **2010,** *5* (1), 113-128.

[89]. Abuchowski, A.; Kazo, G. M.; Verhoest, C. R., Jr.; Van Es, T.; Kafkewitz, D.; Nucci, M. L.; Viau, A. T.; Davis, F. F., Cancer therapy with chemically modified enzymes. I. Antitumor properties of polyethylene glycol-asparaginase conjugates. *Cancer Biochem. Biophys.* **1984,** *7* (2), 175-186.

[90]. Jevsevar, S.; Kunstelj, M.; Porekar, V. G., PEGylation of therapeutic proteins. *Biotechnol. J.* **2010,** *5* (1), 113-28.

[91]. Yamada, H.; Imoto, T.; Fujita, K.; Okazaki, K.; Motomura, M., Selective modification of aspartic acid-101 in lysozyme by carbodiimide reaction. *Biochemistry* **1981,** *20* (17), 4836-4842.

[92]. Hoare, D. G.; Koshland, D. E., A procedure for the selective modification of carboxyl groups in proteins. *J. Am. Chem. Soc.* **1966,** *88* (9), 2057-2058.

[93]. Ban, H.; Gavrilyuk, J.; Barbas, C. F., Tyrosine bioconjugation through aqueous ene-type reactions: a click-like reaction for tyrosine. *J. Am. Chem. Soc.* **2010,** *132* (5), 1523-1525.

[94]. Jones, M. W.; Mantovani, G.; Blindauer, C. A.; Ryan, S. M.; Wang, X.; Brayden, D. J.; Haddleton, D. M., Direct peptide bioconjugation/PEGylation at tyrosine with linear and branched polymeric diazonium salts. *J. Am. Chem. Soc.* **2012,** *134* (17), 7406-7413.

[95]. Iwai, K.; Maeda, H.; Konno, T., Use of oily contrast medium for selective drug targeting to tumor: enhanced therapeutic effect and X-ray image. *Cancer Res.* **1984,** *44* (5), 2115-2121.

[96]. Maeda, H.; Ueda, M.; Morinaga, T.; Matsumoto, T., Conjugation of poly(styrene-co-maleic acid) derivatives to the antitumor protein neocarzinostatin: pronounced improvements in pharmacological properties. *J. Med. Chem.* **1985,** *28* (4), 455-461.

[97]. Caliceti, P.; Veronese, F. M., Pharmacokinetic and biodistribution properties of poly(ethylene glycol)-protein conjugates. *Adv. Drug Deliv. Rev.* **2003,** *55* (10), 1261-1277.

[98]. Veronese, F. M.; Pasut, G., PEGylation, successful approach to drug delivery. *Drug Discov. Today* **2005,** *10* (21), 1451-1458.

[99]. Hoffman, A. S.; Stayton, P. S., Conjugates of stimuli-responsive polymers and proteins. *Prog. Polym. Sci.* **2007,** *32* (8-9), 922-932.

[100]. Chen, J. P.; Hoffman, A. S., Polymer-protein conjugates. II. Affinity precipitation separation of human immunogammaglobulin by a poly(N-isopropylacrylamide)-protein A conjugate. *Biomaterials* **1990,** *11* (9), 631-634.

[101]. Chilkoti, A.; Chen, G.; Stayton, P. S.; Hoffman, A. S., Site-specific conjugation of a temperature-sensitive polymer to a genetically engineered protein. *Bioconjugate Chem.* **1994,** *5* (6), 504-507.

[102]. Ding, Z.; Chen, G.; Hoffman, A. S., Unusual properties of thermally sensitive oligomer–enzyme conjugates of poly(N-isopropylacrylamide)–trypsin. *J. Biomed. Mater. Res.* **1998,** *39* (3), 498-505.

[103]. Salmaso, S.; Semenzato, A.; Bersani, S.; Mastrotto, F.; Scomparin, A.; Caliceti, P., Site-selective protein glycation and PEGylation. *Eur. Polym. J.* **2008,** *44* (5), 1378-1389.

[104]. Roberts, M. J.; Bentley, M. D.; Harris, J. M., Chemistry for peptide and protein PEGylation. *Adv. Drug Deliv. Rev.* **2002,** *54* (4), 459-476.

[105]. Shimoboji, T.; Larenas, E.; Fowler, T.; Kulkarni, S.; Hoffman, A. S.; Stayton, P. S., Photoresponsive polymer-enzyme switches. *Proc. Natl. Acad. Sci. U.S.A.* **2002,** *99* (26), 16592-16596.

[106]. Stayton, P. S.; Shimoboji, T.; Long, C.; Chilkoti, A.; Ghen, G.; Harris, J. M.; Hoffman, A. S., Control of protein-ligand recognition using a stimuli-responsive polymer. *Nature* **1995,** *378* (6556), 472-474.

[107]. Chin, J. W.; Cropp, T. A.; Anderson, J. C.; Mukherji, M.; Zhang, Z.; Schultz, P. G., An expanded eukaryotic genetic code. *Science* **2003,** *301* (5635), 964-967.

[108]. Wang, L.; Brock, A.; Herberich, B.; Schultz, P. G., Expanding the genetic code of Escherichia coli. *Science* **2001,** *292* (5516), 498-500.

[109]. Chin, J. W.; Santoro, S. W.; Martin, A. B.; King, D. S.; Wang, L.; Schultz, P. G., Addition of p-azido-l-phenylalanine to the genetic code of Escherichia coli. *J. Am. Chem. Soc.* **2002,** *124* (31), 9026-9027.

[110]. Liu, H.; Wang, L.; Brock, A.; Wong, C.-H.; Schultz, P. G., A method for the generation of glycoprotein mimetics. *J. Am. Chem. Soc.* **2003,** *125* (7), 1702-1703.

[111]. Liu, C. C.; Schultz, P. G., Adding new chemistries to the genetic code. *Annu. Rev. Biochem.* **2010,** *79* (1), 413-444.

[112]. Link, A. J.; Mock, M. L.; Tirrell, D. A., Non-canonical amino acids in protein engineering. *Curr. Opin. Biotechnol.* **2003,** *14* (6), 603-609.

[113]. de Graaf, A. J.; Kooijman, M.; Hennink, W. E.; Mastrobattista, E., Nonnatural amino acids for site-specific protein conjugation. *Bioconjugate Chem.* **2009,** *20* (7), 1281-1295.

[114]. Green, N. M., Avidin. *Adv Protein Chem* **1975,** *29*, 85-133.

[115]. Hannink, J. M.; Cornelissen, J. J. L. M.; Farrera, J. A.; Foubert, P.; De Schryver, F. C.; Sommerdijk, N. A. J. M.; Nolte, R. J. M., Protein-polymer hybrid amphiphiles. *Angew. Chem. Int. Ed.* **2001,** *40* (24), 4732-4734.

[116]. Bontempo, D.; Maynard, H. D., Streptavidin as a macroinitiator for polymerization: *in situ* protein-polymer conjugate formation. *J. Am. Chem. Soc.* **2005,** *127* (18), 6508-6509.

[117]. Boerakker, M. J.; Hannink, J. M.; Bomans, P. H. H.; Frederik, P. M.; Nolte, R. J. M.; Meijer, E. M.; Sommerdijk, N. A. J. M., Giant amphiphiles by cofactor reconstitution. *Angew. Chem. Int. Ed.* **2002,** *41* (22), 4239-4241.

[118]. Reynhout, I. C.; Cornelissen, J. J. L. M.; Nolte, R. J. M., Self-assembled architectures from biohybrid triblock copolymers. *J. Am. Chem. Soc.* **2007,** *129* (8), 2327-2332.

[119]. Lee, W.-R.; Shen, S.-C.; Lai, H.-H.; Hu, C.-H.; Fang, J.-Y., Transdermal drug delivery enhanced and controlled by erbium:YAG laser: a comparative study of lipophilic and hydrophilic drugs. *J. Control. Release* **2001,** *75* (1-2), 155-166.

[120]. Medina, C.; Santos-Martinez, M. J.; Radomski, A.; Corrigan, O. I.; Radomski, M. W., Nanoparticles: pharmacological and toxicological significance. *Br. J. Pharmacol.* **2007,** *150* (5), 552-558.

[121]. Frokjaer, S.; Otzen, D. E., Protein drug stability: a formulation challenge. *Nat. Rev. Drug Discov.* **2005,** *4* (4), 298-306.

[122]. Dong, H.; Dong, C.; Feng, Y.; Ren, T.; Zhang, Z.; Li, L.; Li, Y., Engineering of peglayted camptothecin into core-shell nanomicelles for improving solubility, stability and combination delivery. *MedChemComm* **2012**, 1555-1561.

[123]. Sun, Q.; Radosz, M.; Shen, Y., Challenges in design of translational nanocarriers. *J. Control. Release* **2012,** *164* (2), 156-169.

[124]. Matsumura, Y.; Maeda, H., A new concept for macromolecular therapeutics in cancer chemotherapy: mechanism of tumoritropic accumulation of proteins and the antitumor agent smancs. *Cancer Res.* **1986,** *46* (12 Part 1), 6387-6392.

[125]. Lu, Y.; Low, P. S., Folate-mediated delivery of macromolecular anticancer therapeutic agents. *Adv. Drug Deliv. Rev.* **2002,** *54* (5), 675-693.

[126]. Danhier, F.; Breton, A. L.; Preat, V., RGD-based strategies to target alpha(v) beta(3) integrin in cancer therapy and diagnosis. *Mol. Pharm.* **2012,** *9* (11), 2961-2973.

[127]. Kimura, R. H.; Cheng, Z.; Gambhir, S. S.; Cochran, J. R., Engineered knottin peptides: a new class of agents for imaging integrin expression in living subjects. *Cancer Res.* **2009,** *69* (6), 2435-2442.

[128]. Gan, H. K.; Burgess, A. W.; Clayton, A. H. A.; Scott, A. M., Targeting of a conformationally exposed, tumor-specific epitope of EGFR as a strategy for cancer therapy. *Cancer Res.* **2012,** *72* (12), 2924-2930.

[129]. Hong, C. W.; Zeng, Q., Awaiting a new era of cancer immunotherapy. *Cancer Res.* **2012,** *72* (15), 3715-3719.

[130]. Tolcher, A. W.; Sugarman, S.; Gelmon, K. A.; Cohen, R.; Saleh, M.; Isaacs, C.; Young, L.; Healey, D.; Onetto, N.; Slichenmyer, W., Randomized phase II study of BR96-doxorubicin conjugate in patients with metastatic breast cancer. *J. Clin. Oncol.* **1999,** *17* (2), 478-484.

[131]. Trail, P.; Willner, D.; Lasch, S.; Henderson, A.; Hofstead, S.; Casazza, A.; Firestone, R.; Hellstrom, I.; Hellstrom, K., Cure of xenografted human carcinomas by BR96-doxorubicin immunoconjugates. *Science* **1993,** *261* (5118), 212-215.

[132]. Uadia, P.; Blair, A. H.; Ghose, T., Tumor and tissue distribution of a methotrexate-anti-EL4 immunoglobulin conjugate in EL4 lymphoma-bearing mice. *Cancer Res.* **1984,** *44* (10), 4263-4266.

[133]. Yang, L.; Zhang, X.; Ye, M.; Jiang, J.; Yang, R.; Fu, T.; Chen, Y.; Wang, K.; Liu, C.; Tan, W., Aptamer-conjugated nanomaterials and their applications. *Adv. Drug Deliv. Rev.* **2011,** *63* (14-15), 1361-1370.

[134]. Brown, K. C., Hitting the target with bifunctional phage. *Chem. Biol.* **2004,** *11* (8), 1033-1035.

[135]. Rialon, K. L.; White, R. R., Aptamers: potential applications to pancreatic cancer therapy. *Anticancer Agents Med. Chem.* **2011,** *11* (5), 434-441.

[136]. Bae, Y.; Fukushima, S.; Harada, A.; Kataoka, K., Design of environment-sensitive supramolecular assemblies for intracellular drug delivery: polymeric micelles that are responsive to intracellular pH change. *Angew. Chem. Int. Ed.* **2003,** *42* (38), 4640-4643.

[137]. Yoo, H. S.; Lee, E. A.; Park, T. G., Doxorubicin-conjugated biodegradable polymeric micelles having acid-cleavable linkages. *J. Control. Release* **2002,** *82* (1), 17-27.

[138]. Choi, S.-H.; Kwon, I. C.; Hwang, K. Y.; Kim, I.-S.; Ahn, H. J., Small heat shock protein as a multifunctional scaffold: integrated tumor targeting and caspase imaging within a single cage. *Biomacromolecules* **2011,** *12* (8), 3099-3106.

[139]. Lin, J.; Zhu, J.; Chen, T.; Lin, S.; Cai, C.; Zhang, L.; Zhuang, Y.; Wang, X.-S., Drug releasing behavior of hybrid micelles containing polypeptide triblock copolymer. *Biomaterials* **2009,** *30* (1), 108-117.

[140]. Wang, K.; Luo, G.-F.; Liu, Y.; Li, C.; Cheng, S.-X.; Zhuo, R.-X.; Zhang, X.-Z., Redox-sensitive shell cross-linked PEG-polypeptide hybrid micelles for controlled drug release. *Polym. Chem.* **2012,** *3* (4), 1084-1090.

[141]. McDaniel, J. R.; Callahan, D. J.; Chilkoti, A., Drug delivery to solid tumors by elastin-like polypeptides. *Adv. Drug Deliv. Rev.* **2010,** *62* (15), 1456-1467.

[142]. Yokoyama, M.; Sugiyama, T.; Okano, T.; Sakurai, Y.; Naito, M.; Kataoka, K., Analysis of micelle formation of an adriamycin-conjugated poly(ethylene glycol)-poly(aspartic acid) block copolymer by gel permeation chromatography. *Pharmaceut. Res.* **1993,** *10* (6), 895-899.

[143]. Osada, K.; Cabral, H.; Mochida, Y.; Lee, S.; Nagata, K.; Matsuura, T.; Yamamoto, M.; Anraku, Y.; Kishimura, A.; Nishiyama, N.; Kataoka, K., Bioactive polymeric metallosomes self-assembled through block copolymer-metal complexation. *J. Am. Chem. Soc.* **2012,** *134* (32), 13172-13175.

[144]. Christian, D. A.; Cai, S.; Bowen, D. M.; Kim, Y.; Pajerowski, J. D.; Discher, D. E., Polymersome carriers: from self-assembly to siRNA and protein therapeutics. *Eur. J. Pharm. Biopharm.* **2009,** *71* (3), 463-474.

[145]. Christian, D. A.; Cai, S.; Bowen, D. M.; Kim, Y.; Pajerowski, J. D.; Discher, D. E., Polymersome carriers: from self-assembly to siRNA and protein therapeutics. *Eur. J. Pharm. Biopharm.* **2009,** *71* (3), 463-74.

[146]. Osada, K.; Christie, R. J.; Kataoka, K., Polymeric micelles from poly(ethylene glycol)-poly(amino acid) block copolymer for drug and gene delivery. *J. R. Soc. Interface* **2009,** *6* (Suppl 3), S325-S339.

[147]. Nishiyama, N.; Okazaki, S.; Cabral, H.; Miyamoto, M.; Kato, Y.; Sugiyama, Y.; Nishio, K.; Matsumura, Y.; Kataoka, K., Novel cisplatin-incorporated polymeric micelles can eradicate solid tumors in mice. *Cancer Res.* **2003,** *63* (24), 8977-8983.

[148]. Zhao, Z.-X.; Gao, S.-Y.; Wang, J.-C.; Chen, C.-J.; Zhao, E.-Y.; Hou, W.-J.; Feng, Q.; Gao, L.-Y.; Liu, X.-Y.; Zhang, L.-R.; Zhang, Q., Self-assembly

nanomicelles based on cationic mPEG-PLA-b-Polyarginine(R15) triblock copolymer for siRNA delivery. *Biomaterials* **2012,** *33* (28), 6793-6807.

[149]. Kumagai, M.; Shimoda, S.; Wakabayashi, R.; Kunisawa, Y.; Ishii, T.; Osada, K.; Itaka, K.; Nishiyama, N.; Kataoka, K.; Nakano, K., Effective transgene expression without toxicity by intraperitoneal administration of PEG-detachable polyplex micelles in mice with peritoneal dissemination. *J. Control. Release* **2012,** *160* (3), 542-551.

[150]. Christie, R. J.; Matsumoto, Y.; Miyata, K.; Nomoto, T.; Fukushima, S.; Osada, K.; Halnaut, J.; Pittella, F.; Kim, H. J.; Nishiyama, N.; Kataoka, K., Targeted polymeric micelles for siRNA treatment of experimental cancer by intravenous injection. *ACS Nano* **2012,** *6* (6), 5174-5189.

[151]. Dash, B. C.; Mahor, S.; Carroll, O.; Mathew, A.; Wang, W.; Woodhouse, K. A.; Pandit, A., Tunable elastin-like polypeptide hollow sphere as a high payload and controlled delivery gene depot. *J. Control. Release* **2011,** *152* (3), 382-392.

[152]. Numata, K.; Reagan, M. R.; Goldstein, R. H.; Rosenblatt, M.; Kaplan, D. L., Spider silk-based gene carriers for tumor cell-specific delivery. *Bioconjugate Chem.* **2011,** *22* (8), 1605-1610.

[153]. Numata, K.; Hamasaki, J.; Subramanian, B.; Kaplan, D. L., Gene delivery mediated by recombinant silk proteins containing cationic and cell binding motifs. *J. Control. Release* **2010,** *146* (1), 136-143.

[154]. Apostolovic, B.; Danial, M.; Klok, H.-A., Coiled coils: attractive protein folding motifs for the fabrication of self-assembled, responsive and bioactive materials. *Chem. Soc. Rev.* **2010,** *39* (9), 3541-3575.

[155]. Ma, Y.; Nolte, R. J. M.; Cornelissen, J. J. L. M., Virus-based nanocarriers for drug delivery. *Adv. Drug Deliv. Rev.* **2012,** *64* (9), 811-825.

[156]. Lewis, J. D.; Destito, G.; Zijlstra, A.; Gonzalez, M. J.; Quigley, J. P.; Manchester, M.; Stuhlmann, H., Viral nanoparticles as tools for intravital vascular imaging. *Nat. Med.* **2006,** *12* (3), 354-360.

[157]. Manchester, M.; Singh, P., Virus-based nanoparticles (VNPs): Platform technologies for diagnostic imaging. *Adv. Drug Deliv. Rev.* **2006,** *58* (14), 1505-1522.

[158]. Ren, Y.; Wong, S. M.; Lim, L.-Y., Folic acid-conjugated protein cages of a plant virus: a novel delivery platform for doxorubicin. *Bioconjugate Chem.* **2007,** *18* (3), 836-843.

[159]. Flenniken, M. L.; Liepold, L. O.; Crowley, B. E.; Willits, D. A.; Young, M. J.; Douglas, T., Selective attachment and release of a chemotherapeutic agent from the interior of a protein cage architecture. *Chem. Commun.* **2005,** (4), 447-449.

[160]. Wang, Q.; Raja, K. S.; Janda, K. D.; Lin, T.; Finn, M. G., Blue fluorescent antibodies as reporters of steric accessibility in virus conjugates. *Bioconjugate Chem.* **2002,** *14* (1), 38-43.

[161]. Flenniken, M. L.; Willits, D. A.; Harmsen, A. L.; Liepold, L. O.; Harmsen, A. G.; Young, M. J.; Douglas, T., Melanoma and lymphocyte cell-specific targeting incorporated into a heat shock protein cage architecture. *Chem. Biol.* **2006,** *13* (2), 161-170.

[162]. Stayton, P. S.; Hoffman, A. S.; Murthy, N.; Lackey, C.; Cheung, C.; Tan, P.; Klumb, L. A.; Chilkoti, A.; Wilbur, F. S.; Press, O. W., Molecular engineering of proteins and polymers for targeting and intracellular delivery of therapeutics. *J. Control. Release* **2000,** *65* (1-2), 203-220.

[163]. Meyer, B. F.; Stoner, M. L.; Raphael, C. L.; Davis, R. E.; Herrmann, R. P., Streptavidin-biotin immunotoxins: a new approach to purging bone marrow. *Exp. Hematol.* **1991,** *19* (7), 710-713.

[164]. Paganelli, G.; Pervez, S.; Siccardi, A. G.; Rowlinson, G.; Deleide, G.; Chiolerio, F.; Malcovati, M.; Scassellati, G. A.; Epenetos, A. A., Intraperitoneal radio-localization of tumors pre-targeted by biotinylated monoclonal antibodies. *Int. J. Cancer* **1990,** *45* (6), 1184-1189.

[165]. Sheldon, K.; Baumal, R.; Marks, A., Targeting of [111In]biocytin to cultured ovarian adenocarcinoma cells using covalent monoclonal antibody-streptavidin conjugates. *Int. J. Radiat. Applic. Instrum., Part A* **1992,** *43* (11), 1399-1402.

[166]. Albarran, B.; To, R.; Stayton, P. S., A TAT-streptavidin fusion protein directs uptake of biotinylated cargo into mammalian cells. *Protein Eng. Des. Sel.* **2005,** *18* (3), 147-152.

[167]. Ehrich, P., *Collected studies on immunity*. John Wiley: New York 1906.

[168]. Janib, S. M.; Moses, A. S.; MacKay, J. A., Imaging and drug delivery using theranostic nanoparticles. *Adv. Drug Deliv. Rev.* **2010,** *62* (11), 1052-1063.

[169]. Huang, J.; Bonduelle, C.; Thévenot, J.; Lecommandoux, S.; Heise, A., Biologically active polymersomes from amphiphilic glycopeptides. *J. Am. Chem. Soc.* **2012,** *134* (1), 119-122.

[170]. Christie, R. J.; Matsumoto, Y.; Miyata, K.; Nomoto, T.; Fukushima, S.; Osada, K.; Halnaut, J.; Pittella, F.; Kim, H. J.; Nishiyama, N.; Kataoka, K., Targeted polymeric micelles for siRNA treatment of experimental cancer by intravenous injection. *ACS Nano* **2012,** *6* (6), 5174-89.

[171]. Simnick, A. J.; Amiram, M.; Liu, W.; Hanna, G.; Dewhirst, M. W.; Kontos, C. D.; Chilkoti, A., *In vivo* tumor targeting by a NGR-decorated micelle of a recombinant diblock copolypeptide. *J. Control. Release* **2011,** *155* (2), 144-151.

[172]. Jaiswal, J. K.; Mattoussi, H.; Mauro, J. M.; Simon, S. M., Long-term multiple color imaging of live cells using quantum dot bioconjugates. *Nat. Biotech.* **2003,** *21* (1), 47-51.

[173]. Sperling, R. A.; Rivera Gil, P.; Zhang, F.; Zanella, M.; Parak, W. J., Biological applications of gold nanoparticles. *Chem. Soc. Rev.* **2008,** *37* (9), 1896-1908.

[174]. Atmaja, B.; Lui, B. H.; Hu, Y.; Beck, S. E.; Frank, C. W.; Cochran, J. R., Targeting of cancer cells using quantum dot–polypeptide hybrid assemblies that function as molecular imaging agents and carrier systems. *Adv. Funct. Mater.* **2010,** *20* (23), 4091-4097.

[175]. Collier, J. H.; Rudra, J. S.; Gasiorowski, J. Z.; Jung, J. P., Multi-component extracellular matrices based on peptide self-assembly. *Chem. Soc. Rev.* **2010,** *39* (9), 3413-24.

[176]. de la Rica, R.; Matsui, H., Applications of peptide and protein-based materials in bionanotechnology. *Chem. Soc. Rev.* **2010,** *39* (9), 3499-3509.

[177]. Lowik, D. W.; Leunissen, E. H.; van den Heuvel, M.; Hansen, M. B.; van Hest, J. C., Stimulus responsive peptide based materials. *Chem. Soc. Rev.* **2010,** *39* (9), 3394-3412.

[178]. Hunter, A. C.; Moghimi, S. M., Therapeutic synthetic polymers: a game of Russian roulette? *Drug Discov. Today* **2002,** *7* (19), 998-1001.

[179]. Yang, J.; Gitlin, I.; Krishnamurthy, V. M.; Vazquez, J. A.; Costello, C. E.; Whitesides, G. M., Synthesis of monodisperse polymers from proteins. *J. Am. Chem. Soc.* **2003,** *125* (41), 12392-12393.

[180]. Dill, K. A.; Shortle, D., Denatured states of proteins. *Annu. Rev. Biochem.* **1991,** *60* (1), 795-825.

[181]. Calmettes, P.; Durand, D.; Desmadril, M.; Minard, P.; Receveur, V.; Smith, J. C., How random is a highly denatured protein? *Biophys. Chem.* **1994,** *53* (1–2), 105-113.

Chapter 2

Rational Design and Synthesis of Protein Based Polypeptide Copolymers

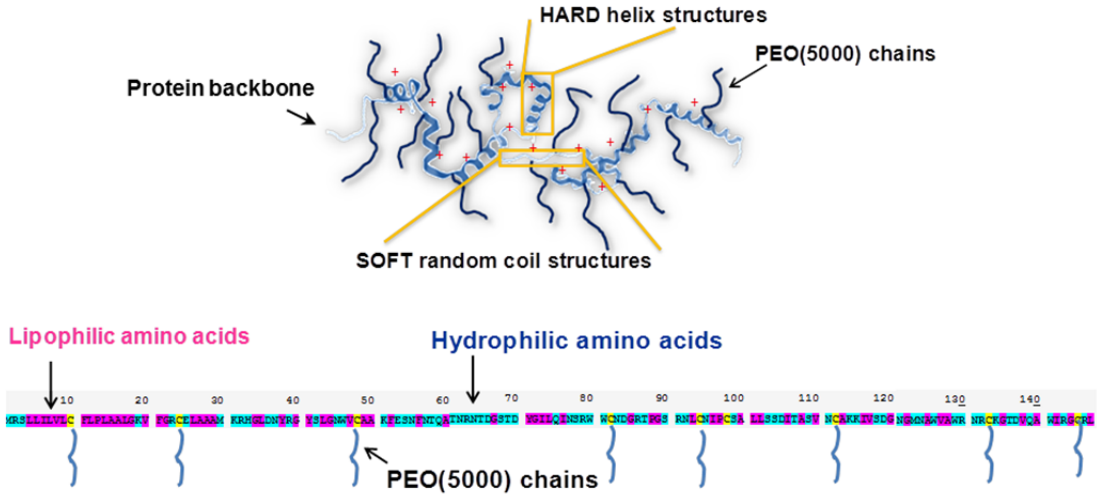

Reproduced with permission [1]. Copyright 2012, American Chemical Society.

This Chapter contains experimental results published previously in (1) *Biomacromolecules*, 2012, 13(6):1890-1898. written by Wu Y., Pramanik G., Eisele K., Weil T.; (2) *Macromol. Rapid Commun.*, 2012, 33(15):1304-1309. written by Wu Y. and Weil T; (3) *Biointerphases*. 2012, 7(1-4):5. written by Wu Y., Er K. S., Ramanathan A., Vasudevan S., Weil T.; (4) *Macromol. Rapid Commun.*, 2012, doi: 10.1002/marc.201200227. written by Wu Y., Wang T., Ng D.Y.W., Weil T.; and (5) *Adv. Healthcare Mater.*, 2012, DOI: 10.1002/adhm.201200296. written by Wu Y., Ihme S., Buske M. F-, Kuan S. L., Eisele K., Lamla M., Wang Y, Buske C., and Weil T. The dissertation author was the primary investigator and first author of these papers.

2.1 Introduction

Peptide materials are of emerging interest due to their biocompatibility, biodegradability and their potential to achieve unique macromolecular architectures with tailored properties [2, 3, 4]. They have been successfully applied in a number of applications such as self-assembly into complex nanostructures [5, 6] or to improve the pharmacokinetic properties of protein therapeutics [7, 8]. To date, there is an increasing interest in the preparation of peptide materials for biomedical applications, e.g. tissue engineering [9, 10] or as carriers for the delivery of drug molecules [11, 12]. Polypeptides for biomedical applications often require precisely controllable biological and physical properties [13] which is rather challenging to achieve.

Ring-opening polymerization of α-amino acid *N*-carboxyanhydrides represents one of the most commonly used synthetic schemes to prepare polypeptides with repeating amino acid sequences [14]. However, monodisperse polypeptides composed of different kinds of amino acids or particular peptide sequences with defined structures and distinct molecular weights are often challenging to achieve *via* classical polymerization reactions [15]. As complementary strategies, the expression of recombinant polypeptides [16, 17] and the solid phase peptide synthesis [18] yield polypeptides with more diverse sequences and defined molecular weights. Still, common limitations, including sophisticated expression or synthetic procedures, low yields and high costs, are yet to overcome. Therefore, it is highly desirable to develop more efficient approaches for the synthesis of defined polypeptides with tunable properties.

Proteins are polypeptides with precisely defined sequences, molecular weights, structures and 3D architectures and they are ubiquitous in nature [19]. It was proposed that the chemical modification of the side chains of proteins should facilitate monodisperse polymers with sequences of natural diversity and functionalities [15]. However, due to the tightly folded polypeptide backbone of native proteins, functional groups are mostly hidden inside the protein structure and thus not accessible for efficient chemical reactions at the protein surface. Denaturing the 3D structure of proteins usually leads to precipitation and destabilization of the polypeptide backbone [20, 21], thus preventing the use of proteins as polypeptide sources. To overcome these problems and explore the potential of proteins as biopolymers, a comprehensive and highly versatile synthetic approach was developed to access stable protein based polypeptide copolymers (PbPs) by a "denaturation and stabilization" strategy.

In this chapter, the general scheme for the synthesis and functionalization of PbPs will be discussed. Starting from different protein precursors, functionalized PbPs with distinct molecular weights, chain lengths, ordered secondary structural elements were prepared. Such copolymers were well soluble in water, stable for long time and fast degradable by proteases. In addition, various reactive groups were distributed along the polypeptide backbone available for further chemical modifications. Other functionalities and properties could be further easily introduced into PbPs either before denaturation or after denaturation *via a priori* and *a posteriori* modification strategies. For instance, PbPs with different charges and hydrophobicities as well as additional functional moieties, such as anticancer drugs and imaging

molecules, were prepared. These highly versatile copolymers synthesized herein represent a novel class of materials featuring high biocompatibility, high biodegradability, multiple reactive groups along the backbone as well as the presence of ordered structural elements. Such biopolymers are highly attractive for a broad range of applications such as bioimaging and drug delivery, which will be further demonstrated in the following chapters. This "semi-synthetic" approach provides a valuable alternative to conventional polypeptide synthesis and expression approaches providing fast and efficient access to various polypeptides of natural diversity.

2.2 Preparation of PbPs from different protein precusors

PbPs with varying lengths of their main chains were achieved from different native precursor proteins. Lysozyme from hen egg white (LY, 24 kDa) was selected as the example of a small protein. The abundant albumins from human serum (HSA, 66 kDa) and bovine serum (BSA, 66 kDa) were chosen as representatives of high molecular weight proteins. Moreover, by connecting several protein building blocks, polypeptides with extremely high molecular weight could also be achieved.

The general scheme to synthesize PbPs was based on a "denaturation and stabilization" process. Proteins were denatured under controlled denaturing conditions to break down the hydrogen bondings and disulfide bridges. The unfolded backbone of proteins was *in situ* stabilized by grafting appropriate numbers of polyethylene(oxide) (PEO) chains. The specific

reaction conditions were dependent on the nature of the protein precursor and will be discussed individually in the following sections.

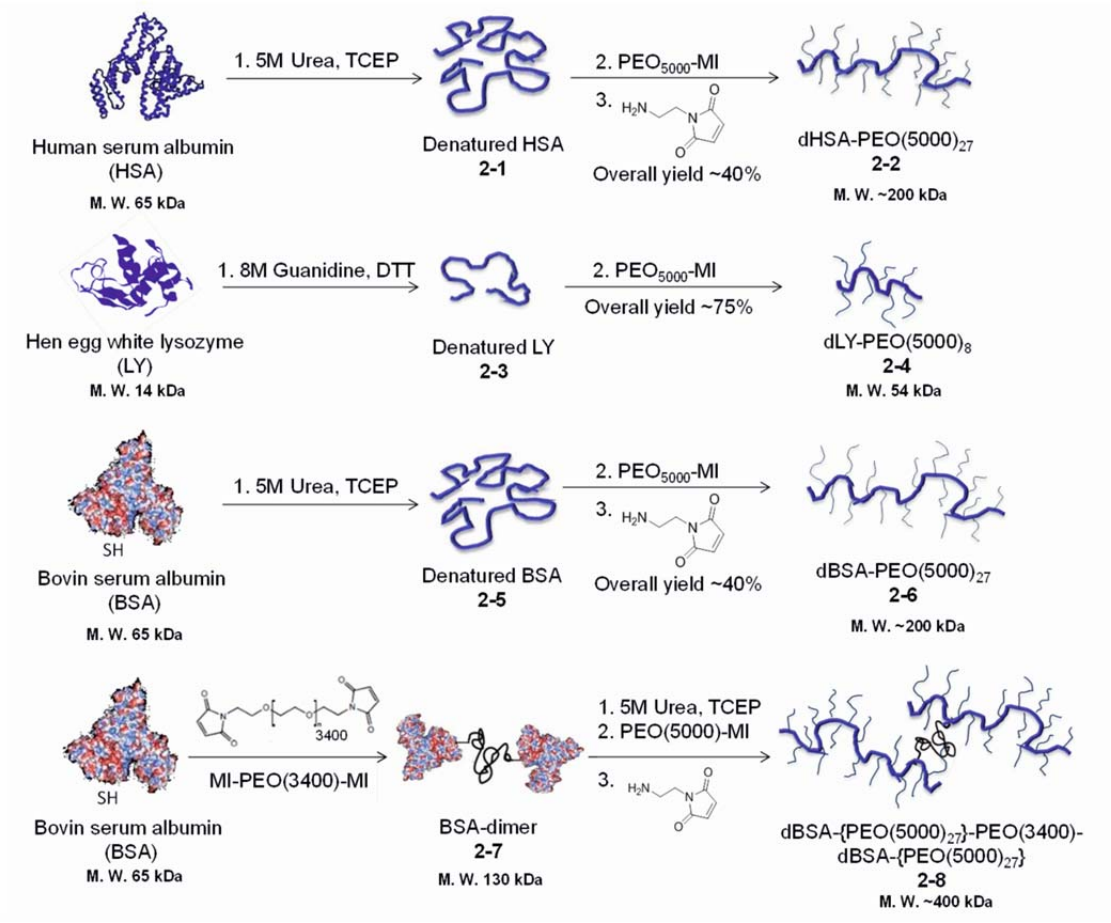

Scheme 2-1. Preparation of albumin and LY derived polypeptide copolymers. Adapted with permission [1]. Copyright 2012, American Chemical Society.

2.2.1 Preparation of long polypeptide copolymers from albumins

HSA is an abundant and non-toxic human protein with a molecular weight of 66 kDa. According to the primary sequence of 609 amino acids in HSA, it contains a large number of functional groups available for chemical modifications, including 100 carboxylic acid groups and 60 amino groups. In addition, there are 35 cysteine residues in the sequence forming 17 disulfide bridges, which are important for maintaining the 3D structure of the protein. Other than the 34 bridged cysteine residues, there is an additional single

cysteine (Cys-34) at an accessible position which could be attractive for mono-functionalization. Therefore, HSA was selected as the first protein precursor for preparing polypeptide copolymers.

Denaturation of albumin proteins was accomplished in the presence of high urea concentrations (5 M) destabilizing the tertiary protein structure by diminishing secondary interactions. Subsequently, tris(2-carboxyethyl)phosphine (TCEP) was added as a mild reducing agent to cleave all disulfide bridges. Under such condition, the protein backbone was virtually unfolded but unstable and tended to precipitate once the urea solution was removed. Therefore, the denatured proteins needed to be stabilized *in situ* by reacting the reduced thiol groups with O-(2-maleimidoethyl)-O'-methyl-polyethylene(oxide)-5000 (PEO(5000)-MI) (**Scheme 2-1**). The PEO chains shielded the hydrophobic amino acids with a hydrophilic layer and, therefore, prevented the backfolding of the polypeptides and significantly improved their stability of the denatured protein copolymers. Sufficient number and length of the PEO chains were found to be critical for achieving stable polypeptide copolymers. *Via* this procedure, the HSA-based copolymer (**2-2**) was achieved carrying ~27 PEO-chains according to molecular weight studies, indicating that 27 out of 35 cysteine residues had reacted with PEO(5000)-MI. Since the presence of remaining free sulfhydryl groups had a negative impact on the long term stability of such polypeptides, N-(2-aminoethyl)maleimide was added after the pegylation step in order to further increase shelf life of the copolymer. The pure protein copolymer dHSA-PEO(5000)$_{27}$ (**2-2**) was isolated as a white fluffy powder after size exclusion chromatography and desalting. The resulting copolymers were soluble in

water at more than 100 mg/mL concentration, and were stable in solid form for up to one year or in solution for a few months.

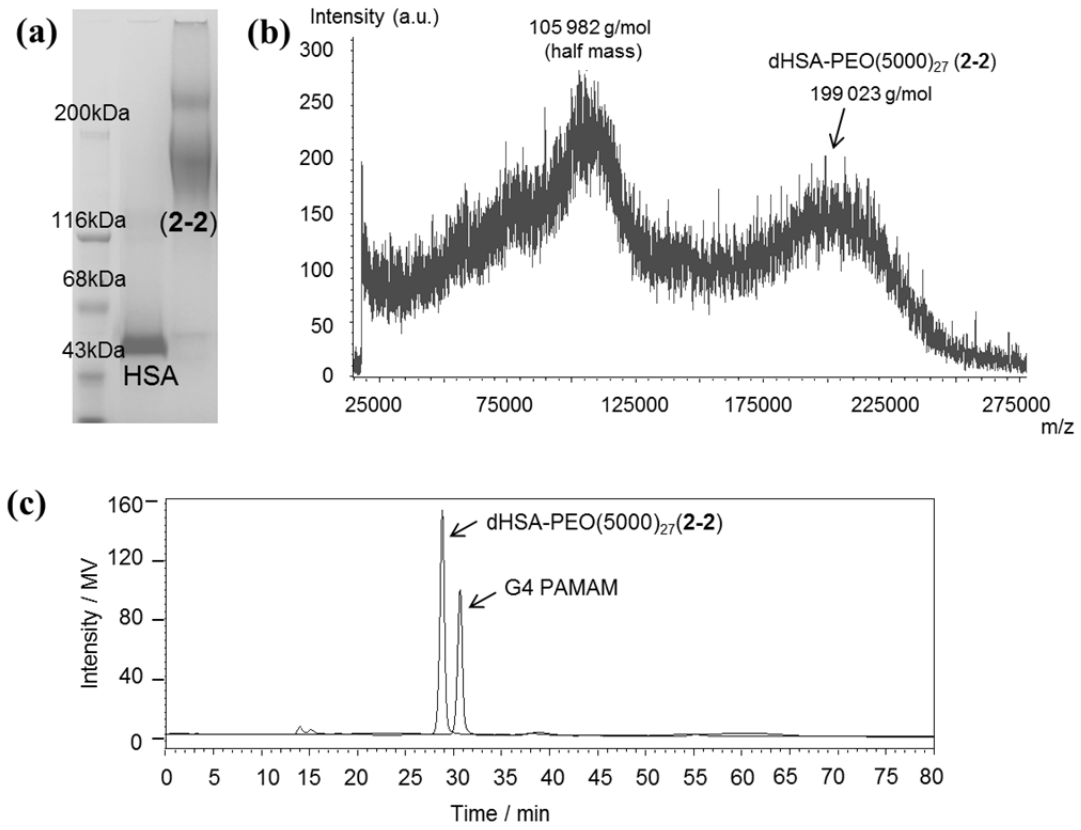

Figure 2-1. Characterization of dHSA-PEO(5000)$_{27}$ (**2-2**). (a). SDS-PAGE of HSA, and the copolymers (**2-2**); (b). MALDI-ToF mass spectrum dHSA-PEO(5000)$_{27}$ (**2-2**), matrix: sinapinic acid; (c). Gel permeation chromatogram of dHSA-PEO(5000)$_{27}$ (**2-2**) (compared with a commercial, monodisperse polyamidoamine "PAMAM" generation 4.0 dendrimer). The first signal corresponds to dHSA-PEO(5000)$_{27}$ (**2-2**) and the second, lower signal refers to the commercial PAMAM 4.0 dendrimer. dHSA-PEO(5000)$_{27}$ (**2-2**) has a similar elution profile as the commercial PAMAM dendrimer (which is considered monodisperse) supporting the narrow dispersity of (**2-2**). Adapted with permission [1]. Copyright 2012, American Chemical Society.

The molecular weight of (**2-2**) was assessed by MALDI-ToF MS which revealed a molecular weight of 199 kDa (**Figure 2-1b**). SDS-PAGE (sodium

dodecyl sulfate polyacrylamide gel electrophoresis) also showed a protein band at around 190 kDa (**Figure 2-1a**). Due to the interaction among PEO chains, the band of (**2-2**) on SDS-PAGE was a bit smeary compared to the native protein. The polymer dispersity of (**2-2**) was also investigated by gel permeation chromatography (GPC). A sharp signal was detected, indicative of a narrow size-distribution and low dispersity (**Figure 2-1c**). However, due to the unique architecture of (**2-2**), no GPC standard with a similar structure and polarity could be identified, thus preventing size estimation *via* GPC. In this context, commonly used standards such as PEO of different chain lengths and Dextran were not applicable. But the polydispersity of (**2-2**) was comparable with the commercial PAMAM dendrimer, which was considered monodisperse. In order to prove the quantitative capping of all free thiol groups, the 4,4'-dithiodipyridine (DPS) test was applied. DPS is a reagent readily being reduced in the presence of free thiol groups and forming 4-thiopyridone with a characteristic absorbance maximum at 325 nm (see experimental section). A good correlation between the free thiol concentration and the absorption of 4-thiopyridone was observed, allowing a quantification of the free thiol groups of (**2-2**). This test showed that less than 1 thiol group in each copolymer was observed, suggesting a nearly quantitative capping of all free thiol groups.

The attachment of ~27-28 substituents along each albumin main chain was very reproducible, which from the view point of polypeptide sequence, might be because of seven cysteine residues located directly next to each other (**Figure 2-2**). Therefore, it was very unlikely that a second PEO-chain was attached after the attachment of the first chain. In this way, even though

the PEO substituents might not be located at the same cysteine residue, the number and distribution of the PEO chains along the backbone could be still considered well defined.

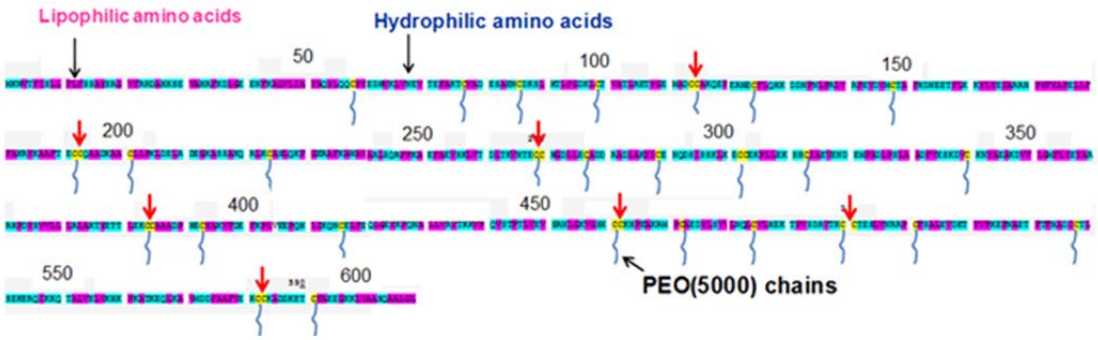

Figure 2-2. Amino acid sequence of HSA. Blue color denotes hydrophilic amino acid residues, purple color stands for lipophilic amino acids and yellow color indicates cystein residues. Red arrows indicate the presence of two neighboring cysteine residues. Due to steric hindrance, the PEO chain was most likely only attached to one of these cysteine residues. Reproduced with permission [1]. Copyright 2012, American Chemical Society.

2.2.2 Preparation of short polypeptide copolymers from lysozyme*

Lysozyme (LY) from hen egg white with a molecular weight of 14 kDa was then selected as a representative of small proteins. A polypeptide copolymer based on LY was successfully synthesized by a similar “denature-pegylation” strategy (the protocol and characterization were first developed by Mr. Goutam Pramanik and are included in his PhD thesis). But unlike HSA, denaturation of LY required more drastic reaction conditions, such as 8 M guanidinium hydrochloride, excess of stronger reduction reagent dithiothreitol (DTT) instead of TCEP as well as prolonged reaction times (>24 hr).

* This method was first developed by Mr. Goutam Pramanik and will be described in detail in his PhD thesis.

According to the primary sequence of LY, there are 8 cysteine residues well separated along the protein backbone. Therefore, the subsequent pegylation with PEO(5000)-MI led to a quantitative reaction of all eight thiol groups and no further capping of remaining thiol groups was needed. After purification with size exclusion chromatography and desalting, dLY-PEO(5000)$_8$ (**2-4**) was obtained as a white fluffy solid. Similar to HSA derivative (**2-2**), dLY-PEO(5000)$_8$ (**2-4**) also displayed significant water solubility as well as long term stability. The molecular weight of dLY-PEO(5000)$_8$ (**2-4**) was also assessed by MALDI-ToF MS and SDS-PAGE. A very sharp peak of 54 kDa was observed from MALDI-ToF MS (**Figure 2-3a**), indicating that all eight thiol groups of the LY backbone were reacted with PEO(5000)-MI and a narrowly dispersed copolymer was formed. In agreement with MALDI-ToF MS, a very sharp protein band at ~50 kDa was also observed on SDS-PAGE (**Figure 2-3b**). In the case of LY, the location of the PEO-chains of (**2-4**) was precisely defined due to the exactly known location of all eight cysteine residues along the main chain (**Figure 2-4**).

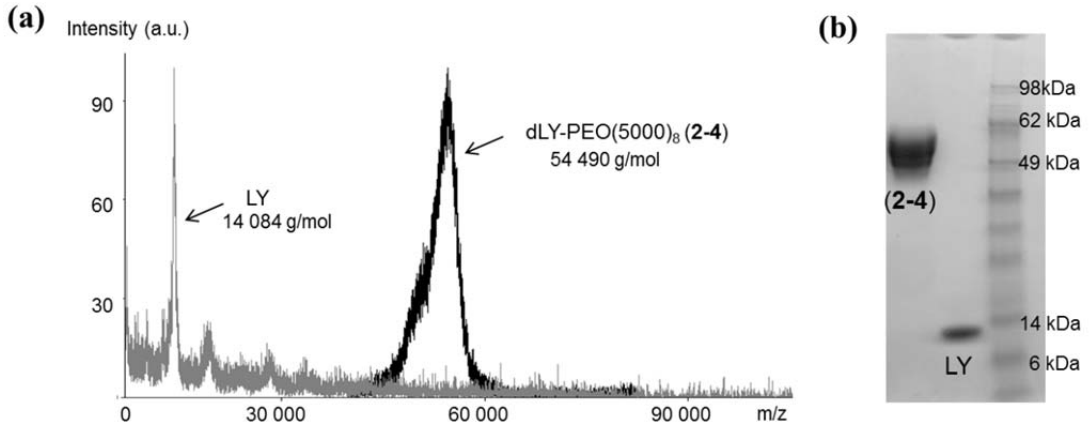

Figure 2-3. Characterization of dLY-PEO(5000)$_8$ (**2-4**). (a). MALDI-ToF mass spectrum of dLY-PEO(5000)$_8$ (**2-4**), matrix: sinapinic acid; (b). SDS-PAGE of

LY and the copolymers (**2-4**)†. Adapted with permission [1]. Copyright 2012, American Chemical Society.

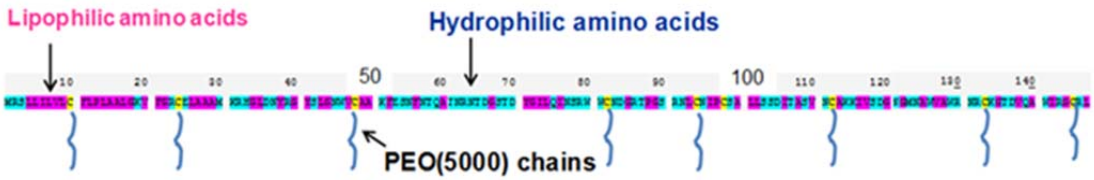

Figure 2-4. Amino acid sequence of lysozyme. Blue color denotes hydrophilic amino acid residues, purple color stands for lipophilic amino acids and yellow color indicates cystein residues. In case of LY, all eight cysteine residues carry a PEO chain. Reproduced with permission [1]. Copyright 2012, American Chemical Society.

2.2.3 Preparation of giant polypeptide copolymers from dimeric BSA

Since HSA and BSA share high sequence similarity [22], the same synthetic approach for HSA copolymers (**2-2**) could be also used to prepare BSA derived copolymers. In addition, to obtain PbPs with even higher molecular weight, a unique giant block copolymer architecture (**2-8**) was achieved based on a more complex precursor from BSA. Briefly, two BSA molecules, each bearing a single free and accessible cysteine group (Cys-34), were connected by a PEO-chain (M_n = 3400 g/mol) bearing two maleimide (MI) groups (MI-PEO(3400)-MI) *via* a Michael reaction to give BSA-dimer (**2-7**). This dimer was sequentially purified by centrifugal filtration (100 kDa MWCO) and flash protein liquid chromatography (FPLC) using a

† This data was provided by Mr. Goutam Pramanik and would be in part of his PhD thesis.

procedure developed by our group [23]. The resulting BSA-dimer (**2-7**) represented a narrowly dispersed, macromolecular precursor with a defined M.W. of ~132 kDa (**Figure 2-5a**). BSA-dimer (**2-7**) was then subjected to strong denaturing conditions (5 M urea). A mild reducing reagent (TCEP) was added to reduce all 34 disulfide bridges of (**2-7**) and stabilize the denatured architecture of (**2-7**) in solution (**Scheme 2-1**). Subsequently, PEO(5000) chains bearing a single thiol-reactive maleimide group (PEO(5000)-MI) were added and the Michael addition product with ~54 out of 68 thiol groups was achieved (see discussion in section 2.2.1). In order to further improve the stability of the PEO-grafted copolymers in solution,[2] similar as for copolymer (**2-2**), the remaining unreacted sulfhydryls groups were capped with N-(2-aminoethyl)maleimide yielding the triblock copolymer dBSA-{PEO(5000)$_{27}$}-PEO(3400)-dBSA-{PEO(5000)$_{27}$} (**2-8**). The absence of any unreacted sulfhydryl group along the BSA-derived polypeptide backbone was confirmed by the DPS test.

The characterization of globular proteins is relatively straightforward compared to their denatured analogues since analysis *via* mass spectrometry is often successful. In this way, the MALDI-ToF mass spectrum of the precursor protein dimer (**2-7**) (BSA-dimer) using sinapinic acid as matrix was recorded and a single peak at m/z = 132 kDa in accordance to the calculated M.W. of 133 kDa was detected (**Figure 2-5a**). BSA-dimer (**2-7**) represented a high M.W. precursor with high structural perfection and complexity.

For a head to head comparison with giant copolymer (**2-8**), a BSA derived polypeptide (**2-6**) (a close analogue of **2-2**) was also synthesized using the same procedure for HSA copolymer (**2-2**). The BSA copolymer (**2-6**) was also

characterized by SDS-PAGE, revealing an average M.W. of ~200 kDa which corresponds to about 27 PEO chains. The increase in M.W. from BSA, (**2-7**) and (**2-6**) to (**2-8**), was well detectable and is depicted in **Figure 2-5b** and **2-5c**. Considerably shorter elution times of (**2-8**) and the PEO-grafted copolymer (**2-6**) were found. According to gel electrophoresis (NuPAGE® tris-acetate gel and HiMark® Pre-stained Protein Standard (Invitrogen)), an approximate M.W. of 400 kDa for triblock copolymer (**2-8**) was obtained. Considering the precise M.W. of precursor (**2-7**) (132 kDa) and assuming a similar grafting efficiency as in (**2-2**) and (**2-6**), theoretically, 27 PEO chains were grafted onto each polypeptide backbone. Thus, a giant polypeptide triblock copolymer (**2-8**) with an approximate M.W. of 400-410 kDa and narrow size dispersity was produced. This was in good agreement with the gel electrophoresis result.

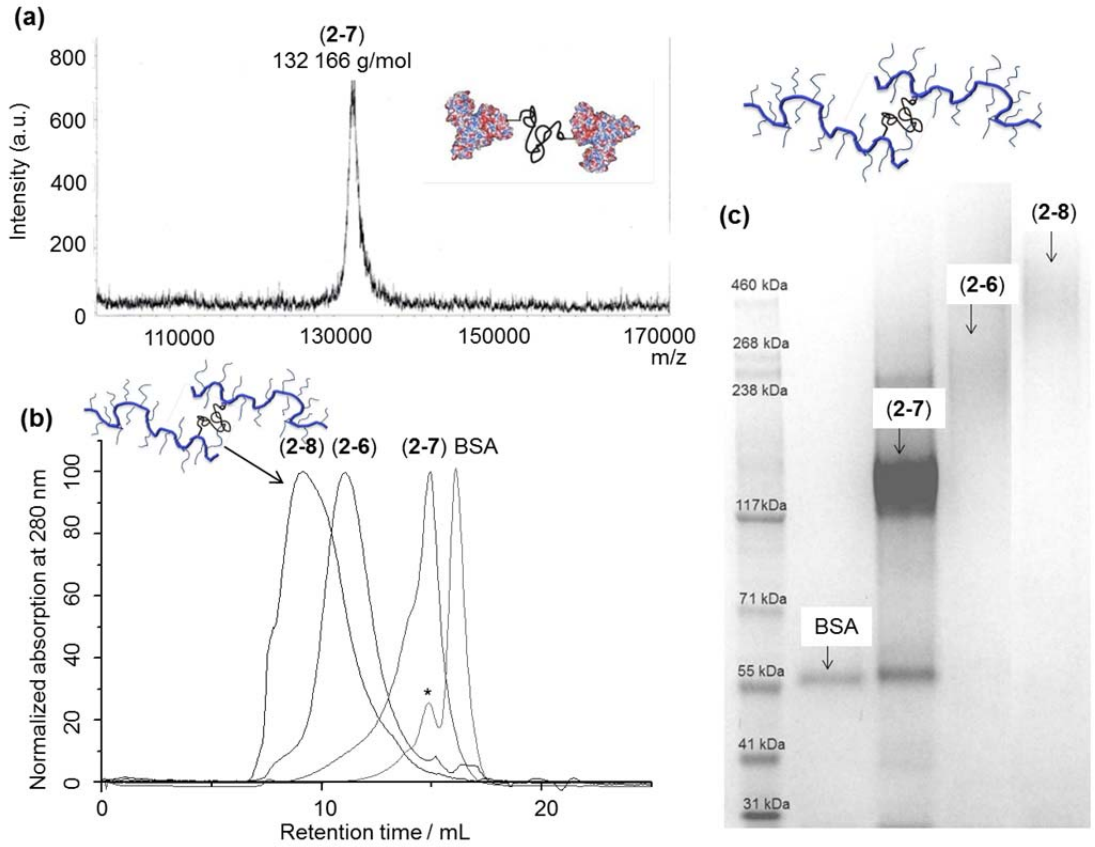

Figure 2-5. Characterization of BSA-derived polypeptide block copolymer architectures. a) MALDI-ToF mass spectrum of BSA-dimer **2-7**, matrix: sinapinic acid; b) elugrams of BSA, **2-7**, **2-6** and **2-8** after size exclusion chromatography (*the minor high molecular weight peak in native BSA corresponds to dynamic dimerization due to inter-molecular thiol-disulfide exchange [24, 25]); c) SDS gel electrophoresis of native BSA (66.7 kDa), BSA-dimer (**2-7**, 132 kDa), dBSA-PEO(5000)$_{27}$ (**2-6**, ~200 kDa), dBSA-{PEO(5000)$_{27}$}-PEO(3400)-dBSA-{PEO(5000)$_{27}$} (**2-8**, ~400 kDa). Adapted with permission [26]. Copyright 2012, Wiley-VCH.

2.2.4 Polypeptide copolymers with highly defined structures and secondary elements

The primary amino acid sequence of the protein backbone folds into secondary structures (e.g. helical and beta sheet structures) due to non-

covalent interactions among the amino acid residues. The presence of regular structural elements in polymers is highly attractive since secondary interactions could impart additional features, for instance, the formation of superstructures like amyloid fibers [27] from β-sheet structures. The far-UV circular dichroism (CD) spectrum of a protein generally reflects its secondary structure content with remarkable sensitivity [28]. Using reference spectra derived from proteins of known structure, various empirical methods have been developed to quantitatively estimate secondary structure fractions from CD spectra [29]. According to circular dichroism studies, the predominant secondary structure elements of the precursor proteins were partially conserved in all protein-derived polypeptide copolymers reported herein (**Figure 2-6**). For instance, native HSA revealed a high content of α-helix (~60%) and only 20% of β-sheet elements, which was also reflected in the respective polypeptide copolymer (**2-2**) containing mainly α-helix (~43%) structures. A parallel trend was also observed for (**2-4**). However, in all cases, a lower content of α-helix structures and higher content of β-sheet or random structural elements were observed compared with their globular protein precursors indicating less densely packed architectures. This might be due to the attached PEO chains blocking the forming of helix structures. In comparison, since random coil and β-sheet structures were more extended and require less restricted interactions, they were less disturbed by pegylation.

Similar to the native protein derived polypeptides, we also studied the secondary structure elements in triblock copolymer (**2-8**) using far-UV CD spectroscopy. According to these investigations (**Figure 2-6**), triblock

copolymer (**2-8**) still maintained ordered secondary structures. Interestingly, the CD spectrum of triblock copolymer (**2-8**) was almost the same as the native albumin derived copolymer (**2-6**). A higher content of β-sheet elements and less α-helix structures were also found compared to the protein precursors BSA and BSA-dimer (**2-7**). This data supported that the secondary structure elements in PbPs were predominantly determined by the precursor proteins and were not much affected by conjugating several blocks together. Therefore, in principle, once a short PbP with desired secondary structures was identified, the giant PbPs with the similar structure but longer chain length could in principle be easily achieved by linking several precursor proteins together. The presence of ordered secondary structure elements in PbPs was highly attractive for introducing various novel features, such as membrane permeability, liquid crystallinity [30] or self-organization into nano- and mesoscopic structures [31].

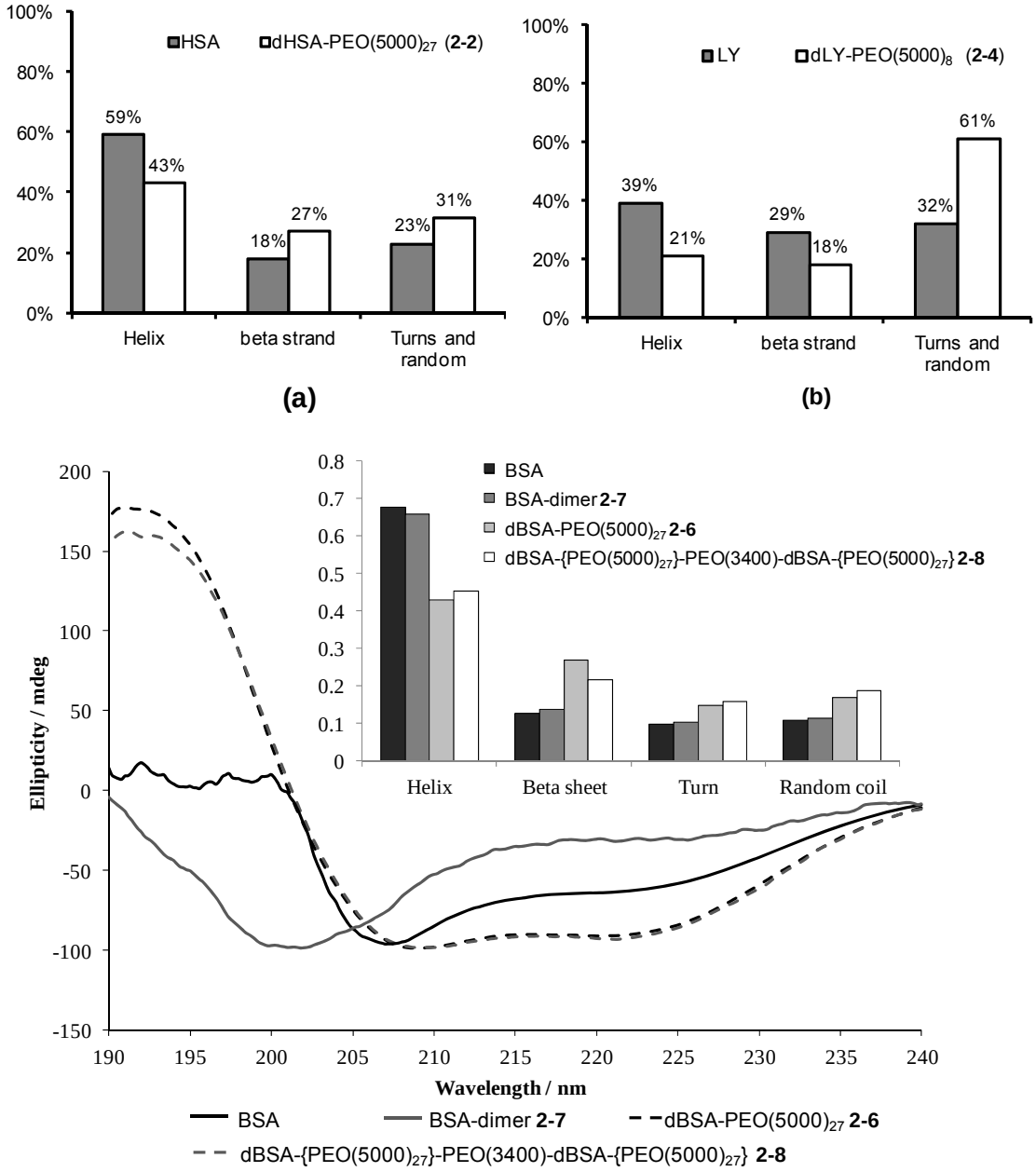

Figure 2-6. Secondary structure analysis of (a) (**2-2**), (b) (**2-4**) and (c) (**2-8**) compared with their corresponding native protein precursors. The percentage of the secondary structure elements is calculated from circular dichroism (CD) spectra using CDSSTR method [29]. Adapted with permission [1, 26]. Copyright 2012, American Chemical Society and Copyright 2012, Wiley-VCH.

2.2.5 Alternating hydrophilic and lipophilic amino acids and induced formation of nanoscopic micelles

According to the amino acid sequences of the native precursor proteins, all polypeptide copolymers contained hydrophobic and hydrophilic amino acids as well as PEO chains distributed along their main chain (**Figure 2-2** and **Figure 2-4**). The polarity of the side chains in proteins is essential for protein folding to adopt a defined and compact 3D structure in aqueous solution. Therefore, it was also very likely that polypeptide copolymers fold into micellar structures in aqueous solution, which was also known for other polypeptides [32]. The precursor proteins HSA and LY exhibited hydrodynamic diameters (d_H) of ~5 nm and 3 nm, respectively, according to the number average diameter obtained by dynamic light scattering (DLS) (**Table 2-1**). In contrast, the size distribution by light scattering intensity yielded slightly larger d_H as well as a second population with d_H between 80 and 150 nm. It was described before that serum albumins as well as LY formed supramolecular structures in solution [33], which could be detected by DLS. These results again reflected the extreme sensitivity of DLS intensity toward large aggregates. The size distribution profiles of the polypeptide copolymers obtained by light scattering intensity indicated that two populations of (**2-2**) coexisted in aqueous solution. The smaller species with diameters of ~40 nm (**2-2**) consisted most likely single chain macromolecules, whereas the larger polypeptide aggregates exhibited diameters of ~187 nm. In the case of (**2-4**), only polypeptide aggregates of ~170 nm were observed. If the number distribution was considered, the majority of species of (**2-2**) in solution were present as single chains with average d_H of 13 nm, indicating that the number

of polypeptide aggregates generated was much smaller than the number of nonaggregated, single chain polypeptides. Differences in the sizes of the different polypeptide species found in solution could be attributed to a variety of effects; for instance, electrostatic repulsion of the negatively charged backbone leading to coil expansion, different levels of counterion condensation depending on the average spacing between backbone charges, a hydrophobic collapse due to a larger content of hydrophobic amino acids, or a higher degree of more compact secondary structures such as α-helix or β-sheet structures. This property could be exploited for the design of efficient nanocarriers for medicinal applications.

Table 2-1. Summary of molecular weight (M.W.), zeta potential, size distribution in aqueous solution and complete proteolysis digestion time of various polypeptide copolymers and their precursor proteins.

Sample name	M.W. (kDa)	Zeta potential (mV)	Diameter (H_2O, nm)[c]	PDI[a]	Diameter (H_2O, nm)[d]	Digestion time[e] (min)
HSA	66[a]	-3±1	5±1	0.34	7±0 121±9	/
dHSA-PEO(5000)$_{27}$	200[a]	-1±2	13±3	0.46	40±4 187±15	90
LY	14[a]	5±1	3±1	0.35	4±1 78±7	/
dLY-PEO(5000)$_8$	54[a]	-8±3	115±12	0.28	170±3	60

[a.] Molecular weight obtained by MALDI-ToF spectrum.
[b.] Molecular weight according to SDS-PAGE and theoretical calculation.
[c.] According to DLS measurements based on number using approximately 0.1 mg/mL of each protein in aqueous solution.
[d.] According to DLS measurements based on intensity using approximately 0.1 mg/mL of each protein in aqueous solution.
[e.] Digestion time was estimated with 0.1% trypsin and analyzed by SDS-PAGE. Detailed SDS-PAGE pictures are shown in **Figure 2-8**.

2.2.6 Non-cytotoxic and biodegradable polypeptide copolymers

Ideal biomaterials are expected to have sufficient stability in the blood stream, no or low cell toxicity as well as biodegradability into non-toxic metabolites. Since polypeptide copolymers were derived from proteins, they

should offer promising biocompatibility and high degradability in cell endosomes and lysosomes in the presence of high concentrations of proteases. We investigated the cytoxicity of HSA and LY derived copolymers (**2-2**) and (**2-4**) in A549 cells at concentration from 0.1 μM to 50 μM and no significant cytoxicities were observed (**Figure 2-7**). Moreover, after *in vitro* treatment with 0.1% trypsin, all the copolymers (**2-2**), (**2-4**) and (**2-8**) were digested immediately into small peptide fragments. A further degradation of the peptide fragments was also observed within 2 hr (**Table 2-1** and **Figure 2-8**). Notably, in the absence of proteases, all these copolymers displayed high stability in the solid state as well as in aqueous solution for several months.

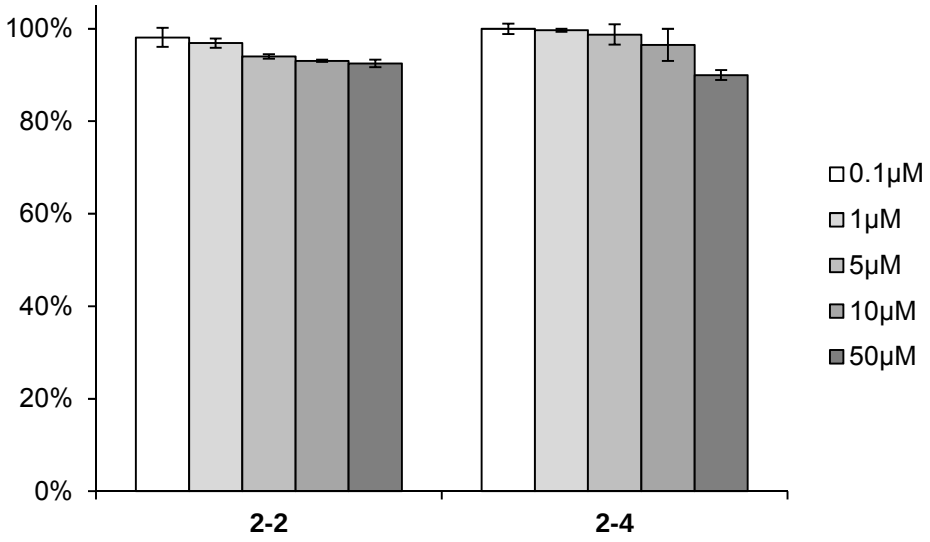

Figure 2-7. Cell viability assays showing no significant cytotoxicity of polypeptide copolymer (**2-2**) and (**2-4**). (n=3, standard deviation presented as error).

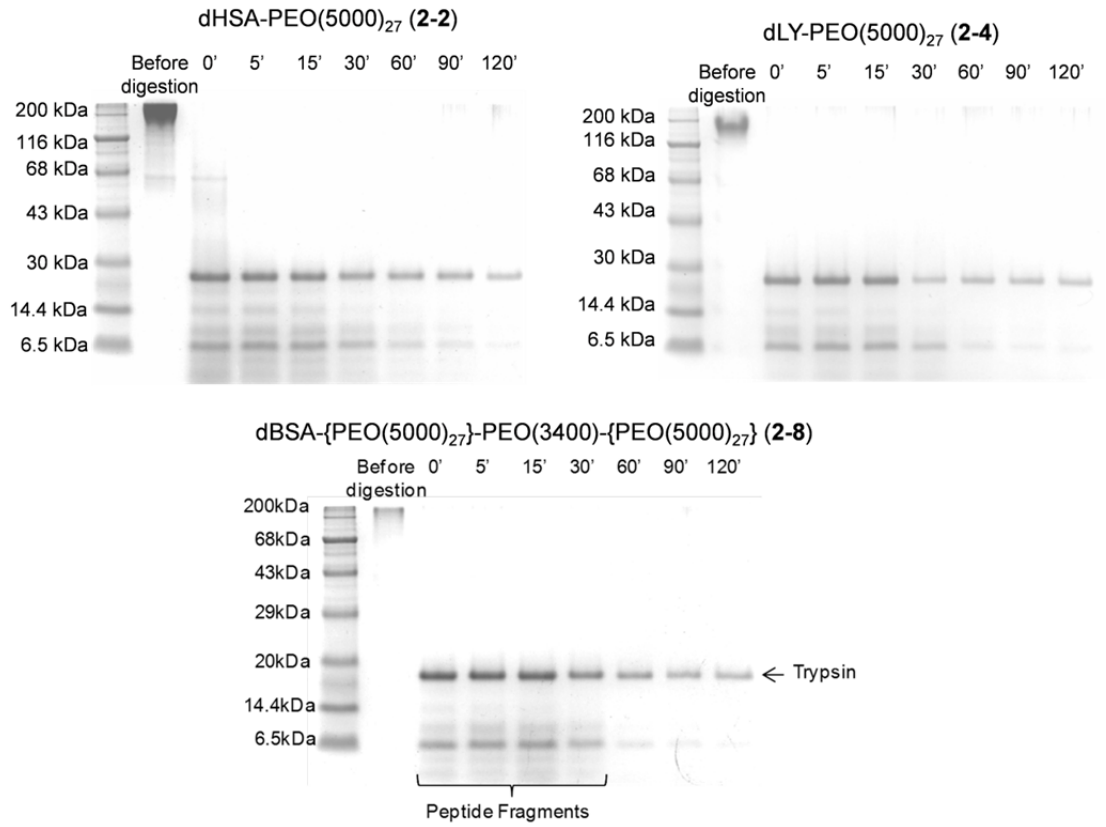

Figure 2-8. Trypsin digestion of polypeptide copolymer (**2-2**), (**2-4**) and (**2-8**) analyzed by 4%-10% SDS-PAGE. Adapted with permission [1]. Copyright 2012, American Chemical Society.

2.3 Synthesis of polypeptide polyelectrolytes *via a priori* modification of precursor proteins

2.3.1 Preparation of polycationic and polyanionic polypeptide copolymers by *a priori* modification of serum albumin

Proteins bear a large number of reactive groups on their surface which are readily available for chemical modification. Thus, the introduction of

additional functional groups could be accomplished by *a priori* modification of the native globular protein precursor before protein denaturation. Such modifications allowed further expanding the repertoire of the protein derived copolymers reported so far to provide particular properties which native protein precursors do not possess. Based on this strategy, we prepared protein derived polyelectrolytes with polycationic charges or polyanionic charges (**Scheme 2-2**).

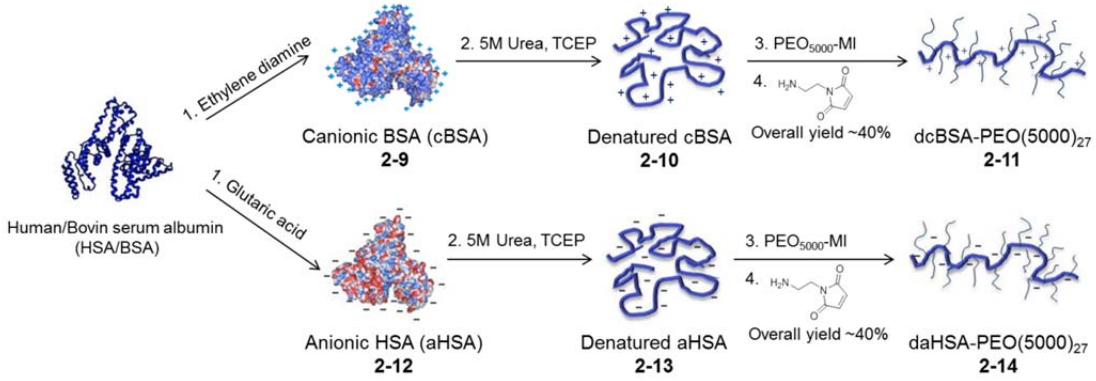

Scheme 2-2. Preparation of polycationic (**2-11**) and polyanionic (**2-14**) PbPs by *a priori* modification of serum albumin. Adapted with permission [1]. Copyright 2012, American Chemical Society.

Charges play an important role in cell biology, such as regulation of cell-cell interaction [34], intracellular communication [35] as well as ligand-receptor interaction [36]. Chemical modification of the serum albumin precursor allows the preparation of polycationic or polyanionic polypeptides that are attractive for cellular uptake, cell trafficking, targeting of subcellular structures [37, 38] and complex formation with DNA [39]. For instance, the polycationic albumin derivative cBSA (**2-9**) has been previously reported, which facilitates fast cell uptake and efficient DNA delivery [39, 40] as well as cell [41] and vesicle

immobilization [42] to surfaces. The synthesis of cBSA (**2-9**) was accomplished by treating the accessible carboxylic acid residues on native BSA with ethylenediamine. By using a large access of etyhlenediamine, the maximum of 147 primary amino groups on average (according to the MALDI-ToF mass spectrum as shown in **Figure 2-9a** and isothermal titration studies reported previously [40]) could be achieved on cBSA (**2-9**) which yielded a high number of positive charges at physiological pH. Following a similar approach, the polyanionic serum albumin derivative aHSA (**2-12**) was prepared by reacting ~40 accessible lysine residues with glutaric acid (according to MALDI-ToF mass spectrum, see **Figure 2-9c**) to introduce additional carboxylic acid groups. The globular precusor proteins were characterized conveniently *via* MALDI-ToF MS whereas it is very challenging to detect the polypeptide copolymers, most likely due to their high molecular weights as well as fragmentation during the measurement [43]. Therefore, in contrast to the functionalization of the polypeptide backbone, a *priori* modification of the native precursor proteins offers the great advantage that the number of functional groups could be assessed from the MALDI-ToF mass spectra. Chemically modified globular proteins such as cBSA (**2-9**) or aHSA (**2-12**) displayed well-defined signals in the MALDI-ToF mass spectra with comparable resolution to those of native proteins (**Figure 2-9a and c**). Preparation of denatured polypeptide copolymers from both modified albumin precursor proteins could be achieved *via* a similar procedure discussed above for dHSA-PEO(5000)$_{27}$ (**2-2**) (**Scheme 2-1**). The resulting polypeptide copolymers dcBSA-PEO(5000)$_{27}$ (**2-11**) and daHSA-PEO(5000)$_{27}$ (**2-14**) had

similar molecular weight as dHSA-PEO(5000)$_{27}$ (**2-2**) according to SDS-PAGE (**Figure 2-9b and d**).

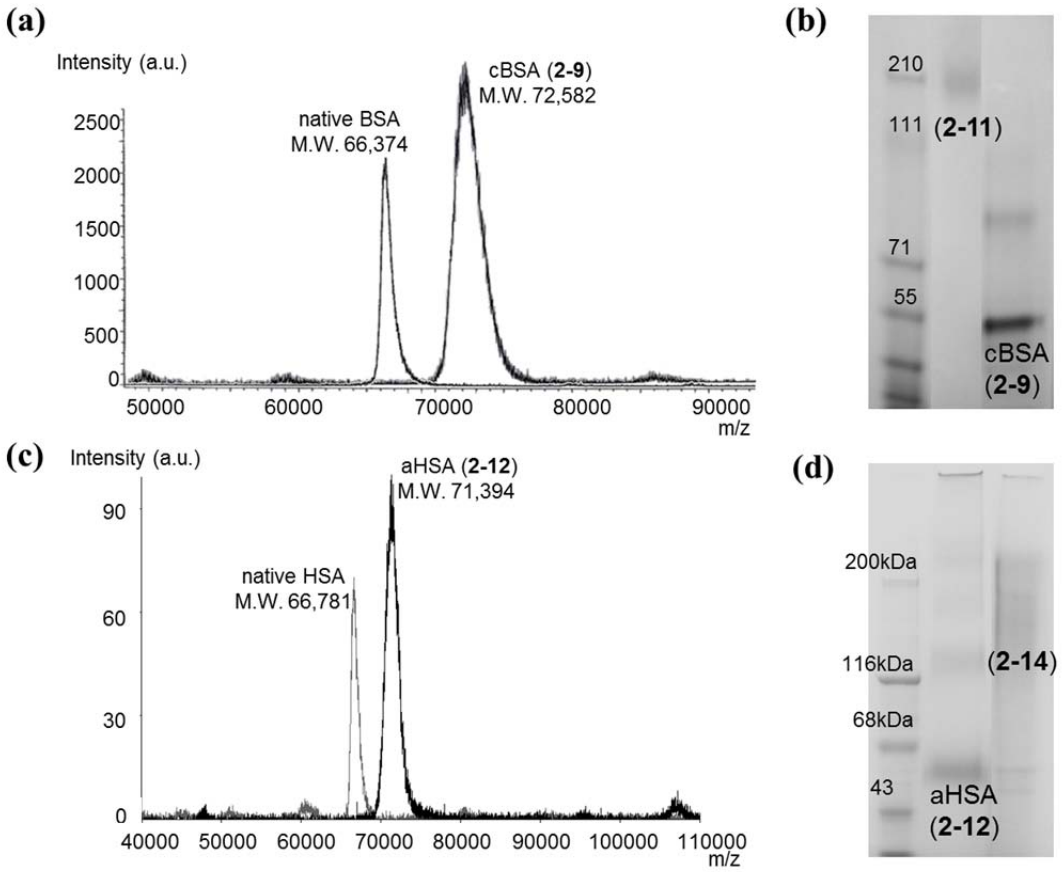

Figure 2-9. a) MALDI-ToF mass spectra of native BSA and cBSA (**2-9**); Matrix: Sinapinic acid. b). SDS-PAGE of cBSA and the corresponding PbPs (**2-11**). c). MALDI-ToF mass spectrum of aHSA (**2-12**) compared to native HSA. b). SDS-PAGE of aHSA and the corresponding polypeptide copolymers (**2-14**). Adapted with permission [1]. Copyright 2012, American Chemical Society.

2.3.2 Polypeptide copolymers containing multiple positive and negative charges along their backbones.

The distinct differences in the net surface charges between cBSA, aHSA and native HSA were demonstrated by gel electrophoresis at pH 7.4 (**Figure**

2-10a): cBSA shifted towards the negative electrode with a strong tailing due to its interaction with the agarose gel, whereas aHSA moved towards the positive electrode, indicating that it carried a negative net charge. Native HSA also bears slightly negative net charge therefore moved towards the positive electrode, however, at a significantly slower speed compared to aHSA. dcBSA-PEO(5000)$_{27}$ (**2-11**), daHSA-PEO(5000)$_{27}$ (**2-14**) and dHSA-PEO(5000)$_{27}$ (**2-2**) showed similar characteristics at physological pH (pH 7.4) as their native precursor proteins (**Figure 2-10a**), suggesting similar net charges.

The surface charges of all polypeptide copolymers were also characterized by zeta potential measurements and the results are summarized in **Figure 2-10b** and **Table 2-2**. A positive surface zeta potential of 23±3 mV and 5±1 mV was obtained for cBSA and LY, respectively, whereas a negative zeta potential of -10±4 mV was found for aHSA. The surface zeta potential of the respective polypeptide copolymers revealed some differences compared to the precursor proteins: dHSA-PEO(5000)$_{27}$ (**2-2**) and dcBSA-PEO(5000)$_{27}$ (**2-11**) revealed similar net charges as HSA and cBSA. In contrast, daHSA-PEO(5000)$_{27}$ (**2-14**) and dLY-PEO(5000)$_{8}$ (**2-4**) exhibited high negative net charges. These findings underlined that polypeptide polyelectrolytes with tunable charges and charge densities could be achieved. Polypeptides with fine tunable surface charges are highly significant for the synthesis of biopolymers with desired cell and tissue penetration properties [44]. In addition, the presence of multiple functional groups located along the polypeptide backbone would allow further

functionalization into complex biohybrid materials such as polymer-drug micelles [45, 46].

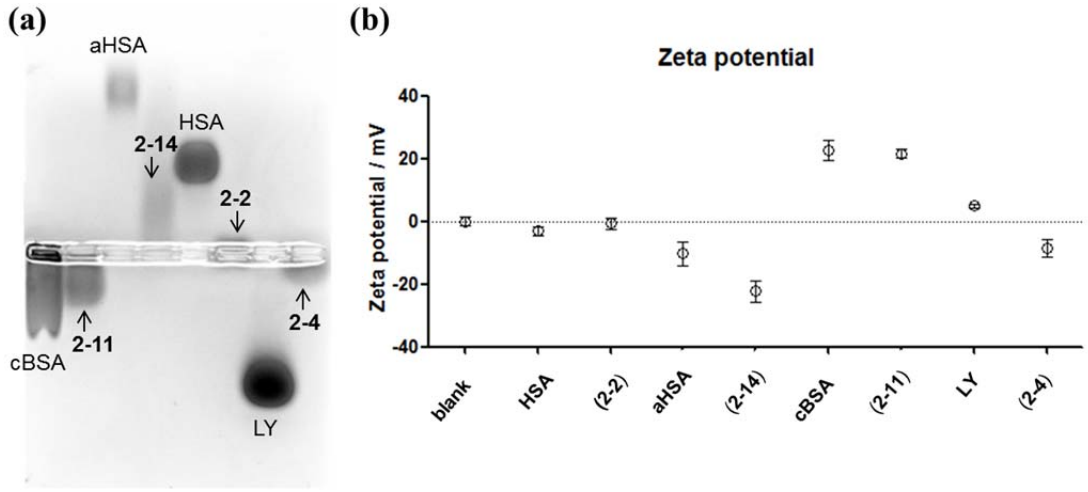

Figure 2-10. Characterization of the charge properties of polypeptide copolymers. a). Agarose gel electrophoresis at pH 7.4 compares charge properties of HSA, LY, cBSA, aHSA and their corresponding polypeptide copolymers (**2-2**), (**2-4**), (**2-11**) and (**2-14**). b). Zeta potential of all polypeptide copolymers compared with their precursor proteins. Reproduced with permission [1]. Copyright 2012, American Chemical Society.

2.3.3 Self-assembly of polyelectrolytes in aqueous solution.

As was also the case with the native protein derived polypeptides, the polycationic copolymer (**2-11**) and polyanionic copolymer (**2-14**) had a tendency to form micelles in aqueous solution due to the alternative hydrophobic and hydrophilic batches along the protein sequence [32]. The precursor proteins aHSA and cBSA revealed hydrodynamic diameters (d_H) of ~10 nm and 7 nm respectively according to the number average diameter obtained by dynamic light scattering (DLS) (**Table 2-2**). The extended structure of aHSA and cBSA compared to the native proteins (d_H = 5 nm for

HSA and d_H = 3 nm for LY) was most likely due to electrostatic repulsion as well as a larger solvent shell as discussed before [40]. In contrast, the size distribution by light scattering intensity yielded slightly larger d_H as well as a second population with d_H of ~150 nm and 120 nm respectively, which should correspond to some protein aggregations similar as observed in native proteins. The size distribution profiles of the polypeptide copolymers obtained by LS intensity indicated that two populations of (**2-11**) coexisted in aqueous solution. The smaller species with diameters of ~23 nm were most likely single chain macromolecules, whereas the larger polypeptide aggregates exhibited diameters of ~151 nm (**2-11**). A similar aggregation behavior was observed for copolymer (**2-2**). In the case of (**2-14**), only polypeptide aggregates of 163 nm were observed. Taking the number distribution into consideration, the majority of species of (**2-11**) in solution were present as single chains with average d_H of 15 nm, indicating that the number of polypeptide aggregates generated was much smaller than the number of non-aggregated, single chain polypeptides. Differences in the size of the polypeptide species found in solution could be due to a variety of effects, including electrostatic repulsion of the negatively charged backbone leading to coil expansion, different levels of counterion condensation depending on the average spacing between backbone charges, a hydrophobic collapse caused by a larger content of hydrophobic amino acids, and a higher degree of more compact secondary structures such as α-helix or β-sheet structures [32], etc. This feature could be highly attractive to design efficient nanocarriers for medicinal applications.

Table 2-2. Summary of molecular weight (M.W.), zeta potential, size distribution in aqueous solution, complete proteolysis digestion time and cell uptake efficiency of various polypeptide copolymers and their precursor proteins.

Sample name	M.W. (kDa)	Zeta potential (mV)	Diameter (H_2O, nm)[c]	PDI [a]	Diameter (H_2O, nm)[d]	Digestion time[e] (min)	Cell Uptake
cBSA	71[a]	23±3	7±1	0.27	13±1 149±36	/	+
dcBSA-$PEO(5000)_{27}$	205[b]	22±2	15±4	0.41	23±4 151±28	30	+
aHSA	71[a]	-10±4	10±2	0.26	12±1 119±38	/	/
daHSA-$PEO(5000)_{27}$	205[b]	-22±3	120±21	0.27	163±18	120	/

[a.] Molecular weight obtained by MALDI-ToF spectra.
[b.] Molecular weight according to SDS-PAGE and theoretical calculation.
[c.] According to DLS measurements based on number using approximately 0.1 mg/mL of each protein in aqueous solution.
[d.] According to DLS measurements based on intensity using approximately 0.1 mg/mL of each protein in aqueous solution.
[e.] Digestion time was estimated with 0.1% trypsin and analyzed by SDS-PAGE. Detailed SDS-PAGE pictures are shown in **Figure 2-12**.

2.3.4 Modified polypeptide copolymers with non-cytotoxicity and biodegradability

Polypeptides with different charge properties could be very attractive for drug delivery applications. Therefore, we further studied the biocompatibility of the *a priori* modified polypeptide copolymers. Similar as for the native protein derived polypeptides, we investigated the cytotoxicity of these copolymers in A549 cells from 0.1 μM to 50 μM concentrations and no significant cytotoxicity was observed for any copolymer (**Figure 2-11**). Moreover, after *in vitro* treatment with 0.1% trypsin, copolymers (**2-11**) were digested into small peptide fragments within 2 hr only (**Table 2-2** and **Figure 2-12**), which is comparable with the native protein derived copolymers (**2-2**), (**2-4**) and (**2-8**). Interestingly, the polyanionic copolymer (**2-14**) exhibited a significantly slower

digestion rate most likely due to the modification on lysine residues since trypsin was known to cleave peptide chains at the C-terminus of lysine and arginine [47]. Notably, in the absence of proteases, all copolymers showed high stability in the solid state as well as in aqueous solution for up to 6 months.

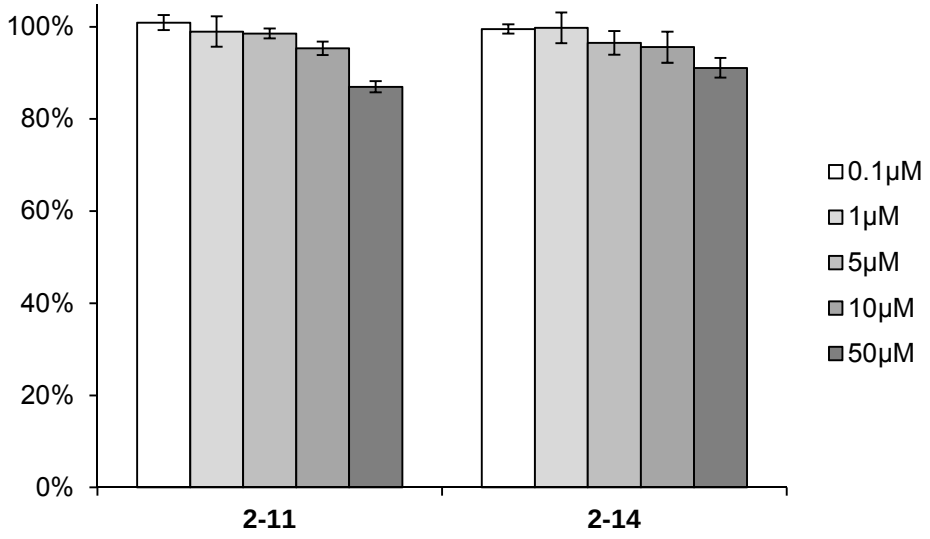

Figure 2-11. Cell viability assay showing no significant cytotoxicity of polypeptide copolymer (**2-11**) and (**2-14**). (n=3, standard deviation presented as error).

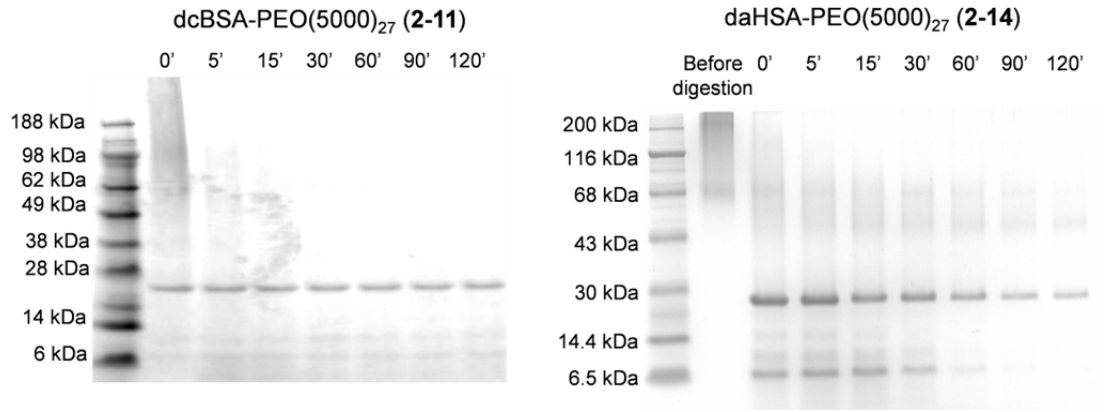

Figure 2-12. Trypsin digestion of polypeptide copolymer (**2-11**) and (**2-14**) analyzed by 4%-10% SDS-PAGE. Adapted with permission [1]. Copyright 2012, American Chemical Society.

2.3.5 Tunable cell uptake efficiency

Cell uptake of positively charged and negatively charged copolymers was studied by applying the respective rhodamine-labeled derivatives in A549 cells. It was shown previously that cBSA could be quickly uptaken by clathrin-mediated endocytosis and released into the cytoplasm [40], in contrast, HSA revealed no significant cellular uptake. The corresponding copolymers displayed a very similar uptake profile. By laser scanning confocal microscopy (LSCM), cBSA derived cationic polypeptide (**2-11**) was significantly uptaken by cells whereas HSA-derived polyanionic polypeptide (**2-2**) was not found inside the cell most likely due to repulsive forces between the biopolymer and the negatively charged cellular membranes (**Figure 2-13**). In this way, cell uptake of the copolymers could be fine-tuned by attaching e.g. positively charged functionalities to the precursor proteins. There might be certain situation where cell uptake of the copolymer might not be desirable, e.g. extracellular targets such as membrane receptors or structures of the extracellular matrix should be addressed for bioimaging purposes. In this case, high non-specific cell uptake might lead to reduced contrast and undesired intracellular effects might occur. In contrast, efficient cell uptake and low proteolytic stability were particularly attractive for drug delivery systems. In particular, cBSA derived polypeptide (**2-11**) represented promising platform for transporting drug molecules into cells.

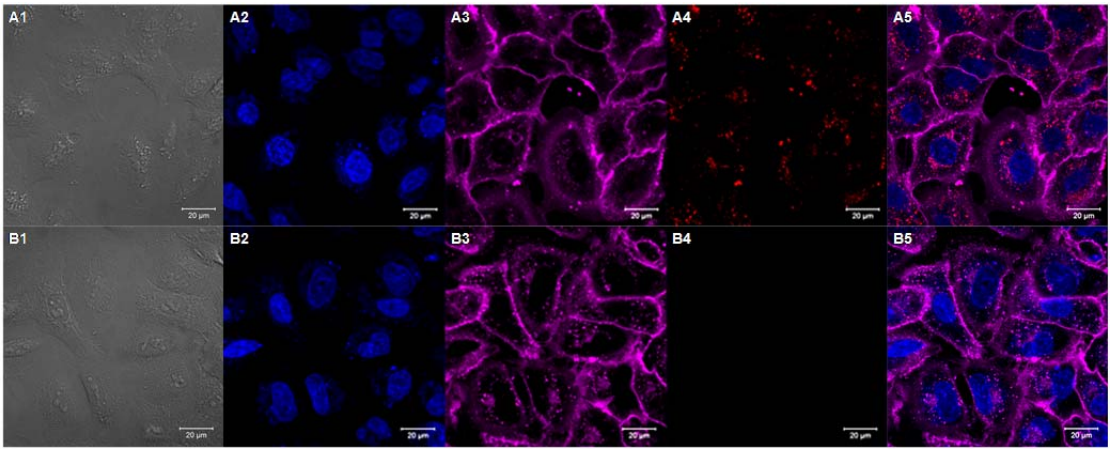

Figure 2-13. LSCM imaging of rhodamine labeled (**2-2**) (B1-B5) and (**2-11**) (A1-A5) incubated with A549 cells for 24 hr. A1 and B1 represent bright field images; A2 and B2 are cell nucleus stained by DAPI nucleus staining; A3 and B3 are cell membranes stained by CellMask® Deep Red plasma membrane stain; A4 and B4 are fluorescence channel for rhodamine emission; A5 and B5 are overlay of channel 2 to 4. Reproduced with permission [1]. Copyright 2012, American Chemical Society.

2.4 *A posteriori* modification to introduce tunable copolymer properties

Functionalized protein-derived copolymers could be achieved by *a priori* modification of the native globular protein precursor, as demonstrated in section 2.3. Alternatively, further functionalities could also be introduced by *a posteriori* modification of the pegylated denatured protein copolymers. Native proteins consist of 20 amino acids with diverse functional groups on the side chains. Therefore, the resulting polypeptide copolymers also contained a large number of reactive groups ready for further chemical modifications. Moreover, since the location of these functional groups could were precisely defined based on the sequence of protein precursors, the position of further

modified functionaliites could be predicted in principle. Such a unique property of protein-derived polymers cannot be achieved for synthetic high molecular weight polymers. *Via* this approach, we successfully introduced different functional moieties into these polypeptide copolymers, including bio-orthogonal functional groups (e.g. ethynyl group), nanoparticle attachment units (e.g. thioctic acid), chromophore molecules (e.g. coumarin) and anticancer drugs (e.g. DOX) (**Figure 2-14**).

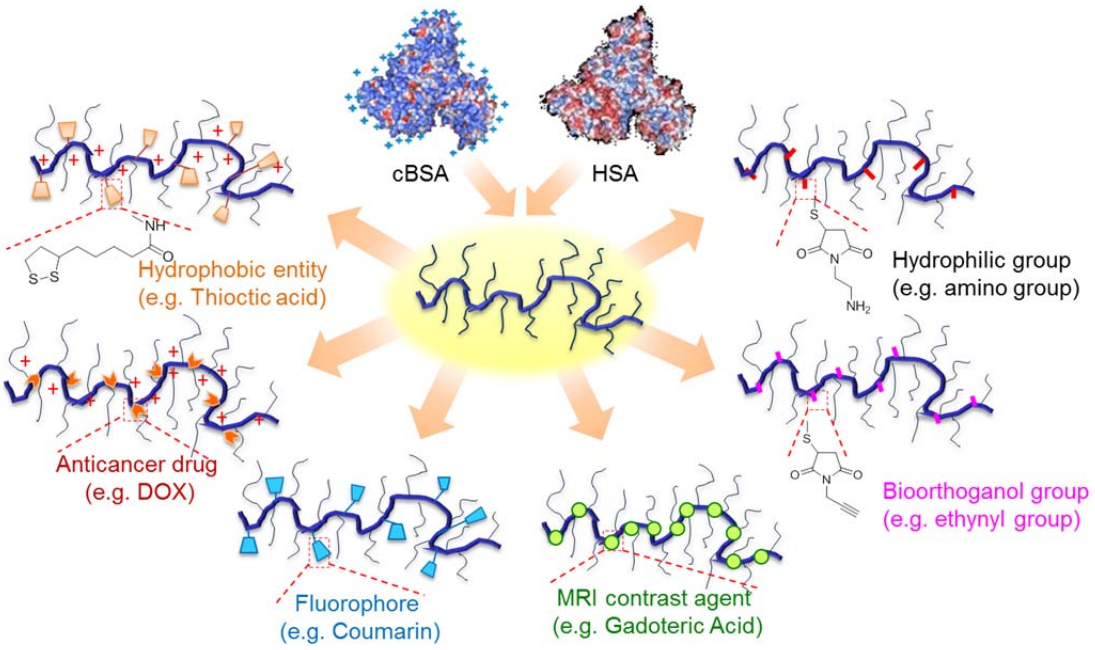

Figure 2-14. Illustration of *a posteriori* modification of PbPs for different applications.

2.4.1 *A posteriori* modification tuning the hydrophobicity of the polypeptides

Albumin derived polypeptide copolymer (**2-11**) consists of 27 PEO chains conjugated on 35 cysteine residues as described in the previous sections.

The remaining, unmodified 8 cysteine residues need to be capped with appropriate small molecules during preparation in order to achieve denatured polypeptides with long term stability and no cross-linking between the chains. In the previous sections, we demonstrated a capping step using *N*-(2-aminoethyl)maleimide which introduces additional amino groups into the resulting polypeptides. In principle, other functional groups can also be introduced into the polypeptide sequence in the same way at this step by using appropriate maleimide-containing reagents to tailor the properties of these biopolymers. For instance, *N*-propargyl maleimide was successfully applied as an alternative capping molecule instead of *N*-(2-aminoethyl)maleimide. As a result, a more hydrophobic polypeptide dcBSA-PEO(5000)$_{27}$-alkyne (**2-15**) was achieved that facilitated bioorthogonal chemical ligation reactions on the alkyne groups. Complete capping of all thiol groups was also confirmed by the thiol quantification assay (DPS test).

The primary amino groups of biopolymer (**2-11**) were positively charged at physiological pH, whereas ethynyl groups were significantly more hydrophobic. The introduction of additional hydrophobic groups along the polypeptide backbone, such as shown in (**2-15**), would lead to subtle changes of the lipophilicity of the polypeptide chain and influence the 3D structure of such polymers in solution. According to DLS studies, the attachment of only 8 ethynyl groups had a considerable impact on the average hydrodynamic diameters of the polypeptide copolymers (**Table 2-3**). Native BSA had a hydrodynamic diameter (d_H) of ~2.1 nm, in contrast, the d_H increased to ~7.2

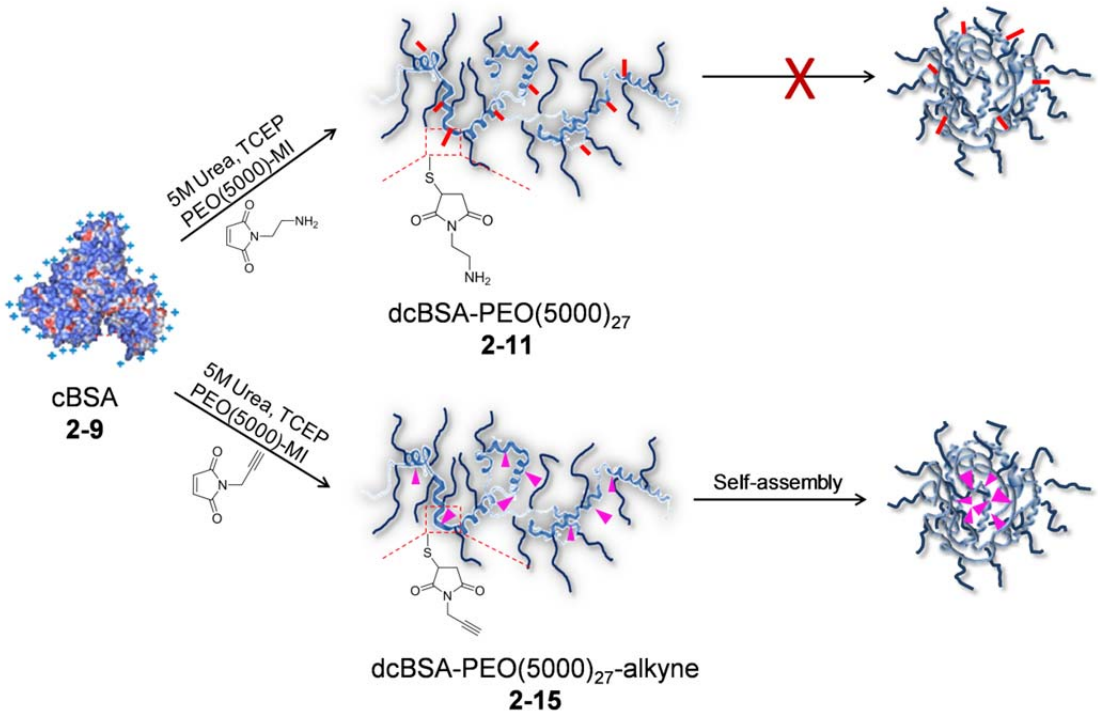

Scheme 2-3. Tune the hydrophobicity of polypeptide copolymer *via* ethynyl decoration.

nm for cBSA with additional amino groups. Such an increase most likely resulted from a larger solvent shell as well as a more extended 3D architecture due to electrostatic repulsion forces [42]. The attachment of additional PEO chains and capping with *N*-(2-aminoethyl)maleimide led to a further increase in the d_H to ~15.2 nm, accompanied by larger aggregates (~150 nm) according to DLS intensity distributions. However, after capping with *N*-propargyl maleimide, the d_H of polypeptide (**2-15**) was only 5.1 nm, which suggested the formation of more compact architectures in solution most likely due to the presence of additional hydrophobic interactions.

The morphologies of copolymer (**2-15**), in parallel to copolymer (**2-11**), were also examined by TEM with uranyl acetate staining (**Figure 2-15a**).

Copolymer (**2-2**) with additional amino groups formed more amorphous structures. In contrast, copolymer (**2-15**) with additional ethynyl side chains adopted more globular architectures. These observations suggested micelle formation of copolymer (**2-15**). Such globular, compact micelles exhibited even smaller dimensions compared to the precursor protein cBSA and most likely provided a hydrophobic interior where the ethynyl groups were facing to the inside. In this way, a protein-like nanoreactor bearing ethynyl functionalities was formed, which in principle allowed click reactions with azido-containing reagents.

In order to assess the capacity of polypeptides (**2-11**) and (**2-15**) to upload lipophilic guest molecules *via* hydrophobic interactions, extraction experiments were undertaken. The hydrophobic chromophore 3-azidocoumarin (**Scheme 2-8**) was dissolved in ethyl acetate (EA) and the solution was extracted with the same amount of water containing either 1 μM polypeptide (**2-11**) or 1 μM copolymer (**2-15**) solution. As shown in (**Figure 2-15b**), the extraction tube containing polypeptide (**2-15**)**,** upon visual comparison, displayed the highest colour intensity in the aqueous layer and correspondingly the lowest intensity in the EA layer. Moreover, according to the absorbance spectrum, the highest coumarin absorbance was also detected in solution containing polypeptide (**2-15**), whereas a similar absorbance was observed for the solution with polypeptide (**2-11**) compared with water solution indicating that (**2-11**) is not able to extract 3-azidocoumarin.

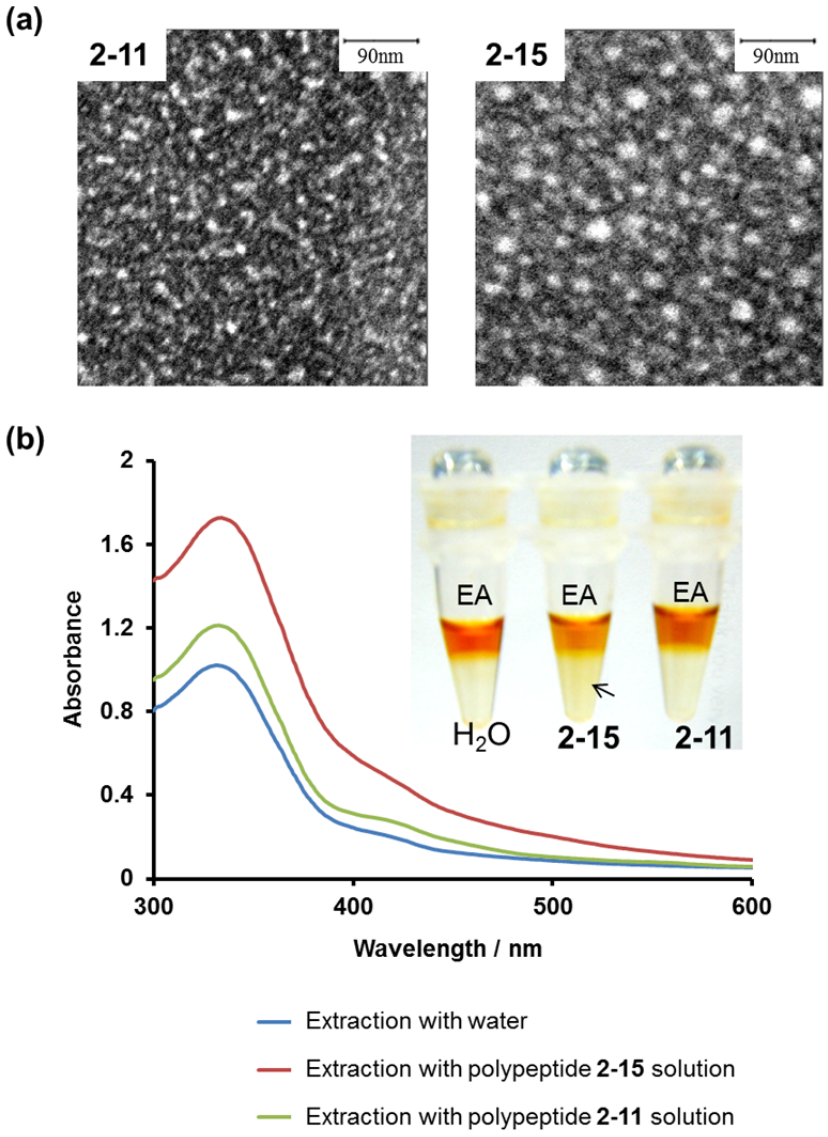

Figure 2-15. (a) TEM imaging after uranyl acetate staining (90 nm scale bar) of dcBSA-PEO(5000)$_{27}$ (**2-11**) and dcBSA-PEO(5000)$_{27}$-alkyne (**2-15**). (b) Extraction of 3-azidocoumarin with water (blue line), 1 μM copolymer (**2-11**) solution (green line) and 1 μM copolymer (**2-15**) solution (red line). Absorbance spectra are recorded with 100 μL of extracted aqueous layer, respectively. Reproduced with permission [48]. Copyright 2012, Wiley-VCH.

Table 2-3. Summary of hydrodynamic radii and PDI determined by DLS (n=5, standard deviation presented as error).

Name of copolymer	Hydrodynamic radius	PDI
BSA	2.1±0.1 nm	0.38
cBSA	7.2±0.5 nm	0.27
dcBSA-PEO(5000)$_{27}$ **2-11**	15.2±3.9 nm	0.41
dcBSA-PEO(5000)$_{27}$-alkyne **2-15**	5.1±0.4 nm	0.32

The observed differences of the architectures and drug loading capacities between copolymer (**2-11**) and (**2-15**) could be attributed to subtle polarity changes of their polypeptide backbones since only ~8 additional substituents were introduced to the biopolymers. These findings highlighted the unique features of copolymers derived from proteins since dense packing into stable, nanoscopic and homogeneous monomolecular micelles represented one of the major characteristics of proteins. Therefore, due to the amphiphilic nature of such polypeptides resulting from the hydrophobic amino acids statistically distributed along the polypeptide backbone, just a few additional lipophilic groups were sufficient to induce a collapse of the 3D structure leading to the formation of ultra-small micelles. Moreover, serum albumin proteins act as transport proteins in blood due to their several hydrophobic pockets that can accommodate hydrophobic guest molecules, such as lipids [49]. Notably, such important features were retained after the formation of the micelles of polypeptide (**2-15**).

2.4.2 *A posteriori* modification tuning the surface patterning of the polypeptides

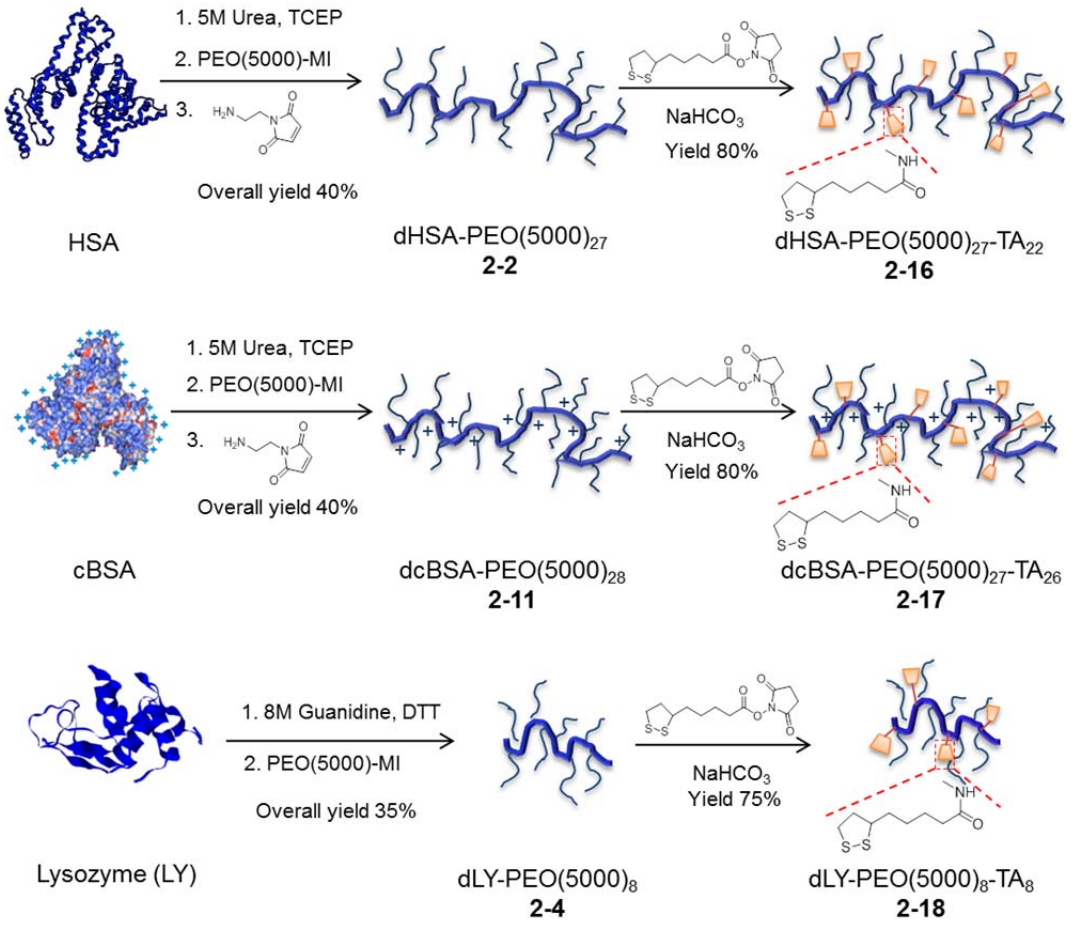

Scheme 2-4. Preparation of thioctic acid functionalized PbPs.

All polypeptide copolymers (**2-2**), (**2-4**) and (**2-11**) provide several reactive primary amino functionalities that allow attaching multiple lipophilic thioctic acid (TA) groups. The attachment of TA substituents is particularly attractive since they can facilitate interactions with a broad range of metal or semiconductor surfaces *via* controlled disulfide reductions. In addition, they can give rise to a higher lipophilicity along the polypeptide backbone which is expected to affect the amount of secondary structure elements. After

treatment of copolymers (**2-2**), (**2-4**) and (**2-11**) with N-hydroxysuccinimide (NHS)-activated TA, copolymers dHSA-PEO(5000)$_{27}$-TA$_{22}$ (**2-16**), dcBSA-PEO(5000)$_{27}$-TA$_{26}$ (**2-17**) and dLY-PEO(5000)$_{8}$-TA$_{8}$ (**2-18**) were isolated in good yields carrying 22±5, 26±3 and 8±3 TA groups, respectively, as quantified by the DPS test and SDS-PAGE (**Figure 2-16**). According to DLS, similar as polypeptide (**2-15**), the attachment of a large number of lipophilic TA groups in polypeptide (**2-17**), also yields a significant decrease of the d_H to 4.2 nm, indicating a similar collapse of the polypeptide architecture as in case of (**2-15**).

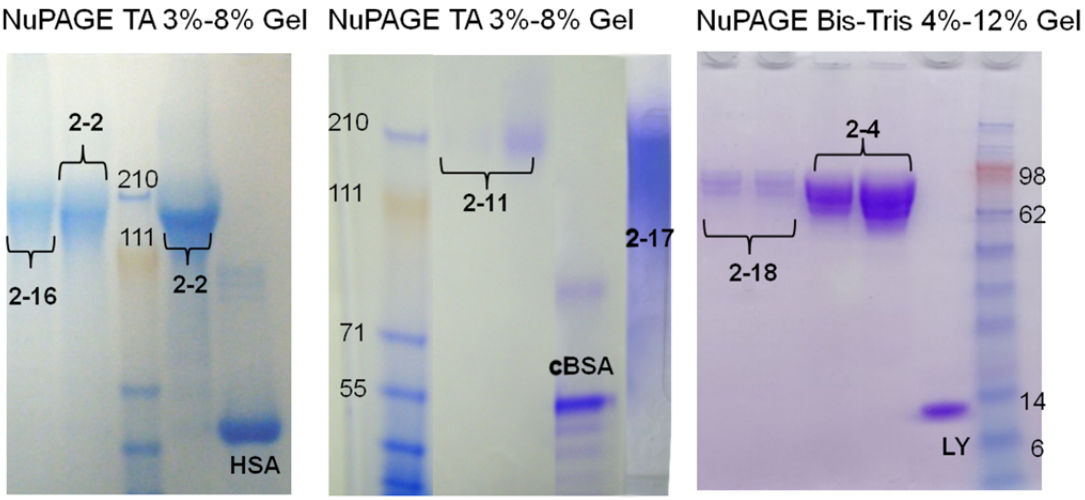

Figure 2-16. SDS-PAGE analysis of thioctic acid functionalized PbPs. Adapted with permission [1]. Copyright 2012, American Chemical Society.

CD spectra of copolymers (**2-2**), (**2-4**) and (**2-7**) displayed relatively low percentages of α-helical structures (0%~13%). In contrast, the attachment of TA along the backbone induced a significant increase of α-helix elements in copolymers (**2-16**), (**2-17**) and (**2-18**) (19% ~44%) (**Figure 2-17 and Figure 2-18**). Although this phenomenon was still barely understood, we speculated that TA motifs contributed to the formation of lipophilic patches along the polypeptide backbone and thus stabilized more compact α-helical structures.

In contrast, previous reports showed an increase in β-sheet structures after introducing additional lipophilic patches that facilitated amyloid fiber formation [27].

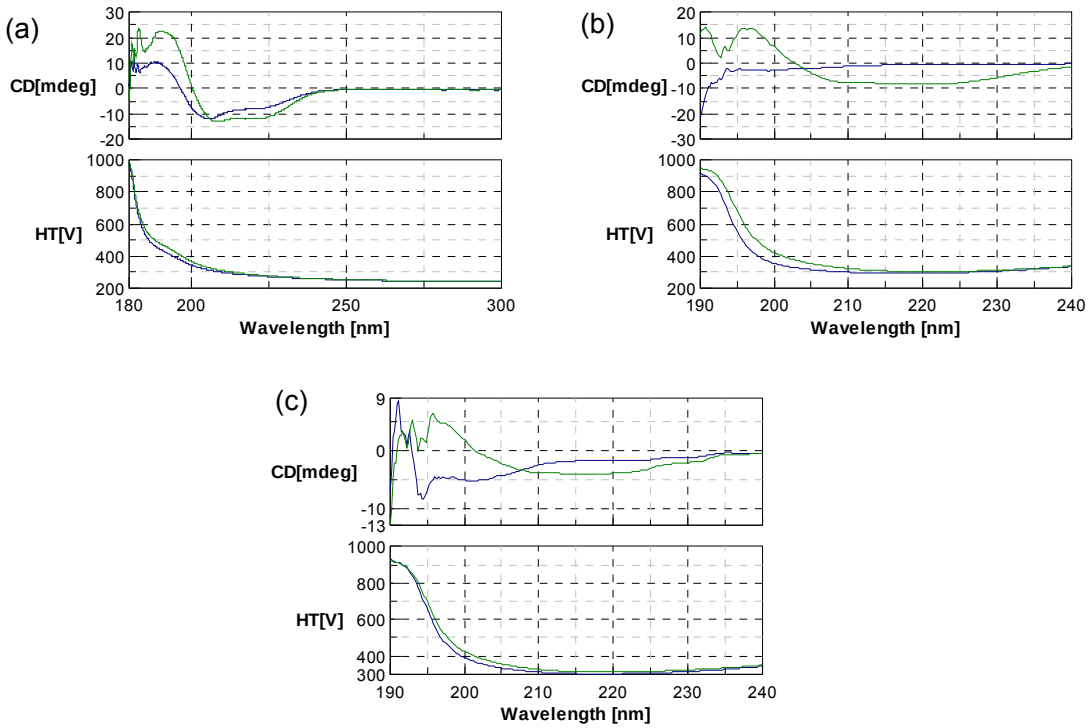

Figure 2-17. CD spectra of a) dHSA-PEO(5000)$_{27}$ (**2-2**, blue line) and dHSA-PEO(5000)$_{27}$-TA$_{22}$ (**2-16**, green line); b) dcBSA-PEO(5000)$_{27}$ (**2-11**, blue line) and dcBSA-PEO(5000)$_{27}$-TA$_{26}$ (**2-17**, green line) and c) dLY-PEO(5000)$_{8}$ (**2-4**, blue line) and dLY-PEO(5000)$_{8}$-TA$_{8}$ (**2-18**, green line).

It is well known that native albumins and lysozyme form amorphous aggregates on surfaces [50], whereas single layer proteins, responsible for important processes on the surface of cellular membrane, crystallize into highly ordered superstructures [51]. It has been previously shown for that hierarchical self-assembly on the mica surface of α-helical-enriched coiled-coil peptides resulted in the formation of fractal superstructures [52]. Heat induced transition of the secondary structure of a short coiled-coil peptide yielded the

formation of different aggregate morphologies [27]. Up to now, there are only a few studies on the self-assembly of protein- or polypeptide- polymer hybrid molecules on surfaces [53]. In particular, the impact of the nature of secondary structure elements as well as their frequency of occurrence on surface supported self-assembly has not been investigated yet despite their great potential for bio- and nanotechnological applications. Therefore, in our study, the 2D crystallization behavior of copolymers (**2-16**), (**2-17**) and (**2-18**) was investigated and compared with copolymers (**2-2**), (**2-11**) and (**2-4**) on a mica surface *via* atomic force microscopy (AFM) analysis (these experiments were performed by Dr. Christoph Meier). All copolymers crystallized upon evaporation of the solvent into distinct aggregates and superstructures (**Figure 2-18**). Among them, both HSA copolymers (**2-2**) and (**2-16**) contained significant amount of folded peptide backbone with highest CD signal intensity (**Figure 2-17**) and deposited into globular particles regardless of the presence or absence of $MgCl_2$. In contrast, the large amount of primary amines caused charge repulsion in cBSA derived copolymers (**2-11**) and (**2-17**) induced a decrease of secondary structure elements and particularly copolymer (**2-11**) exhibited an almost completely denatured structure (**Figure 2-17**). Such high degree of denaturation imposed a high exposure of hydrophobic residues and therefore copolymers (**2-11**) and (**2-17**) self-assembled into branched superstructures during crystallization most likely due to hydrophobic interactions. Interestingly, β-sheet-rich derivative (**2-11**) contained additional linear fine structures which were absent in the superstructure of the α-helix-rich derivative (**2-17**). This observation indicated that more compact aggregates were formed most likely due to the overall higher amount of

secondary structures, thus yielding more compact and rigid molecules. In the case of copolymer (**2-4**), a distinctively different 2D crystallization behavior was observed. Here, linear fiber-like aggregates with a uniform thickness of ~10 nm were formed, which acted as nucleation points for branches of ~6 nm in height. In contrast, the corresponding TA-derivative (**2-18**) formed highly branched structures with a uniform height of ~6 nm. In addition to their similar nm heights, the lateral dimensions of the formed superstructures well exceeded into the sub-mm range (**Figure 2-18**). This remarkable feature addressed one of the main challenges in nanotechnology, namely producing self-assembled structures that incorporate structural features ranging from the nano- to the macro-scale. Since the TA groups were buried within the comparatively long PEO side chains, it is believed that polymer-substrate interactions were mainly governed by the PEO side chains. The TA residues, as indicated by the CD measurement, altered the secondary structure and further 3D conformation *via* hydrophobic interactions and thus formed lipophilic patches buried in the protein core. Our findings indicated that the 3D conformation of the investigated protein copolymers had a significant impact on intermolecular and molecule-substrate interactions. The individual 3D conformation, the rigidity of the peptide backbone and the non-covalent interactions between the PEO side chains could be considered as the main structure-determining parameters for these novel grafted polypeptide copolymers. Therefore, manipulation of the content of lipophilic patches, rigid and flexible secondary structure elements as well as the length of the polymer backbone opened up access to unique nanostructured multifunctional and biocompatible surface coatings.

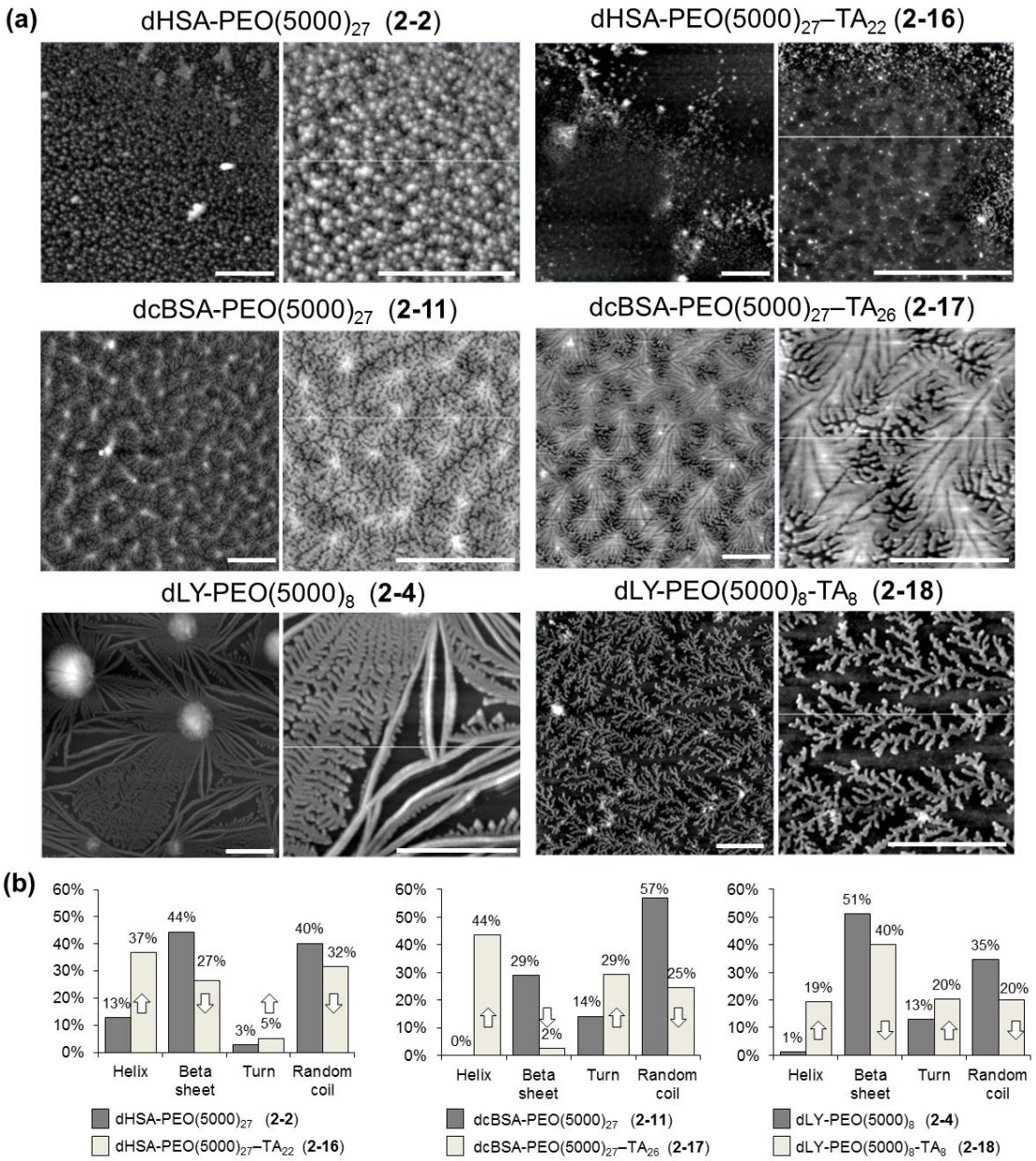

Figure 2-18. (a) AFM image of Protein-derived copolymers deposited on mica *via* drop casting. Left panel: Pegylated copolymers (**2-2**), (**2-11**) and (**2-4**), Right panels: Thiolated copolymers (**2-16**), (**2-17**) and (**2-18**). Scale bars are 2 μm.[‡] (b) Relative amounts of secondary structure elements of all copolymers as measured by circular dichroism (dark color: Pegylated copolymers, light color: Thiolated copolymers).

[‡] This data was provided by Dr. Christoph Meier.

2.4.3 Introduction of functional moieties *via a posteriori* modification.

Beside of tuning the material properties, additional functional entities could also be conjugated to the polypeptide copolymers *via a posteriori* modification strategy. Such modifications were especially significant and attractive since the attachment of multiple functional moieties, such as drug molecules, imaging reagents or cell targeting units, on a degradable polymer is important for biomedical applications. In view of this, we successfully introduced therapeutic molecules, chromophores and MRI contrast agents to the protein backbone by reaction with its native functional groups. The synthetic concept will be briefly introduced in this chapter, and more variations and detailed applications will be discussed in Chapter 4.

2.4.3.1 Conjugation of a chromophore and anti-cancer drug *via* click reaction

It was demonstrated that ethynyl functionalized PbPs (**2-15**) exhibited higher hydrophobicity and higher capacity to interact with hydrophobic molecules (Section 2.4.1). The successful extraction of 3-azidocoumarin with an aqueous solution of polypeptide (**2-15**) suggested a high capacity of (**2-15**) to interact with and accommodate 3-azidocoumarin guest molecules in its hydrophobic interior, leading to significant increase in the local concentration of 3-azidocoumarin in water. Therefore, in principle, this polypeptide could serve as an efficient nanoreactor for concentrating hydrophobic molecules in its interior. 3-Azidocoumarin has emerged as a widely applicable labeling agent that only fluoresces when the triazole moiety is formed [54], which was thus used to monitor and quantify click conjugation reactions in the present study. As shown in **Scheme 2-5**, 3-azidocoumarin (50 equivalents) was

treated with polypeptide (**2-15**) in a 1:1 mixture of water and THF, followed by the addition of $CuSO_4$ (25 equivalents) and sodium ascorbate (50 equivalents) as catalyst and reducing agent, respectively. After the reaction, THF was evaporated and the residue was extracted by dichloromethane (DCM) to remove the unreacted 3-azidocoumarin. Subsequently, any non-specifically adsorbed 3-azidocoumarin was removed by ultrafiltration in concentrated urea buffer and pure water to afford coumarin-labeled copolymer (**2-20**) in 70% yield after lyophilisation.

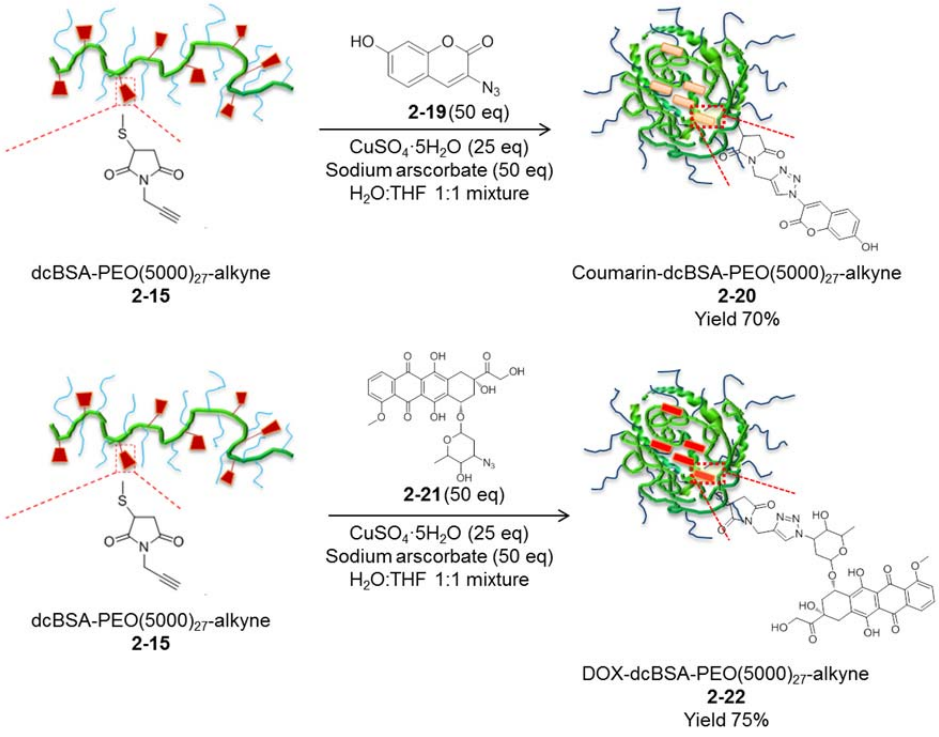

Scheme 2-5. Conjugation of 3-azidocoumarin and azido-DOX with dcBSA-PEO(5000)$_{27}$-alkyne (**2-15**) *via* click reactions. Adapted with permission [48]. Copyright 2012, Wiley-VCH.

The emission and absorbance spectra of coumarin-polypeptide (**2-20**) dissolved in water were shown in **Figure 2-19c**. The characteristic emission of

the coumarin chromophore proved successful formation of the triazol group *via* click reaction. Besides, a fluorescent band corresponding to the Coomassie stained protein band was observed on the SDS-PAGE, indicating a newly formed covalent linkage of coumarin to the polypeptide backbone. According to DLS analysis, the coumarin-polypeptide micelles had an average d_H of ~7.6 nm (**Figure 2-20**), which was slightly larger compared to the polypeptide (**2-15**) micelles due to the presence of guest molecules. The amount of coumarin molecules conjugated into (**2-20**) was calculated based on the absorbance ratio. On average about ~5.5 coumarin molecules had reacted with each polypeptide, which was in accordance with the approximate number of available ethynyl-groups and indicated an efficient conversion. The coumarin-polypeptide (**2-20**) represented a new class of fluorescent biopolymer and cell studies were firstly performed to assess the cytotoxicity as well as cell uptake of (**2-20**). As shown in **Figure 2-19d**, when treating HeLa cells (a mammalian cancer cell line widely used in laboratory) with (**2-20**) for 24 hr, a significant fluorescence signal was found inside cells compared with the blank control without treatment of (**2-20**), indicating a successful cell uptake of (**2-20**). No significant cytotoxicity was observed in HeLa cells at relevant concentrations as shown in **Figure 2-21a,** suggesting that they could be of interest for drug delivery applications.

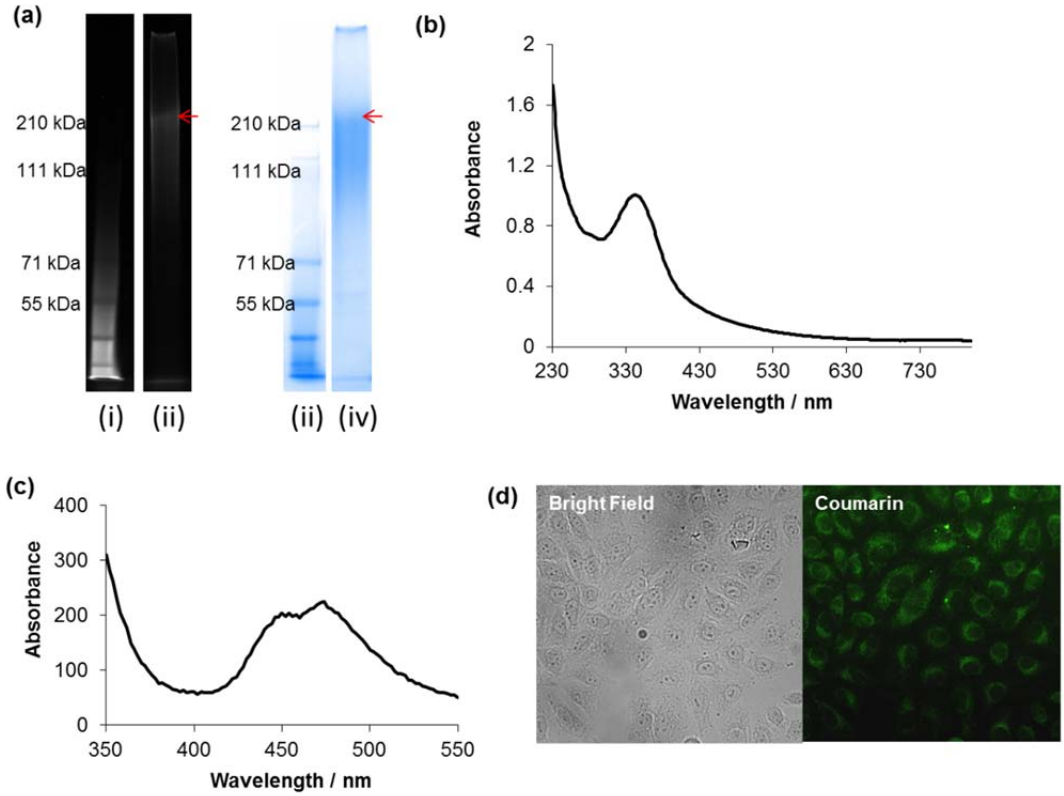

Figure 2-19. (a). SDS-PAGE characterization of coumarin conjugated polypeptide (**2-20**). Fluorescent image of (i) protein makers and (ii) (**2-20**) and the Coomassie stained image of (iii) protein makers and (iv) (**2-20**) are compared. Protein bands are indicated with arrow. (b). Absorbance spectrum and (c) emission spectrum (λ_{ex} = 254 nm) of the conjugate coumarin-polypeptide (**2-20**). (d) Cell imaging of using coumarin-polypeptide (**2-20**) by fluorescence microscopy (λ_{ex} = 405 nm). Reproduced with permission [48]. Copyright 2012, Wiley-VCH.

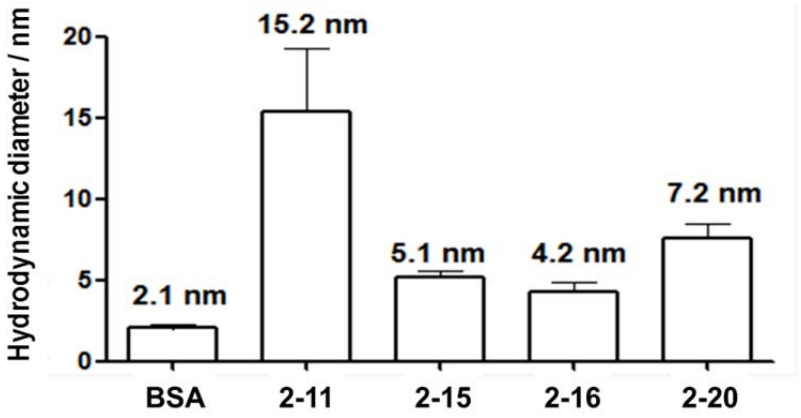

Figure 2-20. Size distribution of functionalized PbPs in solution according to DLS.

In the next step, the well-known anti-cancer drug doxorubicin (DOX) was also attached to the polypeptide (**2-15**) *via* click reactions. As shown in **Scheme 2-5**, azido functionalized DOX (**2-21**) was synthesized and underwent click reaction with polypeptide (**2-15**) to give DOX conjugated PbP (**2-22**), followed by the purification procedure described above for the preparation of (**2-20**). The average number of DOX molecules along the backbone was also calculated according to absorbance. About 5 DOX molecules were conjugated to polypeptide (**2-22**), which was in good agreement with the number of coumarin molecules conjugated to (**2-20**).

In contrast to the coumarin conjugated (**2-20**) which showed negligible cytotoxicity at 1 μM concentration, the DOX conjugate (**2-22**) revealed significant cytotoxicity (IC_{50} of 1.13 ±1.07 μM), which is in a similar range as the free DOX HCl (IC_{50} of 1.39 ±1.06 μM) (**Figure 2-21b**). In addition, notably, the denatured protein backbone released many more functional groups of the amino acid side chains available for further chemical modifications, such as introducing cell targeting entities. In view of these advantages, dcBSA-

PEO(5000)$_{27}$-alkyne (**2-15**) represents an attractive biopolymer allowing various post modification which might be particularly suited as a versatile drug delivery platform.

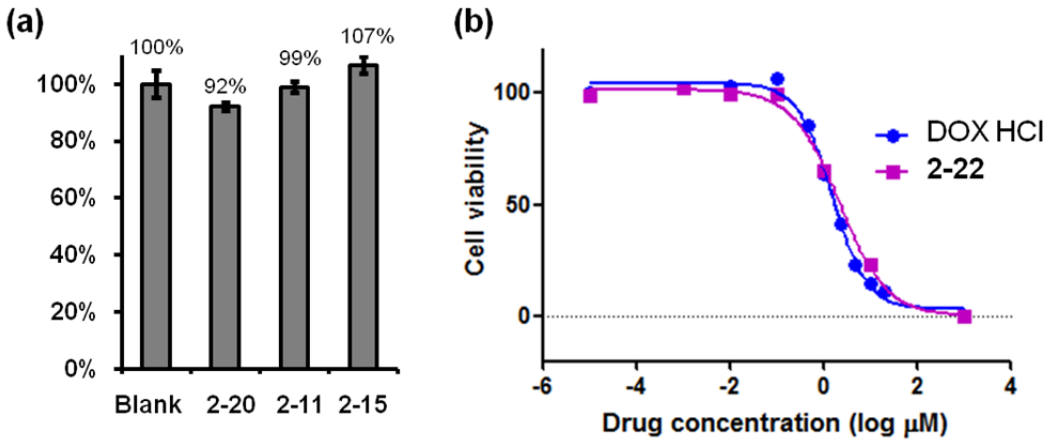

Figure 2-21. (a) Cytotoxicity of 1 µM of polypeptide (**2-11**), (**2-15**) and coumarin-conjugated copolymer (**2-20**). (b) Cytotoxicity of DOX loaded copolymer (**2-22**) compared with free DOX HCl. Reproduced with permission [48]. Copyright 2012, Wiley-VCH.

2.4.3.2 Conjugation of anti-cancer drugs *via* Michael addition reaction

The thiol groups of cysteine residues is known to undergo rapid Michael addition to maleimide functionalized molecules. This reaction provides an alternative method for efficient bioconjugation. In the previous synthetic approach introduced in Section 2.2, all the accessible cysteine residues were capped with PEO chains to maintain the stability of these biopolymers. However, the PEO chains alternatively could also be conjugated to lysine residues on protein surface before denaturation, so that the cysteine residues would be available for functionalization which provided additional possibilities toward multifunctional materials. This novel strategy will be demonstrated by

conjugating anticancer prodrug DOX-EMCH in the following section (**Scheme 2-6**).

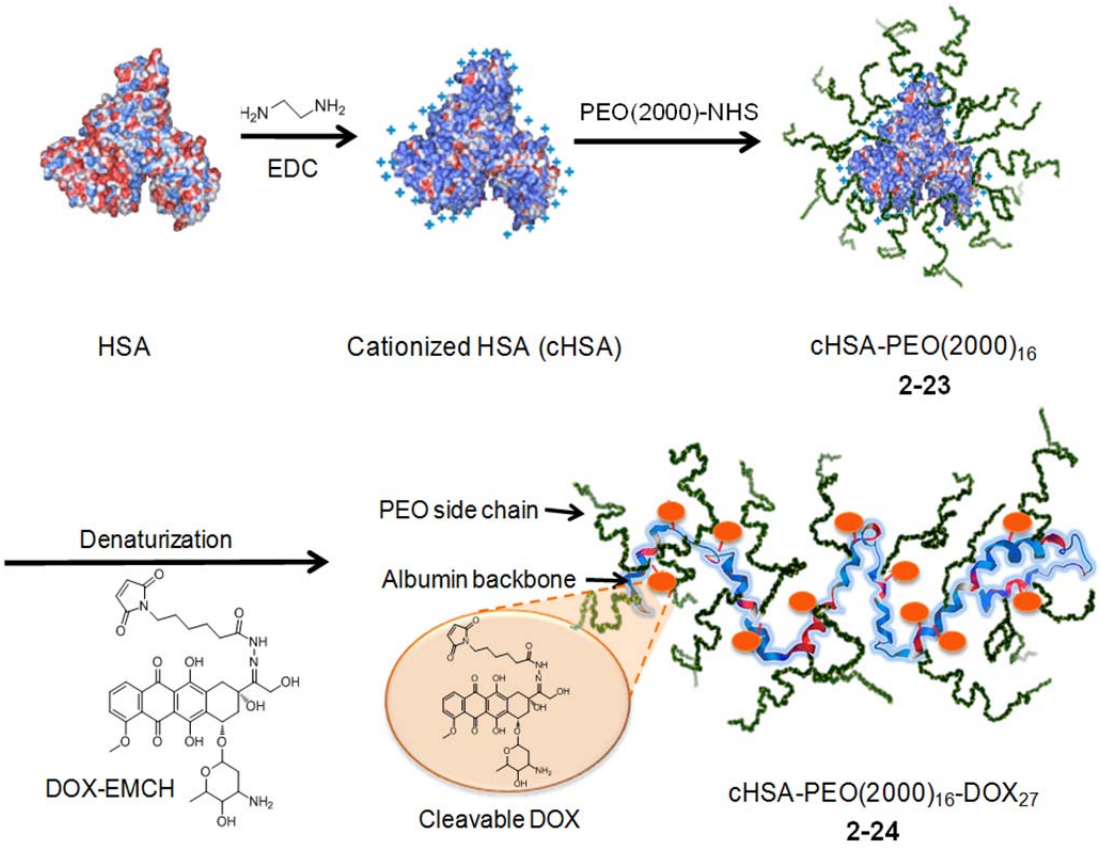

Scheme 2-6. Preparation of cHSA-PEO(2000)$_{16}$-DOX$_{27}$ (**2-24**). Adapted with permission [55]. Copyright 2012, Wiley-VCH.

DOX-EMCH contained a thiol-reactive maleimide group at the terminus of a small spacer ready for conjugation to cysteine residues of proteins and an acid sensitive hydrazone linker at the DOX-C-13 keto-position. The hydrazone linkage would allow pH triggered drug release under acidic environment in tumor tissue [56, 57]. In our study, in order to conjugate DOX-EMCH with cysteine residues of albumin derived PbP, the pre-pegylated albumin cHSA-PEO(2000)$_{16}$ (**2-23**) was prepared by reacting the surface lysine residues of HSA with N-hydroxysuccinimide ester (NHS) activated PEO(2000). The

resulting (**2-23**) exhibited high water solubility (up to 150 mg/mL) and high stability at 4°C for more than 6 months. The molecular weight of (**2-23**) is 102 kDa as characterized by MALDI-ToF MS and SDS-PAGE (**Figure 2-22**). According to the same denaturation procedure described in Section 2.2, denatured cHSA-PEO(2000)$_{16}$ (**2-23**) was achieved in 5 M Urea buffer and the disulfide bridges were reduced by TCEP to expose all cysteine residues. The sufficient pre-pegylation stabilized the denatured structure so that no further pegylation was necessary. An excess of DOX-EMCH was subsequently *in situ* reacted with the reduced thiol groups of denatured (**2-23**). The resulting DOX loaded PbP (**2-24**) was then washed in 5 M Urea buffer using a Vivaspin® centrifugal membrane concentrator with a molecular weight cutoff of 30 kDa to remove any non-bound DOX-EMCH. It is noteworthy that the high concentration urea buffer helped with maintaining the protein conjugate under denaturing conditions and allowed elimination of non-specifically adsorbed DOX molecules. After rising in urea buffer for 3 to 5 times, the DOX loaded denatured protein conjugate was brought into water to allow backfolding of the polypeptide backbone into a globular architecture. As demonstrated in section 2.4.1, the introduction of hydrophobic moieties could lead to a backfolding of PbPs backbones into micellar structures. In the case of (**2-24**), the presence of both the hydrophobic DOX molecules and lipophilic amino acids located along the main chain of the HSA-derived polypeptide could also induce the backfolding of albumin backbone and therefore encapsulate the conjugated DOX molecules inside the protein shell. Notably, the term “backfolding” does not imply refolding of the secondary or tertiary structure of the native protein but refers to the spontaneous assembly of the polypeptide chain into a

globular architecture in aqueous solution due to hydrophobic interactions. Complete removal of non-bound DOX was further achieved by continuously washing with water until no DOX was detected in the elution anymore. The remaining protein solution exhibited a deep red color. As a control experiment, cHSA-PEO(2000)$_{16}$ was mixed with free DOX hydrochloride and washed following the same protocol. No DOX was detected in the protein solution after washing, suggesting a complete removal of non-specifically adsorbed DOX.

After the above intensive washing steps, cHSA-PEO(2000)$_{16}$-DOX$_{27}$ (**2-24**) was obtained with a molecular weight of ~122 kDa according to MALDI-ToF MS analysis, indicating successful covalent loading of 27 DOX-EMCH molecules (increase of 20 kDa M.W., **Figure 2-22b**). In addition, the characteristic absorbance of DOX at 488 nm was used as a second approach to calculate DOX loading. It was found that each polymer contains ~28±4 DOX molecules, which agreed very well with the MALDI-ToF results and again supported the efficient washing and low non-specific adsorption (**Figure 2-22a** and **b**). Covalent conjugation of DOX was also demonstrated by the co-localization of the DOX emission and the cHSA-PEO(2000)$_{16}$ band on denaturing SDS-PAGE (**Figure 2-22c**). Notably, the attachment of 28 substituents to the cysteine residues of denaturized albumin backbone was also observed when preparing polypeptide (**2-2**) and (**2-6**). It had been observed that only 28 PEO chains can be attached on the 35 cysteine residues since 7 thiol groups were reproducibly not accessible as discussed in section 2.2.1. This DOX conjugated copolymer could facilitate efficient drug delivery as well as controlled drug release in endosomal condition. The

structural and pharmaceutical characterization of (**2-24**) and the anticancer activities of this macromolecular drug will be discussed in Chapter 4.

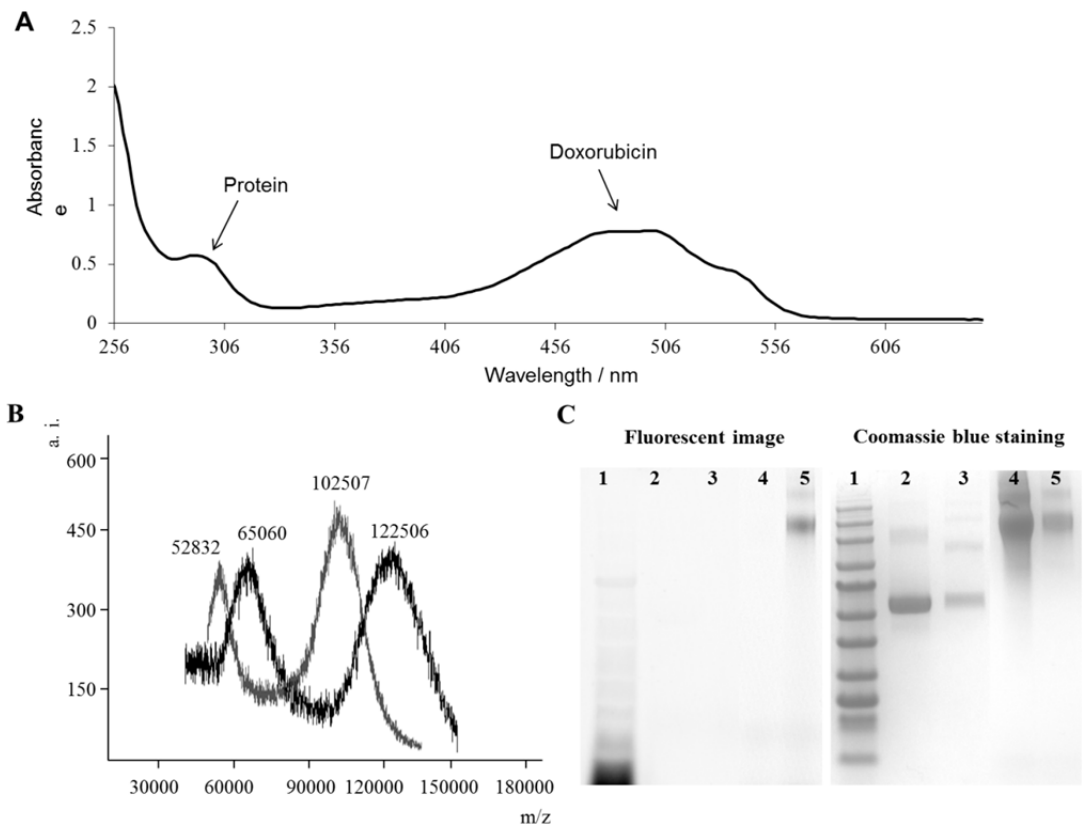

Figure 2-22. Characterization of cHSA-PEO(2000)$_{16}$ (**2-23**) and cHSA-PEO(2000)$_{16}$-DOX$_{27}$ micelles (**2-24**). (A) UV-Vis spectrum of (**2-24**); (B). MALDI-ToF mass spectra of (**2-23**) (grey line) and (**2-24**) (black line). (M^+: the highest peak on the right; M^{2+}: the lower peak on the left); (C) SDS-PAGE (lane 1: protein marker, lane 2: native HSA, lane 3: cationized HSA, lane 4: (**2-23**) and lane 5: (**2-24**). Adapted with permission [55]. Copyright 2012, Wiley-VCH.

2.4.3.3 Conjugation of MRI contrast agents *via* amide coupling[§].

In addition to the 16 PEO groups coupled to lysine side chains, there were still more than 100 amino groups available in cHSA-PEO(2000)$_{16}$ (**2-23**), which could be further conjugated with small functional moieties *via* amide coupling. In this case, gadolinium-based MRI (magnetic resonance imaging) contrast agent "gadoteric acid" was conjugated to (**2-23**) to form a macromolecular MRI contrast particle (**Scheme 2-7**).

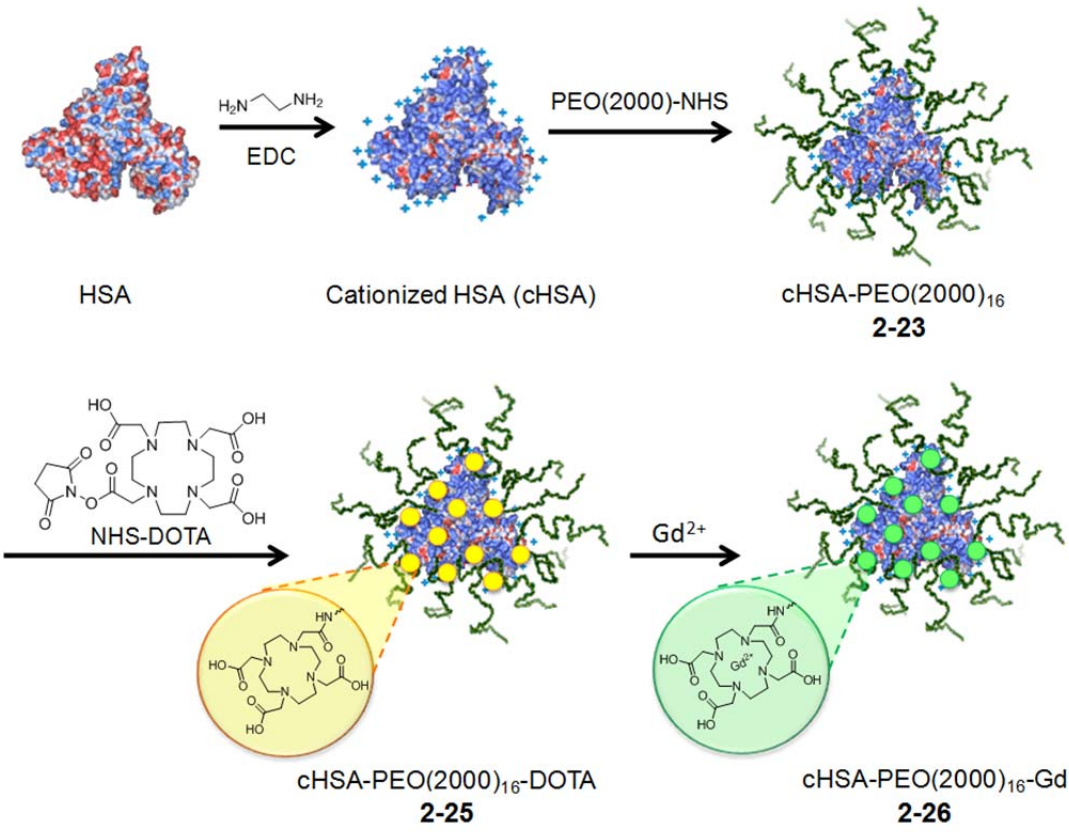

Scheme 2-7. Preparation of biopolymers containing MRI contrast agents.

DOTA (1,4,7,10-tetraazacyclododecane-1,4,7,10-tetraacetic acid) is commonly used as a complexing agent, especially for lanthanide ions and

[§] These studies were performed in close cooperation with Ms Tao Wang and will also be included in her PhD thesis. Ms Tao Wang synthesized NHS-DOTA and prepared (**2-25**) and (**2-26**).

actinide ions. The DOTA-Gd^{3+} complex is a gadolinium-based MRI contrast agent widely used in clinic named “gadoteric acid”. However, small molecular gadoteric acid had a relatively low relaxivity and extravasated non-selectively from blood into the interstitium of both normal tissue and tumor, which significantly limited their clinical applications [58]. To overcome these limitations, macromolecular Gd complexes were intensively studied to achieve enhanced contrast as well as prolong the blood circulation time. Attaching gadoteric acids to macromolecules could slow down the rotational motion of the complexes, thus increase relaxivities [59]. In addition, macromolecular contrast agents also provided a longer blood circulation and preferentially accumulated in tumor tissue with leaky vasculature *via* passive targeting [60]. In this context, various of macromolecular platforms were developed to conjugate with Gd-complexes, including linear polymers [61], branched dendrimers [62] as well as liposomes [63]. Especially, Brasch’s group reported in 1987 the first albumin conjugated macromolecular contrast agent, Albumin-(Gd-DTPA) [64], which was found effective in characterizing the vascularity of various tumors [65] and for early assessment of tumor response to antiangiogenic therapy [66].

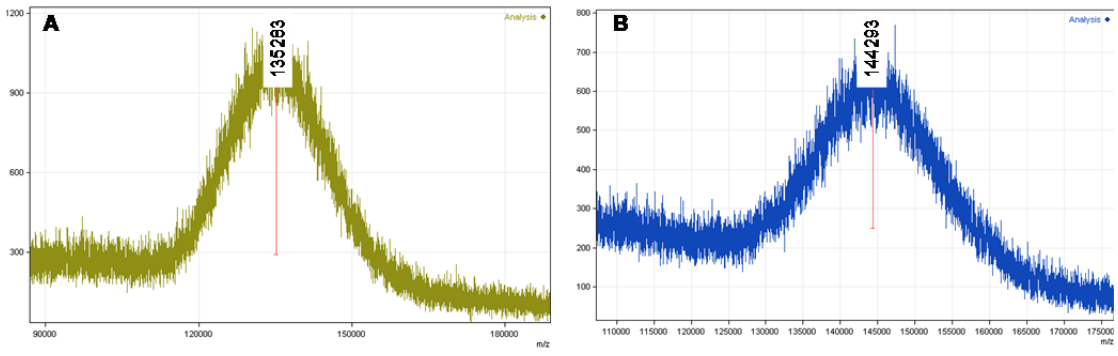

Figure 2-23. MALDI-ToF mass spectra of (A) cHSA-PEO(2000)$_{16}$-DOTA (**2-25**) and (B) cHSA-PEO(2000)$_{16}$-Gd (**2-26**).

To demonstrate a new protein based platform for preparation of macromolecular MRI contrast agent, we successfully conjugated a high number of Gd-DOTA complexes to pegylated albumin (**2-23**). The NHS-DOTA was firstly prepared to facilitate efficient amide coupling with protein (**2-23**) under neutral aqueous conditions (**Scheme 2-7**), which was provided by Ms. Tao Wang. The conjugated cHSA-PEO(2000)$_{16}$-DOTA (**2-25**) had a molecular weight of 135 kDa (**Figure 2-23a**), indicating a successful conjugation of 85 DOTA molecules. Gadolinium (Gd^{3+}) was further loaded to cHSA-PEO(2000)$_{16}$-DOTA (**2-25**) to achieve the albumin derived contrast molecule cHSA-PEO(2000)$_{16}$-Gd (**2-26**) with a further increased molecular weight of 144 kDa (**Figure 2-23b**). According to the molecular weight difference, ~57 of Gd^{3+} was loaded onto (**2-26**) which is significantly more than the Albumin-(Gd-DTPA) reported by Brasch's group (typical 25~30 Gd^{3+}) [64]. Therefore, complex (**2-26**) was expected to have a promising potential of for *in vivo* MRI imaging, which will be further discussed in Chapter 4.

Similar to protein (**2-23**), the gadoteric acid conjugated protein (**2-26**) could be further denatured to prepare a PbP containing MRI contrast agent. Denaturation could further expose the functional groups inside albumin, such as the thiol groups, and allow introducing additional functional moieties, e.g. DOX. By this way, 28 of DOX molecules were conjugated into (**2-26**) by the similar method as demonstrated in section 2.4.3.2. Thus, a protein based theranostic nanoparticle was prepared for simultaneous MRI imaging and cancer therapy. The detailed characterization and application of this system will be discussed in Chapter 4.

2.5 Summary

In summary, we have presented a general reaction scheme toward various protein based polypeptides (PbPs) with well-defined structures and narrow molecular weight distribution compared to classical polymers as well as attractive physical and biological properties. These polypeptides were prepared by controlled denaturation of native proteins and *in situ* stabilization with several PEO chains. In this way, PbPs with different chain lengths (e.g. dHSA-PEO$(5000)_{27}$ (**2-2**) and dLY-PEO$(5000)_{8}$) (**2-4**) and dBSA-{PEO$(5000)_{27}$}-PEO(3400)-dBSA-{PEO$(5000)_{27}$} (**2-8**)) were successfully achieved. This reaction scheme could be in principle applicable for other precursor proteins, but the required denaturing conditions to achieve polypeptide copolymers might be dependent on the stability of the respective native protein. These copolymers contained ordered secondary structural elements inherited from precursor proteins. The presence of alternating hydrophobic and hydrophilic "patches" along polypeptide backbone contributed to the formation of micellar architectures in diluted aqueous solution, which was attractive for drug encapsulation and drug delivery.

All these copolymers exhibited excellent solubility and stability in aqueous media, no cytotoxicity at relevant concentrations as well as fast enzymatic degradability, suggesting promising potential as nanotransporter scaffolds for medicinal applications. Since biomedical application often impose that no immune responses are elicited, polypeptide copolymers derived from human albumin such as (**2-2**) could be particularly attractive for therapeutic applications.

Diverse native functional groups available at precise positions along protein backbone allowed further orthogonal modifications. *Via a priori* and *a posteriori* modification strategies, PbPs containing additional functionalities were prepared with adjustable properties, such as varing net charges (e.g. dcBSA-PEO(5000)$_{27}$ (**2-11**) and daHSA-PEO(5000)$_{27}$ (**2-14**)), tunable hydrophobicities (e.g. dcBSA-PEO(5000)$_{27}$ (**2-11**) and dcBSA-PEO(5000)$_{27}$-alkyne (**2-15**)) as well as diverse surface patterning properties (e.g. dHSA-PEO(5000)$_{27}$-TA$_{22}$ (**2-16**), dcBSA-PEO(5000)$_{27}$-TA$_{26}$ (**2-17**) and dLY-PEO(5000)$_{8}$-TA$_{8}$ (**2-18**)). Moreover, functional moieties, such as chromophores, anti-cancer drugs or MRI contrast agents, could be also introduced into PbPs, which demonstrated PbPs as a highly versatile platform for broad applications.

In view of these unique features, protein-derived polypeptide copolymers represent an attractive and versatile type of biomaterial for drug delivery, self-assembly induced nanopatterning as well as tissue engineering. The “semi-chemistry” polypeptide preparation approach reported herein denotes a novel concept for producing synthetic polypeptides from native protein resources, which complements conventional polypeptide synthesis and expression approach and opens new avenues to unique macromolecular architectures.

2.6 Materials and Methods

2.6.1 Materials.

All chemical reagents were obtained from commercial suppliers and used without further purification unless otherwise noted. Albumins from human serum (HSA), lysozyme from hen egg white (LY), albumins from bovin serum

(BSA) and monomaleimide modified PEO (Mn = 5000 g/mol) (PEO(5000)-MI) were purchased from Sigma-Aldrich Chemie Gmbh (Munich, Germany). Bismaleimide modified PEO (Mn = 3400 g/mol) (MI-PEO(3400)-MI) was provided by Creative PEG-Works (Winston Salem, USA). Mono-NHS activated PEO(2000) (MeO-PEO(2000)-NHS) was purchased from RAPP Polymere GmbH (Tuebingen, Germany). DL-thioctic acid (TA) 98% and 4,4-dipyridyl disulfide (DPS) 98% were obtained from Alfa Aesar. Succinimide activated thioctic acid (TA-NHS) was prepared according to a literature procedure [67]. Mon-succinimide activated 1,4,7,10-tetraazacyclododecane-1,4,7,10-tetraacetic acid (NHS-DOTA) ** was synthesized according to a literature procedure [68]. Bio-Gel P30 from Bio-Rad Laboratories GmbH (Munich, Germany) was used for desalting column. Vivaspin® centrifugal concentrators were purchased from GE Healthcare Europe GmbH (Freiburg, Germany). Dulbecco's Modified Eagle Medium (DMEM) (1X) liquid (high glucose), Fetal Bovine Serum (FBS) Standard Quality (EU approved) from PAA Laboratories GmbH (Cölbe, Germany) and MEM Non-Essential Amino Acids Solution 10 mM (100X) from Invitrogen Life Technologies GmbH (Darmstadt, Germany) were used for cell culture. CellTiter-Glo® Luminescent Cell Viability Assay was obtained from Promega GmbH (Mannheim, Germany).

2.6.2 Instrumentation.

ÄKTA Purifier FPLC and Sephacyl S-100 HR gel filtration column was used for protein copolymer purification. Precast NuPAGE TA 3%-8% Gel and

** NHS-DOTA was synthesized and provide by Ms. Tao Wang.

NuPAGE Bis-Tris 4%-12% Gel were purchased from Invitrogen Life Technologies GmbH (Darmstadt, Germany) and gel electrophoresis was performed in Novek® Mini-Cell. Agarose gel electrophoresis was performed using Mini-Sub Cell GT horizontal electrophoresis system from Bio-Rad Laboratories GmbH (Munich, Germany). Circular dichroism spectra were measured on a JASCO J-810 Spectropolarimeter (JASCO Germany GmbH, Gross-Umstadt, Germany). The MALDI-ToF mass spectrum was obtained on a Bruker Reflex® III MALDI-ToF spectrometer (Bruker Daltonik GmbH, Bremen, Germany). Dynamic light scattering (DLS) and zeta potential measurements were performed on a Malvern Zetasizer ZEN3600 (Malvern Ltd, Malvern, UK).

2.6.3 Protocols for the preparation of PbPs from different protein precusors

*2.6.3.1 Preparation of dHSA-PEO(5000)$_{27}$ (**2-2**) and dBSA-PEO(5000)$_{27}$ (**2-6**).*

HSA or BSA (20 mg, 0.3 μmol) were dissolved in degassed urea-phosphate buffer (10 mL, 20 mM phosphate buffer, pH 7.4, 5 M urea and 2 mM ethylenediamine tetraacetic acid (EDTA)) and stirred at room temperature for 15 min. Tris(2-carboxy-ethyl)phosphine hydrochloride (TCEP) (8.6 mg, 30 μmol) was then added as a solid and the solution was stirred for additional 30 min under argon atmosphere. Subsequently, PEO(5000)-MI (154 mg, 31 μmol) was allowed to react with the protein solution under argon atmosphere for 3 hr. After the attachment of the PEO chains, *N*-(2-aminoethyl)maleimide trifluoroacetate salt (8 mg, 31.5 μmol) was introduced and stirred for another 3 hr to react with the remaining thiol groups. Thereafter, the reaction mixture

was pre-purified five times by ultrafiltration using Vivaspin® 20 (MWCO 30k) centrifugal concentrator with 20 mM Tris-HCl buffer (pH 7.4, containing 150 mM NaCl, 2 mM EDTA), and then further purified by size exclusion FPLC (ÄKTA Purifier, Sephacyl S-100 HR gel filtration column, 20 mM Tris-HCl pH 7.4 buffer with 150 mM NaCl). The first protein peak was collected and concentrated by Vivaspin® 20 (MWCO 30k) centrifugal concentrator. Subsequently, the product mixture was passed through a Bio-Gel P30 desalting column and lyophilized to afford 24 mg dHSA-PEO(5000)$_{27}$ (**2-2**) or dBSA-PEO(5000)$_{27}$ (**2-6**) as white solid (overall yield ~40%).

*2.6.3.2 Preparation of dLY-PEO(5000)$_8$ (**2-4**) (This protocol was first developed by Mr. Goutam Pramanik and will also be described in his PhD thesis).*

5mg LY was denatured using 5mL Guanidine-Tris buffer (8M Guanidine, 0.2 M NaCl, 1 mM EDTA, and 0.1 M Tris/HCl) and stirred at room temperature for 4 hr. Then, the disulfide bond of LY was reduced in 1mL 1M DL-Dithiothreitol (DTT) by stirring at room temperature for 24 hr. After reduction, the pH of the reaction mixture was brought below 4 using HCl. Thereafter, DTT was removed from the reaction mixture by a Sephadex® G25 column using 0.1 M acetic acid. Subsequently, the denatured protein was lyophilized to obtain denatured lysozyme (**2-3**).

PEO(5000)-MI (41 mg, 8.2 μmol) was dissolved in degassed urea-phosphate buffer (10 mL, 10 mM phosphate buffer, pH 7.4, 5 M urea and 2 mM EDTA) and then (**2-3**) (5 mg, 0.34 μmol) was added and stirred under argon atmosphere overnight. The reaction mixture was pre-purified by

ultrafiltration 5-times with pure water using Vivaspin® 20 (MWCO 10 kDa) centrifugal concentrator, and then further purified through a Bio Gel P-30 desalting column and lyophilized to afford dLY-PEO(5000)$_8$ (**2-4**) as white solid (Overall yield 35%). MALDI-ToF MS: 54 kDa.

*2.6.3.3 Synthesis of BSA-PEO(3400)-BSA (**2-7**).*

BSA-PEO(3400)-BSA (**2-7**) was prepared according to our previously reported procedure with minor modifications [69]. BSA (340 mg, 5.3 μmol, 4 eq.) was dissolved in degassed phosphate buffer (70 mL, 50 mM, pH 7.0) under argon atmosphere. MI-PEO(3400)-MI (4.5 mg, 1.3 μmol, 1 eq.) was then added to the mixture and stirred overnight at 4 ^{o}C. Subsequently, the reaction mixture was prepurified by ultrafiltration in water using an Amicon® Ultra (100kDa MWCO) centrifugal filter for 3 times, followed by size exclusion chromatography (SEC) on an ÄKTA Purifier FPLC system using sequentially HiPrep® 16/60 Sephacryl® S-100HR column and Superose® 6 10/300GL column with Tris buffer (20 mM, pH 7.4, 150 mM NaCl, degassed). The first protein peak was collected and analyzed by SDS-PAGE. The pure fractions were desalted using Amicon® Ultra (100kDa MWCO) centrifugal filter device and lyophilized to obtain (**2-7**) as a white fluffy solid (70 mg, yield = 10%). BSA-PEO(3400)-BSA (**2-7**) was characterized by MALDI-ToF MS and SDS-PAGE indicating a molecular weight (M.W.) of 132 kDa.

*2.6.3.4 Synthesis of dBSA-{PEO(5000)$_{27}$}-PEO(3400)-dBSA-{PEO(5000)$_{27}$} (**2-8**).*

BSA-PEO(3400)-BSA (**2-7**) (2 mg, 15 nmol) was dissolved in 1 mL degassed urea-phosphate buffer (5 M urea, 10 mM sodium phosphate, 2 mM EDTA, pH 7.4) under argon atmosphere. TCEP (0.9 mg, 3 μmol, 200 eq) was

added and the reaction mixture was stirred for 15 min. PEO(5000)-MI (15 mg, 3 μmol, 200 eq) was then added and the reaction was continued at room temperature for 3hr. After pegylation, *N*-(2-aminoethyl)maleimide trifluoroacetate salt (0.8 mg, 3 μmol, 200 eq) was introduced to cap any unreacted thiol groups. The solution was left for an additional 3 hr. The resulting copolymer was prepurified by ultrafiltration in water using an Amicon® Ultra (100kDa MWCO) centrifugal filter 3 times and further purified by SEC on an ÄKTA Purifier FPLC system using Superose® 6 10/300GL column with Tris buffer (20 mM, pH 7.4, 150 mM NaCl, degassed). The first protein peak was collected and analyzed by SDS-PAGE. The pure fractions were desalted through a Bio-Gel P30 desalting column and lyophilized to afford (**2-8**) as a white fluffy solid (1.3 mg, yield = 50%).

2.6.4 Protocols for the preparation of polypeptide polyelectrolytes *via a priori* modification of precursor proteins.

*2.6.4.1 Synthesis of cationic BSA (cBSA, **2-9**)*[††].

cBSA was synthesized according to the our previous report [40]. 150 mg (~2.25 μmol) of BSA was allowed to completely dissolve in 15 ml of degassed 2.5 M ethylenediamine-HCl solution (pH 4.75), followed by adding EDC (4 mmol, 621 mg) and stirring for 75 min. The reaction was then terminated by adding 1 ml acetate buffer (4 M, pH 4.75). After reaction, cBSA was washed twice with acetate buffer (4 M, pH 4.75) and 3 times with deionized distilled water using Vivaspin® 20 (MWCO 30k) centrifugal concentrator and then

[††] This protocol was first developed by Dr. Klaus Eisele.

lyophilized to obtain 154 mg cBSA (**2-9**) as white fluffy solid (yield: 94%). MALDI-ToF MS: 69.3 kDa.

*2.6.4.2 Synthesis of anionic HSA (aHSA, **2-12**)*[‡‡]*.*

50 mg (~0.75 μmol) of HSA and glutaric acid (26.4 mg, 0.2 mmol) were allowed to completely dissolve in 7.5 ml of degassed phosphate buffer (50mM, pH8.4), followed by adding 1-Ethyl-3-(3-dimethylaminopropyl)carbodiimide (EDC) (62 mg, 0.4 mmol) and stirring for 2.5 hr at room temperature. Reaction mixture was then directly added to a Vivaspin® 20 (MWCO 30k) centrifugal concentrator and washed five times with deionized distilled water. After washing, aHSA (**2-12**) can be lyophilized to obtain 48 mg white fluffy solid (yield: 90%). MALDI-ToF MS: 71.4 kDa.

*2.6.4.3 Preparation of daHSA-PEO(5000)$_{27}$ (**2-14**) and dcBSA-PEO(5000)$_{27}$ (**2-11**).*

daHSA-PEO(5000)$_{27}$ (**2-14**) and dcBSA-PEO(5000)$_{27}$ (**2-11**) was prepared based on the same protocol as described in section 2.6.3.1 but using aHSA and cBSA as precursors respectively.

*2.6.4.4 Preparation of rhodamine labeled dHSA-PEO(5000)$_{27}$ (**2-2**) and dcBSA-PEO(5000)$_{27}$ (**2-11**).*

Rhodamine labeled dHSA-PEO(5000)$_{27}$ (**2-2**) and dcBSA-PEO(5000)$_{27}$ (**2-11**) were prepared from rhodamine mono-labeled native HSA and BSA, respectively. To a solution of HSA or BSA (300 mg, 4.5 μmol) in phosphate

[‡‡] This protocol was first developed by Dr. Klaus Eisele.

buffer (300 ml, 50 mM, pH 7.4), a freshly prepared aqueous solution of TCEP (1 ml, 1 mM, 1 mmol) was added and the reaction mixture was stirred for 10 min at room temperature. Then, a solution of tetramethylrhodamine-5-maleimide (TMRh-MI, from Sigma-Aldrich, 4.3 mg, 9 µmol, 200% excess) in DMSO (1 ml) was added and the reaction mixture was stirred at RT for another 1 hr under argon atmosphere. The non-reacted TMRh-MI was removed by ultrafiltration and size-exclusion chromatography (BioGel P 30, MQ water). The first colored layer was lyophilized to afford rhodamine monolabeled HSA/BSA as a bright pink solid (260 mg, yield 86%). MALDI-ToF MS: 66.9 kDa. From these rhodamine labeled precursors, Rho-dHSA-PEO(5000)$_{27}$ and Rho-dcBSA-PEO(5000)$_{27}$ can be prepared using the same protocol mentioned in Section 2.6.3.1.

2.6.5 Protocols for post-modification of PbPs.

2.6.5.1 Synthesis of N-propargyl maleimide

Maleic anhydride (980 mg, 10 mmol) was reacted with propargylamine (550 mg, 10 mmol) in 20 mL glacial acetic acid at room temperature overnight. Then, sodium acetate (164 mg, 2 mmol) and acetic anhydride (10 mL) were added and the reaction mixture was heated to 65°C for 2 hr. After reaction, all solvent was removed under vacuum and the residue was purified by silica gel column chromatography (EtOAc:Hexane 1:3) to yield 60 mg of a white solid (yield 5%). Rf 0.56 (EtOAc/heptane, 1:1 v/v), ^{1}H NMR ($CDCl_3$, 300 MHz): δ 6.75 (s, 2H), 4.28 (d, 2H, J 1.8 Hz,); 2.20 (t,1H, J 1.8 Hz); ^{13}C NMR ($CDCl_3$, 300 MHz): δ 169.2, 134.4, 76.9, 71.5, 26.8. MS-ESI, 136 $[M+H]^+$.

*2.6.5.2 Synthesis of dcBSA-PEO(5000)$_{27}$-alkyne (**2-15**).*

dcBSA-PEO(5000)$_{27}$-alkyne (**2-15**) were prepared using a similar procedure as described in section 2.6.3.1. cBSA (**2-9**, 10 mg, 0.15 μmol) was first denatured in degassed urea-phosphate buffer (10 mL, 10 mM phosphate buffer, 5 M urea and 2 mM EDTA, pH 7.4) for 10 min, and then reducing agent TCEP (4.3 mg, 15 μmol) was added under argon athmosphere for 30 min. Subsequently, PEO(5000)-MI (77 mg, 15 μmol) was added to the reaction and stir at RT for 3 hr. After pegylation, *N*-propargyl maleimide (4.1 mg, 30 μmol) was given to the reaction and allow reacting for 3 hr. The reaction mixture was then purified by ultrafiltration with Tris-HCl buffer (20 mM Tris, 150 mM NaCl, 2 mM EDTA, pH 7.4), and followed by further size exclusion purification using HiPrep® Sephacyl® S-100 HR gel filtration column on ÄKTA Purifier flash protein liquid chromotography with Tris-HCl buffer (20 mM Tris, 150 mM NaCl, pH 7.4). Then, the purified material was desalted and lyophilized to yield dcBSA-PEO(5000)$_{27}$-alkyne (**2-15**) as white fluffy solid (overall yield 35%~50%). The product was characterized by gel electrophoresis using precast NuPAGE® TA 3%-8% Gel (Invitrogen) in Novek® Mini-Cell.

*2.6.5.3 Synthesis of dHSA-PEO(5000)$_{27}$-TA$_{22}$ (**2-16**) and dcBSA-PEO(5000)$_{27}$-TA$_{26}$ (**2-17**).*

(**2-2**) or (**2-11**) (1 mg, ~ 0.4 μmol amino groups) was dissolved in Milli-Q water (1 mL). Then, thioctic acid, activated by NHS (TA-NHS, 2.4 mg, 8 μmol) was dissolved in DMF (0.2 mL). $NaHCO_3$ (0.2 mL, 5 mg/mL) was added and the reaction mixture was vigorously stirred overnight. The insoluble TA-NHS residue was filtered off after reaction. A clear solution was obtained and transferred to an ultrafiltration tube (Vivaspin® 20, 30 MWCO), washed 5-times

with pure water and further purified through a Bio Gel P-30 desalting column. The product was further lyophilized to obtain a white solid (80% yield). The resulting dHSA-PEO(5000)$_{27}$-TA$_{22}$ (**2-16**) or dcBSA-PEO(5000)$_{27}$-TA$_{26}$ (**2-17**) was analyzed by SDS-PAGE and a thiol quantification assay (DPS assay, see section 2.6.6.1).

*2.6.5.3 Synthesis of dLY-PEO(5000)$_8$-TA$_8$ (**2-18**).*

Denatured dLY-PEO(5000)$_8$ (**2-4**, 5.4 mg, ~ 6 µmol amino groups) was dissolved in Milli-Q water (3 mL). Then, TA-NHS (2.4 mg, 8 µmol) was dissolved in DMF (0.2 mL). $NaHCO_3$ (0.6 mg) was added and the reaction mixture was vigorously stirred overnight. The insoluble TA-NHS residue was filtered off after reaction. A clear solution was obtained and transferred to an ultrafiltration tube (Vivaspin® 20, 10 MWCO), washed five times with pure water and further purified through a Bio Gel P-30 desalting column. The resulting dLY-PEO(5000)$_8$-TA$_8$ (**2-18**) was analyzed by MALDI-ToF MS (m/z = 56 kDa) which indicating eleven thioctic acids attached (yield 75%). The number of thioctic acid groups in (**2-18**) has also been detected by DPS assay which resulted eight detectable thioctic acids.

*2.6.5.4 Synthesis of azido-coumarin (**2-19**)*[§§]

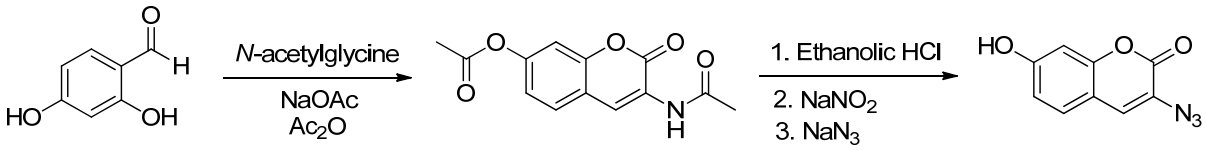

Scheme 2-8. Synthesis of azido-coumarin.

[§§] Azido-coumarin was prepared by Mr. Ng. Y. W. David.

The synthesis of azido-coumarin (**2-19**) followed a previous published protocol and afforded highly similar results [54]. To a mixture of anhydrous NaOAc (4.8 g, 60 mmol) in acetic anhydride (100 mL) was added 2,4-dihydroxy benzaldehyde (2.76 g, 20 mmol) and N-acetylglycine (2.34 g, 20 mmol). The reaction mixture was put under reflux for 4 hr and poured onto ice to give a yellow precipitate. The precipitate was filtered and washed with copious amounts of ice water before transfering into 30 mL 1:2 ethanolic solution of HCl (ethanol : conc. HCl). The mixture was then reflux for 1 hr followed by dilution using ice water (40 mL). The soluton was cooled in an ice bath and added $NaNO_2$ (2.76 g, 40 mmol). The reaction was stirred for 10 min and NaN_3 (3.9 g, 60 mmol) was added in small portions. The resultant brown precipitate was filtered off after an additional 15 min. The precipitate was washed with water and dried under high vacuum to afford the product without further purification. Yield 45% (1.83 g). ^{1}H NMR (DMSO-d6, 400 MHz) δ 7.56 (s, 1H), 7.47 (d, J = 8.5 Hz, 1H),), 6.79 (m, 1H), 6.74 (d, J = 2.2 Hz, 1H).

*2.6.5.5 Synthesis of azido-doxorubicin (**2-21**)***.*

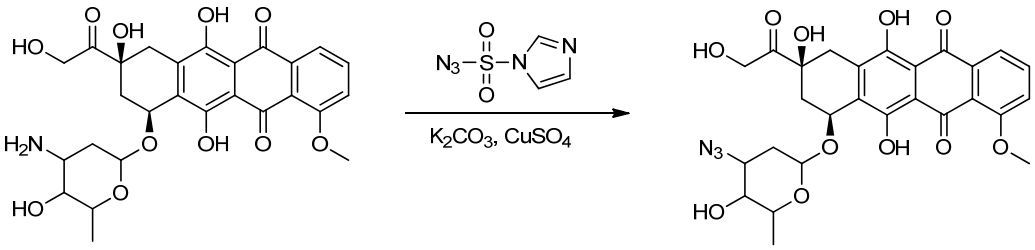

Scheme 2-9. Synthesis of azido-doxorubicin.

Imidazole-1-sulfonyl azide hydrochloride (22 mg, 0.10 mmol) was added to the doxorubicin hydrochloride (50 mg, 0.086 mmol), potassium carbonate

*** Azido-doxorubicin was prepared by Ms. Tao Wang.

(18 mg, 0.13 mmol) and copper sulfate (0.14 mg, 0.86 µmol) in 1ml of methanol. The reaction mixture was stirred at room temperature overnight. The mixture was concentrated, diluted with water (30 ml) and extracted with DCM (3x20 ml). The combined organic layers were washed by saturated brine and dried over anhydrous sodium sulfate, filtered and concentrated. The crude product was purified by flash chromatography using 10% methanol in chloroform to give 34 mg of the azido-doxorubicin (**2-21**) in 70% yield. ^{1}H NMR (400MHz, $CDCl_3$): δ 1.34 (d, 3H), 1.933 (m, 2H), 2.14 (m, 2H), 2.34 (d, 1H), 3.02 (m, 2H), 3.28 (d, 1H), 3.59 (m, 1H), 3.74 (s, 1H), 3.92 (s, 1H), 4.09 (s, 3H), 4.51 (s, 1H), 4.75 (d, 2H), 5.31 (d, 1H), 5.59 (d, 1H), 7.41 (d, 1H), 7.80 (t, 1H), 8.04 (d, 1H), 13.24 (s, 1H), 14.01 (s, 1H). ^{13}C NMR (400MHz, $CDCl_3$): δ 16.76, 28.18, 33.50, 35.25, 56.44, 65.30, 67.27, 69.34, 69.68, 76.49, 77.20, 100.59, 110.99, 111.11, 118.37, 119.57, 120.17, 133.25, 134.85, 135.65, 155.04, 155.88, 160.72, 186.04, 186.33, 213.35. ESI-MS: 568 $[M+H]^+$.

*2.6.5.6 Click reaction inside dcBSA-PEO(5000)$_{27}$-alkyne (**2-15**) micelle*

cBSA-PEO(5000)$_{27}$-alkyne (**2-15**) 2 mg was dissolved in 0.49 mL distilled water and mixed with azido-coumarin (**2-19**, 101 µg) in 0.5 mL tetrahydrofuran (THF). $CuSO_4 \cdot 5H_2O$ (62.5 µg, 6.25 µL from 10 mg/mL stock solution in water) and sodium ascorbate (99 µg, 9.9 µL from 10 mg/mL stock solution in water) were premixed and transfer to the solution of (**2-19**). The reaction was shaken overnight in dark. After reaction, THF was evaporated and the aqueous solution was extracted once with DCM. The residue was washed with 3 mL of urea buffer (5M Urea, 10 mM sodium phosphate, pH 7.4) using ultrafiltration

tube for three times and subsequently with water for another three times. 1.4 mg of coumarin-cBSA-PEO(5000)$_{27}$-alkyne (**2-20**) can be obtained after lyophilization (yield 70%).

For preparation of doxorubicin-cBSA-PEO(5000)$_{27}$-alkyne (**2-22**), azido-doxorubicin (**2-21**) (284 µg) was used and the same procedure was followed.

*2.6.5.7 Synthesis of cHSA-PEO(2000)$_{16}$ (**2-23**)*

50 mg of cHSA was allowed to completely dissolve in 50 ml of degassed phosphate buffer (50 mM, pH 8.0), followed by adding 45 mg MeO-PEO(2000)-NHS dissolved in 500 µl DMSO and stirring for 2 hr. After reaction, cHSA-PEO(2000)$_{16}$ was washed 8 times with deionized distilled water using Vivaspin® 20 (MWCO 30k) centrifugal concentrator and then lyophilized to obtain cHSA-PEO(2000)$_{16}$ (**2-23**) as white fluffy solid (59 mg, yield 78%). MALDI-ToF MS: 102.5 kDa.

*2.6.5.8 Preparation of cHSA-PEO(2000)$_{16}$-DOX$_{27}$ (**2-24**)*

cHSA-PEO(2000)$_{16}$ (10 mg, 50 nmol) was dissolved in degassed urea-phosphate buffer (10 ml, 50 mM sodium phosphate buffer, pH 7.4, 5 M urea and 2 mM EDTA) and stirred at room temperature for 15 min. TCEP (0.29 mg, 1 µmol) was added as a solid and the solution was stirred for additional 30 min under argon atmosphere. Then, DOX-EMCH (15 mg, 10 µmol) was added and stirred under argon atmosphere overnight. Thereafter, the reaction mixture was purified by ultrafiltration with urea-phosphate buffer (10 mM sodium phosphate buffer, pH 7.4, 5 M urea and 2 mM EDTA) for 3 times and with water for >5 times until no red color in the filtrate, then lyophilized to

obtain cHSA-PEO(2000)$_{16}$-DOX$_{27}$ as red solid (5.4 mg, yield 45%). MALDI-ToF MS: 122.5 kDa.

*2.6.5.9 Preparation of cHSA-PEO(2000)$_{16}$-DOTA (**2-25**) and cHSA-PEO(2000)$_{16}$-Gd (**2-26**).*

cHSA-PEO(2000)$_{16}$ (**2-23**, 50 mg) was allowed to completely dissolve in phosphate buffer (50 mL, 50 mM, pH 7.8), followed by adding NHS-DOTA (100 mg, 400 eq) and stirring for 24 hr. After reaction, the product was washed 8 times with deionized distilled water using Vivaspin® 20 (MWCO 30k) centrifugal concentrator and then lyophilized to obtain cHSA-PEO(2000)$_{16}$-DOTA (**2-25**) as white fluffy solid (61 mg, yield 90%).

To load Gd^{3+}, (**2-25**) (50 mg) was allowed to dissolve in $GdCl_3$ solution (25 mL, 6 mM) and stirred at room temperature overnight. The resulted product was washed 8 times with deionized distilled water using Vivaspin® 20 (MWCO 30k) centrifugal concentrator and then lyophilized to obtain cHSA-PEO(2000)$_{16}$-Gd (**2-26**) as white fluffy solid (49 mg, yield 92%).

2.6.6 Characterization of PbPs.

2.6.6.1 DPS test

The procedure of the DPS test is modified from a method described previously [70]. 4,4'-Dithiodipyridine can be reduced by free –SH groups to form 4-thiopyridone with a unique absorption maximum at 325 nm (**Scheme 2-10**). A stock solution of 2 mg/mL thioctic acid in 20mM Tris buffer was firstly prepared at pH 7.4, which was diluted to different concentrations by pure water to give the standard solution. The sample or thioctic acid standard (20 μL) and freshly prepared 2% (w/v) $NaBH_4$ solution (80 μL) were added into

Eppendorf tubes. The solution was then cooled to 0 °C and incubated for 3 hr while shaking. After reduction, 6 M HCl (1 µL) was added to adjust the pH to 1, and the solution was votexed until no gas release was observed anymore. Subsequently, 1.5 M citrate buffer (1.5 µL) was added to bring the pH to 4.5. Then, 5 mM DPS (50 µL) aqueous solution was added and incubated for 1 min. 200 µL of each solution were added to Greiner UVStar® Microplate 96 wells and the absorbance at 325 nm was recorded on a Tecan® Infinite M1000 microplate reader. The concentration of thiol group or thioctic acids was calculated based on the calibration curve (**Figure 2-24**). The read-out was repeated 3 times on average. This assay was sensitive down to 1 µg/mL thioctic acid with excellent correlation.

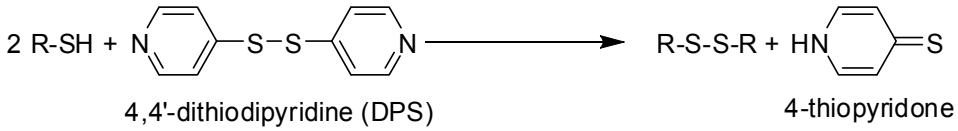

Scheme 2-10. DPS test reaction.

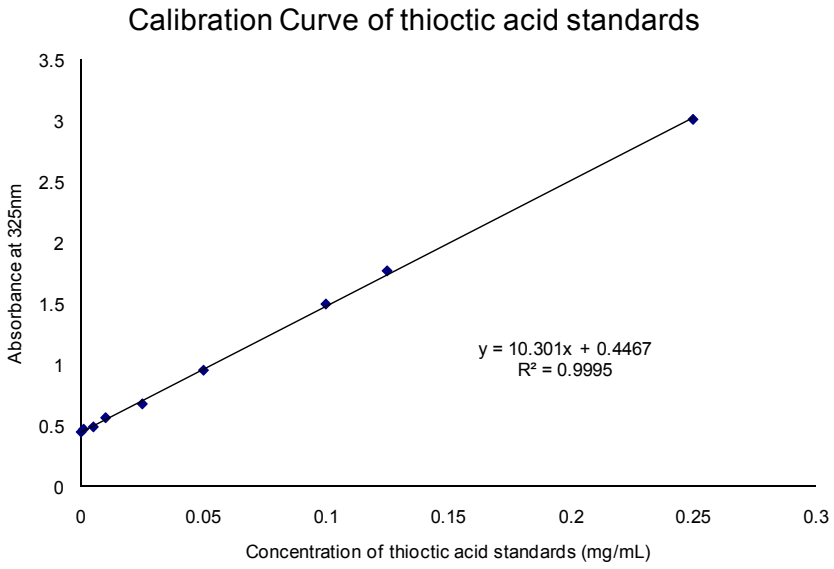

Figure 2-24. Calibration of thioctic acid concentration.

2.6.6.2 Gel permeation chromatography.

Gel permeation chromatography was recorded by Waters 515 HPLC pump, Waters 244 refractive index detector, PL Aquagel-OH 30/40/50 and PL Guard Column (Agilent). Pure water was used as solvent with a flow rate of 1 mL/min.

2.6.6.3 Dynamic light scattering (DLS).

Protein copolymers were prepared at 0.1 mg/ml in aqueous solution and measured at 25°C using a Malvern Zetasizer ZEN3600 (Malvern Ltd, Malvern, UK) The analysis was accomplished with a laser wavelength of 633 nm and a scattering angle of 173°. Solutions were filtered through a 0.2 μm pore size Supor Membrane (Life Science) filter prior to data acquisition. Autocorrelation functions were analyzed by applying the cumulants method and COTIN routine to estimate the hydrodynamic diameter and polydispersity index (PDI). The hydrodynamic diameter distribution was discussed based on both intensity distribution and number distribution.

2.6.6.4 Characterization of the polymer surface charge.

The net surface charges of all samples were characterized by agarose gel electrophoresis using 0.5% agarose gel in pH 7.4 TAE (Tris-Acetate-EDTA) buffer. Positively charged species move toward the negative electrode whereas the negatively charged molecules move toward the positive electrode. The Zeta potential of all samples was also aquired in 1mM KCl solution using a Malvern Zetasizer ZEN3600 (Malvern Ltd, Malvern, UK).

2.6.6.5 Proteolysis of polypeptides - stability study.

1 mg/mL of each sample was prepared in PBS buffer at pH 7.4 and incubated in 0.1% trypsin at 37 °C. To monitor the digestion process on SDS-PAGE, 7 µL of the sample was taken out of the reaction mixture at desired time points and immediately treated by phenylmethanesulfonyl fluoride (PMSF) (1 µL, 10 mM), DTT (1 µL, 1 M) and 3 µL NuPAGE LDS sample buffer (Invitrogen) and boiled at 95 °C for 5 min. The samples were then directly analyzed by SDS-PAGE.

2.6.6.6 Circular dichroism (CD).

All copolymer materials were dissolved in pure water in ~2 mg/mL concentration respectively. Tris buffer (0.75 mL, 50 mM, pH7) was added to 0.1 mL of this solution separately. The sample was measured in a 1 mm cuvette with a volume of 700 µL. The CD signal was recorded from 240 nm down to 190 nm. The bandwidth was set to 1 nm and a response at 1 sec. Standard sensitivity was used with the data pitch 0.1 nm and 100 nm/min scanning speed. Temperature was kept constant at 20 °C. The data was recorded using 5 times data accumulation. The secondary structure elements were estimated using the CDSSTR program in CDPro software package (available at website: http://lamar.colostate.edu/~sreeram/CDPro/main.html).

2.6.6.7 Negative staining transmission electron microscopy (TEM)

The morphology of dcBSA-PEO(5000)$_{27}$ (**2-11**) and dcBSA-PEO(5000)$_{27}$-alkyne (**2-15**) micelles was characterized *via* TEM applying the negative staining technique. A drop of 1 mg/mL aqueous solution of (**2-11**) or (**2-15**) was deposited onto a hydrophilic copper grid with a carbon film for approximately 1 min and then blotted excess of the sample by filter paper.

The grid was allowed to dry at RT for overnight and then stained with 1% uranyl acetate solution for 30 sec before TEM investigations.

2.6.6.8 AFM and fluorescence microscopy[†††]

The AFM samples were prepared by drop-casting 10 µL aliquots of 0.3 mg/mL solutions in Mili-Q water on freshly cleaved Mica and drying in air. AFM measurements were performed on a Vecco Multimode IIIa AFM with extender module using silicon nitride cantilevers (Olympus) with a spring constant of 1.7 N/m. The raw data was processed (plane correction only) and analysed with the SPIP 5.1.5 software (Image Metrology).

The hierarchical self-assembly of the protein copolymer layer with rhodamine monolabeled HSA was carried out as follows. To a mica surface decorated with dLY-PEO(5000)$_8$-TA$_8$ a saturated solution of rhodamine monolabeled HSA in EtOH/H_2O (3:1 v/v) was added and the solvent evaporated in air. The as modified surface was imaged using a Zeiss fluorescence microscope.

2.6.7 Study of PbPs in mammalian cells.

2.6.7.1 Cell culture.

HeLa cells (human cervix carcinomic cell line) and A549 (a carcinomic human alveolar basal epithelial cell line) were obtained from DSMZ (German Collection of Microorganisms and Cell Cultures, Braunschweig) and cultured in DMEM medium with high glucose supplemented and with 10% fetal bovine

[†††] This experiment was performed by Dr. Christoph Meier.

serum (FBS), 100 U/ml Penicillin, 0.1 mg/ml Streptomycin, 0.1 mM non-essential amino acids at 37°C in a humidified 5% CO_2 incubator.

2.6.7.2 Cytotoxicity assay.

Eight thousand of A549 cells or HeLa cells per well were plated onto a white 96-well plate and incubated overnight for attachment. The wells were 70–80 % confluent on the day of the experiment. The cells were then treated with desired concentration of PbP samples as well as 1 μM doxorubicin as control and incubated for another 24 hrs. Cells without treatment were used as blank control. After treatment, Cell-Titer Glo® cell viability assay kit was used to quantify the viability of the cell culture in each well, according to the manufacturer's manual.

2.6.7.3 Confocal laser scanning microscope (CLSM).

A549 cells were plated in a Coverglass Lab-Tek 8-well chamber (Nunc, Denmark) at a density of 30,000 cells per well in 300 μl DMEM containing 10% FCS, 1% penicillin/streptomycin and 1% MEM. The cells were incubated overnight at 37°C in 5% CO_2 to allow adhesion. The next day, 4 μg of rhodamine labeled (**2-2**) and (**2-11**) were added to cells respectively and incubated for 24 hr. Before imaging, cells were washed three times with PBS buffer. Cell nuclei were stained with 1 μl of DAPI solution (5 mg/ml) for 15 mins and the cell membrane was further stained with 0.5 μl of CellMask® Deep Red plasma membrane stain solution for 5 mins (0.5 mg/ml). Imaging was then performed using a LSM 710 laser scanning confocal microscope system (Zeiss, Germany) coupled to an XL-LSM 710 S incubator and equipped with a 63× oil immersion objective. The DAPI nuclei stain and

CellMask® Deep Red plasma membrane stain was excited with a Diode405-30 laser and a HeNe633 laser, respectively, and the emission was collected using 410-582 nm and 647-759 nm filters, respectively. The fluorescence of rhodamine was recorded separately using a 531-648 nm filter and a 514 nm Argon laser for excitation. The acquired images were processed with Zen software developed by Carl Zeiss.

2.7 References

[1]. Wu, Y.; Pramanik, G.; Eisele, K.; Weil, T., Convenient approach to polypeptide copolymers derived from native proteins. *Biomacromolecules* **2012,** *13* (6), 1890-1898.

[2]. Collier, J. H.; Rudra, J. S.; Gasiorowski, J. Z.; Jung, J. P., Multi-component extracellular matrices based on peptide self-assembly. *Chem. Soc. Rev.* **2010,** *39* (9), 3413-24.

[3]. de la Rica, R.; Matsui, H., Applications of peptide and protein-based materials in bionanotechnology. *Chem. Soc. Rev.* **2010,** *39* (9), 3499-3509.

[4]. Lowik, D. W.; Leunissen, E. H.; van den Heuvel, M.; Hansen, M. B.; van Hest, J. C., Stimulus responsive peptide based materials. *Chem. Soc. Rev.* **2010,** *39* (9), 3394-3412.

[5]. Cui, H.; Muraoka, T.; Cheetham, A. G.; Stupp, S. I., Self-assembly of giant peptide nanobelts. *Nano Lett.* **2009,** *9* (3), 945-951.

[6]. Verch, A.; Hahn, H.; Krause, E.; Colfen, H.; Borner, H. G., A modular approach towards functional decoration of peptide-polymer nanotapes. *Chem. Commun. (Cambridge, U. K.)* **2010,** *46* (47), 8938-8940.

[7]. Apostolovic, B.; Deacon, S. P.; Duncan, R.; Klok, H. A., Hybrid polymer therapeutics incorporating bioresponsive, coiled coil peptide linkers. *Biomacromolecules* **2010,** *11* (5), 1187-1195.

[8]. Deacon, S. P.; Apostolovic, B.; Carbajo, R. J.; Schott, A. K.; Beck, K.; Vicent, M. J.; Pineda-Lucena, A.; Klok, H. A.; Duncan, R., Polymer coiled-coil conjugates: potential for development as a new class of therapeutic "molecular switch". *Biomacromolecules* **2011,** *12* (1), 19-27.

[9]. Gil, E. S.; Mandal, B. B.; Park, S. H.; Marchant, J. K.; Omenetto, F. G.; Kaplan, D. L., Helicoidal multi-lamellar features of RGD-functionalized silk biomaterials for corneal tissue engineering. *Biomaterials* **2010,** *31* (34), 8953-8963.

[10]. Sahoo, S.; Toh, S. L.; Goh, J. C., A bFGF-releasing silk/PLGA-based biohybrid scaffold for ligament/tendon tissue engineering using mesenchymal progenitor cells. *Biomaterials* **2010,** *31* (11), 2990-2998.

[11]. van Dongen, S. F. M.; de Hoog, H.-P. M.; Peters, R. J. R. W.; Nallani, M.; Nolte, R. J. M.; van Hest, J. C. M., Biohybrid polymer capsules. *Chem. Rev.* **2009,** *109* (11), 6212-6274.

[12]. Wenk, E.; Wandrey, A. J.; Merkle, H. P.; Meinel, L., Silk fibroin spheres as a platform for controlled drug delivery. *J. Control Release* **2008,** *132* (1), 26-34.

[13]. Hunter, A. C.; Moghimi, S. M., Therapeutic synthetic polymers: a game of Russian roulette? *Drug Discov. Today* **2002,** *7* (19), 998-1001.

[14]. Hadjichristidis, N.; Iatrou, H.; Pitsikalis, M.; Sakellariou, G., Synthesis of well-defined polypeptide-based materials *via* the ring-opening polymerization of α-amino acid N-carboxyanhydrides. *Chem. Rev.* **2009,** *109* (11), 5528-5578.

[15]. Yang, J.; Gitlin, I.; Krishnamurthy, V. M.; Vazquez, J. A.; Costello, C. E.; Whitesides, G. M., Synthesis of monodisperse polymers from proteins. *J. Am. Chem. Soc.* **2003,** *125* (41), 12392-12393.

[16]. Rabotyagova, O. S.; Cebe, P.; Kaplan, D. L., Protein-based block copolymers. *Biomacromolecules* **2011,** *12* (2), 269-289.

[17]. van Hest, J. C.; Tirrell, D. A., Protein-based materials, toward a new level of structural control. *Chem. Commun. (Cambridge, U. K.)* **2001,** (19), 1897-904.

[18]. Brunsveld, L.; Kuhlmann, J.; Alexandrov, K.; Wittinghofer, A.; Goody, R. S.; Waldmann, H., Lipidated ras and rab peptides and proteins--synthesis, structure, and function. *Angew. Chem., Int. Ed.* **2006,** *45* (40), 6622-6646.

[19]. Klok, H.-A., Protein-inspired materials: Synthetic concepts and potential applications. *Angew. Chem., Int. Ed.* **2002,** *41* (9), 1509-1513.

[20]. Calmettes, P.; Durand, D.; Desmadril, M.; Minard, P.; Receveur, V.; Smith, J. C., How random is a highly denatured protein? *Biophys. Chem.* **1994,** *53* (1–2), 105-113.

[21]. Dill, K. A.; Shortle, D., Denatured states of proteins. *Annu. Rev. Biochem.* **1991,** *60* (1), 795-825.

[22]. Steinhardt, J.; Krijn, J.; Leidy, J. G., Differences between bovine and human serum albumins. Binding isotherms, optical rotatory dispersion, viscosity, hydrogen ion titration, and fluorescence effects. *Biochemistry* **1971,** *10* (22), 4005-4015.

[23]. Zöphel, L.; Eisele, K.; Gropeanu, R.; Rouhanipour, A.; Koynov, K.; Lieberwirth, I.; Müllen, K.; Weil, T., Preparation of defined albumin–polymer hybrids for efficient cell transfection. *Macromol. Chem. Phys.* **2010,** *211* (2), 146-153.

[24]. Williams, E. J.; Foster, J. F., The aggregation of bovine plasma albumin at low pH1. *J. Am. Chem. Soc.* **1960,** *82* (14), 3741-3745.

[25]. Ware, B. R.; Flygare, W. H., Light scattering in mixtures of BSA, BSA dimers, and fibrinogen under the influence of electric fields. *J. Colloid Interface Sci.* **1972,** *39* (3), 670-675.

[26]. Wu, Y.; Weil, T., An efficient approach for preparing giant polypeptide triblock copolymers by protein dimerization. *Macromol. Rapid Commun.* **2012,** *33* (15), 1304-1309.

[27]. Dong, H.; Hartgerink, J. D., Role of hydrophobic clusters in the stability of α-helical coiled coils and their conversion to amyloid-like β-sheets. *Biomacromolecules* **2007,** *8* (2), 617-623.

[28]. Whitmore, L.; Wallace, B. A., Protein secondary structure analyses from circular dichroism spectroscopy: methods and reference databases. *Biopolymers* **2008,** *89* (5), 392-400.

[29]. Sreerama, N.; Woody, R. W., Estimation of protein secondary structure from circular dichroism spectra: Comparison of CONTIN, SELCON, and CDSSTR methods with an expanded reference set. *Anal. Biochem.* **2000,** *287* (2), 252-260.

[30]. Fotiadis, D.; Scheuring, S.; Muller, S. A.; Engel, A.; Muller, D. J., Imaging and manipulation of biological structures with the AFM. *Micron* **2002,** *33* (4), 385-97.

[31]. Rosler, A.; Klok, H. A.; Hamley, I. W.; Castelletto, V.; Mykhaylyk, O. O., Nanoscale structure of poly(ethylene glycol) hybrid block copolymers containing amphiphilic beta-strand peptide sequences. *Biomacromolecules* **2003,** *4* (4), 859-63.

[32]. Siddique, B.; Duhamel, J., Effect of polypeptide sequence on polypeptide self-assembly. *Langmuir* **2011,** *27* (11), 6639-6650.

[33]. Georgalis, Y.; Umbach, P.; Raptis, J.; Saenger, W., Lysozyme aggregation studied by light scattering. I. Influence of concentration and nature of electrolytes. *Acta Crystallogr. D Biol. Crystallogr.* **1997,** *53* (Pt 6), 691-702.

[34]. Cosson, P.; Lankford, S. P.; Bonifacino, J. S.; Klausner, R. D., Membrane protein association by potential intrarnembrane charge pairs. *Nature* **1991,** *351* (6325), 414-416.

[35]. Catterall, W. A., From ionic currents to molecular mechanisms: the structure and function of voltage-gated sodium channels. *Neuron* **2000,** *26* (1), 13-25.

[36]. Ding, X.-Q.; Pinon, D. I.; Furse, K. E.; Lybrand, T. P.; Miller, L. J., Refinement of the Conformation of a Critical Region of Charge-Charge Interaction between Cholecystokinin and Its Receptor. *Molecular Pharmacology* **2002,** *61* (5), 1041-1052.

[37]. Boddohi, S.; Kipper, M. J., Engineering nanoassemblies of polysaccharides. *Adv. Mater.* **2010,** *22* (28), 2998-3016.

[38]. He, Q.; Cui, Y.; Li, J., Molecular assembly and application of biomimetic microcapsules. *Chem. Soc. Rev.* **2009,** *38* (8), 2292-2303.

[39]. Zöphel, L.; Eisele, K.; Gropeanu, R.; Rouhanipour, A.; Koynov, K.; Lieberwirth, I.; Müllen, K.; Weil, T., Preparation of Defined Albumin–Polymer

Hybrids for Efficient Cell Transfection. *Macromolecular Chemistry and Physics* **2010,** *211* (2), 146-153.

[40]. Eisele, K.; Gropeanu, R. A.; Zehendner, C. M.; Rouhanipour, A.; Ramanathan, A.; Mihov, G.; Koynov, K.; Kuhlmann, C. R. W.; Vasudevan, S. G.; Luhmann, H. J.; Weil, T., Fine-tuning DNA/albumin polyelectrolyte interactions to produce the efficient transfection agent cBSA-147. *Biomaterials* **2010,** *31* (33), 8789-8801.

[41]. Ng, J. F.; Jaenicke, S.; Eisele, K.; Dorn, J.; Weil, T., cBSA-147 for the preparation of bacterial biofilms in a microchannel reactor. *Biointerphases* **2011,** *5* (3), FA41-7.

[42]. Ritz, S.; Eisele, K.; Dorn, J.; Ding, S.; Vollmer, D.; Putz, S.; Weil, T.; Sinner, E. K., Cationized albumin-biocoatings for the immobilization of lipid vesicles. *Biointerphases* **2010,** *5* (3), FA78-87.

[43]. Li, L., *Overview of MS and MALDI MS for polymer analysis*. John Wiley & Sons, Inc.: 2009; p 8.

[44]. Ganta, S.; Devalapally, H.; Shahiwala, A.; Amiji, M., A review of stimuli-responsive nanocarriers for drug and gene delivery. *Journal of Controlled Release* **2008,** *126* (3), 187-204.

[45]. Wu, Y.; Chakrabortty, S.; Gropeanu, R. A.; Wilhelmi, J.; Xu, Y.; Er, K. S.; Kuan, S. L.; Koynov, K.; Chan, Y.; Weil, T., pH-Responsive quantum dots *via* an albumin polymer surface coating. *J. Am. Chem. Soc.* **2010,** *132* (14), 5012-5014.

[46]. Wu, Y.; Er, K. S.; Ramanathan, A.; Vasudevan, S.; Weil, T., Nano-sized albumin-copolymer micelles for efficient doxorubicin delivery. *Biointerphases* **2012,** *7* (1-4), 5.

[47]. Strader, M. B.; Tabb, D. L.; Hervey, W. J.; Pan, C.; Hurst, G. B., Efficient and specific trypsin digestion of microgram to nanogram quantities of proteins in organic-aqueous solvent systems. *Anal Chem* **2006,** *78* (1), 125-34.

[48]. Wu, Y.; Wang, T.; Ng, D. Y. W.; Weil, T., Multifunctional polypeptide–PEO nanoreactors *via* the hydrophobic switch. *Macromol. Rapid Commun.* **2012,** *33* (17), 1474-1481.

[49]. Bhattacharya, A. A.; Grune, T.; Curry, S., Crystallographic analysis reveals common modes of binding of medium and long-chain fatty acids to human serum albumin. *J. Mol. Biol.* **2000,** *303* (5), 721-732.

[50]. Mori, O.; Imae, T., AFM investigation of the adsorption process of bovine serum albumin on mica. *Colloids Surf., B* **1997,** *9* (1-2), 31-36.

[51]. Fotiadis, D.; Scheuring, S.; Müller, S. A.; Engel, A.; Müller, D. J., Imaging and manipulation of biological structures with the AFM. *Micron* **2002,** *33* (4), 385-397.

[52]. Lomander, A.; Hwang, W.; Zhang, S., Hierarchical self-assembly of a coiled-coil peptide into fractal structure. *Nano Lett.* **2005,** *5* (7), 1255-1260.

[53]. Foubert, P.; Hannink, J. M.; Köhn, F.; Gronheid, R.; Sommerdijk, N. A. J. M.; Nolte, R. J. M.; De Feyter, S.; De Schryver, F. C., Morphology of protein polymer hybrid films studied by atomic force microscopy and scanning confocal fluorescence microscopy. *Thin Solid Films* **2003,** *443* (1-2), 124-135.

[54]. Sivakumar, K.; Xie, F.; Cash, B. M.; Long, S.; Barnhill, H. N.; Wang, Q., A fluorogenic 1,3-dipolar cycloaddition reaction of 3-azidocoumarins and acetylenes. *Org. Lett.* **2004,** *6* (24), 4603-4606.

[55]. Wu, Y.; Ihme, S.; Feuring-Buske, M.; Kuan, S. L.; Eisele, K.; Lamla, M.; Wang, Y.; Buske, C.; Weil, T., A core-shell albumin copolymer nanotransporter for high capacity loading and two-step release of doxorubicin with enhanced anti-leukemia activity. *Adv. Healthcare Mater.* **2013**, DOI: 10.1002/adhm.201200296.

[56]. Unger, C.; Haring, B.; Medinger, M.; Drevs, J.; Steinbild, S.; Kratz, F.; Mross, K., Phase I and pharmacokinetic study of the (6-maleimidocaproyl)hydrazone derivative of doxorubicin. *Clin. Cancer Res.* **2007,** *13* (16), 4858-4866.

[57]. Lammers, T.; Hennink, W. E.; Storm, G., Tumour-targeted nanomedicines: principles and practice. *Br. J. Cancer.* **2008,** *99* (3), 392-397.

[58]. Zhou, Z.; Lu, Z.-R., Gadolinium-based contrast agents for magnetic resonance cancer imaging. *Wiley Interdisciplinary Reviews: Nanomedicine and Nanobiotechnology* **2013,** *5* (1), 1-18.

[59]. Botta, M.; Tei, L., Relaxivity enhancement in macromolecular and nanosized GdIII-based MRI contrast agents. *European Journal of Inorganic Chemistry* **2012,** *2012* (12), 1945-1960.

[60]. Daldrup, H.; Shames, D. M.; Wendland, M.; Okuhata, Y.; Link, T. M.; Rosenau, W.; Lu, Y.; Brasch, R. C., Correlation of dynamic contrast-enhanced magnetic resonance imaging with histologic tumor grade: comparison of macromolecular and small-molecular contrast media. *Pediatr Radiol* **1998,** *28* (2), 67-78.

[61]. Curtet, C.; Maton, F.; Havet, T.; Slinkin, M.; Mishra, A.; Chatal, J. F.; Muller, R. N., Polylysine-Gd-DTPAn and polylysine-Gd-DOTAn coupled to anti-CEA F(ab')2 fragments as potential immunocontrast agents. Relaxometry, biodistribution, and magnetic resonance imaging in nude mice grafted with human colorectal carcinoma. *Invest. Radiol.* **1998,** *33* (10), 752-761.

[62]. Venditto, V. J.; Regino, C. A. S.; Brechbiel, M. W., PAMAM dendrimer based macromolecules as improved contrast agents. *Mol. Pharm.* **2005,** *2* (4), 302-311.

[63]. Hak, S.; Sanders, H. M.; Agrawal, P.; Langereis, S.; Grull, H.; Keizer, H. M.; Arena, F.; Terreno, E.; Strijkers, G. J.; Nicolay, K., A high relaxivity Gd(III)DOTA-DSPE-based liposomal contrast agent for magnetic resonance imaging. *Eur J Pharm Biopharm* **2009,** *72* (2), 397-404.

[64]. Ogan, M. D.; Schmiedl, U.; Moseley, M. E.; Grodd, W.; Paajanen, H.; Brasch, R. C., Albumin labeled with Gd-DTPA. An intravascular contrast-enhancing agent for magnetic resonance blood pool imaging: preparation and characterization. *Invest. Radiol.* **1987,** *22* (8), 665-671.

[65]. Dafni, H.; Kim, S.-J.; Bankson, J. A.; Sankaranarayanapillai, M.; Ronen, S. M., Macromolecular dynamic contrast-enhanced (DCE)-MRI detects reduced vascular permeability in a prostate cancer bone metastasis model following anti–platelet-derived growth factor receptor (PDGFR) therapy, indicating a drop in vascular endothelial growth factor receptor (VEGFR) activation. *Magnetic Resonance in Medicine* **2008,** *60* (4), 822-833.

[66]. Raatschen, H.-J.; Simon, G. H.; Fu, Y.; Sennino, B.; Shames, D. M.; Wendland, M. F.; McDonald, D. M.; Brasch, R. C., Vascular Permeability

during Antiangiogenesis Treatment: MR Imaging Assay Results as Biomarker for Subsequent Tumor Growth in Rats1. *Radiology* **2008,** *247* (2), 391-399.

[67]. Howarth, M.; Liu, W.; Puthenveetil, S.; Zheng, Y.; Marshall, L. F.; Schmidt, M. M.; Wittrup, K. D.; Bawendi, M. G.; Ting, A. Y., Monovalent, reduced-size quantum dots for imaging receptors on living cells. *Nat. Meth.* **2008,** *5* (5), 397-399.

[68]. Li, C.; Winnard, P. T.; Takagi, T.; Artemov, D.; Bhujwalla, Z. M., Multimodal image-guided enzyme/prodrug cancer therapy. *Journal of the American Chemical Society* **2006,** *128* (47), 15072-15073.

[69]. Zöphel, L.; Eisele, K.; Gropeanu, R.; Rouhanipour, A.; Koynov, K.; Lieberwirth, I.; Müllen, K.; Weil, T., Preparation of defined albumin–polymer hybrids for efficient cell transfection. *Macromol. Chem. Phys.* **2010,** *211* (2), 146-153.

[70]. Hansen, R. E.; Østergaard, H.; Nørgaard, P.; Winther, J. R., Quantification of protein thiols and dithiols in the picomolar range using sodium borohydride and 4,4'-dithiodipyridine. *Analytical Biochemistry* **2007,** *363* (1), 77-82.

Chapter 3

Protein Based Polypeptide Copolymers Coated Biocompatible QDs for Imaging, Biosensoring and Gene delivery

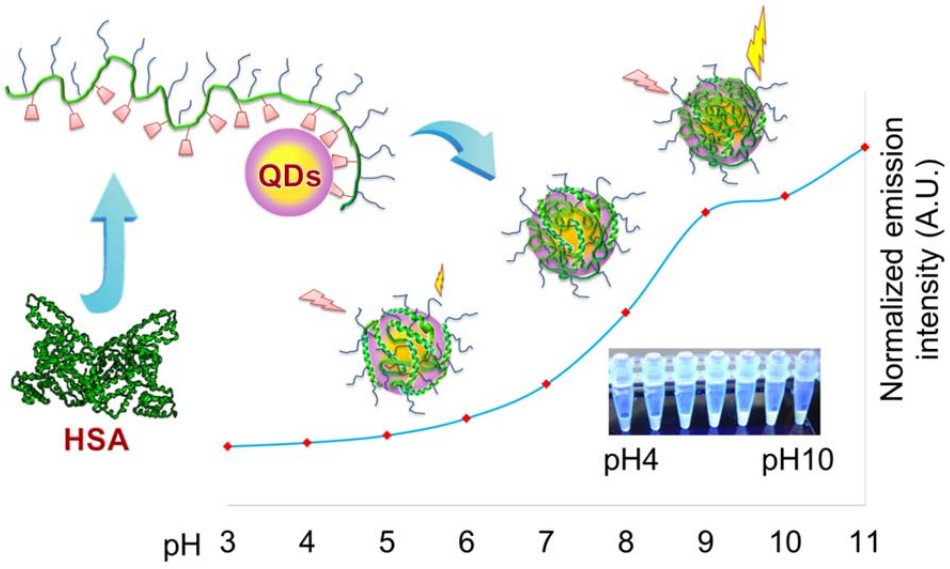

Reproduced with permission [1]. Copyright 2012, American Chemical Society.

This Chapter contains experimental results published previously in (1) *J. Am. Chem. Soc.*, 2010, 132(14):5012-5014. written by Wu Y., Chakrabortty S., Gropeanu R. A., Wilhelmi J., Xu Y., Er K. S., Kuan S. L., Koynov K., Chan Y. T. and Weil T. and (2) *Small*, 2012, 8 (22): 3465–3475. written by Wu Y., Eisele K., Doroshenko M., Algara-Siller G., Kaiser U., Koynov K., Weil T., The dissertation author was the primary investigator and first author of these papers.

3.1 Introduction

Fluorescence microscopy techniques are rapidly developing with respect to resolution, sensitivity and versatility and emerged as powerful tools for monitoring the dynamics of live cells as well as tracking of target molecules and cells *in vivo*. [2] However, challenges are still associated with fluorescence microscopy including cell auto-fluorescence in the visible spectrum which can mask signals from labelled molecules and the limited observation times due to the photobleaching of conventional organic fluorophores [3]. From this aspect, there is a high demand for new fluorescent probes that emit above 550 nm and that are photo-stable for long time excitation. [4]

Quantum dots (QDs) are fluorescent colloidal semiconductor nanoparticles made from II/VI and III/V semiconductors [5, 6], carbon [7] and silicon nanoparticles [8]. The absorption and emission properties of QDs can be precisely controlled by the composition and particle size during synthesis (**Figure 3-1**). In comparison to organic chromophores, QDs reveal a number of unique features attractive for bioimaging. (i). The absorption spectra of QDs are broad and range from the UV region to the first excitonic absorption band in visible region, which allow excitation of mixed QD populations at a single wavelength far from their respective emissions. (ii) Their photoluminescence (PL) spectra are mostly narrow and symmetric with large Stokes shifts, which is straightforward for the separation of excitation and emission while imaging. (iii). The fluorescence from QDs is normally very bright with high quantum yield and excitation coefficient, and photobleaching and chemical degradation

does usually not occur. Such photostability is essential for long term imaging and single-molecule tracking. (iv). The emission of QDs could be fine-tuned from the visible region to the NIR region allowing even flexible color selection in special cases. These outstanding properties make QDs highly attractive as fluorophores for biomedical diagnostic applications. [4]

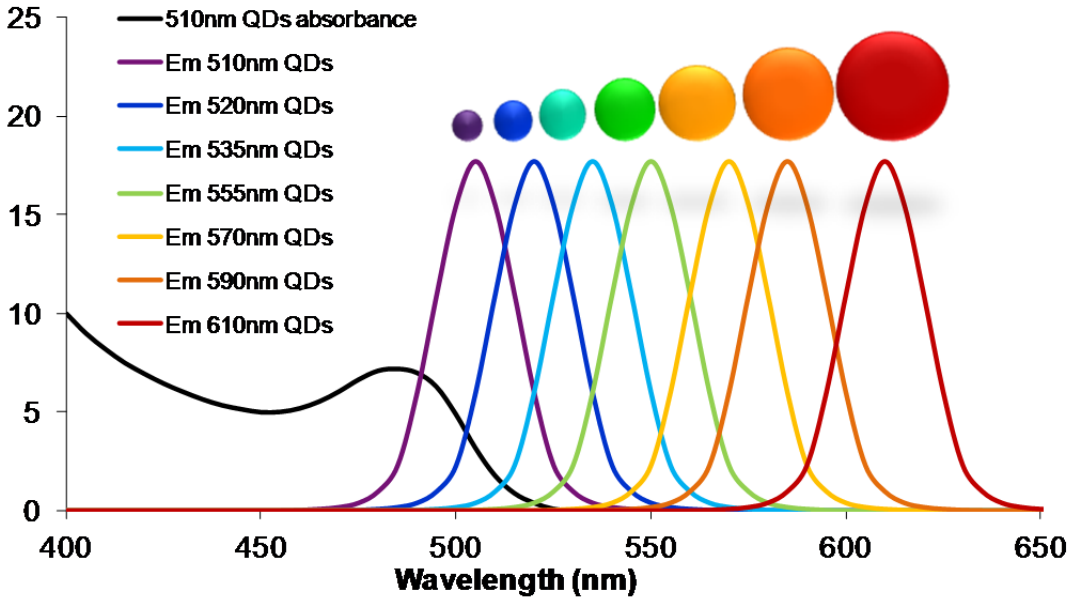

Figure 3-1. Representative absorbance and emission spectra of QDs [9].

One of the most widely used QD fluorophores are based on CdSe cores overcoated with a layer of ZnS. The passivation layer of ZnS protects the CdSe cores from oxidation, prevents leeching of Cd and Se and also substantially improved the quantum yield [10, 11]. The reproducible preparation of high-quality CdSe/ZnS core-shell QDs was firstly reported by the Bawendi group [12]. CdSe QDs cores grew at high-temperature solvents/ligands (mixture of trioctyl phosphine/trioctyl phosphine oxide, TOP/TOPO), combined with pyrolysis of organometallic precursors (such as CdO and Cd-acetate). The crystallization duration was critical for controlling the size and spectra of

the QDs. This method yielded highly crystalline CdSe cores with size distributions of 8-11%. The same reaction could be further applied to grow the passivation shell using wider-bandgap semiconducting material (e.g. ZnS or CdS) [12, 13].

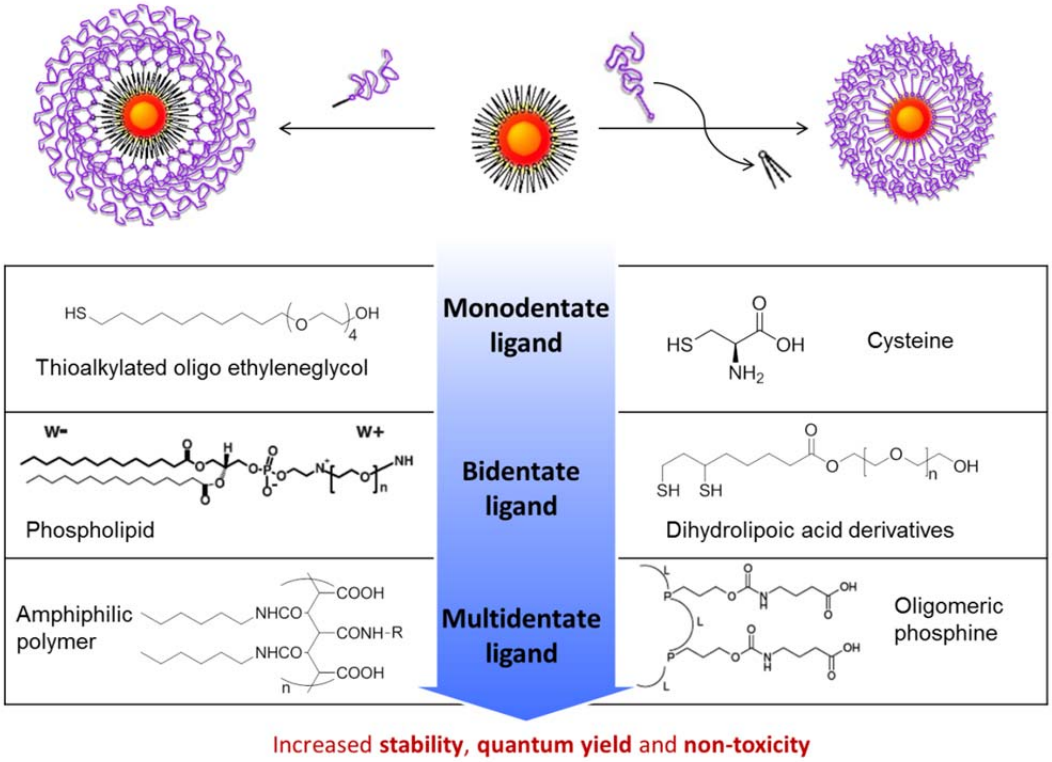

Figure 3-2. Ligand exchange to make water soluble QDs.

Notably, QDs prepared using high-temperature crystallization were insoluble in aqueous solution. Thus, for biological applications, surface functionalization of QDs with hydrophilic ligands was required. This process could be accomplished either through 'capping exchange' to replace TOP/TOPO ligands with hydrophilic ligands, or by encapsulating the TOP/TOPO-capped QDs in another thick heterofunctional organic coating driven by hydrophobic interactions [9] (**Figure 3-2**). Thiol group (-SH) [14] and phorsphine groups [15] were identified as high affinity anchor groups to interact

with QDs and replace TOP/TOPO capping. For hydrophobic encapsulation strategies, amphiphilic polymers consisting C8 to C18 lipid chains were found efficient [15]. According to the number of interaction points in each ligand, the ligands used for QDs phase transfer could be classified into three groups: simple monodentate ligands (e.g. cysteine [3], mercaptocarbonic acids [16]), small molecular bidentate ligand (e.g. dihydrolipoic acid (DHLA) derivatives [17, 18]) and polymeric multidentate ligand (e.g. lipid chain modified acrylic acid polymer [15], oligomeric phosphines [19] and amphiphilic block copolymers [20]). Although the small molecular ligands were popular due to their facile synthesis, QDs capped by these ligands revealed limitations such as short shelf lives due to dynamic thiol-ZnS interactions [21]. Bidentate small molecular ligands, such as dihydrolipoic acid derivatives containing two thiol groups, significantly improved the QDs stability in aqueous solution compared with mono-mercapto ligands. However, multidentate polymeric ligands were still recognized as the most preferred capping materials to stabilize QDs for biological studies [22]. In addition, the surface functionalization ligands on the one hand contributed to the water solubility of QDs and on the other hand provided modification points for further conjugations with biomolecules. Therefore, these ligands normally required multifunctionalities including anchor groups for QDs interactions and chemical reactive groups for further modification chemistries.

In the last Chapter, the preparation of a new class protein derived polypeptide copolymers (PbPs) was introduced. These polypeptides revealed high water solubility, attractive biocompatibility as well as multiple accessible

functional groups. Therefore, they are expected to be very suitable for the stabilization and functionalization of QDs. The synthesis of albumin derived PbP decorated thioctic acid, which formed special nanopatterning on mica surfaces (section 2.4.2), was introduced in Chapter 2. Reduction of the thioctic acid moieties yielded dihydrolipoic acid (DHLA) which had been widely used for high affinity interactions with QDs [17, 18]. Thus we have applied the thioctic acid modified PbPs (**2-16**), (**2-17**) and (**2-18**) for QDs ligand exchange.

In this Chapter, the preparation of PbPs coated QDs will be described. Such QDs are found to be highly stable in a biological environment and not toxic to cells even at high concentrations. In addition, the cell uptake efficiency of such QDs could be tuned depending on the PbPs used for coating. An interesting responsiveness has also been observed for some coated QDs, e.g. a pH responsiveness and responsiveness to DNA concentration, which makes them particularly attractive for *in vivo* cell imaging.

3.2 Preparation and characterization of PbPs coated biocompatible QDs

3.2.1 Preparation of water soluble QDs with serum albumin copolymer coatings

Differently colored CdSe/CdZnS QDs were firstly synthesized according to literature procedures [23]. Two different colors with emission maxima at 561nm and 599nm were prepared and kindly provided by Dr. Yinthai Chan

from National University of Singapore. Their absorption and PL spectra are shown in **Figure 3-3**.

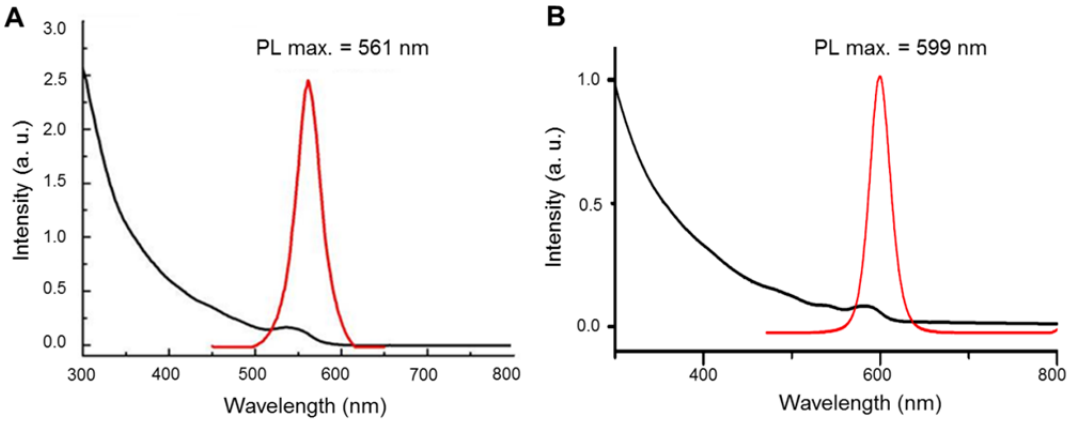

Figure 3-3. Absorption (black) and PL (red) spectra of (a) 561nm quantum dots and (b) 599nm quantum dots. Adapted with permission [1]. Copyright 2012, American Chemical Society.

To couple thioctic acid modified PbPs to hydrophobic, as-synthesized CdSe/CdZnS QDs, the disulfide group of the thioctic acid substituents were firstly reduced with $NaBH_4$ under argon to afford dihydrolipoic acid (DHLA). The ligand exchange with CdSe/CdZnS QDs was subsequently achieved *in situ* by adding a QDs dispersion in a minimum amount of THF under vigorous stirring. The solution was stirred overnight and the non-reacted QDs were filtered out. The coated QDs were then homogeneously dispersed in water. By this way, QDs coated with (**2-16**), (**2-17**) and (**2-18**) were all prepared and named as HSA-QDs, cBSA-QDs and LY-QDs. The emission spectra of PbPs coated QDs in water revealed a slight bathochromic shift compared with the as-synthesized QDs in hexane, consistent with previous reports on ligand-exchange with thioalkyl acids [24] (**Figure 3-5**). The quantum yields (QY) of the thus formed coated core-shell QDs decreased from ~48% in hexane to

10~20% on average in water, which is typical of QD ligand-exchange processes. [25, 26] Furthermore, the number of thoictic acid groups attached to these three materials was also different due to the various amounts of available amino groups, which was strongly influent the quantum yields of stabilized QDs. dcBSA-PEO(5000)$_{27}$-TA$_{26}$ (**2-17**) contained the highest number of TA groups (26±3 TA), which also gave the highest quantum yield (21%) of the coated QDs (cBSA-QDs), whereas the dHSA-PEO(5000)$_{27}$-TA$_{22}$ (**2-16**) coated HSA-QDs had quantum yields of 15% and the QDs from dLys-PEO5000$_8$-TA$_8$ (**2-18**) coating had quantum yield of only 11%. This observation clearly indicated that introducing sufficient anchoring groups is important for maintaining high quantum yields.

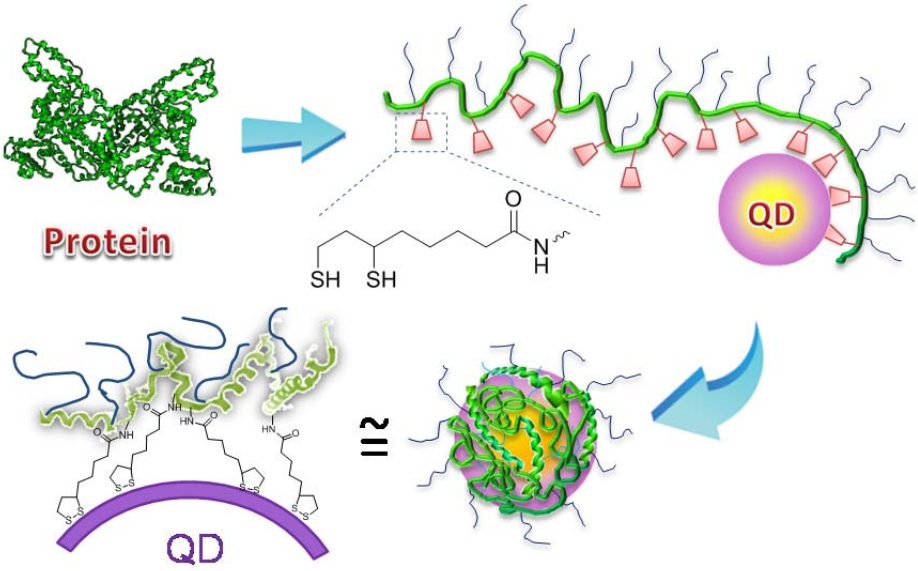

Figure 3-4. An illustration of a QD coated with PbPs. While it is possible that each PbP chain may include more than one QD, such occurrences were rare and the majority of conjugates comprised of single QDs. Adapted with permission [1]. Copyright 2012, American Chemical Society.

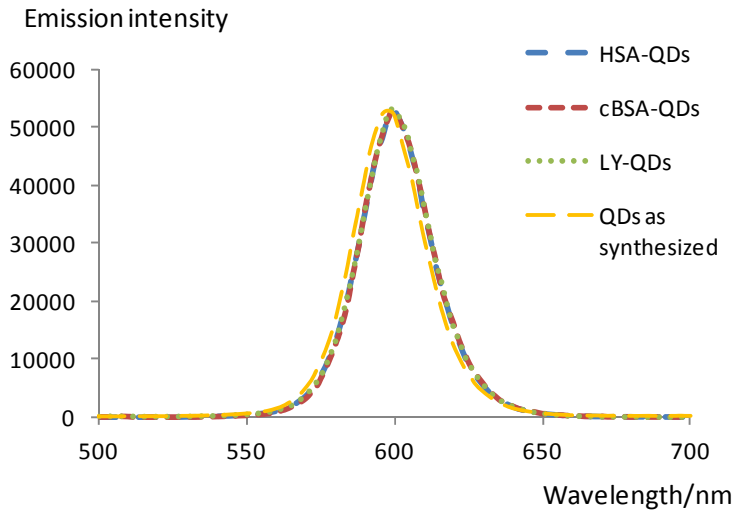

Figure 3-5. Emission spectra of HSA-QDs, cBSA-QDs and LY-QDs compared with as-synthesized QDs.

3.2.2 Size distribution and composition of PbP-QDs

The sizes of the nanoparticles have a significant impact on their cell uptake efficiency [27], biodistribution [28] as well as cytotoxicity [29] and are therefore critical for biomedical application. The size distribution of HSA-QDs and cBSA-QDs was assessed by transmission electron microscopy (TEM), dynamic light scattering (DLS) and fluorescence correlation spectroscopy (FCS). Electron microscopy is a powerful technique to visualize inorganic nanoparticles, since they normally possess high electron densities. However, flexible organic materials such as the protein shells of HSA-QDs and cBSA-QDs are difficult to be directly visualized by TEM. Therefore, we observed mainly homogeneously dispersed CdSe/CdZnS cores with average diameters of ~ 8nm *via* TEM (**Figure 3-6a** and **b**). In order to also visualize the protein shell, negative staining with Uranyl acetate was applied. The differential electron scattering by the heavy metal stain versus the lower atomic mass

samples under investigation generated reverse-contrast negative electron optical images [30], which showed the protein shell as white color spots on a dark background. Thus, the HSA-QDs coated with protein shells were observed with average diameters of 55 nm (**Figure 3-6c**). The detailed structure of cBSA-QDs was also investigated by high resolution TEM on a grapheme substrate at 80 kV acceleration voltage (this data was obtained in close collaboration with Prof. Kaiser and Prof. Walter in Ulm University). As shown in **Figure 3-6d**, the atomic crystal lattice fringes of CdSe/CdZnS QD cores were clearly visualized, which are surrounded by shell-like structures. It can be suggested that these structures are formed by the dcBSA-PEO$(5000)_{27}$-TA_{26} protein shells. Such shell structures were always found around the quantum dots cores. The average diameters of the QD cores were about 6.55 nm and the compressed protein gaps between agglomerated QD cores were about 2 nm. Very flexible polymer structures were found around the QDs and the polymer around the QDs increased from 5 to 15 nm.

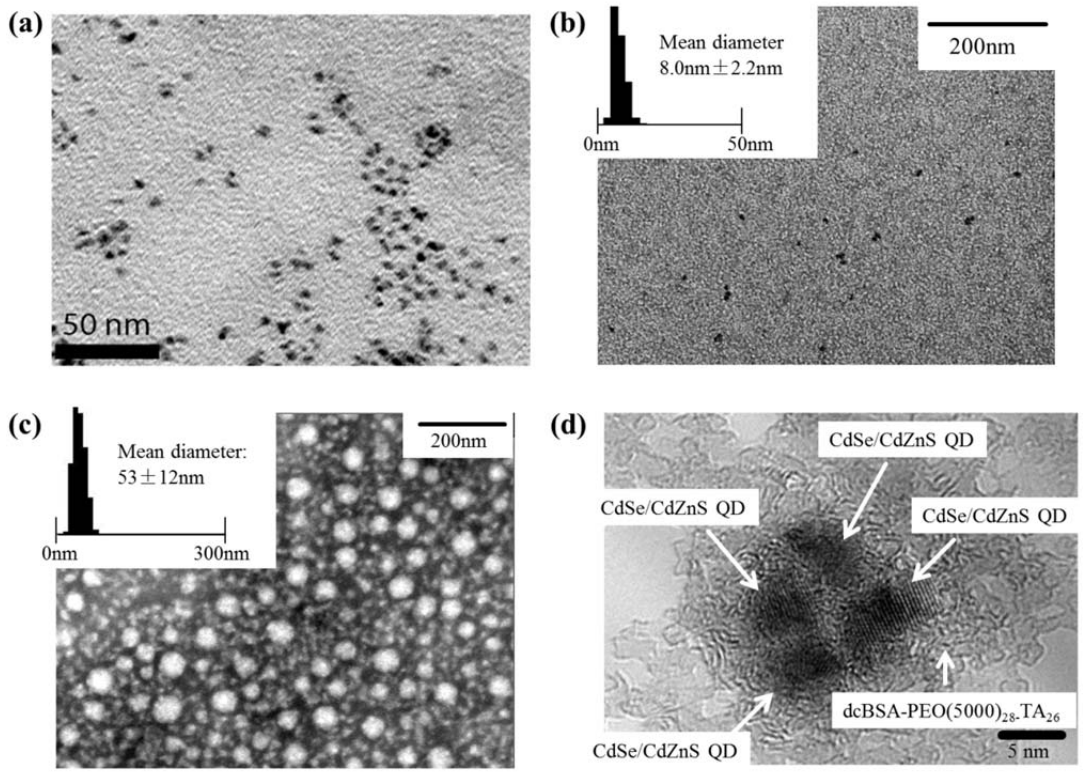

Figure 3-6. TEM micrographs of (a) HSA-QDs and (b) cBSA-QDs. (c) Negative staining TEM of HSA-QDs. (d) High resolution TEM of cBSA-QDs*. The insert reveals the size distribution based on statistic of 106 particles (mean ± standard deviation). Adapted with permission [50]. Copyright 2012, Wiley-VCH.

Notably, although the protein structures were observed under high resolution TEM, such structures only reflected the morphology of PbPs coated QDs under dry conditions. In order to investigate the size distribution of the biopolymer-coated QDs in solution, DLS and FCS were applied. DLS is a convenient method to determine the hydrodynamic size distribution profile of small particles in suspension or solution. According to DLS, the average diameters of HSA-QDs and cBSA-QDs were ~30 nm and ~33 nm respectively

* The high resolution TEM was done by Prof. Kaiser´s group in Ulm University.

(PDI ~ 0.2) (**Figure 3-7**). Similarly, FCS† also obtained a hydrodynamic diameter of ~34 nm for HSA-QDs, and the hydrodynamic diameter of ~44 nm for cBSA-QDs (**Figure 3-8**). (The FCS experiments were performed in close collaboration with Dr. Koynov in Max Planck Institute of Polymer Research). Both methods are in good agreement with each other, and also in the same range of the results measured by negative staining TEM. The significantly increased hydrodynamic diameters of coated QDs compared to the CdSe/CdZnS core reflected the successful coating by the PbP shell.

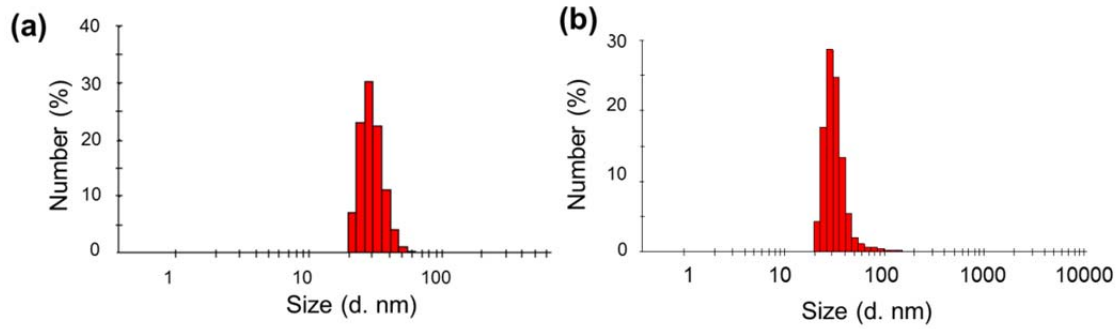

Figure 3-7. Hydrodynamic diameter distributions of (a) HSA-QDs and (b) cBSA-QDs measured by DLS. Adapted with permission [50]. Copyright 2012, Wiley-VCH.

† Fluorescence correlation spectroscopy (FCS) is a correlation analysis of the concentration fluctuations of fluorescent particles (molecules) in solution. In this technique, the fluorescence emitted from a very tiny space in solution containing a small number of fluorescent particles (molecules) is observed. The fluorescence intensity is fluctuating due to Brownian motion of the particles. In other words, the number of the particles in the sub-space defined by the optical system is randomly changing around the average number. The analysis gives the average number of fluorescent particles and average diffusion time, when the particle is passing through the space. Eventually, both the concentration and size of the particle (molecule) are determined.

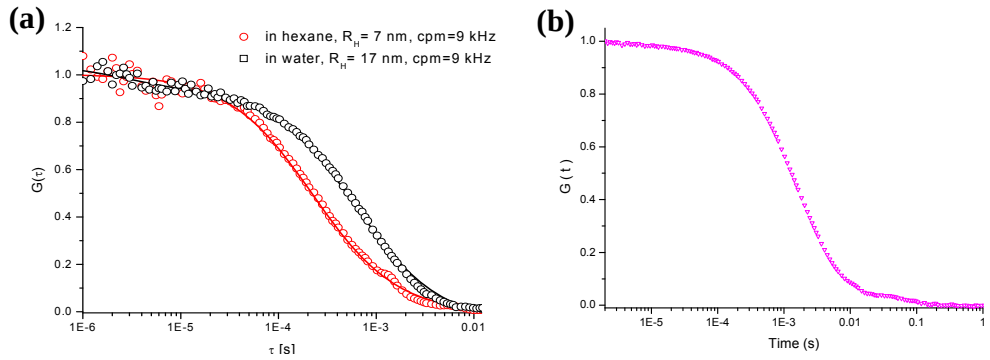

Figure 3-8. Hydrodynamic diameter distributions of (a) HSA-QDs and (b) cBSA-QDs measured by FCS. Adapted with permission [50]. Copyright 2012, Wiley-VCH.

The theoretical sizes of the PbPs coated QDs were calculated based on literature data. The cBSA-QDs with emission maxima at ~600 nm were taken as an example. According to the literature [10], CdSe/CdZnS QDs emission at ~600 nm originated from 5 nm CdSe and a CdZnS shell of approximately 3 nm, which was consistent with our findings. When considering the BSA-derived protein shell, native, globular BSA has a hydrodynamic diameter of ~7 nm [31]. Therefore, the BSA shell added at least 14 nm to the total diameter of cBSA-QDs considering that the QDs were encapsulated by the biopolymer. In addition, the polyethylene oxide side chains of the cBSA-PEO copolymer were hydrophilic, and most likely, they adopted a more extended architecture in aqueous solution. Theoretically, each repeat unit of PEO contributes about 3.5 Å. Therefore, fully extended PEO(5000) (consisting of 114 repeating units) would add to a total length of ~ 40 nm. Taking into consideration that the PEO chains were flexible and could fold back; we could assume that the hydrodynamic length of a PEO(5000) chain was about 3-times shorter than the fully extended chain length, which gave about 12 nm. In the literature, PEO(2000) chains on liposomes have been estimated to contribute a

"hydrodynamic thickness" of 3.5 to 4.5nm [32], which also supported that the PEO(5000) chains contributed about 9 to 11 nm. Therefore, the theoretical hydrodynamic diameter of cBSA-QDs should be at least 8 nm (QD core) +7 nm (Protein shell) +2*12 nm (PEO(5000) shell) = 39 nm (**Figure 3-9**). The experimental dimensions of the cBSA-QDs determined by negative staining TEM, DLS and FCS showed an average hydrodynamic diameter of about 43 nm as discussed above, which was close to the theoretical value calculated.

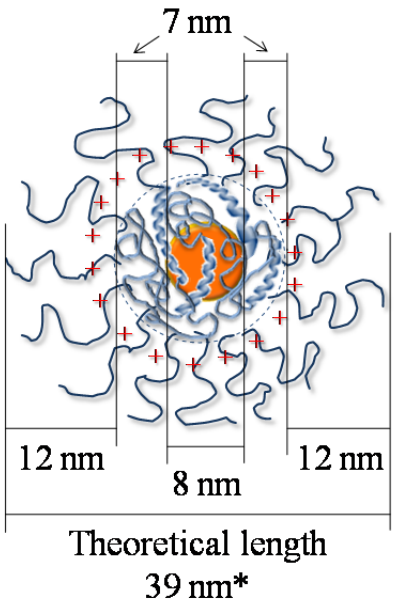

Figure 3-9. Scratch of quantum dots diameter. Reproduced with permission [50]. Copyright 2012, Wiley-VCH.

3.2.3 The stability of PbP-QDs under biological conditions

The high number of TA groups attached along the copolymer backbone allowed multivalent interactions stabilizing the QDs in solution thus yielding tremendously stable core-shell particles even under extreme conditions [33]. No changes in the optical spectra occurred even after 6 months of storage in

aqueous solution at 4°C. High stability was also found in PBS buffer and cell culture media (**Figure 3-10**). Furthermore, although the PbPs undergoes fast enzymatic degradation in solution, the QDs coated with PbPs exhibited very high resistance to proteolysis. For instance, the incubation of cBSA-QDs with 0.1 mg/mL trypsin and proteinase K for 1 hr resulted in only a slight decrease in the QY (**Figure 3-10** and **Figure 3-11**), suggesting strong interactions of multiple thiol groups with the QD surface. SDS-PAGE also shows the stable QDs band on top of the pocket even after trypsin digestion (**Figure 3-11**).

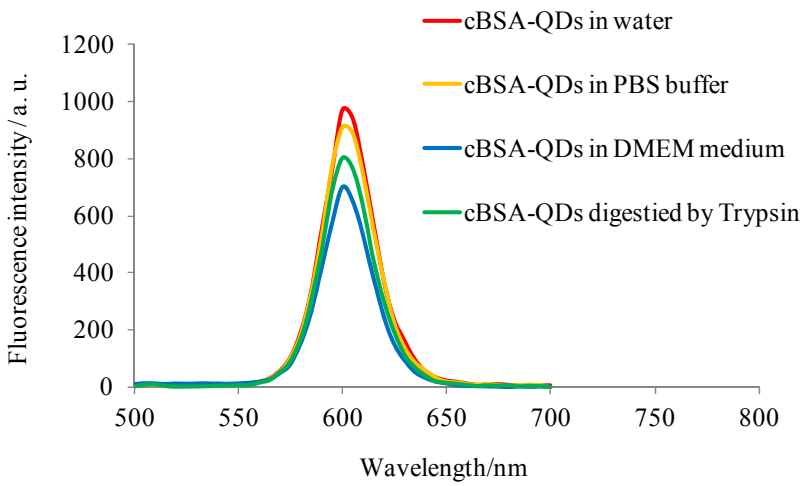

Figure 3-10. cBSA-QDs emission spectra under different condition. Adapted with permission [50]. Copyright 2012, Wiley-VCH.

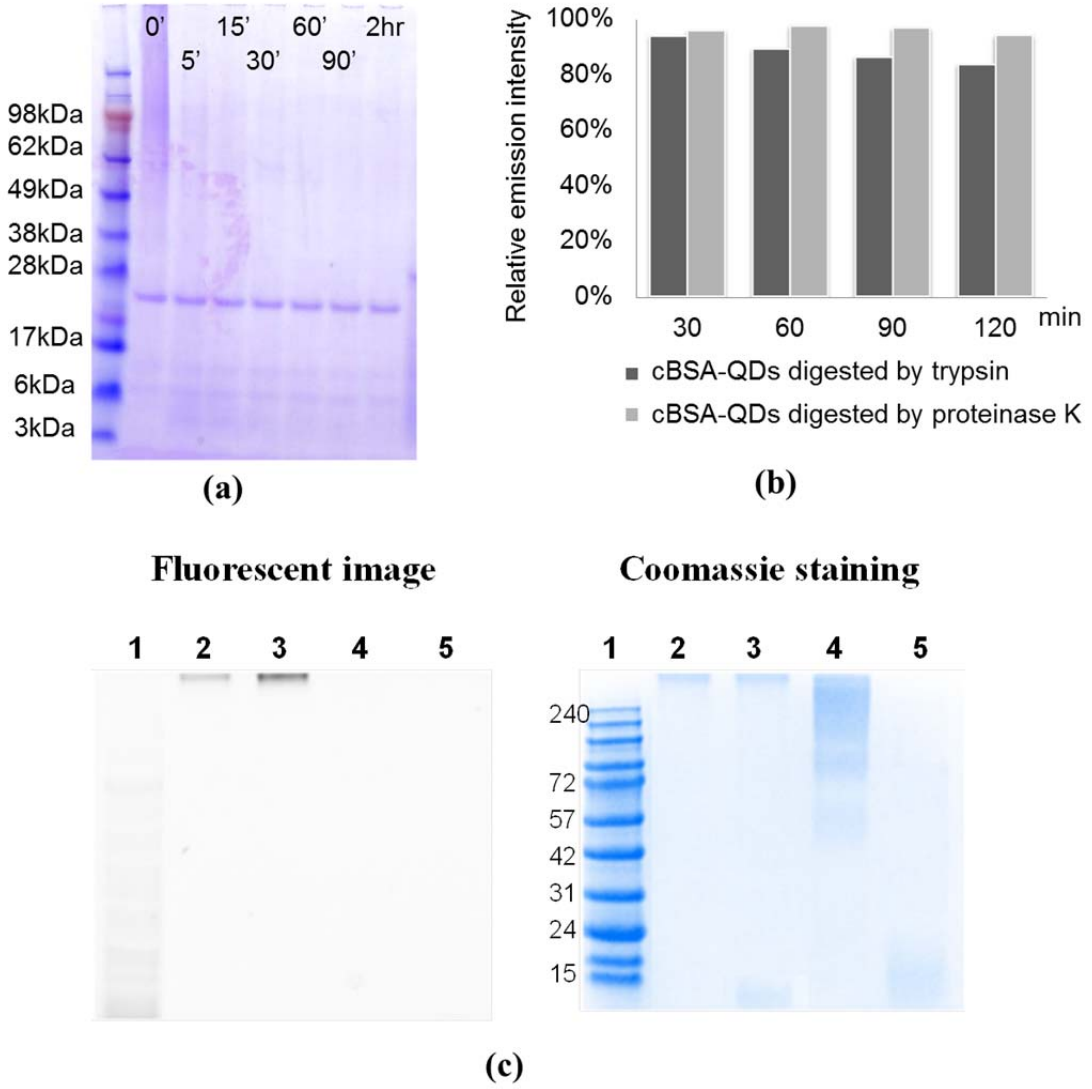

Figure 3-11. Proteolytic stability of cBSA-QDs. a). SDS-PAGE showed fast degradation of cBSA-PEO(5000)$_{27}$ by Trypsin within 2hr. b). Relative emission intensity at 600 nm (λ_{ex}=254 nm) of cBSA-QDs after digestion by trypsin and proteinase K compared to same concentrations of cBSA-QDs in water without enzyme treatment. c). SDS-PEGE shows stable cBSA-QDs after Trypsin digestion for 2hr. Line 1: Protein marker; line 2: cBSA-QDs; line 3: cBSA-QDs treated with trypsin for 2 hr; line 4: dcBSA-PEO(5000)$_{27}$; line 5: dcBSA-PEO(5000)$_{27}$ treated with trypsin for 2 hr. The digestion fragments of dcBSA-PEO(5000)$_{27}$ were observed at the bottom of the gel after trypsin digestion, but the cBSA-QD band remained on top of the gel even after treating with trypsin. Adapted with permission [50]. Copyright 2012, Wiley-VCH.

3.2.4 Test of biocompatibility of PbP-QDs

One of the critical concerns limiting the application of QDs for biomedical applications is the toxicity of QDs due to the presence of cytotoxic metals such as cadmium, selenium as well as organic stabilizers. Therefore, it is always important to assess the potential cytotoxity of functionalized QDs before applying them for bioimaging. The *in vitro* toxicity of PbP-QDs was assessed in a A549 human lung adenocarcinoma cell line (**Figure 3-12**). No significant cytotoxicity was found for both HSA-QDs and cBSA-QDs at relevant concentrations of up to 5 μM after a 24-hr incubation. Compared to synthetic polymer QD coatings that have been applied for bioimaging before [34], the PbP-QDs reported herein exhibited significantly lower cytotoxicities. This low cytotoxicity is attributed to the non-cytotoxic nature of the protein-based polymer coating and its effective protection of the QD core *via* multivalent interactions. In addition, the presence of a PEO shell should potentially minimize reactions with immune cells, reduce plasma protein binding and enhance metabolic stability as demonstrated in many studies [35]. All of these results strongly suggested that PbP-QDs were highly attractive for live-cell imaging experiments.

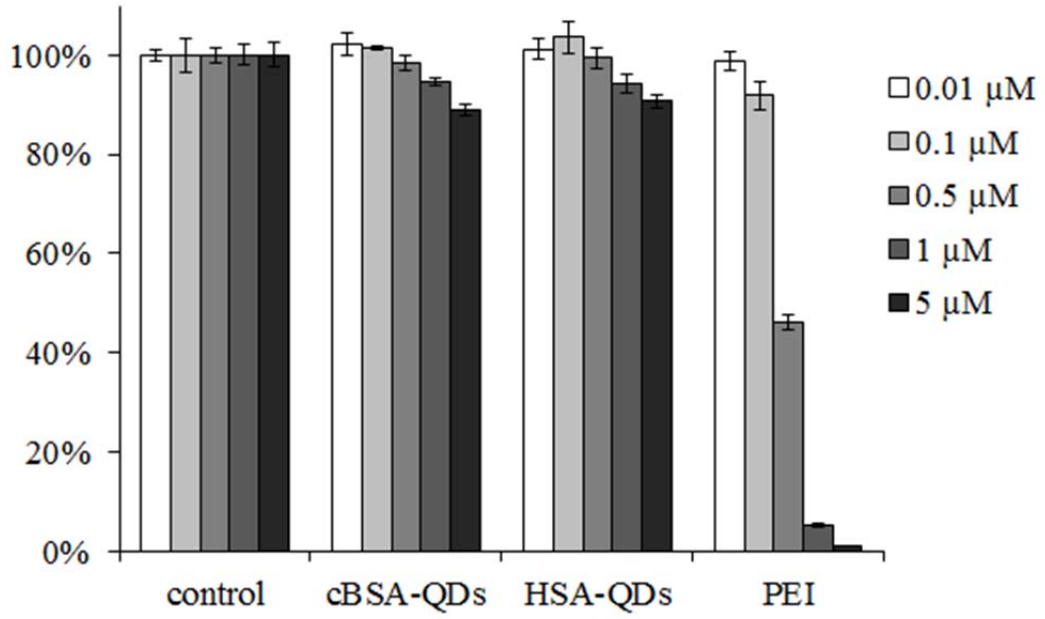

Figure 3-12. Cytotoxicity of cBSA-QDs and HSA-QDs comparing with the gene transfection standard polyethyleneimine (PEI). Adapted with permission [50]. Copyright 2012, Wiley-VCH.

3.2.5 Tuning of cell uptake efficiency of PbP-QDs

Charges play an important role in cellular uptake, cell trafficking, targeting of subcellular structures [36, 37] and the presence of positive or negative charges will determine the location and function of QDs *in vivo*. For PbP-QDs, the polypeptide coating allowed fine-tuning of the surface properties of QDs such as surface charges and functionalities, which were crucial factors for cell imaging experiments. For instance, the plasma protein HSA had an isoelectric point of 4.9, whereas cBSA (**2-9**) displays an isoelectric point of 9.5 (**Figure 3-13a**). Gel electrophoresis at pH 7.4 (**Figure 3-13b**) showed that HSA modified QDs moved toward the positive electrode and cBSA modified QDs

moved toward the negative electrode, demonstrating net negative and net positive charges of HSA-QDs and cBSA-QDs, respectively.

The cellular uptake efficiency into A549 cells was studied with both cBSA-QDs and HSA-QDs and in the case of anionic HSA-QDs, no significant cellular uptake was observed after 24-hr incubation, most likely due to electrostatic repulsion between the negatively charged QDs and the cell membranes (**Figure 3-13c**). In contrast, polycationic cBSA-QDs revealed significant cellular uptake and enrichment in the perinuclear region (**Figure 3-13d**). A similar uptake behavior had also been observed for the precursor protein cBSA-147 [38], an efficient gene transporter protein that crosses cell membranes *via* clathrin-mediated endocytosis and localizes in the endoplasmic reticulum (ER) and Golgi apparatus [38]. The cell uptake mechanism of cBSA-QDs has been investigated by applying Filipin, which blocks caveolae mediated endocytosis and chlorpromazine, which inhibits clathrin mediated endocytosis. We observed that treatment with chlorpromazine reduces the cBSA-QDs uptake (p<0.005) while application of Filipin (FIL) did not affect cell uptake (p>0.1) according to confocal microscopy (**Figure 3-14**), which indicated a clathrin mediated endocytosis as one of the major pathways. The opportunity to manipulate the cellular uptake of QDs is of great importance for a wide range of applications: High cellular uptake *via* clathrin-mediated endocytosis and release from vesicles would allow investigating intracellular targets, whereas low level cellular uptake would facilitate imaging of extracellular structures, such as the extracellular matrix or cell surface receptors.

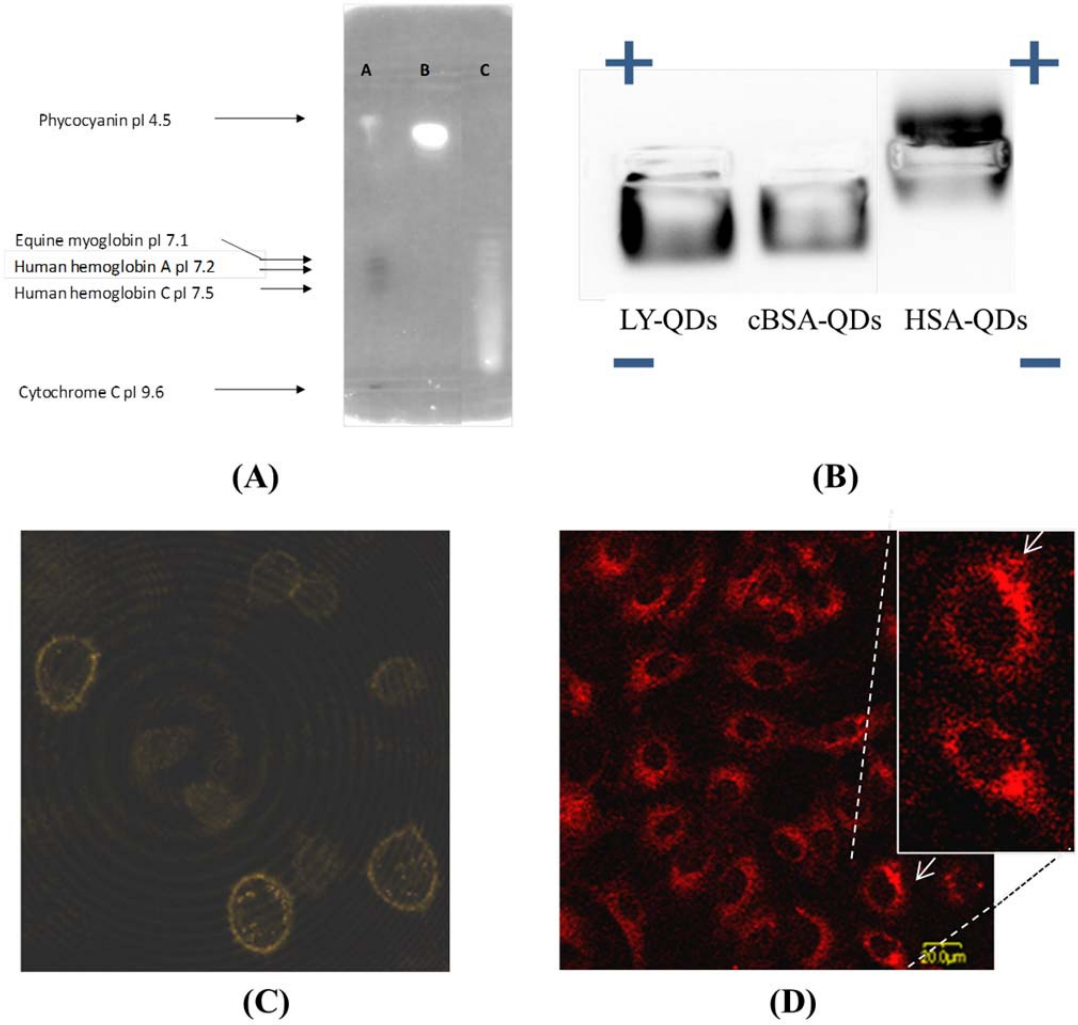

Figure 3-13. (a). Isoelectric focusing (IEF) experiment of native BSA and cBSA. A: IEF Standards, pI range 4.45 - 9.6; B: Native BSA; C: cBSA; (b). Agarose gel electrophoresis showing different net charges of QDs coated by three PbPs at pH7.4; (c). Confocal micrograph of HSA-QDs in A549 cells after a 24-hr incubation. No cell uptake was observed; (d). Confocal micrograph of cBSA-QDs in A549 cells after a 24-hr incubation. cBSA-QDs revealed fast cell uptake as well as enrichment in the perinuclear region showing by the white arrow. Adapted with permission [50]. Copyright 2012, Wiley-VCH.

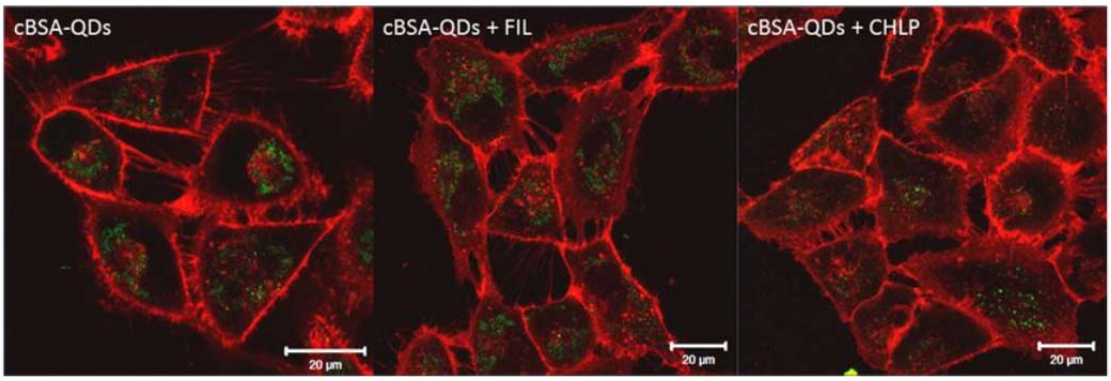

Figure 3-14. Endocytosis mechanism study of cBSA-QDs in A549 cells using confocal microscope. Green color: cBSA-QDs; Red color: cell membrane staining. Treatment with CHLP (50 μM) reduced the cBSA-QDs uptake while application of FIL (1 μg/ml) did not affect cell uptake. Reproduced with permission [50]. Copyright 2012, Wiley-VCH.

3.3 PbPs coated QDs as biosensors

3.3.1 Quantum yield of HSA-QDs responsive to pH change

The structure of native proteins is often sensitive to subtle environmental changes, such as pH, temperature and ionic strength. This was observed also in PbPs coated QDs. While assessing the stability of the HSA-QDs at different pH values, strong optical responses to changes in the pH were observed. A series of universal buffer solutions ranging systematically from pH 3 to pH 12 were prepared as described in the experimental section and the fluorescence intensities from mixtures of HSA-QDs in buffers of different pH were monitored with a fluorescence microplate reader. Significant changes in the emission intensities were observed at different pH, as depicted in **Figure 3-15**.

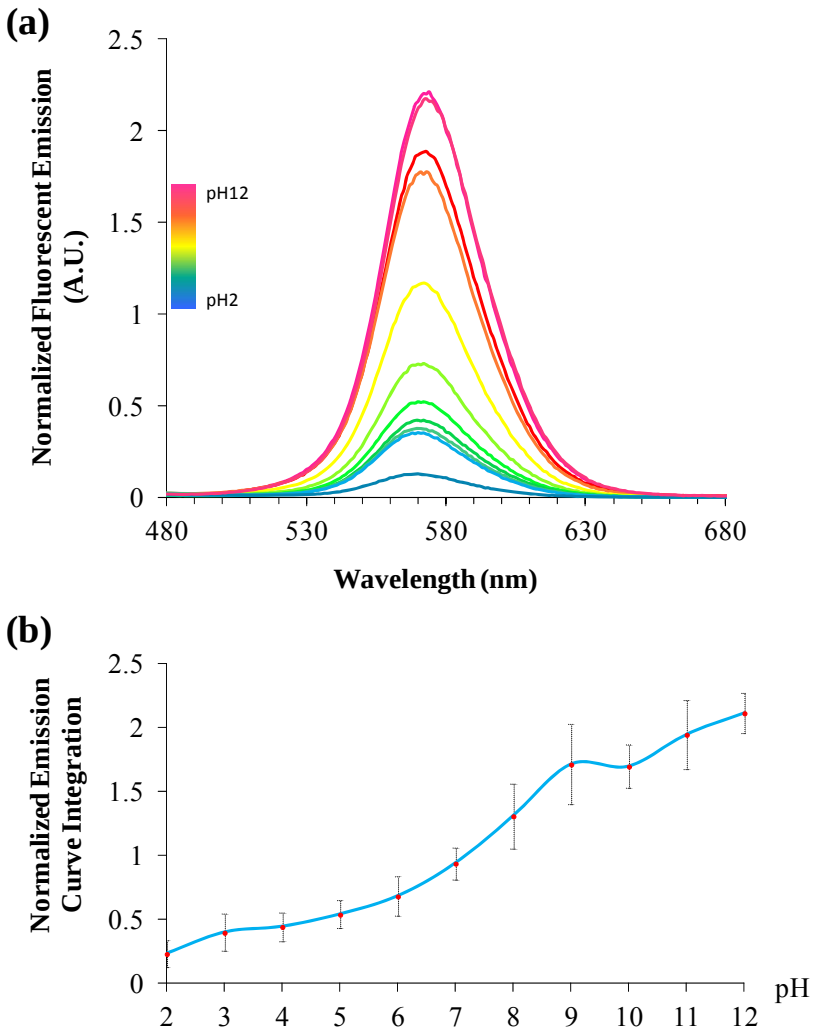

Figure 3-15. (a) Emission intensities of HSA-QDs at different pH (λ_{ex} = 254 nm); (b) Integrated emission intensities *versus* pH based on four consecutive measurements. Adapted with permission [1]. Copyright 2012, American Chemical Society.

Progressing from pH 2 to pH 12, the QYs of HSA-QDs increased by nearly 10 fold (**Table 3-1**). Within the physiological pH range of pH 5 to 9, where the most significant increase in QY emissions were found, we verified that these changes were fully reversible, as shown in **Figure 3-16**. Additionally, no discernible shifts in the peak emission were observed at the different pH values. These findings collectively suggested that neither shell

degradation [39] and hole-trapping [40] from thiolate formation nor aggregation through irreversible ligand loss could explicate the changes in QY.

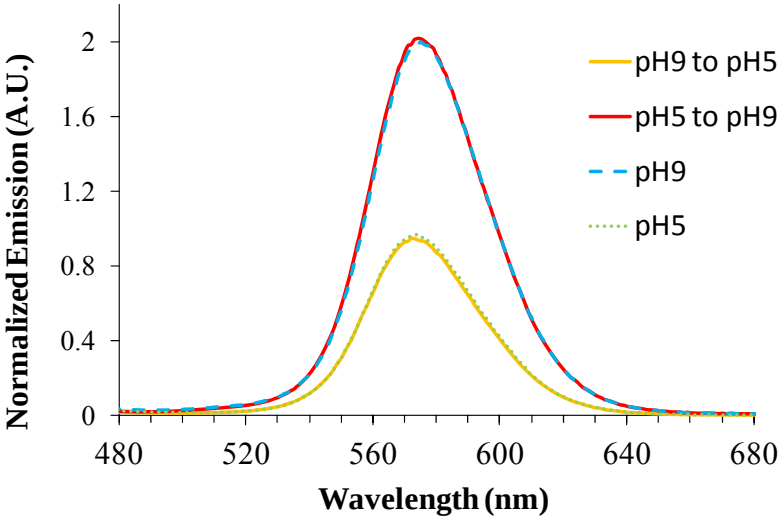

Figure 3-16. Reversibility of the pH responsiveness between pH 5 and pH 9 based on three independent measurements. The emission intensity was recovered after increasing the pH from 5 to 9 as well as decreasing the pH from 9 to 5. Adapted with permission [1]. Copyright 2012, American Chemical Society.

3.3.2 Discussion of the mechanism of the pH responsiveness

The changes in the PL efficiency at different pH may broadly be attributed to the corresponding changes in surface passivation of the QDs. We hypothesized that structural changes in dHSA-PEO(5000)$_{27}$–TA$_{22}$ (**2-16**) at different pH may influence their ability to interact with the QD surface. In order to qualify this assertion, the secondary structure of (**2-16**) was investigated *via* circular dichroism (CD) at different pH values, as summarized in **Figure 3-17** and **Table 3-1**. At acidic pH (pH 3-5), (**2-16**) displayed a significantly larger α-helix content, which represents an opposite trend compared with the secondary structure changes of native albumin proteins [41] at low pH, again

highlighting the unique structural characteristics of (**2-16**). With increasing pH, β-sheet and random coil structural elements became more predominant. The larger content of structurally more rigid α-helix elements at low pH were likely to impose restrictions on the ability of the polymer backbone to conform to the surface of the QD and allow for more ligand-QD interactions. Additionally, we expected a decline in the number of thiol-QD binding interactions in accordance with previously observed dissociation of thiolate ligands from QDs at low pH [42], leading to less surface passivation and low QYs. However, with increasing pH and in particular above pH 7, more beta sheet as well as flexible random coil structural elements occurred which could facilitate more anchoring of the thiol and amine groups on the polymer backbone to the QDs surface, thus leading to increased QYs. These dramatic changes of the secondary structure may thus play a significant role in the observed trends in pH responsiveness of HSA-QDs. The exact identity of the resultant trapped states formed or removed at different pH, appropriately probed with fast time-resolved techniques might give valuable insights into further understanding of the pH responsiveness, which has not been accomplished yet.

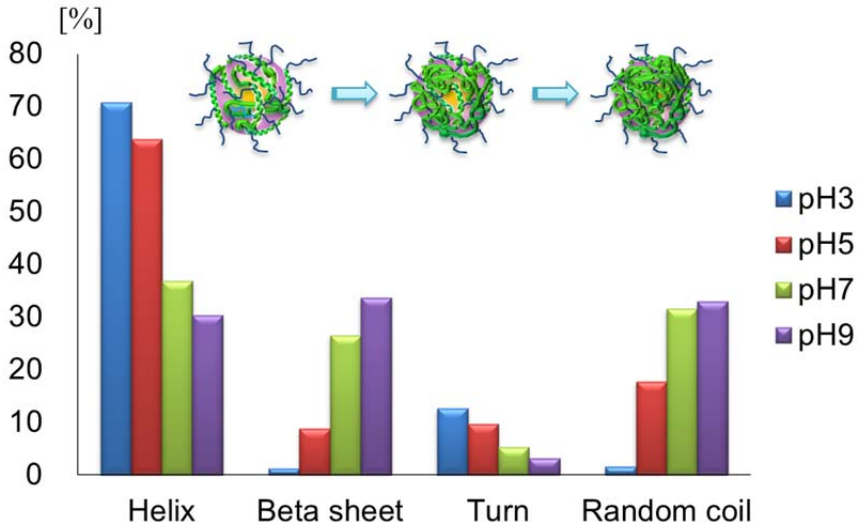

Figure 3-17. Changes in the secondary structure of dHSA-PEO(5000)$_{27}$–TA$_{22}$ (**2-16**) at different pH values. Adapted with permission [1]. Copyright 2012, American Chemical Society.

The average diameters *d* of HSA-QDs at different pH were also investigated using DLS. Only a slight increase of *d* between pH 3 and pH 9 was detected. Therefore, the altered emission intensity was attributed to passivation events on the QD surface and pH-induced aggregate formation was unlikely. The sizes (number distribution) at different pH were shown in **Figure 3-18**. The slight increase of the hydrodynamic radii from pH 3 to pH 9 could be attributed to conformational changes of the copolymer at the surface of the QDs and not to aggregate formation. For example, the diameter of aggregates of HSA-QDs should be well above 40 nm and quenching, rather than an increase of the overall emission would be expected at higher pH. A redshift in the emission wavelength would also be expected, which we did not observe. Therefore, pH-induced aggregate formation was not likely and the

emission intensity changes were most probably due to an improved surface passivation of the QDs.

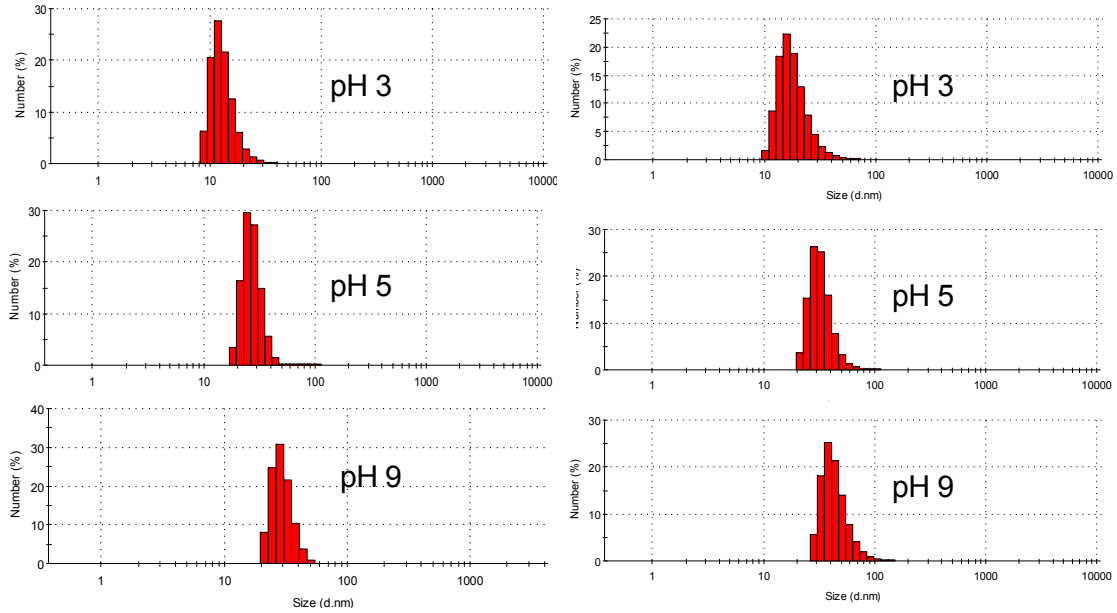

Figure 3-18. Number size distributions of coated HSA-QDs by DLS. At pH 3, 5 and 9, average hydrodynamic radii of 23.5±5.0 nm, 30.2±3.1 nm and 37.0±7.7 nm, respectively, were obtained after two independent measurements. Reproduced with permission [1]. Copyright 2012, American Chemical Society.

Table 3-1. Summary of the fluorescence quantum yields (QY) and total emission intensities (EI) and diameters (d) of HSA-QDs as well as the respective conformational changes of PbP (**2-16**) at different pH values.

pH	EI±S.D.	QY(%) ±S.D.	α-helix (%)	β-turn (%)	β-sheet (%)	R. coil (%)	d (nm)*±S. D.
3	0.40±0.14	5.5±1.7	70.7	12.6	1.2	1.6	23.5 ± 5.0
5	0.54±0.11	12.3±1.6	63.8	9.7	8.8	17.7	30.2 ± 3.1
7	0.94±0.12	16.0±0.9	36.8	5.2	26.5	31.6	29.4 ±3.9
9	1.71±0.31	23.2±1.2	30.3	3.1	33.7	32.9	37.0 ± 7.7

*Average diameter recorded by DLS after minimum two independent measurements at different pH.

3.3.3 cBSA-QDs as DNA sensor

Surface charges are among the key factors affecting the interaction between QDs and guest molecules and polycationic nanoparticles are known to undergo strong interactions with nucleic acids [43, 44, 45]. It was previously shown that cBSA-147 efficiently complexes plasmid DNA and high transfection efficacies were found [38]. Interestingly, *in vitro* experiments on the complex formation of cBSA-QDs with different proportions of two kinds of plasmid DNA of varying lengths (pUC19, 2686 bp, and pGL4.73, 3921 bp) revealed significant changes in the optical properties of the QDs: Increasing the ratio of DNA to cBSA-QDs from 1:8 to 2:1 resulted in a continuous reduction of the PL efficiency to less than 20% of the original PL (**Figure 3-19a**). It is unlikely that the observed significant quenching of the photoluminescence was caused by aggregate formation, which usually causes spectral broadening or spectral shifts, since neither changes in the emission spectra nor shifts in the emission maxima of the QDs were observed (**Figure 3-19b**) in the presence of DNA [46, 47]. Most likely, electron transfer between QDs and nucleotide bases plays a major role, supported by the fact that DNA-induced quenching was recently reported for cysteine-capped QDs [48], which was attributed to electron transfer between QDs and nucleotide bases [48, 49]. Fortunately, the emission of the cBSA-QDs was not quenched entirely, most likely due to the cBSA polymer backbone serving as a distance holder between the cBSA-QDs and the DNA nucleobases. Residual emission of the complexes was of high importance for the investigation of both the complexes and free QDs *via* fluorescence microscopy as discussed later.

Efficient formation of stable cBSA-QD/DNA complexes was further supported by gel electrophoresis (**Figure 3-21**), where neither free DNA nor cBSA-copolymer was detected in cBSA-QD/DNA complexes.

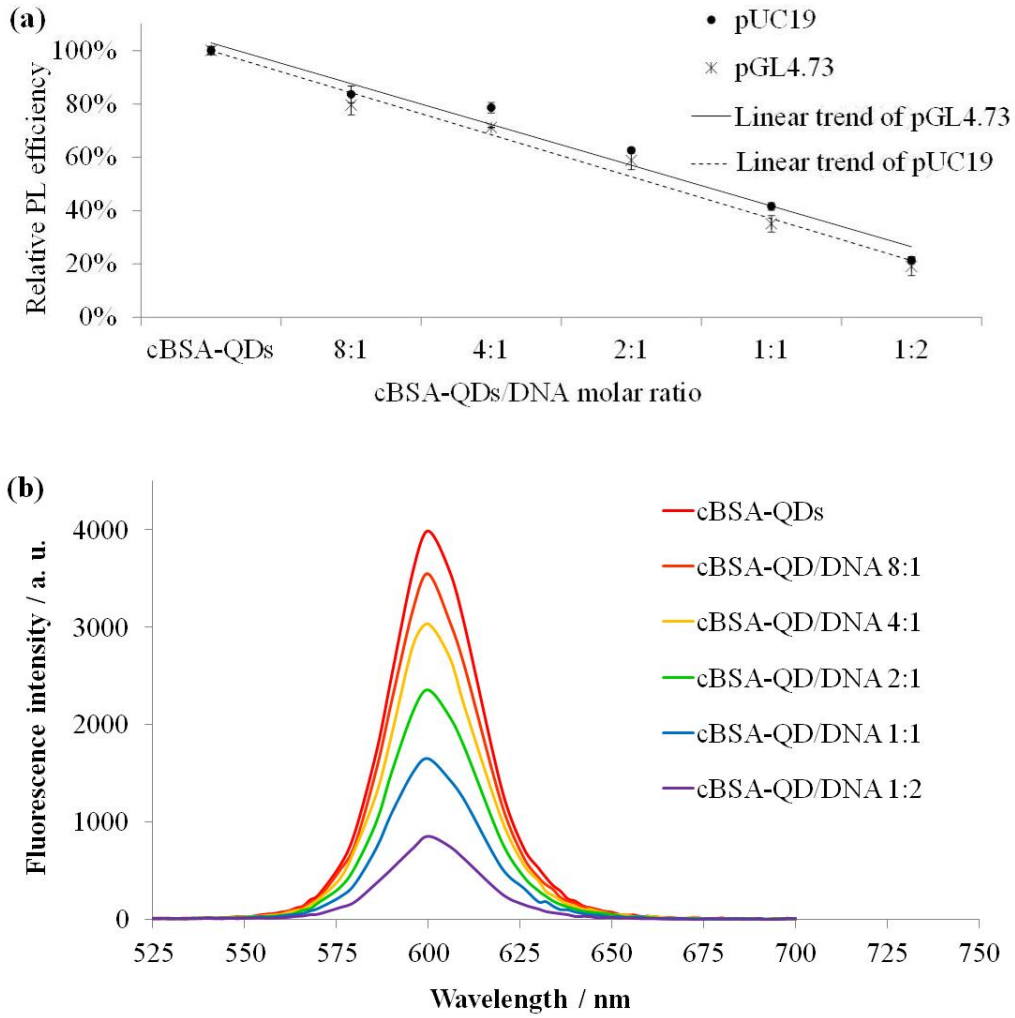

Figure 3-19. Characterization of cBSA-QD/DNA complexes and gene transfection. (a). Relative PL efficiency of complexes with different ratios (cBSA-QD/DNA). pUC19 and pGL4.73 were tested as model DNAs. Data were obtained in triplicate, and standard deviations were shown as error bars. (b). Emission spectra of different complex ratios (cBSA-QD/pUC19-DNA). (λ_{ex} = 254 nm). Adapted with permission [50]. Copyright 2012, Wiley-VCH.

The morphologies of the complexes formed by different cBSA-QDs-to-DNA ratios were investigated by TEM (**Figure 3-20a and 3-20b**) and FCS (**Figure 3-20c**). In TEM measurements, cBSA-QDs were visualized as individual 7 nm QD cores (**Figure 3-6b**), whereas cBSA-QD/DNA complexes were observed as condensed aggregates with average diameters of 23 nm (**Figure 3-20a and 3-20b**). Varying the cBSA-QD/DNA ratio from 8:1 to 1:1 caused no significant changes of the complex morphologies or sizes. cBSA-QD/DNA 8:1 complexes studied *via* FCS and DLS experiments revealed slightly larger hydrodynamic diameters of 44 nm and 34 nm, respectively, in the same range to those of individual cBSA-QDs in solution (**Figure 3-20c,d** and **Table 3-2**). Most likely, complex formation with DNA condenses the extended, soft and flexible copolymer shell consisting of soft PEO chains thereby yielding nano-sized cBSA-QD/DNA complexes with hydrodynamic radii similar to those of individual cBSA-QDs but with a more dense and compact structure.

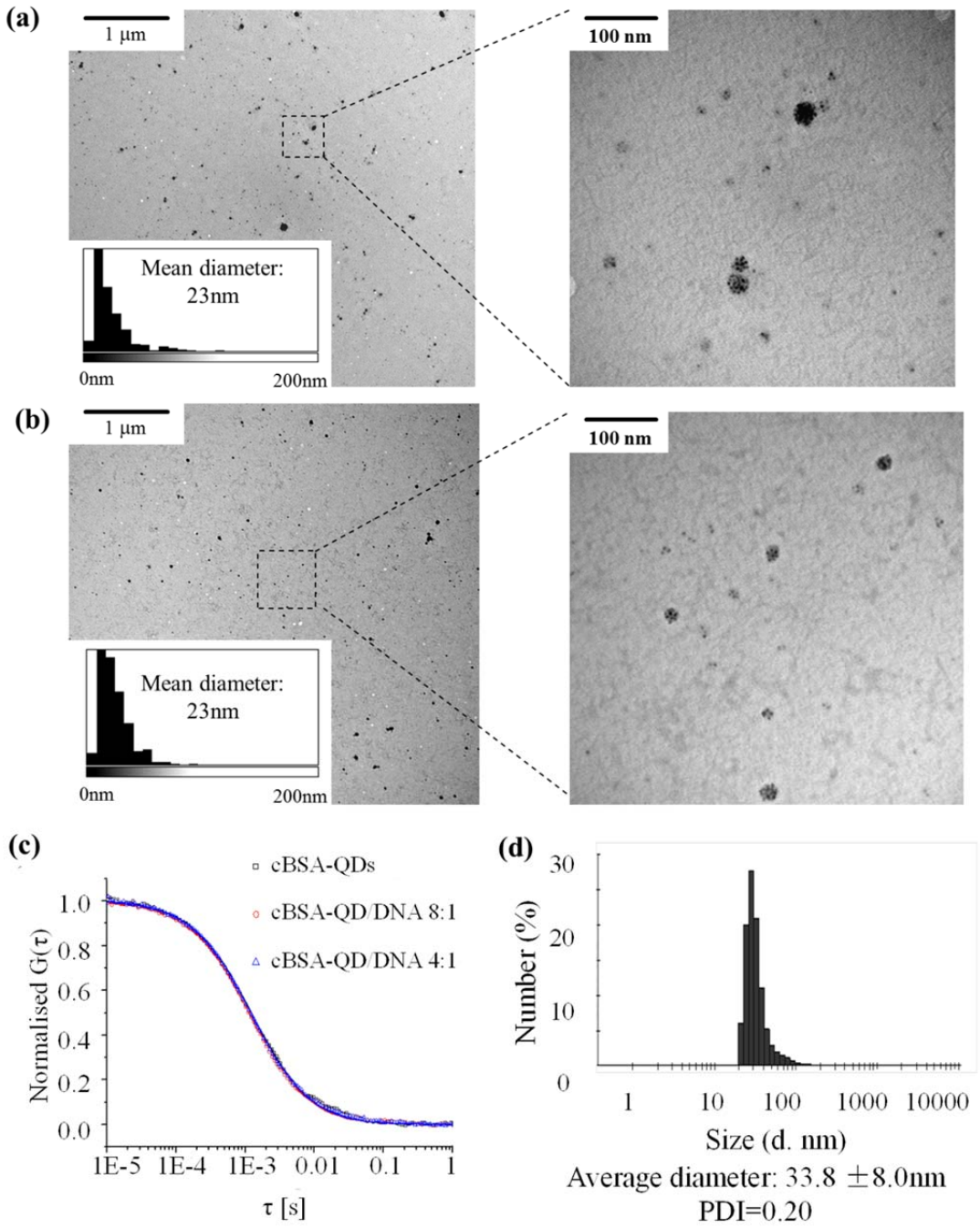

Figure 3-20. TEM images of (a) 8:1 cBSA-QD/DNA complexes and (b) 1:1 cBSA-QD/DNA complexes. (c). FCS autocorrelation curves measured for cBSA-QDs and pUC19 plasmid complexes in aqueous solution at approximately 10 nM concentration. The solid lines represent the corresponding best-fit lines with single component equations. (d). Hydrodynamic diameter distribution measured by DLS. Average diameter was calculated based on three independent measurements and the standard

deviation was presented as error. Adapted with permission [50]. Copyright 2012, Wiley-VCH.

In addition, the changes of the emission intensities of cBSA-QDs upon complexation with DNA were studied with FCS by measuring the average particle brightness (the experiments were done together with Dr. Koynov in Max Planck Institute for Polymer Research), which was directly proportional to the quantum yield of the studied fluorescent species. The particle brightness was determined by dividing the average fluorescent intensity by the number of species in the observation volume. A particle brightness of cBSA-QDs of 24 kHz/particle for free cBSA-QDs, 21 kHz/particle for 8:1 cBSA-QD/DNA complexes and 19 kHz/particle for 4:1 cBSA-QD/DNA complexes was found, suggesting an easily detectable photo-responsiveness with a similar trend as observed in the emission spectra. The remarkable photo-responsiveness of cBSA-QDs represented an efficient indicator of DNA complex formation which could be very attractive for DNA detection and the convenient monitoring of DNA loading and unpacking in live cells without the need to apply other labels or DNA modifications.

Table 3-2. Summary of size and optical properties of cBSA-QDs and cBSA-QD/DNA complexes (8:1).

Sample name	Relative PL efficiency (%)[b]	Diameter (nm) (TEM) [c]	Hydrodyn. diameter (nm, DLS)	Hydrodyn. diameter (nm, FCS)	Theor. hydrodyn. diameter (nm) [d]
cBSA-QDs	100 ± 2 [e]	8 ± 2 [e]	33 ± 6 [e]	~44	46
cBSA-QD/DNA complexes (8:1) [a]	84 ± 3 [e]	23 ± 16 [e]	34 ± 8 [e]	~44	--

[a] pUC19 plasmid was used as DNA. [b] Relative PL efficiency was calculated by considering the PL efficiency of cBSA-QDs as 100%. [c] The statistical diameter of

quantum dots core clusters measured according to direct TEM images. [d] Detailed calculation see section 3.2.2. [e] Average ± standard deviation.

3.4 cBSA-QDs as photoswitch for DNA detection, gene transfection and live-cell imaging

Recently, QDs were used in gene delivery to elucidate non-viral gene delivery mechanisms [43, 51, 52, 53]. FRET (fluorescence resonance energy transfer) between QDs and organic chromophores had been successfully applied and allowed following the internalization of nucleic acids/polyelectrolyte complexes and nucleic acid release processes by independently labeling gene delivery vectors and nucleic acids [51, 52, 53, 54]. However, in most cases, the vectors were covalently combined either with nanometer-sized QDs [54] or lipophilic organic dyes [51, 52], which required additional synthetic steps and might affect the properties of the complexes. Therefore, it would be advantageous to directly investigate QDs as gene delivery vectors. In this context, successful gene silencing had been demonstrated by covalently binding siRNA to amino functionalized QDs *via* disulfide linkages [34, 55] or by non-covalent adsorption of siRNA onto the surface of positively charged QDs [45, 56, 57]. However, in such systems, labeling of nucleic acids is still necessary to investigate siRNA release. Recently, it was also reported that electron transfer between QDs and DNA induces QD emission quenching [48, 49], which was attractive for the development of label-free DNA detection and delivery systems.

Although using QDs to investigate gene delivery was highly promising, several challenges still obstructed the use of QDs *in vivo*. For instance, long-

term investigations of QDs in live cells were often limited by their cytotoxicity at high concentrations, and long-term stability studies of QDs in a biological environment were not conclusive [4, 58]. Therefore, it is still of great interest to develop non-cytotoxic QDs with high *in vivo* stability, which offer the unique possibility to investigate efficient gene delivery and release in live cells.

cBSA-QDs revealed unique properties ideally suited for live-cell imaging, such as efficient cellular uptake, high intracellular stability and low cytotoxicity. Complex formation of cBSA-QDs with plasmid DNA exhibited a significant photo-responsive behavior. Therefore these QDs provided an attractive platform for investigating DNA transportation and DNA unpacking during gene delivery. In addition, it was often time-consuming to identify the optimal ratio of the transfection reagent and DNA. Here, due to the photo-responsive behavior of cBSA-QDs, ideal cBSA-QDs to plasmid DNA ratios for efficient gene transfection could be conveniently assessed from the emission intensities of the cBSA-QD/DNA complexes. In addition, we applied FCS to study the size, aggregation behavior and stability of single QDs in live cells. Individual, freely diffusing cBSA-QDs were observed inside large endosomes and to the best of our knowledge, similar studies collecting the physical properties of QDs inside live cells have not yet been reported. Therefore, cBSA-QDs were attractive for live-cell imaging, and these results paved the way toward mechanistic studies of non-viral gene delivery processes.

3.4.1 cBSA-QD form stable complexes with DNA

cBSA-QDs and cBSA-QD/DNA complex were studied by SDS-PAGE. The fluorescence image was firstly taken after electrophoresis to record the direct

fluorescence from QDs (**Figure 3-21a**). Then, the gel was stained by Sybr® safe (from Invitrogen Life Technologies GmbH, Darmstadt, Germany) DNA staining for 30 min and the fluorescence image was taken again. In this image (**Figure 3-21b**), DNAs displayed as fluorescent bands and the direct fluorescence from QDs was also visible. Thereafter, the gel was further stained by coomassie blue to visualize the protein related bands (**Figure 3-21c**). According to this experiment, cBSA-QDs (line 2 and 3) and cBSA/DNA complexes (line 4 and 5) stacked at the loading pockets, whereas dcBSA-PEO$(5000)_{27}$-TA_{26} copolymer (line 6 and 7) and dcBSA-PEO$(5000)_{27}$-TA_{26} /DNA complexes (line 8 and 9) showed smeary protein bands. No free dcBSA-PEO$(5000)_{27}$-TA_{26} polymer was found in both cBSA-QDs sample and cBSA-QDs/DNA complexes (**Figure 3-21b**). In addition, no free DNA band was detected in cBSA-QDs/DNA complexes indicating successful complex formation.

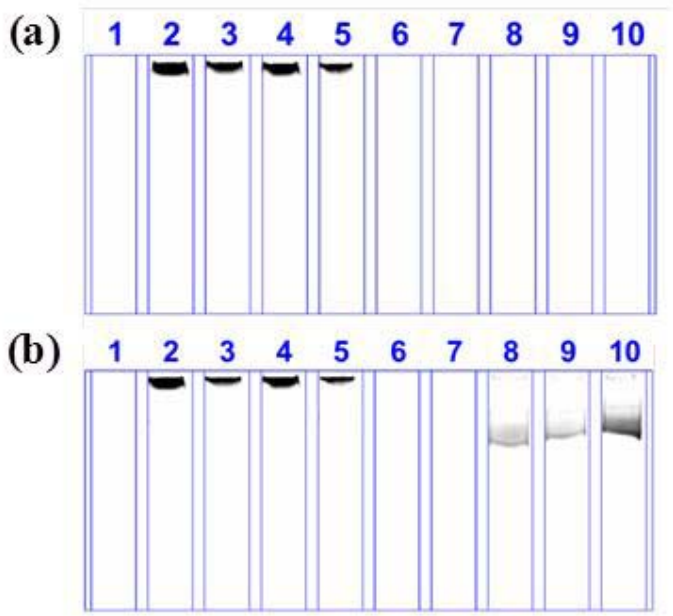

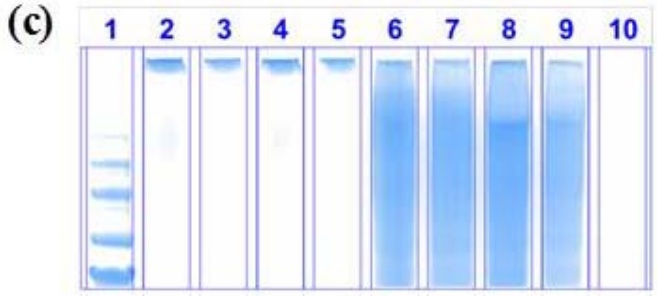

Figure 3-21. SDS-PAGE characterization of cBSA-QDs and cBSA-QDs/DNA* complex. (a) Fluorescent image showing cBSA-QDs emission; (b) Fluorescent image after Sybr® Safe DNA staining; (c) Coomassie protein staining. Line 1. Protein maker; line 2. cBSA-QDs 7.5 μg; line 3. cBSA-QDs 5 μg; line 4. cBSA-QD/DNA 8:1 7.5 μg; line 5. cBSA-QD/DNA 8:1 5 μg; line 6. dcBSA-PEO$(5000)_{27}$-TA_{26} 7.5 μg; line 7. dcBSA-PEO$(5000)_{27}$-TA_{26} 5 μg;line 8. dcBSA-PEO$(5000)_{27}$-TA_{26}/DNA 8:1 7.5 μg; line 9. dcBSA-PEO$(5000)_{27}$-TA_{26}/DNA 8:1 5 μg; line 10. pUC19 plasmid DNA 7.5 ng. *pUC19 plasmid DNA was using as representative DNA. Adapted with permission [50]. Copyright 2012, Wiley-VCH.

3.4.2 cBSA-QD/DNA complexes efficiently transfect mammalian cells

The potential of cBSA-QDs to efficiently deliver plasmid DNA into cells was evaluated by transfecting pGL4.73 plasmid DNA, which encodes for the Renilla firefly luciferase. cBSA-QD/DNA complexes formed with different QD-to-DNA ratios were tested (**Figure 3-22**) and successful expression of luciferase was demonstrated by applying the Renilla-Glo® Luciferase Assay System (Promega GmbH, Mannheim, Germany) based on luminescence detection. Successful gene transfection was achieved but the transfection efficiencies were strongly dependent on the applied cBSA-QD/DNA ratios (**Figure 3-22**).

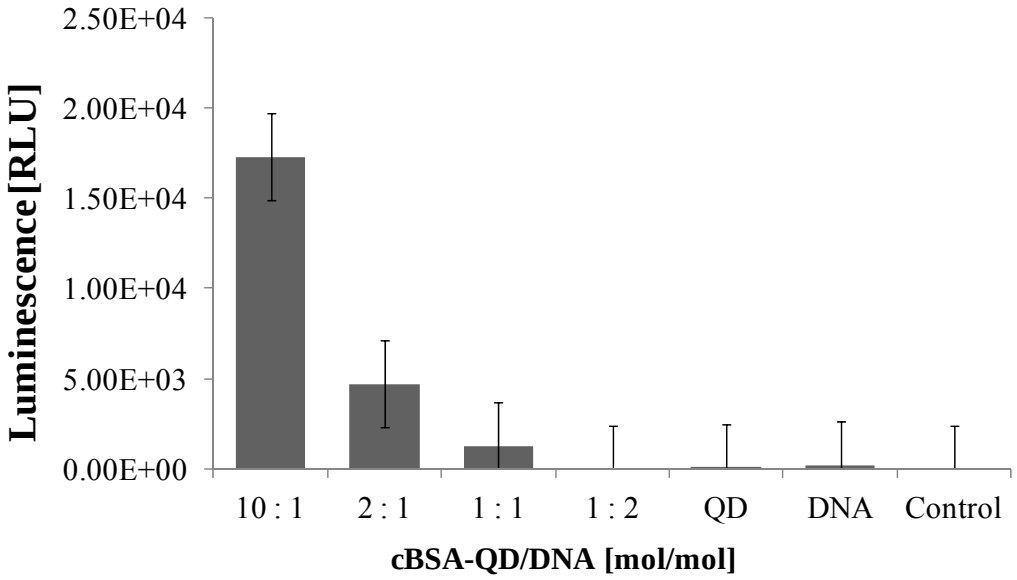

Figure 3-22. Gene transfection efficiencies of cBSA-QDs measured using the Renilla-Glo® Luciferase Assay. Data were obtained in triplicate, and standard deviations were shown as error bars. Experiments were repeated three times independently. Reproduced with permission [50]. Copyright 2012, Wiley-VCH.

It is well-known that optimal positive-to-negative charge ratios of the polyelectrolytes are required to accomplish efficient gene transfection since cellular uptake of the complexes, DNA protection and DNA release are important factors in this process that need to be fine-tuned experimentally [38]. Interestingly, complexes formed with high cBSA-QD content that were strongly fluorescent also revealed increased transfection efficiencies, whereas increased DNA content in the complexes that also displayed low fluorescence intensities yielded strongly reduced transfection efficiencies. Low transfection efficiencies in the presence of high DNA quantities could indicate inefficient cellular uptake of the complexes and/or inefficient DNA protection from proteolysis. cBSA-QD/DNA complexes formed by a 10:1 ratio possess an adequate net positive charge to facilitate efficient cellular uptake and DNA release (higher ratios of cBSA-QDs and DNA were not tested since quenching

of the emission intensities could not be detected anymore which renders such complexes less useful). Usually, the positive-to-negative charge ratios must be calculated and carefully adjusted experimentally, which was often challenging and time consuming, particularly for less well-defined transfection and transduction facilitators. Here, due to the photo-responsive behavior of cBSA-QDs, optimal cBSA-QDs to plasmid DNA ratios for efficient gene delivery could be conveniently assessed from the emission intensities of the complexes.

3.4.3 Investigation of cBSA-QDs and cBSA-QD/DNA complexes in live cells using confocal imaging and FCS

In the next step, the cellular uptake and vesicle trafficking of cBSA-QDs and cBSA-QD/DNA complexes were investigated using confocal imaging and FCS. FCS is a powerful technique that can be used to study dynamic behavior of fluorescent species (small molecules, macromolecules or nanoparticles) in various environments. The method is based on monitoring and recording the fluctuations of the fluorescent intensity signal, caused by the diffusion of the species through a very small observation volume (typically the focus of a confocal microscope) stationary positioned at the point of interest in the studied sample. The recorded fluctuations are evaluated in the form of an autocorrelation curve that is then fitted with appropriate model equations (see experimental section for details) to obtain quantitative information on the physical properties of the species. One of the most common applications of FCS is measuring the hydrodynamic radius of

diffusing fluorescent species as demonstrated in section 3.2.2. Knowing the size of the observation volume, the diffusion coefficient and through the Stokes-Einstein relation, the hydrodynamic radius of the fluorescent species as well as the number of fluorescent species in the observation volume (i.e. the local concentration) and their particle brightness can be assessed from autocorrelation curve. Due to minimal requirements on sample amounts and its high sensitivity and selectivity, FCS has found widespread applications, e.g. for probing quantities such as diffusion coefficients, kinetic rate constants, equilibrium binding constants, etc [59]. Owing to the very small observation volume required for FCS (the focal area of a confocal microscope), such studies can be performed inside living cells or even sub-cellular compartments [60, 61]. Therefore, FCS represents a valuable technique to elucidate the behavior of cBSA-QDs in live cells. To the best of our knowledge, live-cell imaging with QDs has not yet been investigated by FCS.

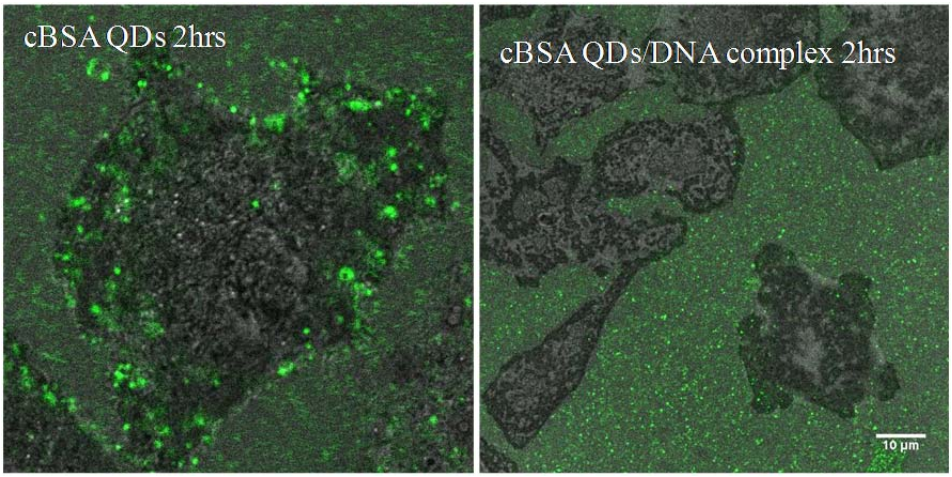

(a) **(b)**

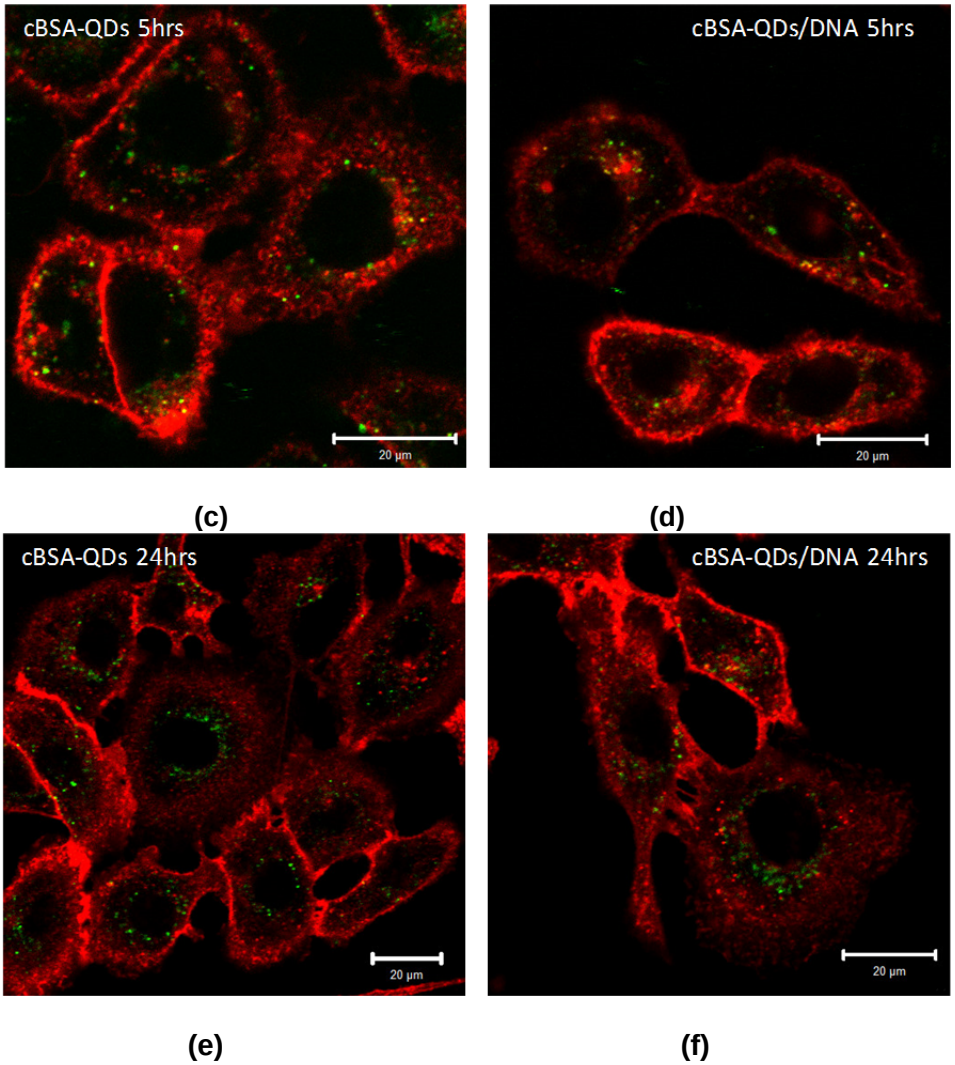

Figure 3-23. Confocal imaging of cBSA-QDs and 8:1 cBSA-QD/DNA complexes. (a) cBSA-QDs incubated with A549 cells for 2 hr showed electrostatic accumulating on the cell membrane. (b) cBSA-QD/DNA complexes incubated with A549 cells for 2 hr showed not obvious accumulation on the cell membrane compared to (a). (c) QDs incubated with A549 cells for 5 hr showed significant cell uptake. All QDs in solution were removed at this time point. (d) cBSA-QD/DNA complexes incubated with A549 cells for 5 hr revealed cell uptake. All QDs in solution were removed at this time point. (e) cBSA-QDs incubated with A549 cells for 24 hr showed accumulation in the perinuclear region. (f) cBSA-QD/DNA complexes incubated with A549 cells for 24 hr revealed accumulation in the perinuclear region. Adapted with permission [50]. Copyright 2012, Wiley-VCH.

A549 cells were treated with ~0.2 μM cBSA-QDs, and the intracellular pathways were followed by time-lapse confocal microscopy and FCS. CellMask® deep red tracker was used to label the cell and intracellular membranes. cBSA-QDs were found to accumulate on the cell surface within 2 hr (**Figure 3-23**), indicating that an adsorptive endocytosis process occurs in which the first step was the electrostatic accumulation of the highly cationic QDs on the negatively charged cellular membrane [62]. Subsequently, the bound QDs were internalized into early endosomes when the cellular membrane invaginated to form endocytic vesicles. Once inside the cells, cBSA-QDs remained in vesicles at different locations in the cells, as confirmed by FCS studies performed after 5-hr incubation. These studies showed no freely diffusing QDs in the cells, and only occasionally were large and bright objects seen. These large objects likely represented endosome vesicles slowly passing through the observation volume. Furthermore, several large endosome lumens were found. By positioning the FCS observation volume (<1 μm^3) inside such lumens (arrow in **Figure 3-24a**), we were able to study the properties of endosome-entrapped QDs. Interestingly, mono-dispersed QDs and no aggregates were observed (**Figure 3-24c**). Assuming the viscosity in the endosome was equal to that of water, the hydrodynamic radii of these QDs were in the range of approximately 24 nm, which is slightly smaller than in aqueous solution. This could be due to partial enzymatic degradation of the accessible, unbound parts of the biopolymer shell. However, the presence of high ion concentrations and the influence of the different viscosities in vesicles and water on diffusion times may also have an impact on the calculated sizes of the cBSA-QDs. QDs with a reduced

brightness of approximately 9 kHz/particle were recorded inside the vesicles. However, due to the different excitation setup for this cell study and the complicated membrane environment in the cells, the brightness of each QD could not be directly compared with that obtained in solution. The ability to investigate coated QDs inside late endosomes strongly supported the excellent stability of the cBSA-QDs, even under high salt concentrations and enzymatic conditions in live cells. Aggregate formation of QDs inside cells and the association of QDs with cell membranes are normally considered important limitations for QD applications *in vivo* [4, 58]. Thus, cBSA-QDs exhibited highly promising live-cell imaging features, most likely due to the multivalent interactions stabilizing the protein coating and to the presence of PEO chains, which minimize the nonspecific adsorption of QDs.

After a 24-hr incubation, cBSA-QDs were found accumulated at a specific pole of the cell perinuclear region, the regions where the endoplasmic reticulum (ER) and Golgi apparatus are located (**Figure 3-24b**), displaying a very similar trafficking behavior as the gene transfection vehicle cBSA-147. [14] This accumulation was further confirmed by staining cell ER with ER-Tracker® Green dye, which showed co-localization of QD signals within the ER region (**Figure 3-25a**). In addition, in some endosomal vesicles, freely diffusing cBSA-QDs could still be detected with similar size distributions and emission intensities as in previous investigations.

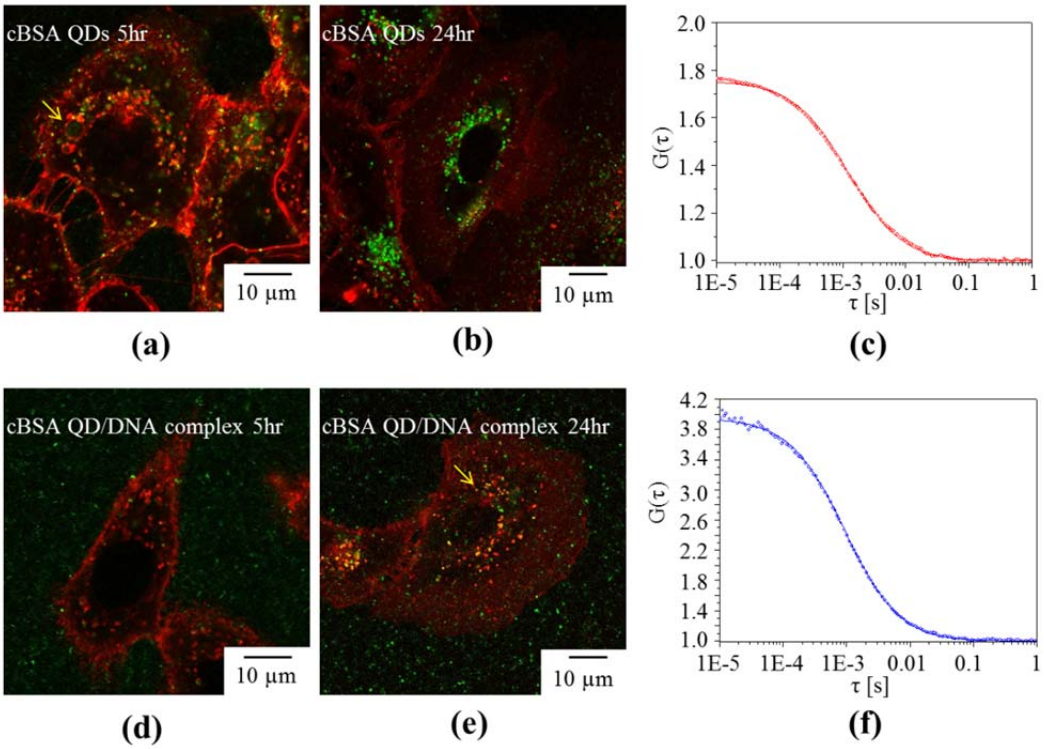

Figure 3-24. Live cell confocal imaging and FCS measurement of cBSA-QDs and 8:1 cBSA-QD/DNA complexes. (a) cBSA-QDs incubated with A549 cells for 5 hr. (b) cBSA-QDs incubated with A549 cells for 24 hr. (c) Representative FCS autocorrelation curves of QDs measured in live cells treated with cBSA-QDs after 5 hr. (d) cBSA-QD/DNA complexes (8:1) incubated with A549 cells for 5 hr. (e) cBSA-QD/DNA complexes (8:1) incubated with A549 cells for 24 hr. (f). Representative FCS autocorrelation curves of QDs measured in live cells treated with cBSA-QD/DNA complexes (8:1) after 24 hr. Cell membranes were labeled with CellMask® deep red tracker and were shown in red in the photomicrographs, and cBSA-QDs (recorded using 488 nm excitation and 555 nm – 605 nm band pass emission filter) were shown as green points. Arrows presented the position where the FCS focus was located to measure QD properties in live cells. Reproduced with permission [50]. Copyright 2012, Wiley-VCH.

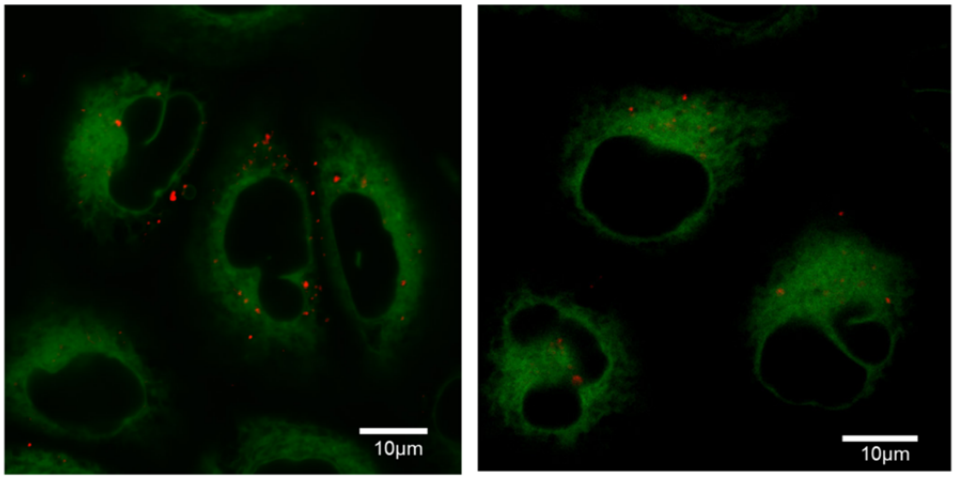

Figure 3-25. Investigation of location of QDs with ER tracker. (a). QDs incubated with A549 cells for 5hr and stained by ER tracker. (b). QDs/DNA complexes incubated with A549 cells for 5hr and stained by ER tracker. Green color corresponds to the ER tracker and red color corresponds to the QDs. Adapted with permission [50]. Copyright 2012, Wiley-VCH.

Thereafter, cBSA-QD/DNA (8:1) complexes that represented a good compromise of sufficient transfection efficiencies as well as detectable changes of the emission intensities were investigated in A549 cells. Slower uptake was observed compared with cBSA-QD/DNA (10:1) complexes due to the presence of fewer net positive charges (**Figure 3-24d** and **3-24e**). Large endosomes containing freely diffusing cBSA-QDs were only found by FCS after the 24-hr incubation time. This observation emphasized the delicate interplay between the number of positive charges and cellular uptake efficiency, which had been previously highlighted for polymers and for cationic lipid carrier systems.[29-31] Interestingly, similar mono-dispersed QDs were observed in these endosomes, and these QDs had size distributions (diameter = 24 nm) and emission intensities (8 kHz/particle) (**Figure 3-24f**)

similar to those of free cBSA-QDs in endosomes, indicating that the cBSA-QDs may have already released their cargo DNA. Since live cells represented highly complex and dynamic systems, additional studies would be required to achieve an improved understanding of the sophisticated interplay of aggregation, disaggregation and membrane association in these vesicles. The co-localization of 8:1 cBSA-QD/DNA complexes with endosomes and the accumulation within the ER region were also observed by membrane staining and ER-Tracker® Green dye staining (**Figure 3-25b**), indicating that the internalization process of 8:1 cBSA-QD/DNA complexes proceeded similar as for cBSA-QDs.

In addition to FCS quantification, a statistical quantification on the total brightness of cBSA-QDs and cBSA-QD/DNA complexes in individual cells was performed at two different time points during the transfection process by applying confocal microscopy. A549 cells were treated in two different experiments with the same amount of (a) cBSA-QDs and (b) cBSA-QD/DNA complexes for 5 hr and confocal images using the same settings (e.g. excitation laser power and detector gain) were acquired. After 5 hr, all QDs that were not uptaken by the cells were removed by multiple washing steps in both experiments and the cells were further cultured in fresh medium. Confocal images of these cells were taken after 5 hr and again after 24 hr with all identical microscope settings. The emission intensities of the QDs of experiment (a) and (b) in each single cell were quantified using ImageJ software based on a statistics of about 25 to 30 cells. As shown in **Figure 3-26** (representative cell images see **Figure 3-23e** and **3-23f**), cBSA-QD/DNA complexes in experiment (b) exhibited a significantly less (~20% less)

emission intensity ($p<0.005$ by ANOVA test) compared to cells treated with cBSA-QDs in experiment (a) after 5 hr whereas the identical emission intensities were regained after 24 hr. These experimental data were in good agreement with the partially quenched fluorescence intensity of cBSA-QD/DNA complexes at the beginning of the gene transfection experiment (about 20% quenching for 8:1 complexes calculated for 100% emission intensity of cBSA-QDs) and recovery of the emission intensity after DNA release after 24 hr. Although comprehensive studies would be still needed to elucidate the entire process of DNA release from cBSA-QDs, both results from FCS and confocal imaging strongly suggested the release of DNA cargoes and recovery of cBSA-QDs after 24 hr which was well in line with the gene transfection experiments.

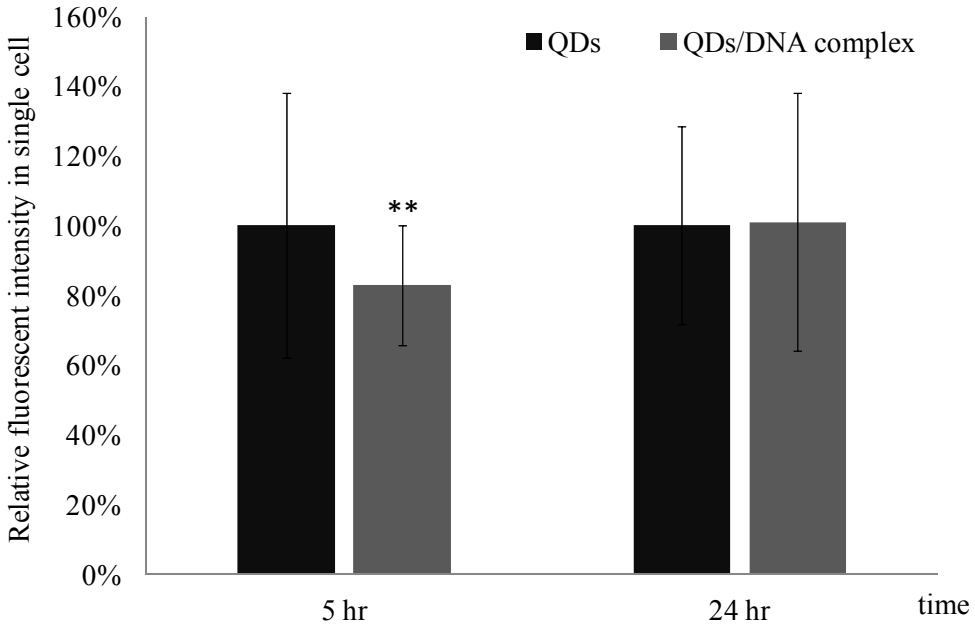

Figure 3-26. Statistical quantification of the emission intensities of QDs in individual cells based on a number of 25 to 30 cells. Significantly less emission intensity (20 % less) was observed after investigating cells treated with cBSA-QD/DNA complexes (8:1) compared to cBSA-QDs after 5 hr. After 24 hr, similar emission intensities were regained for both samples by

investigating the same cells. ** p<0.005 by ANOVA test. Reproduced with permission [50]. Copyright 2012, Wiley-VCH.

3.5 Summary

In summary, we prepared a series of PbPs coated QDs (HSA-QDs, cBSA-QDs and LY-QDs). These QDs were water soluble and biocompatible. Their quantum yield in water was 10% to 20% depending on the length and number of DHLA groups on the PbPs used for coating. Due to the protein-type nature of the coating, these QDs exhibited very low cytotoxicity, even at high concentrations. The multivalent interactions between QDs and DHLAs along the PbPs backbones and the PEG protection shells outside QDs resulted in high QD stabilily under different conditions such as in water, PBS buffer and cell culture medium. Depending on the net charges of the PbPs used for coating, QDs could be prepared containing both negative surface charges and positive surface charges. The positive charged cBSA-QDs facilitated interactions with negatively charged cell membranes and enabled efficient cellular uptake *via* clathrin-mediated endocytosis, whereas the negatively charged HSA-QDs were not uptaken by cells due to charge repulsion.

PbPs coated QDs were highly attractive for several bioimaging applications. HSA-QDs were found significantly responsive to pH changes, and such responsibility was fully reversible within pH 5 to 9. cBSA-QDs were sensitive to DNA interactions due to high numbers of positive charges, which could be useful for DNA detection. The cBSA-QD/DNA complexes were

successfully used for gene transfection with luciferase encoded plasmid. The linear relationship between PL intensities and cBSA-QD/DNA ratios could be used to conveniently determine the best complex ratio for gene transfection. Optimal complex ratios for gene transfection were characterized by high cBSA-QD content (e.g., cBSA-QD/DNA ratios of 8:1 or 10:1) and high emission intensities of the QDs in the complexes. Complexes formed with equimolar quantities or with DNA in excess exhibited low emission intensities due to DNA-induced quenching, and they only displayed low transfection efficiencies most likely due to low cellular uptake or low DNA condensation/protection in the complexes.

For the first time, the physical properties of QDs such as emission intensity and size distributions were investigated in live cells by FCS. These results supported that cBSA-QDs were very stable even inside endosomes which have strong enzymatic hydrolysis, highly ionic strength and low pH environment. The cBSA-QDs/DNA complexes were also investigated by live-cell FCS. Preliminary studies revealed full recovery of PL efficiency after DNA release. These cBSA-QD/DNA complexes have the great potential to evolve as a valuable tool to follow DNA packing and release without the necessity to directly label the DNA.

We envision that PbPs coated QDs, with all of their unique features, could be explored as non-cytotoxic fluorescent markers for *in vivo* bioimaging, as attractive biosensors for live-cell detection and become an important tool to facilitate an improved mechanistic understanding of non-viral gene delivery. Furthermore, the presence of several available functional groups along the

protein backbone provided various opportunities for introducing additional modifications on QDs such as e.g. signaling peptides.

3.6 Materials and Methods

3.6.1 Materials.

All chemical reagents were obtained from commercial suppliers and used without further purification unless otherwise noted. Bio-Rad Bio-Gel P30 was used for desalting. Dulbecco's Modified Eagle Medium (DMEM) (1X) liquid (high glucose), Fetal Bovine Serum (FBS) Standard Quality (EU approved) were obtained from PAA Laboratories GmbH (Cölbe, Germany). MEM (Non-Essential Amino Acids Solution 10 mM (100X)), LysoTracker® Green DND-26, ER-Tracker® Green dye, CellMask® Deep Red plasma membrane stain and Leibovitz's L-15 Medium (1X), containing L-glutamine but no phenol red were purchased from Invitrogen Life Technologies GmbH (Darmstadt, Germany). The CellTiter-Glo® luminescent cell viability assay kit and the Renilla-Glo® luciferase assay system were obtained from Promega GmbH (Mannheim, Germany). CdSe/CdZnS QDs were synthesized according to previously reported procedures [63] and kindly provided by Dr. Yinthai Chan (National University of Singapore, Singapore).

3.6.2 Instruments.

The fluorescence and absorbance were recorded using a Tecan Infinit® M1000 microplate reader. ÄKTA Purifier FPLC and Sephacryl S-100 HR gel filtration columns were used for dcBSA-PEO$(5000)_{28}$ purification. Vivaspin® 20

MWCO 30,000 and Vivaspin® 6 MWCO 10,000 devices obtained from GE Healthcare Europe GmbH (Freiburg, Germany) were used for ultrafiltration and the centrifugation was performed using Eppendorf 5804R centrifuge at 3500 rpm. Precast NuPAGE® TA 3%-8% Gel and NuPAGE® Bis-Tris 4%-12% Gel were purchased from Invitrogen Life Technologies GmbH (Darmstadt, Germany), and gel electrophoresis was performed in a Novek® Mini-Cell. The confocal microscopy and FCS measurements were performed using a FV300 laser scanning confocal system (Olympus, Japan) coupled to an inverted optical microscope IX-70 (Olympus, Japan).

3.6.3 Preparation of HSA-QDs and cBSA-QDs

3.6.3.1 Synthesis of core/shell CdSe/CdZnS [‡]*.*

Synthesis of monodisperse CdSe quantum dots (QDs) proceeded based on a previously reported procedure with slight modifications [23]. A bath comprising of trioctylphosphine oxide (TOPO, 9 g, 90%), hexadecylamine (HDA, 6 g) and diisopropanolamine (DIPA, 0.25 mL) was degassed at 100 °C for 1.5 hr. A precursor solution comprising of $Cd(acac)_2$ (317 mg) and 1,2-hexadecanediol (HDDO, 567 mg) in 1-octadence (ODE, 6 mL) was degassed at 120 ^{o}C for 1.5 hr, followed by addition of TOPSe (1.5 M, 4 mL, obtained by dissolving Se shot in trioctylphosphine (TOP)) at room temperature. The precursor solution was then rapidly injected into the bath at 360 °C and allowed to cool to 80 °C. As-synthesized CdSe QDs were subsequently

[‡] CdSe/CdZnS QDs were prepared by Yang Xu and Sabyasachi Chakrabortty from Dr. Chan's group in National University of Singapore.

processed by 3-4 cycles of precipitation in a butanol / methanol mixture and re-dispersion in hexane for further use.

For the overcoating process, CdSe cores in hexane were first introduced into a 100 mL 4-neck flask containing TOPO (9 g) and HDA (6 g), and the hexane was removed under vacuum at 70 °C. A mixture comprising of $Cd(acac)_2$ (31 mg), $Zn(acac)_2$ (235 mg) and HDDO (512 mg) in ODE (5 mL) was degassed at 130 °C for 1 hr, yielding a cloudy solution that was subsequently loaded into a syringe. Separately, elemental sulfur (32 mg) in ODE (5 mL) was degassed at 160 °C for 1 hr, yielding a pale yellow solution that was loaded into a different syringe. About 1 mL of the mixture containing the Zn and Cd precursors was injected into the bath containing the CdSe cores at 120 °C and the temperature was raised to 230 °C for 10 min. About 1 mL of the sulfur containing mixture was then added dropwise and the temperature was raised further to 240 °C. Following that, the remaining mixtures of Cd/Zn and S precursors in their respective syringes were added dropwise and the solution was left to stir for 20 min before the temperature was lowered to 80 °C. As-synthesized CdSe/CdZnS core/shell QDs were then processed by repeated cycles of precipitation in methanol and re-dispersion in toluene or hexane as needed.

3.6.3.2 General procedure to prepare PbPs coated QDs.

dHSA-PEO$(5000)_{27}$-TA_{22} (**2-16**, 1 mg, ~6.6 nmol), dcBSA-PEO$(5000)_{28}$-TA_{26} (**2-17**, 1 mg, ~6.6 nmol) or LY-PEO$(5000)_8$-TA_8 (**2-18**, 1 mg, ~17.8 nmol) were used to prepare HSA-QDs, cBSA-QDs and LY QDs respectively. The corresponding PbP was dissolved in double distilled water (2 mL). Then,

$NaBH_4$ (1 mg, 26 μmol) was added under argon, and the reaction mixture was stirred for 2 hr to reduce all disulfide bridges of the thioctic acid groups. After reduction, HCl (1 M) was added until no more gas formed. Subsequently, NaOH (1 M) was added to adjust the solution to a neutral pH. To the reduced PbP-DHLA conjugates, 5 equivalents of CdSe/CdZnS QDs (33 nmol) in THF (10 μL) was added under vigorous stirring. After sonication for 1 min, the reaction mixture was constantly stirred overnight. Thereafter, the reaction mixture was filtered through a 0.2 μm micro-syringe filter to eliminate any uncoated QDs. Finally, the water-soluble cBSA-QDs were further purified and concentrated by ultrafiltration (Vivaspin® 6 MWCO 10,000).

3.6.4 Optical Properties of PbPs coated QDs.

UV-Vis absorption spectra and Fluorescence spectra were recorded using Tecan Infinit® M1000 microplate reader. The quantum yields of QDs were determined relative to Fluorescein in ethanol as a fluorescent standard (λ_{ex} = 425 nm), with the possibility of correcting for differences between the refractive index of the reference (n_r), and the sample solutions (n_s) using the expression:

$$\Phi f(s) = \Phi f(r).\{(\int Is(\bar{\upsilon})d\bar{\upsilon})/(\int Ir(\bar{\upsilon})d\bar{\upsilon})\}.(Dr/Ds).(ns^2/nr^2)$$

Here the indices s and r, respectively, denote sample and reference. The integrals over I represent areas of the corrected emission spectra, and D is the optical density at the wavelength of excitation.

3.6.5 Characterization of the size of PbPs coated QDs.

3.6.5.1 Transmission electron microscopy (TEM) of PbPs coated QDs.

A Jeol 1400 Transmissions electron microscope was used to obtain bright field TEM images of the coated QDs. For TEM measurements, a drop of the QDs solution was placed onto a 300 mesh size copper grid covered with a continuous carbon film and electrodeposited. Excess solution was removed by an adsorbent paper and the sample was dried at room temperature. It was found that the PbPs coated QDs samples contained mostly single, isolated QDs. The few clusters that were detected were primarily attributed to the solvent drying process. 8:1, 2:1 and 1:1 cBSA-QD/DNA complexes were also investigated by TEM *via* the sample protocol.

1% Uranyl acetate solution was used to further stain the sample to investigate the polypeptide coating. A drop of uranyl acetate solution was added to the copper grid with sample deposited and allowed to stay for 1 min. The grid was then gently rinsed with water for 3 times and dried under IR lamp. The uranyl acetate deposited on the grid provided a dark background contrast and the protein sample thus could be observed as white spots.

The size distribution of particles was calculated using ImageJ (available at http://rsb.info.nih.gov/ij; developed by Wayne Rasband, National Institutes of Health, Bethesda, MD).

3.6.5.2 High resolution TEM[§]

The morphology of cBSA-QDs was also investigated by high resolution TEM using an imaging-side aberration-corrected FEI TITAN 80-300 operated at 80kV acceleration voltage. A graphene substrate was fabricated *via*

[§] Experiments were done by Dr. Kaiser and Gerardo Algara-Siller from the department of Electron Microscopy of Materials Science, University of Ulm, Germany.

micromechanical cleavage and transferred to a Quantifoil grid. In order to reduce contamination on the substrate, graphene was annealed at 250 °C for 5 minutes and then treated with H_2:O_2 ion plasma. Solutions of cBSA-QDs were deposited by drop coating on graphene.

3.6.5.3 Dynamic light scattering (DLS).

1 μM aqueous solution of PbPs coated QDs were prepared and filtered through 0.2 μm syringe filter before measurement to avoid any dust contaminations. DLS measurements were performed using a Malvern Zetasizer ZEN3600 (Malvern Ltd, Malvern, UK) at 25 °C. Autocorrelation functions were analyzed by cumulants method and COTIN routine to estimate hydrodynamic diameter and polydispersity index (PDI). The hydrodynamic diameter distribution was presented as number distribution. The average hydrodynamic diameter and standard deviation (SDV) were calculated according to 6 independent measurements.

3.6.5.4 Size Determination via Fluorescence Correlation Spectroscopy[**]*.*

A commercial CLSM-FCS setup manufactured by Carl Zeiss (Jena, Germany) consisting of the modules ConfoCor 2, LSM510 and an inverted microscope, model Axiovert 200 was used. In addition, a Zeiss C-Apochromat 40x/1.2 W water immersion objective was applied. The QDs were excited by an Argon laser and the emission was collected after filtering with a LP505 long pass filter. The eight-well, polystyrene chambered cover-glass (Lab-Tek, Nalge Nunc International) was used as a sample cell for the water solutions of

[**] Experiments were done by Dr. Koynov in Max-Planck Institute for Polymer Research, Mainz, Germany

PbPs coated QDs. For each solution, a series of ten measurements with a total duration of five minutes were performed. The confocal observation volume was calibrated using a reference dye with a known diffusion coefficient i.e. Rhodamine 6G. The measured autocorrelation curves were fitted with the model function given below in order to determine the hydrodynamic radii of PbPs coated QDs in independent measurements:

$$G(\tau) = 1 + \frac{1}{N}\left(1 + \frac{\tau}{\tau_D}\right)^{-1}\left(1 + \frac{\tau}{S^2\tau_D}\right)^{-1/2}$$

where N is the average number of fluorescent species in the observation volume V, τD is the lateral diffusion time and $S=z_0/\omega_0$ is the ratio of axial to radial dimension of V. The diffusion coefficient of the fluorescent species D can be determined as $D = \omega_0^2/4\tau$ and their hydrodynamic radius trough $R_H = k_B T / 6\pi\eta D$ where T is the temperature, k_B the Boltzmann constant and η the viscosity of the solution.

3.6.6 Study the stabibility of PbPs coated QDs.

3.6.6.1 Stability of cBSA-QDs in different buffers and media.

The cBSA-QDs were added to water, PBS buffer and DMEM cell culture media as well as 1 mg/mL Trypsin in PBS buffer and incubated for 24 hr at 37 °C and the emission curves were recorded.

3.6.6.2 Proteolysis stability of dcBSA-PEO(5000)$_{27}$ and dBSA-QDs.

1 mg/mL of dcBSA-PEO(5000)$_{27}$ or 0.2 mg/mL of cBSA-QD were prepared in 50 mM Tris buffer at pH 7.4. Then, trypsin or proteinase K were

added to the final concentration of 0.1 mg/mL and incubated at 37°C. To monitor the digestion process on SDS-PAGE, 7 μL of the sample was taken out of the reaction mixture at desired time points and immediately treated by phenylmethanesulfonyl fluoride (PMSF) (1 μL, 10mM), DTT (1 μL, 1M) and NuPAGE® LDS sample buffer (3 μL) and then boiled at 95°C for 5 min. The samples were directly analyzed by SDS-PAGE.

The photoluminescence properties of cBSA-QDs were also monitored. A blank control sample was prepared by using same concentration of cBSA-QDs and incubating at the same conditions in parallel. The emission intensities of cBSA-QDs incubated with Trypsin and proteinase K were recorded after the time intervals indicated, and the relative emission intensities of the experimental samples were calculated by considering the emission intensity of the blank control sample as 100%.

3.6.7 Characterization of the pH responsiveness of HSA-QDs.

3.6.7.1 Study HSA-QDs emission spectrum under different pH.

pH3 to pH11 buffer was prepared according to a procedure reported previously [64]. 10 μL of HSA-QDs in double distilled water and 10 μL of the buffer with the desired pH were combined in PerkinElmer ProxiPlate®-384 F plus microplates and the fluorescence was instantly recorded on a Tecan Infinit® M1000 microplate reader. This experiment was conducted four times with different batches of HSA-QDs. The area under each curve was integrated separately in four replicate measurements and normalized. The average of the integration data was plotted and the standard deviation was included as error bars.

3.6.7.2 pH responsiveness reversibility test.

In order to measure the reversibility of the impact of the pH on the emission intensity and fluorescence quantum yield, 10 μL of HSA-QDs dissolved in pure water was first added to 10 μL of a buffer solution adjusted to pH9 (10 mM) or pH5 (10 mM). Then, 5 μL of this solution was added to 15 μL of 20 mM pH9 or pH5 buffer as shown (**Figure 3-27**) so that the quantum dots were at similar concentration and the emission spectra were taken and compared directly. Measurements were performed three times and the average data was plotted.

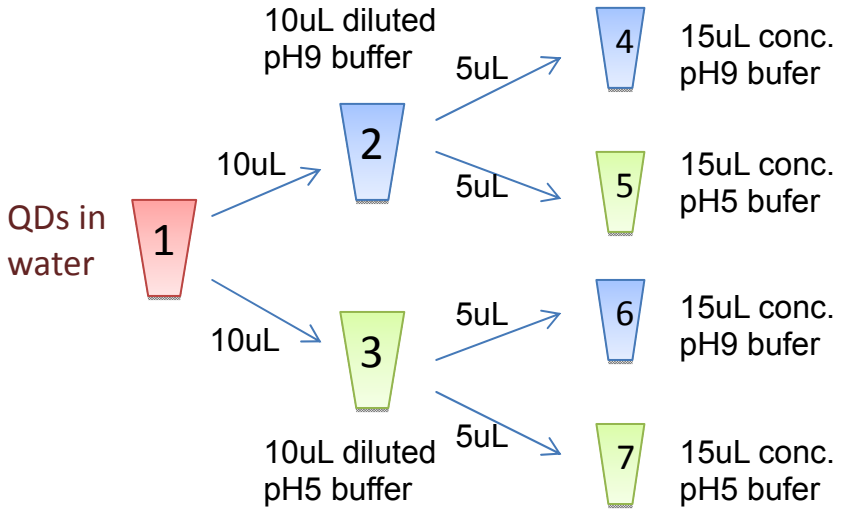

Figure 3-27. pH reversibility test protocol. 4: HSA-QDs in pH9 buffer; 5: HSA-QDs in pH9 first then pH5 buffer; 6: HSA-QDs in pH5 first then pH9 buffer and 7: HSA-QDs in pH5 buffer. Reproduced with permission [1]. Copyright 2012, American Chemical Society.

*3.6.7.3 Circular Dichroism of dHSA-PEO(5000)$_{27}$-TA$_{22}$ (**2-16**) under different pH.*

dHSA-PEO(5000)$_{27}$-TA$_{22}$ (**2-16**) was dissolved in pure water in ~1 mg/mL concentration. 0.75 mL of pH3, pH5, pH7 and pH9 borate-phosphate buffer (50 mM) was added to 0.25 mL of this solution separately. The sample was measured in a 1 mm cuvette with a volume of 400 μL. The CD signal was measured from 260 nm down to 185 nm. The bandwidth was set to 1 nm and a response at 1 sec. Standard sensitivity was used with the data pitch 0.1 nm and 100 nm/min scanning speed. Temperature was kept constant at 20 °C. The data was recorded using 5 times data accumulation.

3.6.8 Measure the relative PL efficiency of cBSA-QDs complexed with different DNAs.

Concentration of cBSA-QDs was firstly estimated by determining dcBSA-PEO(5000)$_{27}$-TA$_{26}$ copolymer concentration using the BCA® (bicinchoninic acid) protein assay kit (Thermo Scientific Pierce Protein Research Products, Illinois, U.S.A.). Desired molar ratio of different plasmid DNAs were then added to the same amount of cBSA-QDs solutions and 20 μL of the complex solutions were transferred to a 384-well small-volume black microplate (Grenier Bio-one). The emission spectra of the QDs and QD/DNA complexes were first checked, and no shift in the spectrum was found. The maximum emission intensity at 600 nm (λ_{ex}=254 nm) was recorded for each sample. The relative PL efficiency was calculated by dividing the emission intensity of each sample by the emission intensity of the original QDs at the same concentration.

3.6.9 Study of PbPs coated QDs in mammalian cells.

3.6.9.1 Cell culture.

A549 cells, a human alveolar basal epithelial carcinoma cell line, were obtained from DSMZ (German Collection of Microorganisms and Cell Cultures, Braunschweig). Cells were cultured in high-glucose DMEM supplemented with 10% fetal bovine serum (FBS), 100 U/mL penicillin, 0.1 mg/mL streptomycin, and 0.1 mM non-essential amino acids at 37°C in a humidified 5% CO_2 incubator.

3.6.9.2 Cytotoxicity assay.

Eight thousand A549 cells per well were plated onto a white 96-well plate and incubated overnight to allow attachment. The wells were 70–80% confluent on the day of the experiment. The cells were treated with 1 μM cBSA-QDs or 1 μM doxorubicin as positive control and incubated for another 24 hr. Blank cells without treatment were used to obtain 100% cell viability. After treatment, the Cell-Titer Glo® (Promega GmbH, Mannheim, Germany) cell viability assay kit was used to quantify the viability of the cells in each well according to the manufacturer's instructions.

3.6.9.3 Confocal microscopy imaging.

A549 cells were plated in a Coverglass Lab-Tek 8-well chamber (Nunc, Denmark) at a density of 30,000 cells per well in 300 μl DMEM containing 10% FCS, 1% penicillin/streptomycin and 1% MEM. The cells were incubated overnight at 37°C in 5% CO_2 to allow adhesion. The next day, the cells were washed gently twice with pre-warmed PBS and then incubated in 100 μL warm PBS containing 2% glucose in 32 μl cBSA-QDs solution (1 μM, sterilized with a 0.2 μm microsyringe filter) or the cBSA-QD/DNA complex (8:1

cBSA-QDs/pUC19 plasmid) (1 μM) for 2 hr. Subsequently, 100 μl L-15 medium without phenol red and supplemented with 10% fetal bovine serum (FBS) and 0.1 mM non-essential amino acids was supplied to cells, which were further incubated for the desired time at 37°C under 5% CO_2. Imaging was then performed using a FV300 laser scanning confocal system (Olympus, Japan) coupled to an inverted optical microscope IX-70 (Olympus, Japan) equipped with a 60×/1.2 NA water immersion objective (Olympus, Japan). The QD fluorescence was excited with the 488-nm line of an argon laser, and fluorescence was detected after a 555 nm - 605 nm band pass emission filter. The membrane dye was excited with a He-Ne laser at 633 nm, and the fluorescence was collected after an LP650 long pass emission filter. During the experiments, the samples were mounted on a temperature-controlled microscope stage (Linkam, UK), which kept the cells at 37°C.

3.6.9.4 Investigation of cell uptake mechanism by pharmacological treatment in A549 cells.

A549 cells were grown and treated for 90 min with chlorpromazine hydrochloride 50 μM (CHLP) or Filipin 1 μg/ml (FIL). FIL blocks caveolae mediated endocytosis (CAME), while CHLP inhibits clathrin mediated endocytosis (CLME). After pharmacological treatment, 0.1 μM cBSA-QDs were further incubated with cells for 4 hr. Cells representing the control groups were not treated with drug molecules, but also treated with cBSA-QDs for 4 hr. After incubation, cells were washed gently three times with PBS buffer and then investigated by confocal microscopy.

3.6.10 Study of cBSA-QDs for gene transfection.

3.6.10.1 Luciferase gene transfection assay.

A549 cells were seeded at a density of 8000 cells per well in a white 96-well plate and were incubated overnight at 37°C in 5% CO_2. Subsequently, cBSA-QD/DNA complexes were prepared at different ratios. All complexes were suspended in a final volume of 50 μl with Tris-HCl 100 mM and 100 mM NaCl, pH 7.2 and were incubated for 5 min. Cells were washed twice gently with pre-warmed PBS. Then, 50 μl warm PBS containing 2% glucose and 50 μl of each complex containing 450 ng of pGL4.73 plasmid in Tris-HCl buffer were added to the corresponding wells and incubated for 45 min. After transfection, A549 cells were supplied with 100 μl fresh supplemented DMEM without antibiotics and then incubated overnight at 37°C in 5% CO_2. The transfection efficiency was quantified using the Luciferase Assay System (Promega GmbH, Mannheim, Germany) according to the manufacturer's protocol with a delay time of 2 sec and a detection time of 15 sec.

3.6.10.2 Live-cell FCS study cBSA-QDs and cBSA-QDs/DNA complexes[††].

FCS was carried out using the FV300-IX-70 system (Olympus, Japan). Cells were treated same as for confocal imaging. An image was firstly acquired using the FV300-IX-70 system, and then the focus of the microscope was positioned at a point of interest using the galvanometric scanning mirrors of the FV300 and its Fluoview software package. The focus was kept there

[††] Experiments were done together with Dr. Koynov in Max-Planck Institute for Polymer research, Mainz, Germany.

during the FCS data acquisition. The measured autocorrelation curves were fitted with the model function given in section 3.6.5.4. The average fluorescent particle brightness, which is directly proportional to the quantum yield of the studied fluorescent species, was evaluated by dividing the average fluorescent intensity (in Khz) by the average number of fluorescent species in the observation volume, N. The calibration of the size of the observation volume V was performed using a tracer with a known diffusion coefficient, Alexa Fluor 488.

3.7 Reference

[1]. Wu, Y.; Chakrabortty, S.; Gropeanu, R. A.; Wilhelmi, J.; Xu, Y.; Er, K. S.; Kuan, S. L.; Koynov, K.; Chan, Y.; Weil, T., pH-responsive quantum dots *via* an albumin polymer surface coating. *J. Am. Chem. Soc.* **2010,** *132* (14), 5012-5014.

[2]. Stephens, D. J.; Allan, V. J., Light microscopy techniques for live cell imaging. *Science* **2003,** *300* (5616), 82-86.

[3]. Resch-Genger, U.; Grabolle, M.; Cavaliere-Jaricot, S.; Nitschke, R.; Nann, T., Quantum dots versus organic dyes as fluorescent labels. *Nat. Meth.* **2008,** *5* (9), 763-775.

[4]. Michalet, X.; Pinaud, F. F.; Bentolila, L. A.; Tsay, J. M.; Doose, S.; Li, J. J.; Sundaresan, G.; Wu, A. M.; Gambhir, S. S.; Weiss, S., Quantum dots for live cells, *in vivo* imaging, and diagnostics. *Science* **2005,** *307* (5709), 538-544.

[5]. Alivisatos, A. P., Semiconductor clusters, nanocrystals, and quantum dots. *Science* **1996,** *271* (5251), 933-937.

[6]. Weller, H., Quantum size colloids: From size-dependent properties of discrete particles to self-organized superstructures. *Curr. Opin. Colloid Interface Sci.* **1998,** *3* (2), 194-199.

[7]. Sun, Y.-P.; Zhou, B.; Lin, Y.; Wang, W.; Fernando, K. A. S.; Pathak, P.; Meziani, M. J.; Harruff, B. A.; Wang, X.; Wang, H.; Luo, P. G.; Yang, H.; Kose, M. E.; Chen, B.; Veca, L. M.; Xie, S.-Y., Quantum-sized carbon dots for bright and colorful photoluminescence. *J. Am. Chem. Soc.* **2006,** *128* (24), 7756-7757.

[8]. Warner, J. H.; Hoshino, A.; Yamamoto, K.; Tilley, R. D., Water-soluble photoluminescent silicon quantum dots. *Angew. Chem. Int. Ed.* **2005,** *44* (29), 4550-4554.

[9]. Medintz, I. L.; Uyeda, H. T.; Goldman, E. R.; Mattoussi, H., Quantum dot bioconjugates for imaging, labelling and sensing. *Nat. Mater.* **2005,** *4* (6), 435-446.

[10]. Dabbousi, B. O.; Rodriguez-Viejo, J.; Mikulec, F. V.; Heine, J. R.; Mattoussi, H.; Ober, R.; Jensen, K. F.; Bawendi, M. G., (CdSe)ZnS core-shell quantum dots: Synthesis and characterization of a size series of highly luminescent nanocrystallites. *J. Phys. Chem. B* **1997,** *101* (46), 9463-9475.

[11]. Hines, M. A.; Guyot-Sionnest, P., Synthesis and characterization of strongly luminescing ZnS-capped CdSe nanocrystals. *J. Phys. Chem.* **1996,** *100* (2), 468-471.

[12]. Murray, C. B.; Norris, D. J.; Bawendi, M. G., Synthesis and characterization of nearly monodisperse CdE (E = sulfur, selenium, tellurium) semiconductor nanocrystallites. *J. Am. Chem. Soc.* **1993,** *115* (19), 8706-8715.

[13]. Peng, Z. A.; Peng, X., Formation of high-quality CdTe, CdSe, and CdS nanocrystals using CdO as precursor. *J. Am. Chem. Soc.* **2000,** *123* (1), 183-184.

[14]. Hong, R.; Fischer, N. O.; Verma, A.; Goodman, C. M.; Emrick, T.; Rotello, V. M., Control of protein structure and function through surface recognition by tailored nanoparticle scaffolds. *J. Am. Chem. Soc.* **2004,** *126* (3), 739-743.

[15]. Dubertret, B.; Skourides, P.; Norris, D. J.; Noireaux, V.; Brivanlou, A. H.; Libchaber, A., *In vivo* imaging of quantum dots encapsulated in phospholipid micelles. *Science* **2002,** *298* (5599), 1759-1762.

[16]. Chan, W. C. W.; Nie, S., Quantum dot bioconjugates for ultrasensitive nonisotopic detection. *Science* **1998,** *281* (5385), 2016-2018.

[17]. Mattoussi, H.; Mauro, J. M.; Goldman, E. R.; Anderson, G. P.; Sundar, V. C.; Mikulec, F. V.; Bawendi, M. G., Self-assembly of CdSe-ZnS quantum dot bioconjugates using an engineered recombinant protein. *J. Am. Chem. Soc.* **2000,** *122* (49), 12142-12150.

[18]. Mei, B. C.; Susumu, K.; Medintz, I. L.; Mattoussi, H., Polyethylene glycol-based bidentate ligands to enhance quantum dot and gold nanoparticle stability in biological media. *Nat. Protocols* **2009,** *4* (3), 412-423.

[19]. Kim, S.; Bawendi, M. G., Oligomeric ligands for luminescent and stable nanocrystal quantum dots. *J. Am. Chem. Soc.* **2003,** *125* (48), 14652-14653.

[20]. Gao, X.; Cui, Y.; Levenson, R. M.; Chung, L. W. K.; Nie, S., *In vivo* cancer targeting and imaging with semiconductor quantum dots. *Nat. Biotech.* **2004,** *22* (8), 969-976.

[21]. Parak, W. J.; Gerion, D.; Pellegrino, T.; Zanchet, D.; Micheel, C.; Williams, S. C.; Boudreau, R.; Gros, M. A. L.; Larabell, C. A.; Alivisatos, A. P., Biological applications of colloidal nanocrystals. *Nanotechnology* **2003,** *14* (7), R15.

[22]. Uyeda, H. T.; Medintz, I. L.; Jaiswal, J. K.; Simon, S. M.; Mattoussi, H., Synthesis of compact multidentate ligands to prepare stable hydrophilic quantum dot fluorophores. *J. Am. Chem. Soc.* **2005,** *127* (11), 3870-3878.

[23]. Snee, P. T.; Chan, Y.; Nocera, D. G.; Bawendi, M. G., Whispering-gallery-mode lasing from a semiconductor nanocrystal/microsphere resonator vomposite. *Adv. Mater.* **2005,** *17* (9), 1131-1136.

[24]. Algar, W. R.; Krull, U. J., Luminescence and Stability of Aqueous Thioalkyl Acid Capped CdSe/ZnS Quantum Dots Correlated to Ligand Ionization. *ChemPhysChem* **2007,** *8* (4), 561-568.

[25]. Liu, W.; Howarth, M.; Greytak, A. B.; Zheng, Y.; Nocera, D. G.; Ting, A. Y.; Bawendi, M. G., Compact Biocompatible Quantum Dots Functionalized for Cellular Imaging. *J. Am. Chem. Soc.* **2008,** *130* (4), 1274-1284.

[26]. Uyeda, H. T.; Medintz, I. L.; Jaiswal, J. K.; Simon, S. M.; Mattoussi, H., Synthesis of Compact Multidentate Ligands to Prepare Stable Hydrophilic Quantum Dot Fluorophores. *J. Am. Chem. Soc.* **2005,** *127* (11), 3870-3878.

[27]. Chithrani, B. D.; Ghazani, A. A.; Chan, W. C. W., Determining the size and shape dependence of gold nanoparticle uptake into mammalian cells. *Nano Lett.* **2006,** *6* (4), 662-668.

[28]. He, C.; Hu, Y.; Yin, L.; Tang, C.; Yin, C., Effects of particle size and surface charge on cellular uptake and biodistribution of polymeric nanoparticles. *Biomaterials* **2010,** *31* (13), 3657-3666.

[29]. Oh, W.-K.; Kim, S.; Choi, M.; Kim, C.; Jeong, Y. S.; Cho, B.-R.; Hahn, J.-S.; Jang, J., Cellular uptake, cytotoxicity, and innate immune response of silica-titania hollow nanoparticles based on size and surface functionality. *ACS Nano* **2010,** *4* (9), 5301-5313.

[30]. Harris, J. R.; Roos, C.; Djalali, R.; Rheingans, O.; Maskos, M.; Schmidt, M., Application of the negative staining technique to both aqueous and organic solvent solutions of polymer particles. *Micron* **1999,** *30* (4), 289-298.

[31]. Yohannes, G.; Wiedmer, S. K.; Elomaa, M.; Jussila, M.; Aseyev, V.; Riekkola, M.-L., Thermal aggregation of bovine serum albumin studied by asymmetrical flow field-flow fractionation. *Anal. Chim. Acta* **2010,** *675* (2), 191-198.

[32]. Garbuzenko, O.; Barenholz, Y.; Priev, A., Effect of grafted PEG on liposome size and on compressibility and packing of lipid bilayer. *Chem. Phys. Lipids* **2005,** *135* (2), 117-129.

[33]. Stewart, M. H.; Susumu, K.; Mei, B. C.; Medintz, I. L.; Delehanty, J. B.; Blanco-Canosa, J. B.; Dawson, P. E.; Mattoussi, H., Multidentate poly(ethylene glycol) ligands provide colloidal stability to semiconductor and metallic nanocrystals in extreme conditions. *J. Am. Chem. Soc.* **2010,** *132* (28), 9804-9813.

[34]. Jung, J.; Solanki, A.; Memoli, K. A.; Kamei, K.-i.; Kim, H.; Drahl, M. A.; Williams, L. J.; Tseng, H.-R.; Lee, K., Selective inhibition of human brain tumor cells through multifunctional quantum-dot-based siRNA delivery. *Angew. Chem. Int. Ed.* **2010,** *49* (1), 103-107.

[35]. van Hest, J. C. M., Biosynthetic-synthetic polymer conjugates. *Polym. Rev.* **2007,** *47* (1), 63-92.

[36]. Dobrovolskaia, M. A.; Aggarwal, P.; Hall, J. B.; McNeil, S. E., Preclinical studies to understand nanoparticle interaction with the immune system and its potential effects on nanoparticle biodistribution. *Mol. Pharm.* **2008,** *5* (4), 487-495.

[37]. Zhao, F.; Zhao, Y.; Liu, Y.; Chang, X.; Chen, C., Cellular uptake, intracellular trafficking, and cytotoxicity of nanomaterials. *Small* **2011,** *7* (10), 1322-1337.

[38]. Eisele, K.; Gropeanu, R. A.; Zehendner, C. M.; Rouhanipour, A.; Ramanathan, A.; Mihov, G.; Koynov, K.; Kuhlmann, C. R. W.; Vasudevan, S. G.; Luhmann, H. J.; Weil, T., Fine-tuning DNA/albumin polyelectrolyte interactions to produce the efficient transfection agent cBSA-147. *Biomaterials* **2010,** *31* (33), 8789-8801.

[39]. Liu, W.; Choi, H. S.; Zimmer, J. P.; Tanaka, E.; Frangioni, J. V.; Bawendi, M., Compact Cysteine-Coated CdSe(ZnCdS) Quantum dots for *in vivo* applications. *J. Am. Chem. Soc.* **2007,** *129* (47), 14530-14531.

[40]. Jeong, S.; Achermann, M.; Nanda, J.; Ivanov, S.; Klimov, V. I.; Hollingsworth, J. A., Effect of the thiol−thiolate equilibrium on the photophysical properties of aqueous CdSe/ZnS nanocrystal quantum dots. *J. Am. Chem. Soc.* **2005,** *127* (29), 10126-10127.

[41]. El Kadi, N.; Taulier, N.; Le Huerou, J. Y.; Gindre, M.; Urbach, W.; Nwigwe, I.; Kahn, P. C.; Waks, M., Unfolding and refolding of bovine serum albumin at acid pH: Ultrasound and structural studies. *Biophys. J.* **2006,** *91* (9), 3397-3404.

[42]. Aldana, J.; Lavelle, N.; Wang, Y.; Peng, X., Size-dependent dissociation pH of thiolate ligands from cadmium chalcogenide nanocrystals. *J. Am. Chem. Soc.* **2005,** *127* (8), 2496-2504.

[43]. Lee, H.; Kim, I. K.; Park, T. G., Intracellular trafficking and unpacking of siRNA/quantum dot-PEI complexes modified with and without cell penetrating peptide: confocal and flow cytometric FRET analysis. *Bioconjug. Chem.* **2010,** *21* (2), 289-295.

[44]. Li, S. D.; Huang, L., Gene therapy progress and prospects: non-viral gene therapy by systemic delivery. *Gene Ther.* **2006,** *13* (18), 1313-1319.

[45]. Qi, L.; Gao, X., Quantum dot-amphipol nanocomplex for intracellular delivery and real-time imaging of siRNA. *ACS Nano* **2008,** *2* (7), 1403-1410.

[46]. Kim, T.; Noh, M.; Lee, H.; Joo, S.-W.; Lee, S. Y.; Lee, K., Fluorescence-based detection of point mutation in DNA sequences by CdS quantum dot aggregation. *J. Phys. Chem. B* **2009,** *113* (43), 14487-14490.

[47]. Liu, J.; Yang, X.; Wang, K.; Yang, R.; Ji, H.; Yang, L.; Wu, C., A switchable fluorescent quantum dot probe based on aggregation/disaggregation mechanism. *Chem. Commun.* **2011,** *47* (3), 935-937.

[48]. Zhang, B.; Zhang, Y.; Mallapragada, S. K.; Clapp, A. R., Sensing polymer/DNA polyplex dissociation using quantum dot fluorophores. *ACS Nano* **2011,** *5* (1), 129-138.

[49]. Siegberg, D.; Herten, D.-P., Fluorescence quenching of quantum dots by DNA nucleotides and amino acids. *Aust. J. Chem.* **2011,** *64* (5), 512-516.

[50]. Wu, Y.; Eisele, K.; Doroshenko, M.; Algara-Siller, G.; Kaiser, U.; Koynov, K.; Weil, T., A quantum dot photoswitch for DNA detection, gene transfection, and live-cell imaging. *Small* **2012,** *8* (22), 3465-3475.

[51]. Chen, H. H.; Ho, Y. P.; Jiang, X.; Mao, H. Q.; Wang, T. H.; Leong, K. W., Quantitative comparison of intracellular unpacking kinetics of polyplexes by a model constructed from quantum dot-FRET. *Mol. Ther.* **2008,** *16* (2), 324-332.

[52]. Ho, Y. P.; Chen, H. H.; Leong, K. W.; Wang, T. H., Evaluating the intracellular stability and unpacking of DNA nanocomplexes by quantum dots-FRET. *J. Control. Release* **2006,** *116* (1), 83-89.

[53]. Lee, J. I.; Ha, K. S.; Yoo, H. S., Quantum-dot-assisted fluorescence resonance energy transfer approach for intracellular trafficking of chitosan/DNA complex. *Acta Biomater.* **2008,** *4* (4), 791-798.

[54]. Lee, H.; Kim, I. K.; Park, T. G., Intracellular trafficking and unpacking of siRNA/quantum dot-PEI complexes modified with and without cell penetrating peptide: confocal and flow cytometric FRET analysis. *Bioconjug Chem.* **2010,** *21* (2), 289-95.

[55]. Derfus, A. M.; Chen, A. A.; Min, D.-H.; Ruoslahti, E.; Bhatia, S. N., Targeted quantum dot conjugates for siRNA delivery. *Bioconjug. Chem.* **2007,** *18* (5), 1391-1396.

[56]. Yezhelyev, M. V.; Qi, L.; O'Regan, R. M.; Nie, S.; Gao, X., Proton-sponge coated quantum dots for siRNA delivery and intracellular imaging. *J. Am. Chem. Soc.* **2008,** *130* (28), 9006-9012.

[57]. Zhao, M. X.; Li, J. M.; Du, L.; Tan, C. P.; Xia, Q.; Mao, Z. W.; Ji, L. N., Targeted cellular uptake and siRNA silencing by quantum-dot nanoparticles coated with beta-cyclodextrin coupled to amino acids. *Chem. Eur. J.* **2011,** *17* (18), 5171-5179.

[58]. Jovin, T. M., Quantum dots finally come of age. *Nat. Biotech.* **2003,** *21* (1), 32-33.

[59]. Rigler, R.; Elson, E. S., *Fluorescence correlation spectroscopy*. Springer-Verlag: New York, 2001.

[60]. Kim, S. A.; Heinze, K. G.; Schwille, P., Fluorescence correlation spectroscopy in living cells. *Nat. Meth.* **2007,** *4* (11), 963-973.

[61]. Chen, H.; Farkas, E. R.; Webb, W. W., Chapter 1: *In vivo* applications of fluorescence correlation spectroscopy. *Methods Cell Biol.* **2008,** *89*, 3-35.

[62]. Khalil, I. A.; Kogure, K.; Akita, H.; Harashima, H., Uptake pathways and subsequent intracellular trafficking in nonviral gene delivery. *Pharmacol. Rev.* **2006,** *58* (1), 32-45.

[63]. Banerjee, I. A.; Yu, L.; Shima, M.; Yoshino, T.; Takeyama, H.; Matsunaga, T.; Matsui, H., Magnetic nanotube fabrication by using bacterial magnetic nanocrystals. *Adv. Mater.* **2005,** *17* (9), 1128-1131.

[64]. Sober, H. A., *Handbook of biochemistry: selected data for molecular biology*. Chemical Rubber Co: Cleveland, 1968.

Chapter 4

Protein Based Polypeptide Copolymers Derived Drug Delivery Systems

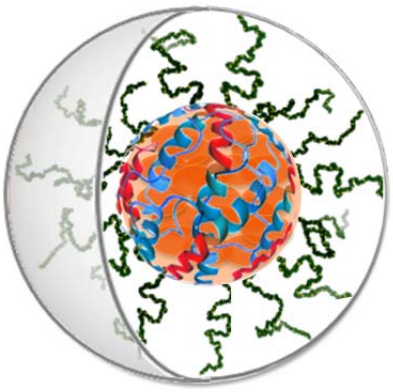

Adapted with permission [61]. Copyright 2012, Wiley-VCH.

This Chapter contains experimental results published previously in (1) *Biointerphases*. 2012, 7(1-4):5. written by Wu Y., Er K. S., Ramanathan A., Vasudevan S., and Weil T. and (2) *Adv. Healthcare Mater.*, 2012, DOI: 10.1002/adhm.201200296. written by Wu Y., Ihme S., Feuring-Buske M., Kuan S. L., Eisele K., Lamla M., Wang Y., Buske C., and Weil T. The dissertation author was the primary investigator and first author of these papers.

4.1 Introduction

The conventional small-molecule chemotherapeutics often elicit severe side effects, such as anemia, vomiting, diarrhea, decreased immunity and hair loss, which is due to the systemic distribution of cytotoxic drugs [1]. In this view, nanomedicines, involving the development of nanoscale particles or macromolecules to improve the biological activity and pharmacokinetic profile of drug candidates, has emerged as an innovative strategy for cancer therapy with great promise for clinical applications [2]. In recent years, a large number of natural and synthetic macromolecules as well as inorganic particles were developed as drug delivery nanocarriers [3], such as liposomes [4], polymeric nanoparticles [5], inorganic nanoparticles [6] as well as proteins [7, 8]. The long systemic circulation times of nano-sized drugs and drug carriers and the increased vascular permeability of tumor tissue led to an accumulation at tumor sites, which was often referred as passive targeting or the “enhanced permeability and retention effect” (EPR effect) [9, 10]. In addition, such nano-sized drug delivery systems could serve as a platform to integrate multiple additional functionalities such as specific targeting ligands or probes suitable for tumor imaging [11, 12].

Although nanomedicine had been developing fast in the past decades, there were major challenges still associated with the design of an ideal macromolecular drug delivery system [1, 3]. One of the key concerns remained the biocompatibility of the nanocarrier, which should be degraded in or cleared from the body without adding further side-effects. In addition, the prevention of drug leakage during blood circulation on the one hand but

achieving efficient drug release at target cells on the other hand represented crucial factors that still appeared challenging to achieve. Other prerequisites included efficient permeability through vascular barriers and cell membranes, great specificity for tumor tissue and high loading of the drug cargo. In view of these criteria, it is not astonishing that only few drug delivery systems have entered clinical trials yet.

While synthetic delivery vehicles often struggled to meet clinical expectations, nature had already created functional macromolecular structures that can be employed as efficient drug carriers [13]. In particular, owing to its beneficial biochemical and pharmacological properties, serum albumin was regarded as a promising drug carrier candidate [8, 14]. Serum albumins could be used as a single molecular carrier, where the drugs were covalently conjugated to the free thiol group in the cysteine-34 position [15] or to introduced free thiols [16]. This strategy maintained the physiochemical properties of albumin while significantly improving the tumor uptake of conjugated drugs. However, only one or a few therapeutic molecules could be carried by each albumin molecule, leading to low delivery efficiency. As an alternative strategy, albumin could also be formulated into microspheres or nanoparticles through precipitation or lyophilization [17, 18, 19]. The formed particles could encapsulate tens to thousands of drug molecules per particle, achieving high drug-loading efficiency. Such albumin particles formulated anticancer drugs, including the FDA approved Abraxane® [20], had been extensively investigated in animals and in clinical studies. However, with sizes in the range of several hundred nanometers to several micrometers, these particles were prone to uptake by the reticuloendothelial system (RES) in the

liver and spleen. And the non-covalent interaction between albumin and drug molecules led to undesired drug leakage in the vascular system, which was difficult to avoid [21]. In this regard, modified albumin nanocarriers displaying high drug loading and minimized drug leakage could be very attractive for clinical applications.

Among many anticancer drugs used clinically, doxorubicin (DOX) continued to be a leading therapeutic for the treatment of various kinds of cancers ever since its discovery in 1971 [22] due to its potency and broad spectrum of activity against diverse cancer types [23, 24]. Especially, it remained one of the most effective therapeutics for the treatment of acute myeloid leukemia (AML), a disease with still very high mortality rates [25, 26]. However, the administration dose of DOX was restricted by serious cardiotoxicity and the development of drug-resistance of tumors [27, 28, 29]. In addition, DOX was known to be rapidly degraded into inactive metabolites after injection into the blood stream [30]. Therefore, various delivery systems had been studied in the past decades in order to improve its therapeutic efficacy.

Physical encapsulation of DOX into polymeric micelles or nanocages [31, 32, 33] was one of the most popular strategies due to their easy preparation, no required modification of the drug molecule and high drug loading capacity. By this way, liposome formulations such as Doxil® containing DOX entered the market [34]. However, for polymer particles and liposomes, a burst drug release was generally observed resulting in undesirable drug leakage in the blood stream and uncontrolled drug release rates [35, 36].

An alternative strategy consisted of conjugating DOX molecules onto polymers to form “polymeric prodrugs” [37]. In order to achieve the release of

the covalently conjugated drugs in tumor tissue, a cleavable linker was normally used between the drug and polymer backbone with tumor selective stimulus reponsiveness. The widely used pH-sensitive hydrazone linker, for instance, was relatively stable at pH 7.4 in the circulation while rapidly cleaved at low pH in the endosomal/lysosomal compartments [38, 39]. Similarly, enzymatic cleavable peptides had also been used as linkers [40]. *Via* these strategies, relatively fast and specific drug release could be achieved in tumor tissue with comparably less drug leakage in the blood stream and in normal tissue. However, notably, slow non-specific drug leakage still remained challenging to prevent completely, which could be serious after long time administration.

In this regard, multi-stimuli responsive carriers attracted increasing attention [41, 42, 43]. For instance, the slight acidic environment of solid tumors caused by the high rate of glycolysis at tumor sites was intensively used to build up pH-sensitive delivery systems [43]. Besides, drug release triggered by enzymatic hydrolysis was also particularly interesting due to the high specificity and fast speed of enzymatic reactions [40, 44]. Especially, some enzymes, such as the lysosomal enzyme Cathepsin B, were found expressed at increased levels in tumor tissue as compared to normal tissue, which were highly attractive for controlled drug release applications [45, 46]. By combining these two strategies, several dual-stimuli tumor-specific delivery systems were developed that enabled the carrier degradation and drug release triggered by both mild acidic conditions and tumor-specific enzymes, both of which modeled the tumor cell microenvironment. Although there were only limited examples of such systems, they revealed promising benefits including

improved stability under blood environment and fast drug release at the tumor site [47, 48].

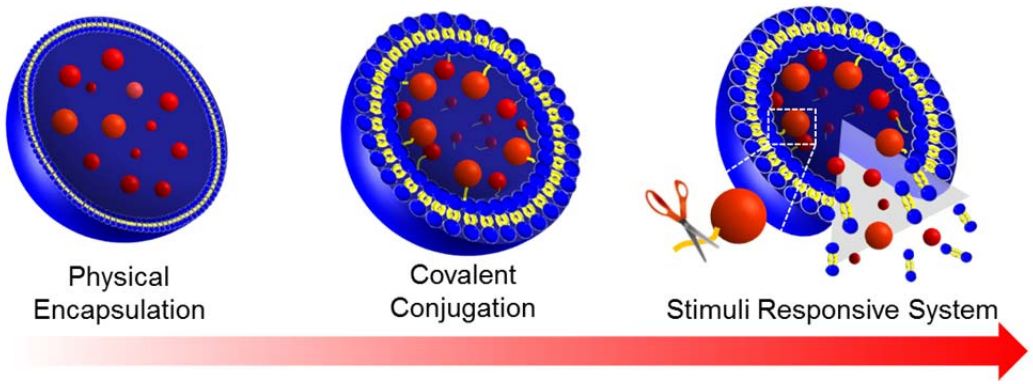

Figure 4-1. Different strategies for DOX delivery.

It was outlined recently that translational nanocarriers suitable for clinical applications should consist of excipientable materials prepared by scalable processes that allow drug retention in the blood circulation versus release in tumor cells to deliver the drug specifically to the tumor with high therapeutic efficacy and few side effects. Up to now, there was no generally applicable transporter available that combines all of these features. Therefore, there is still a considerable interest in novel strategies for achieving improved nanocarriers combining high drug loading efficiency as well as controlled drug release and ideally no systemic toxicity, which was very promising for clinical applications.

Albumin derived PbPs were originated from human proteins, therefore they were found to be highly biocompatible with low cytotoxicity and fast enzymatic degradability as demonstrated in the previous chapters. They formed micelles when interacting with hydrophobic molecules and revealed fast cellular uptake when cationized. Multiple functional groups were available

along the polypeptide backbone providing the opportunity to conjugate drugs or targeting moieties. In addition, PEO side-chains were known to reduce non-specific interactions as well as immunogenicity and antigenicity of proteins and peptides. Therefore, such biohybrid materials represented a novel type of delivery platform offering great potential to effectively transport and release lipophilic drugs into cancer cells.

In this chapter, different drug delivery systems developed from albumin PbPs will be presented. DOX was chosen as representative drug molecule and loaded into PbPs *via* two different strategies - hydrophobic encapsulation and covalent conjugation *via* cleavable hydrazone linker. The hydrophobic modified cationic PbP dcBSA-PEO(5000)$_{27}$-alkyne (**2-15**) was used to form micelles with DOX molecules *via* hydrophobic interactions. The pharmaceutical properties of these micelles were assessed *in vitro*. In addition, in order to achieve more defined structures with minimized drug leakage, covalent drug loading approaches were also investigated. DOX was covalently conjugated with cysteine residues along PbPs *via* pH-sensitive hydrazone linker to allow defined drug loading as well as efficient drug release in targeted tumor tissue. Through a “denaturation-backfolding” strategy, a core-shell drug delivery system could be achieved with a two-step controlled drug released mechanism *via* (1) enzymatic hydrolysis of the albumin scaffold and (2) pH triggered hydrolysis of DOX from the albumin fragments inside the cell. These micelles were carefully characterized and their anti-cancer activities were examined *in vitro* and *in vivo*. In addition, the large number of functional groups available on the protein backbone in principle allowed introducing multi-functionalities into PbPs to create “magic bullets”. To

demonstrate this potential, a protein based "theranostic" system was also constructed by combining anti-cancer therapeutics and magnetic resonance imaging (MRI) contrast agents onto one PbP backbone. Such system would allow controlled delivery of anti-cancer drug and *in situ* monitoring of drug distribution *via* MRI simultaneously.

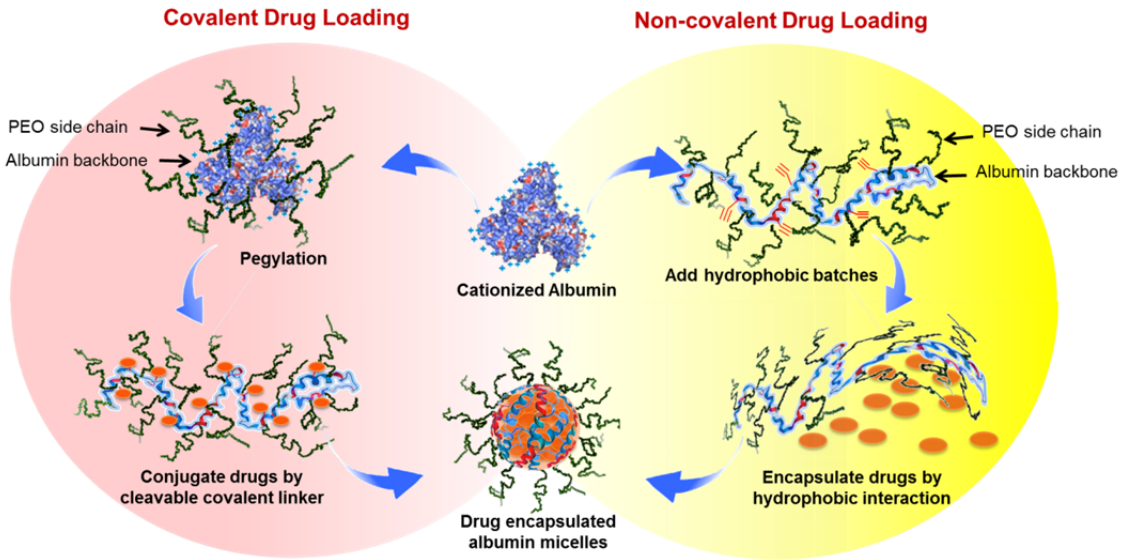

Figure 4-2. Illustration of covalent and non-covalent drug loading into PbPs drug delivery systems. Adapted with permission [61]. Copyright 2012, Wiley-VCH.

4.2 Nano-sized PbP micelles encapsulate doxorubicin by hydrophobic interactions for efficient drug delivery

It was demonstrated in Chapter 1 that PbPs could form stable micellar structures by introducing hydrophobic moieties. Ethynyl group modified PbP (**2-15**) was found to interact with hydrophobic guest molecules with high loading capacity. Based on this hydrophobic interaction, PbP micelles could serve as an anti-cancer drug delivery platform. In this section, PbP (**2-15**)

based micelles encapsulating hydrophobic drug molecules *via* non-covalent interactions will be discussed in view of their potential for drug delivery applications. These nano-sized, stable micelles had high drug loading capacity and they were able to efficiently pass cell membranes and therefore displayed enhanced cytotoxicity compared to the free drugs.

4.2.1 Preparation and characterization of PbP DOX micelles

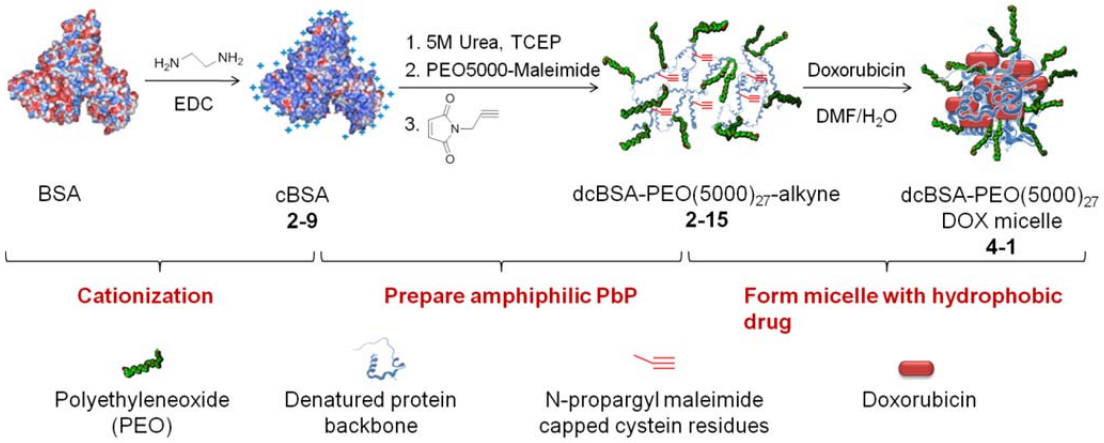

Figure 4-3. Preparation of dcBSA-PEO(5000)$_{27}$-DOX micelles. Reproduced with permission [49]. Copyright 2012, Springer.

PbP (**2-15**) was synthesized from polycationic bovine serum albumin (cBSA **2-9**) as demonstrated in Chapter 2 Section 2.4.1. Denaturation of globular cBSA exposed a large number of functional groups along the backbone, which were previously hidden inside the protein scaffold. Especially, the lipophilic amino acids originating from e.g. hydrophobic pockets were now accessible and, together with the N-propargyl groups, allowed efficient interactions with hydrophobic drug molecules. The presence

of multiple positive charges contributed to an increased membrane permeability and cellular uptake and the high number of PEO side chains distributed along the backbone assisted with reducing nonspecific adsorption and minimizing immunogenicity. Therefore, this grafted polymer represented an attractive platform for conjugating targeting ligands and other functional moieties.

It was known that serum albumin transports water-insoluble lipids in the bloodstream and about eight hydrophobic ligands could be transported [50]. After denaturation, the tertiary structure of dcBSA-PEO(5000)$_{27}$-alkyne (**2-15**) was unfolded but sufficient numbers of lipophilic amino acids and additional N-propargylamine were still present that could non-covalently interact with hydrophobic molecules. DOX was chosen as model drug since it had been well characterized *in vitro* and *in vivo*. DOX has a lipophilic scaffold and emits above 500 nm thus facilitating characterization *via* fluorescence microscopy. The loading of DOX into PbP (**2-15**) was performed according to a published procedure [51] (**Figure 4-3**). Briefly, DOX hydrochloride salt was first neutralized and extracted into a dichloromethane layer. The obtained non-water soluble drug was then re-dissolved in a minimum amount of dimethylformamide and added into an aqueous solution of (**2-15**) (1 mg/mL). After overnight stirring, the formed micelles were purified by dialysis. The purification efficiency was estimated by loading dcBSA-PEO(5000)$_{27}$-DOX (**4-1**) and free DOX HCl into Bio-Gel P30 (Bio-Rad Laboratories GmbH, Munich, Germany) size exclusion columns. Free DOX HCl gave a red colored narrow band, which remained on top of the column, whereas sufficiently stable DOX micelles quickly moved along the column and no traces of free DOX were

present on top of the column suggesting that all DOXs were associated with the copolymer micelles (**Figure 4-4a**).

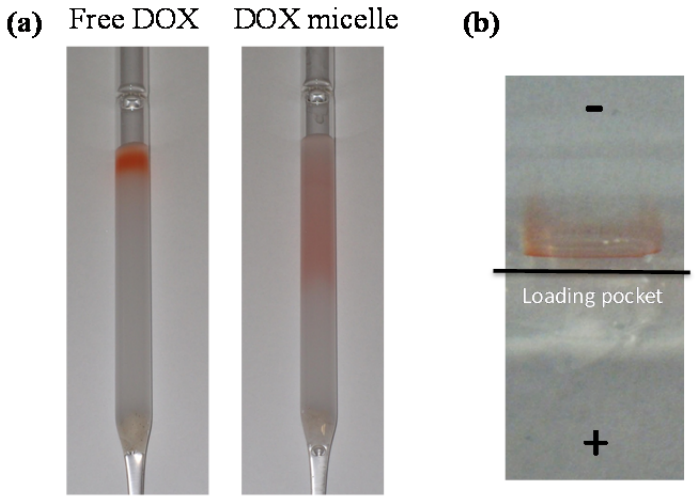

Figure 4-4. Characterization of dcBSA-PEO(5000)$_{27}$-DOX micelles (**4-1**). (a). Loading of DOX HCl and dcBSA-PEO(5000)$_{27}$-DOX micelles onto a Bio-gel P30 size exclusion column using the same amount of eluent. (b). Agarose gel electrophoresis of dcBSA-PEO(5000)$_{27}$-DOX micelles in TAE buffer (Tris base-acetic acid-EDTA buffer, pH7.4). Adapted with permission [49]. Copyright 2012, Springer.

4.2.2 Characterization of dcBSA-PEO(5000)$_{27}$-DOX micelles (4-1)

In order to quantify the average number of encapsulated DOX molecules as well as the maximum drug loading efficiency of the micelle system, different equivalents of DOX were applied for micelle preparation. After dialysis, the absorbance spectra of the micelles were recorded (**Figure 4-5a**) and the characteristic DOX absorbance with a maximum at 488 nm was observed indicating successful DOX loading. The DOX concentration was calculated considering a molar extinction coefficient of 11500 $M^{-1}cm^{-1}$ and the average number of DOX encapsulated in the micelles was given in **Table 4-1**.

DOX loading could be estimated due to a linear correlation of the amount of DOX added in access to the copolymer solution (feed DOX) versus the number of encapsulated DOX molecules (**Figure 4-5b**). By adding 100 equivalents of DOX, a maximum number of about 14 DOX molecules was reproducibly encapsulated by each micelle. In contrast, the native protein carrier HSA was only able to accommodate up to eight lipophilic guest molecules [50] thus indicating an increased drug load after protein denaturation.

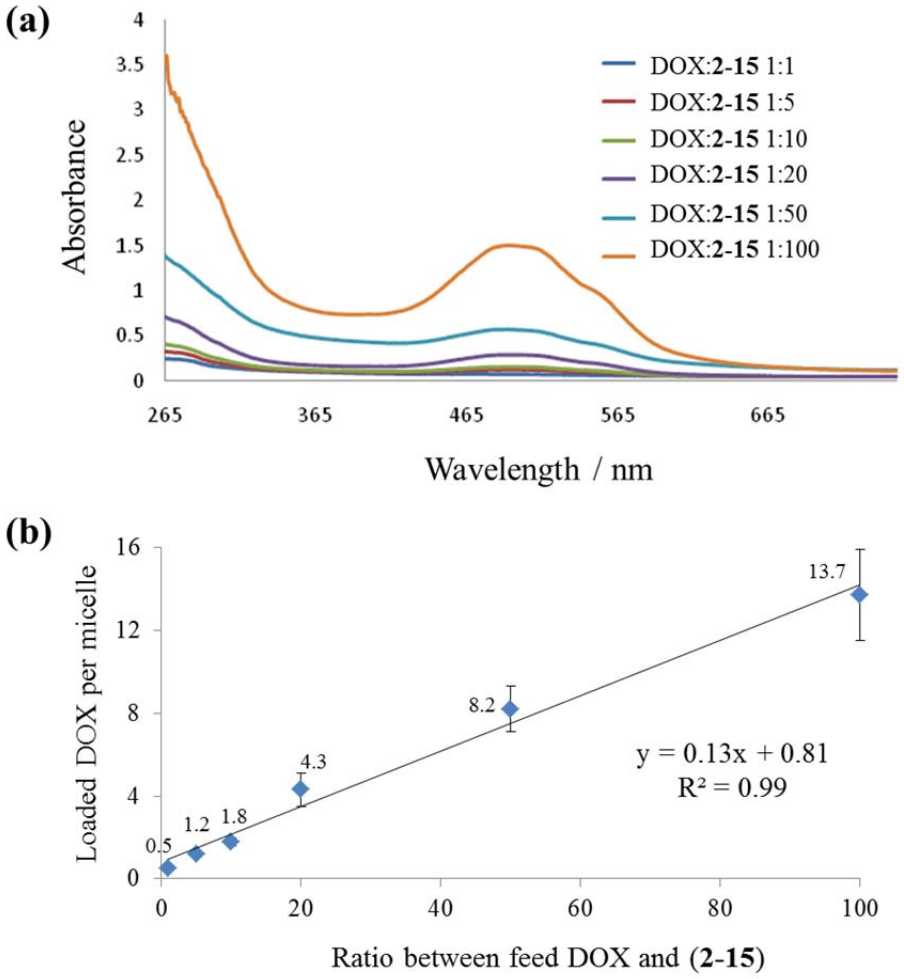

Figure 4-5. Loading of different ratios of DOX into dcBSA-PEO(5000)$_{27}$-DOX micelles (**4-1**). (a) Absorbance spectra of (**4-1**) with different equivalent of DOX loaded (the protein concentration was kept the same); (b). Correlation of the ratio of added DOX (feed DOX) versus (**2-15**) and the amount of DOX

loaded into micelles (**4-1**). Reproduced with permission [49]. Copyright 2012, Springer.

Table 4-1. Summary of the loading efficiencies of DOX molecules into dcBSA-PEO(5000)$_{27}$ micelles (**4-1**).

Ratio added DOX : (2-15)[a]	Loading efficiency (Molar ratio)[b]	Loading efficiency (in Weight%)[c]	Encapsulation efficiency of DOX (%)[d]
1:1	0.5±0.1	0.15±0.03	51.6±9.9
5:1	1.2±0.1	0.34±0.01	23.1±1.0
10:1	1.8±0.2	0.52±0.07	17.2±2.3
20:1	4.3±0.8	1.22±0.23	20.4±3.9
50:1	8.2±1.1	2.33±0.31	15.5±2.0
100:1	13.7±2.2	3.91±0.63	13.1±2.1

[a] Molar ratio of feed DOX added versus dcBSA-PEO(5000)$_{27}$-alkyne (**2-15**) for micelle formation.
[b] Molar ratio of DOX loaded into dcBSA-PEO(5000)$_{27}$ micelles (**4-1**).
[c] Weight percentage of DOX loaded into dcBSA-PEO(5000)$_{27}$ micelles.
[d] Weight percentage of loaded DOX to added DOX (feed DOX).

The morphology and size distribution of micelles containing about 14 DOX were investigated by TEM with uranyl acetate staining. Very homogenous micelles with narrow size-distributions were observed. Their average diameters are ~56 nm (**Figure 4-6a,b**) which was generally considered ideal for passive targeting and accumulation into tumor tissues by the ERP effect [9, 10]. The size distribution of dcBSA-PEO(5000)$_{27}$-DOX micelles (**4-1**) in solution was further investigated using DLS and narrowly dispersed particles were found with average diameters of ~30 nm (**Figure 4-6c**) which was comparable with the particle sizes found by TEM. In addition, DOX-containing micelles (**4-1**) possessed a highly positive surface charge originating from the cationic nature of the cBSA-147 precursor protein, which was confirmed by gel electrophoresis (**Figure 4-4b**). The positive net charges would be beneficial

for electrostatic interactions with cellular membranes and therefore enhance cellular uptake efficiency.

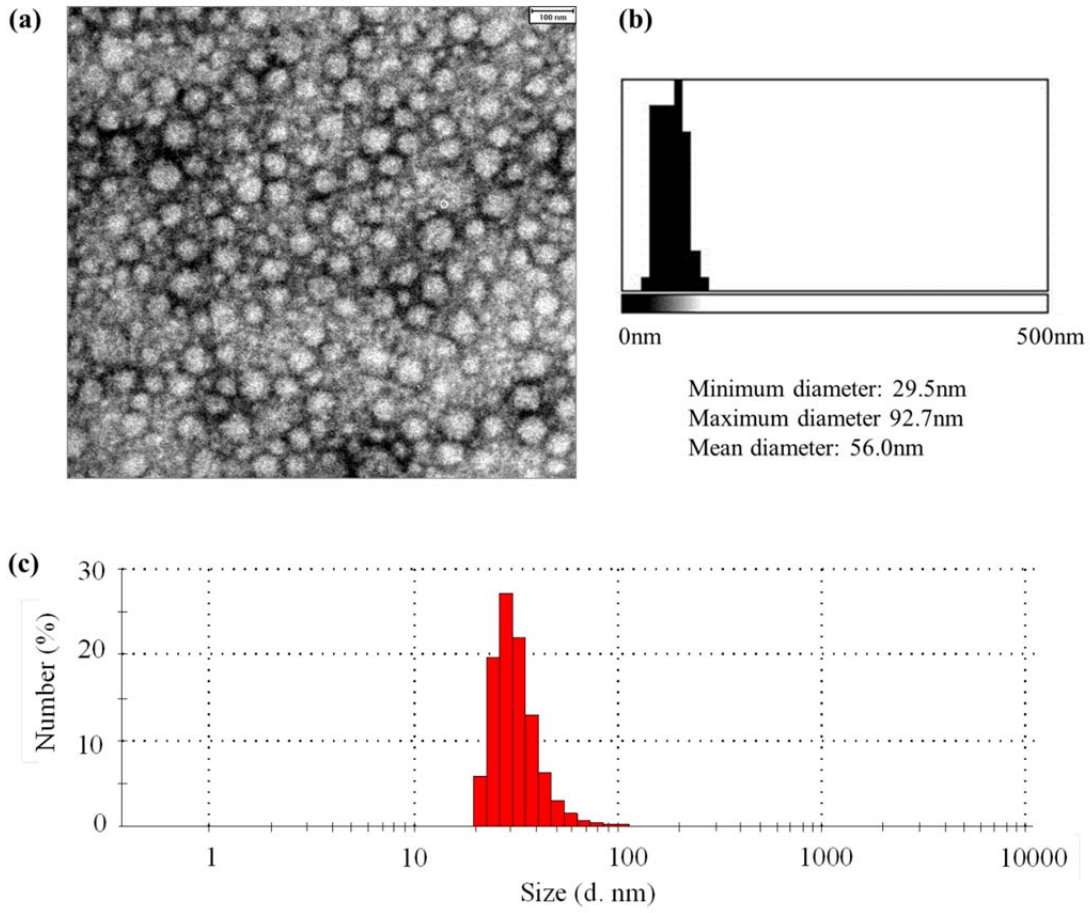

Figure 4-6. (a). Negative staining TEM imaging of (**4-1**); (b) size distribution of (**4-1**) calculated by the NIH ImageJ program with default settings (developed at the U.S. National Institutes of Health and available on the Internet at http://rsb.info.nih.gov/nih-image/). (c). Size distribution of (**4-1**) measured by DLS. Adapted with permission [49]. Copyright 2012, Springer.

4.2.3 *In vitro* assessment of micelle stability

Undesired drug leakage in the blood plasma represented a common limitation for most drug delivery carriers, which was known to cause several serious side effects. To study the stability of (**4-1**) in different media, micelles

containing about 14 DOX molecules were dialyzed in PBS buffer as well as DMEM cell culture medium for 4 days. The absorbance spectra were recorded before and after dialysis (**Figure 4-7**). Notably, no changes of the absorbance occurred indicating high micelle stability under high ion strength and cell culture conditions. Furthermore, the stability of these micelles at different pH was also investigated. Dialysis was performed in the physiological relevant range from pH 3 to pH 9 for 2 days, and the absorbance spectra of these micelles did not reveal any major changes (**Figure 4-7b**). Therefore, the albumin-derived copolymer micelles displayed remarkably high stabilities in solution and no significant drug leakage was observed *in vitro* which is very critical for drug delivery applications. The promising stability could be attributed to multivalent interactions of the hydrophobic moieties on proteins with DOX molecules, which was especially attractive compared to the liposome formulated Doxil® used in clinic.

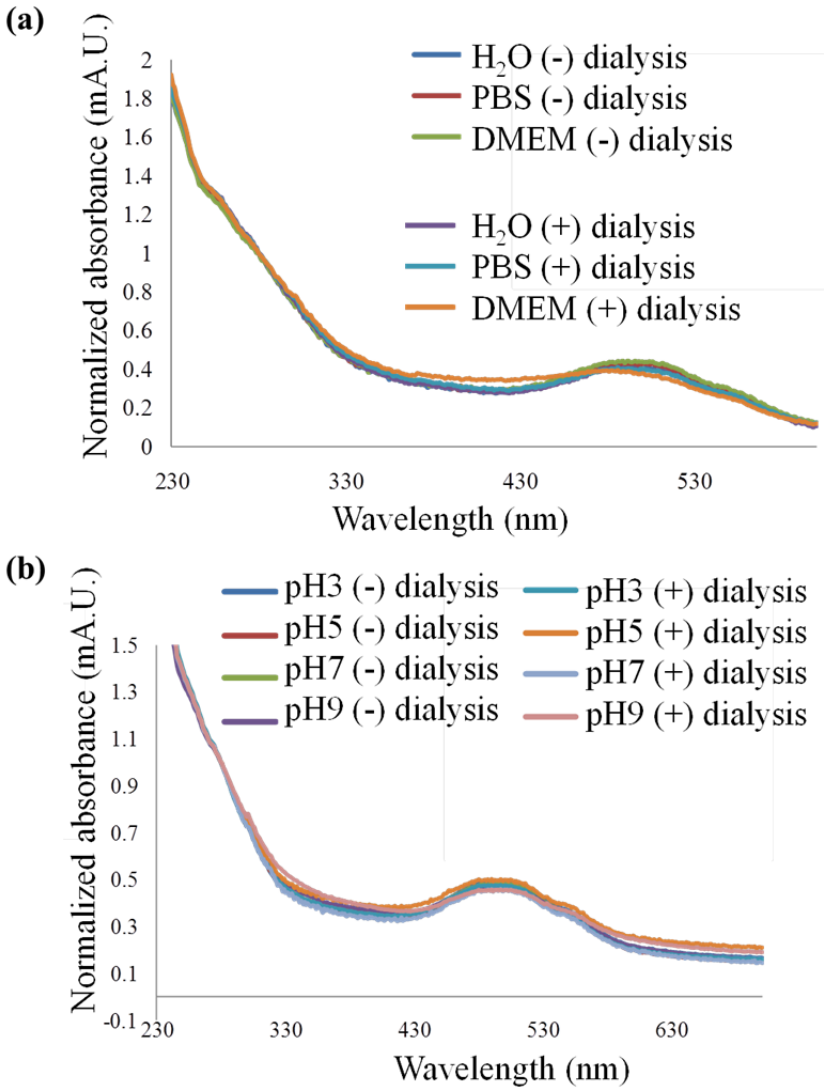

Figure 4-7. (a) Absorbance spectra of dcBSA-PEO(5000)$_{27}$-DOX micelles (**4-1**) before and after dialysis in different physiological buffers; (b) Absorbance spectra of micelles (**4-1**) before and after dialysis in different pH buffer solutions. Reproduced with permission [49]. Copyright 2012, Springer.

4.2.4 Enhanced cellular uptake

The unfavourable cellular uptake efficiency of DOX was known as one of the major limitations of DOX chemotherapy. [52] The stable encapsulation of DOX into positively charged albumin micelles should facilitate cellular uptake *via* endocytosis pathways. Therefore, the cellular uptake efficiency of dcBSA-

$PEO(5000)_{27}$-DOX micelles into A549 cells was followed by confocal microscopy (**Figure 4-8**). Adenocarcinomic human alveolar basal epithelial cells (A549 cells) were used to assess cellular permeability into epithelial tissue. After 1 hr of incubation only, significantly increased cellular uptake of dcBSA-$PEO(5000)_{27}$-DOX at 0.1 μM concentration was observed. In addition, the free DOX hydrochloride salt of the same concentration was applied in parallel as comparison. As shown in **Figure 4-8**, substantial amount of DOX (green channel) was found in such cells treated with the DOX micelles (**4-1**), whereas considerably less emission intensity was collected for such cells incubated with the non-complexed, free DOX molecules. The quantification of DOX uptake was calculated based on these confocal micrographs (**Figure 4-9**). DOX micelles revealed more than 5 times higher uptake efficiency compared to free DOX, which was also reflected by the difference in cytotoxicity of both samples as discussed below.

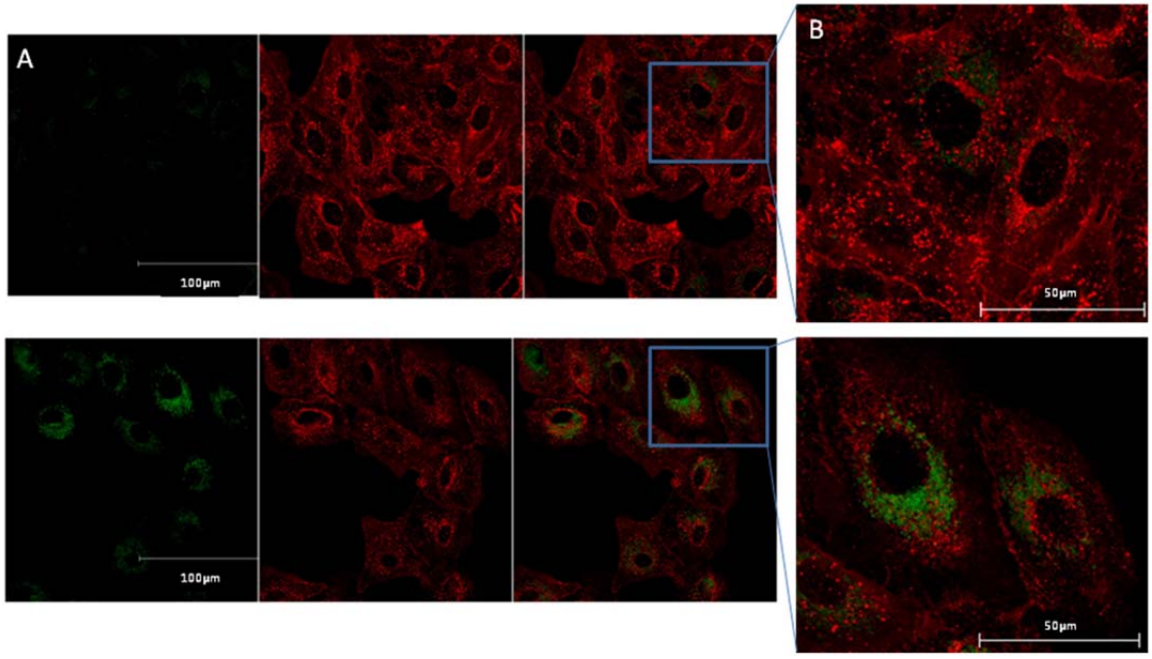

Figure 4-8. Live confocal images of DOX in A549 cells. A. DOX in dcBSA-$PEO(5000)_{27}$-DOX is delivered into the A549 cells, top panel – cells incubated

with free DOX, bottom panel – A549 cells incubated with dcBSA-PEO(5000)$_{27}$-DOX. B. Enlarged view of a field (marked by a square) from panel A. Cell membrane (red color), DOX (green color). Reproduced with permission [49]. Copyright 2012, Springer.

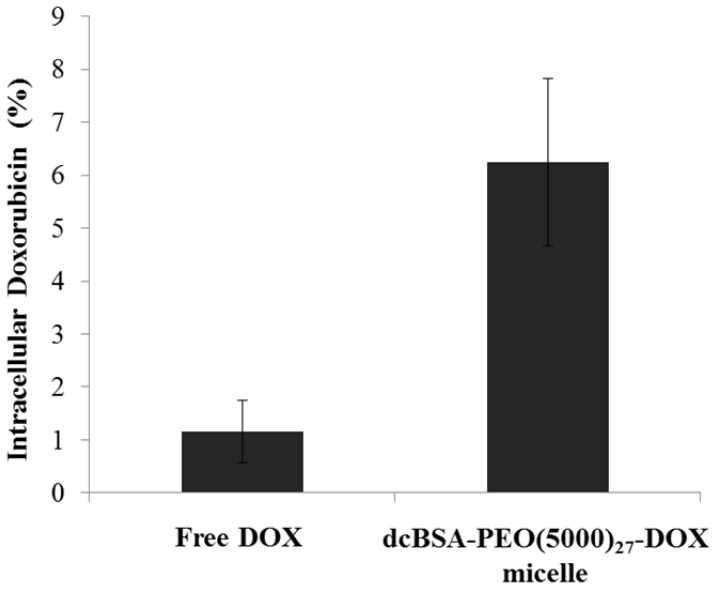

Figure 4-9. Quantification of intracellular DOX in A549 cells after 1 hr incubation time. Reproduced with permission [49]. Copyright 2012, Springer.

4.2.5 *In vitro* cytotoxicity of dcBSA-PEO(5000)$_{27}$-DOX micelle (4-1)

HeLa cells are considered the most common human carcinomic cell model used in cancer research. The cytotoxic activity of dcBSA-PEO(5000)$_{27}$-DOX micelles (**4-1**) was evaluated in HeLa cells and compared with DOX hydrochloride salt. The cells were treated with a series of concentrations of (**4-1**) or the free drug DOX hydrochloride for 12 hr, 24 hr and 48 hr and cell viability at each concentration was tested by applying the CellTiter-Glo® cell viability assay (from Promega GmbH, Mannheim, Germany) and plotted in **Figure 4-10**. For all 3 incubation times, micelles (**4-1**) exhibited an around five-times increased cytotoxicity compared to the free DOX hydrochloride salt.

After 12 hr of incubation, an IC_{50} value of the DOX micelles (**4-1**) of about 1.10±0.20 μM was found (free DOX: IC_{50} of 5.5±0.7 μM), which was further decreased down to 0.40±0.01 μM (free DOX: IC_{50} = 1.5±0.3 μM) and 0.14±0.01 μM after 48 hr of incubation, indicating in all these cases a five-times increased cytotoxicity of (**4-1**) compared with free DOX (**Figure 4-10**). Extended observation times for achieving the maximum biological activity were reported for other delivery systems as well [51] and were most likely due to slow release of active drugs from delivery carriers inside the cell. The attractive *in vitro* cytotoxic activity of dcBSA-PEO(5000)$_{27}$-DOX micelles (**4-1**) could be attributed to their high membrane permeability, improved cell uptake due to multiple positive charges, as well as efficient carrier degradation and drug release in lysosomes.

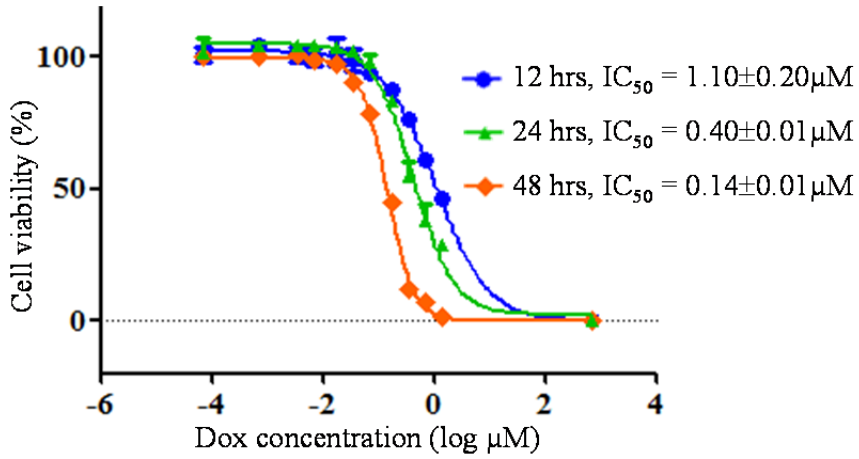

Figure 4-10. Cytotoxicity of free DOX and dcBSA-PEO(5000)$_{27}$-DOX micelles (**4-1**) after 12 hr, 24 hr and 48 hr incubation times. Reproduced with permission [49]. Copyright 2012, Springer.

4.3 Defined PbP based drug carrier for high capacity loading and two-step release of doxorubicin with enhanced anti-leukemia activity

Instead of loading drug molecules into PbP micelles *via* hydrophobic interactions, conjugation of drug molecules with the PbP backbone by covalent linkers could facilitate improved stability of the drug delivery system. In this section, a strategy to covalently conjugate high numbers of DOX *via* a hydrazone linkage to the albumin derived PbP scaffold will be demosntrated. Once the DOX conjugated PbPs were uptaken into the targeted tumor cells, DOX could be released from the carriers *via* a two-step controlled drug release mechanism. The high protease concentration and acidic pH environment in lysosomes and late endosomes led to (1) a rapid degradation of the pegylated albumin shell and (2) the release of the DOX molecules from the hydrazone linker. In this section, the physical properties and drug release mechanism will be comprehensively discussed. The anti-tumor activity of this DOX loaded HSA-based carrier was firstly studied *in vitro* with HeLa cells and thereafter, as an application example, its potential as leukemia treatment was assessed both *in vitro* and *in vivo*.

4.3.1 Preparation of DOX covalently loaded to cationic and pegylated albumin

The preparation of DOX conjugated PbP dcHSA-PEO(2000)$_{16}$-DOX$_{27}$ (**2-24**) has been introduced briefly in Chapter 2, Section 2.4.3.2. The

pharmacological considerations for designing such construct will be discussed in detail here.

Cationized albumin exhibited improved cellular and tissue uptake efficiency as demonstrated in previous studies [53, 54]. It was discussed before that highly cationic bovine serum albumin (cBSA) is an excellent gene delivery carrier and could serve as an ideal cationic protein precursor for PbP preparation [55, 56]. In addition, polymers containing large numbers of amine groups were also beneficial for endosomal escape of the drug delivery system. It was proposed that polymers with multiple amine groups could increase the pH in endosomes, thus a large amount of proton would need to be transported into endosome to neutralize the amine groups which dramatically changed the osmotic pressure and finally caused endosomal membrane disruption. This effect was called “proton sponge” mechanism [57]. Therefore, following a similar approach for preparing cBSA, native HSA was firstly cationized by converting the negatively charged residues (e.g. glutamic acid and aspartic acid) on the protein surface into positively charged amino groups using ethylene diamine (**Figure 4-11a**) to achieve the cationized cHSA. In order to address the potential immunogenicity of cationic albumin derivatives [58], a high degree of pegylation using NHS activated polyethylene(oxide)-2000 (PEO2000-NHS) is subsequently implemented to efficiently shield potential epitopes at the albumin surface. Pegylation represented a well-elaborated approach tested in clinical trials to prolong the circulation time of protein therapeutics and minimize immunogenicity [59, 60]. In this way, cHSA-PEO$(2000)_{16}$ (**2-23**) was obtained with a molecular weight of about 102 kDa as characterized by MALDI-ToF mass spectrometry and SDS-PAGE (**Figure**

2-22b and c). This modified albumin conjugate revealed high water solubility of up to 150 mg/mL and long term stability at 4°C for more than 6 months.

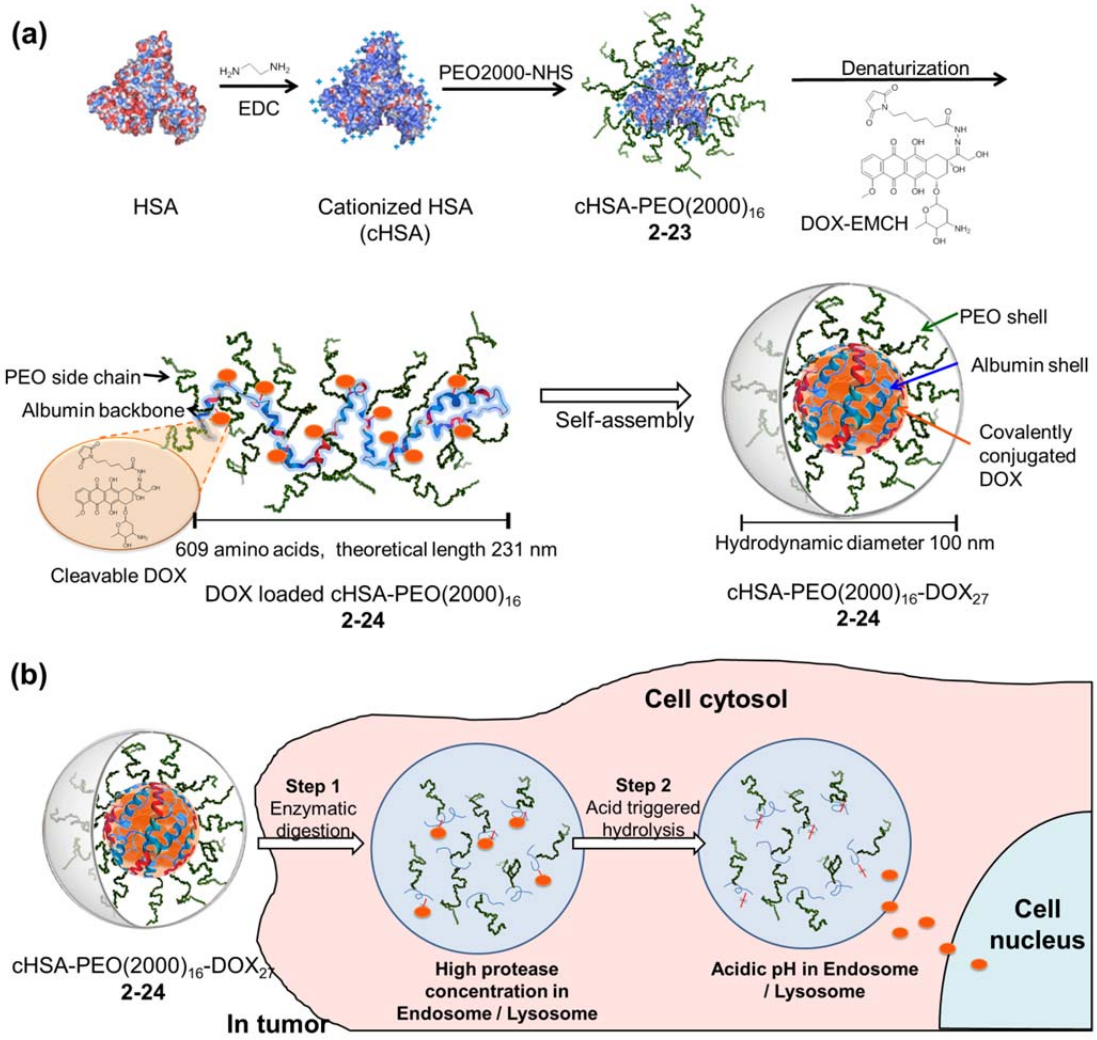

Figure 4-11. (a). Preparation of DOX loaded cHSA-PEO(2000)$_{16}$-DOX$_{27}$ micelles (**2-24**); (b). Illustration of two-step DOX release from cHSA-PEO(2000)$_{16}$-DOX$_{27}$ micelles (**2-24**) in tumor cells. Reproduced with permission [61]. Copyright 2012, Wiley-VCH.

DOX-EMCH (see structure in **Figure 4-11**) represents a well-studied albumin-binding prodrug of doxorubicin which *in situ* binds to the Cys34 position of endogenous albumin and reveals superior anti-tumor efficacy in several tumor models compared to DOX [62, 63]. It bears a thiol reactive

maleimide group at the terminus of a small spacer, which could be readily conjugated to cysteine residues of proteins and an acid sensitive hydrazone linkage at the DOX-C-13 keto-position that allows either extracellular DOX release in the slightly acidic environment often present in tumor tissue or intracellular release in acidic endosomal or lysosomal compartments after cellular uptake by the tumor cells [62, 63]. The DOX-EMCH was efficiently loaded into the hydrophobic interior of cHSA-PEO(2000)$_{16}$ (**2-23**) *via* a "denaturation-backfolding strategy". The globular structure of cHSA-PEO(2000)$_{16}$ was firstly unfolded in 5 M Urea buffer and the disulfide bridges were reduced by TCEP to expose all cysteine residues for DOX-EMCH conjugation. After *in situ* reaction with DOX-EMCH in excess, the unreacted DOX was removed by centrifugal membrane filter (Vivaspin® centrifugal membrane concentrator, MWCO 30 kDa) with Urea buffer (5 M Urea, 20 mM Sodium Phosphate buffer, pH 7.4). The high concentration urea maintained the protein conjugates under denaturing conditions and allowed the maximium elimination of non-specifically adsorbed DOX molecules. After rising in urea buffer for 3 to 5 times, the DOX loaded denatured protein conjugate was brought into water to allow globular repacking of the polypeptide backbone due to the presence of the hydrophobic DOX molecules as well as the presence of lipophilic amino acids located along the main chain of the HSA-derived polypeptide. The product was continuously washed with water until no DOX was detected in the elution anymore. The remaining protein solution exhibited a deep red color. As a control, cHSA-PEO(2000)$_{16}$ was combined with free DOX hydrochloride and washed following the same protocol and no red color was found in the protein solution suggesting efficient removal of non-

specifically adsorbed DOX. The covalent conjugation of DOX was confirmed by denaturing SDS-PAGE (**Figure 2-22**) and the number of DOX-EMCH that have been conjugated was calculated by MALDI-ToF and UV-Vis absorbance (**Figure 2-22**). MALDI-ToF revealed a molecular weight of 122 kDa of cHSA-PEO$(2000)_{16}$-DOX_{27} corresponding to 27 additional DOX-EMCH molecules, which agrees well with the number calculated from UV-Vis spectra (28±4 DOX-EMCH). Since only covalent conjugates could be observed on the mass spectrometer while any DOX absorbed or conjugated could be detected by UV-Vis spectroscopy, the very close numbers obtained from both methods again supported the efficient washing and elimination of non-specific absorbed DOX. The number of 27 DOX molecules was considered as the conjugation number in the following discussion.

4.3.2 cHSA-PEO$(2000)_{16}$-DOX_{27} micelles (2-24) exhibit positive net charge

Zeta potential of cHSA-PEO$(2000)_{16}$-DOX_{27} micelles (**2-24**) was found at 28.6±1.8 mV indicating a positive surface charge of (**2-24**). Agarose gel electrophoresis was also used to demonstrate the positive net charge (**Figure 4-12**) at pH 7.4. In TAE (Tris-acetate-EDTA, pH 7.4) buffer, free DOX moves toward the negatively charged electrode due to the positive charge of the primary amine group of DOX. The cHSA-PEO$(2000)_{16}$ precursor and DOX loaded cHSA-PEO2000_{16}-DOX_{27} (**2-24**) both slowly move to the same direction indicating the net positive charge of these polypeptides. The presence of positive charges is essential to enable efficient interactions with

negatively charged cellular membranes and therefore to promote fast cellular and tissue uptake by absorptive-mediated endocytosis [53]. No free DOX was observed in the DOX loaded cHSA-PEO2000$_{16}$-DOX$_{27}$ (**2-24**) sample again demonstrating the high stability of the protein-derived nanocarrier containing DOX in their interior.

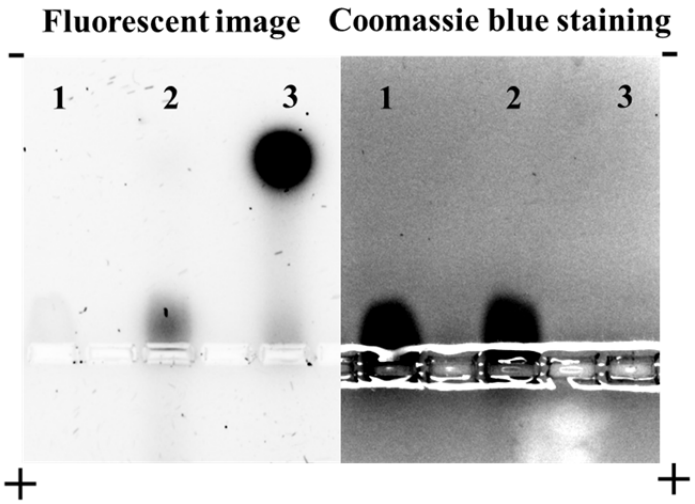

Figure 4-12. Agarose gel electrophoresis characterization of net charge. Lane 1: cHSA-PEO(2000)$_{16}$ (**2-23**), lane 2: cHSA-PEO(2000)$_{16}$-DOX$_{27}$ (**2-24**), lane 3: free DOX hydrochloride. Adapted with permission [61]. Copyright 2012, Wiley-VCH.

4.3.3 Size distribution and morphology of DOX loaded cHSA-PEO(2000)$_{16}$-DOX$_{27}$ (2-24)

The morphology and size distribution of cHSA-PEO(2000)$_{16}$-DOX$_{27}$ (**2-24**) was characterized by TEM and DLS (**Figure 4-13**). According to TEM, cHSA-PEO(2000)$_{16}$-DOX$_{27}$ (**2-24**) were soft-edged, spherical nanoparticles with average diameters of about 43 nm with narrow size distributions. Since cHSA-PEO(2000)$_{16}$ could not be directly detected by TEM due to insufficient

electron absorption, the dark spots observed for DOX loaded cHSA-PEO(2000)$_{16}$-DOX$_{27}$ (**2-24**) micelles indicated a condensed loading of DOX into the polypeptide core due to hydrophobic interactions. However, the size distribution recorded by TEM experiments only gives a first idea of the morphology of the DOX nanocarriers after drying and the soft parts of the polypeptide copolymer carriers were not visible. Therefore, to demonstrate the hydrodynamic size distribution of DOX loaded cHSA-PEO(2000)$_{16}$-DOX$_{27}$ (**2-24**) particles in solution, representative samples were investigated by applying DLS and an average diameter of 100 nm with a narrow polydispersity index (PDI) of 0.21 was obtained (**Figure 4-13**). Compared to the TEM results, the larger hydrodynamic radius originated from the contribution of the highly hydrophilic PEO / water layer. Nanoscopic objects with sizes of about 100 nm in diameter were reported to accumulate very well in tumor tissues *via* the EPR effect [9, 10].

In order to access the stability of cHSA-PEO(2000)$_{16}$-DOX$_{27}$ micelles (**2-24**) in highly salted buffer, the DLS size distribution was also acquired in different buffer conditions including 0.9% NaCl solution (mimicking the salt concentration *in vivo*) and phosphate buffer saline (PBS, mimicking the ion concentration and pH in the human body) (**Figure 4-14**). The similar size distribution was observed in these high ionic strength buffer compared with the size distribution in water, indicating that the structure of (**2-24**) was highly stable under different buffer conditions.

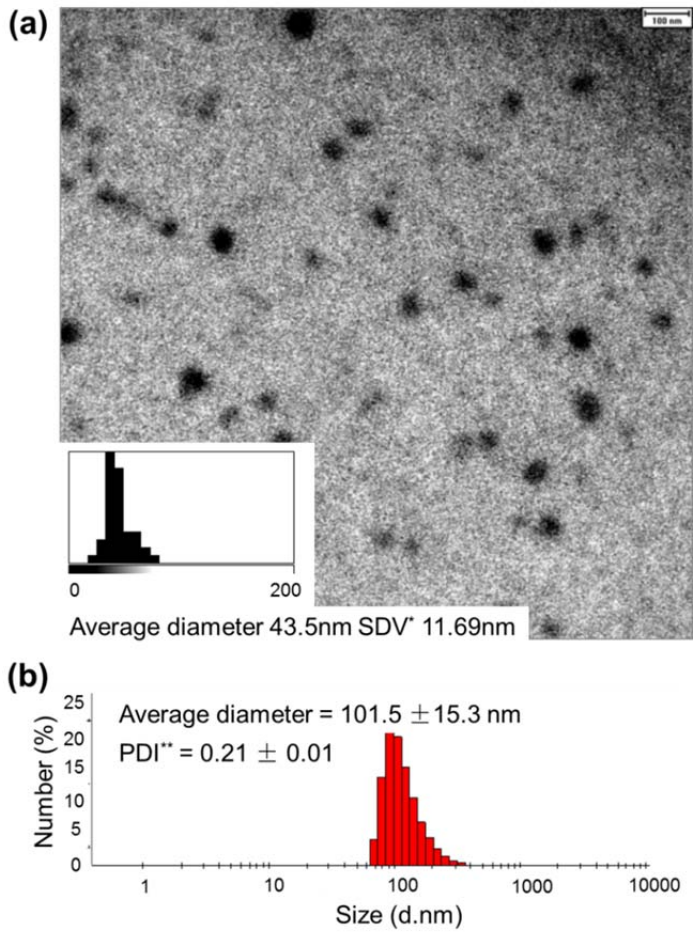

Figure 4-13. Size distribution and morphology of DOX loaded cHSA-PEO(2000)$_{16}$-DOX$_{27}$ (**2-24**) characterized by (A) TEM and (B) DLS. *SDV is standard deviation. **PDI is polydispersity index. Adapted with permission [61]. Copyright 2012, Wiley-VCH.

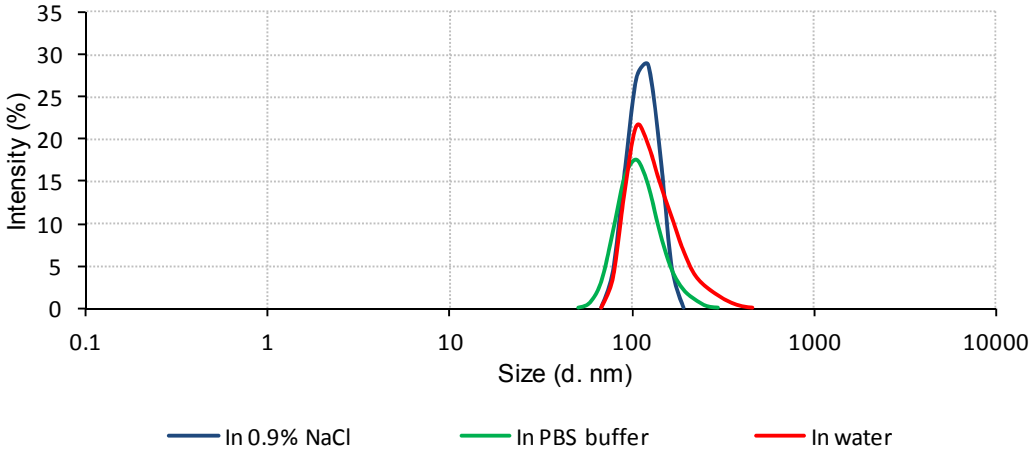

Figure 4-14. Size distribution of cHSA-PEO(2000)$_{16}$-DOX$_{27}$ (**2-24**) under different buffer conditions.

4.3.4 Efficient two-step DOX release with reduced undesirable drug leakage

Release of active DOX from cHSA-PEO(2000)$_{16}$-DOX$_{27}$ micelles (**2-24**) could be achieved under lysosomal condition *via* a two-step release mechanism. At the first step, the polypeptide backbone of cHSA-PEO(2000)$_{16}$-DOX$_{27}$ micelles (**2-24**) was rapidly digested by lysosomal proteases and exposed the DOX containing fragments into the acidic environment in the lysosome. The subsequent acid triggered hydrolysis of the hydrazone linker could then enable the release of active DOX molecules from peptide fragments. We performed several experiments to investigate this two-step release mechanism and monitor the DOX release profile under an *in vitro* condition mimicking the lysosomal environment.

Firstly, the proteolytic degradation of the polypeptide backbone of cHSA-PEO(2000)$_{16}$-DOX$_{27}$ (**2-24**) was investigated in the presence of trypsin, as well as the endosomal/lysosomal endopeptidase cathepsin B (**Figure 4-15**). Digestion was observed immediately after adding trypsin when analyzed by SDS-PAGE, which appeared as a smeary band with various sizes consisting of peptide fragments. The polypeptide backbone of (**2-24**) was found completely digested into very small fragments within 2 hr with trypsin (0.2 mg/ml) treatment, whereas the complete digestion with cathepsin B (0.05 mg/ml) was observed after 24 hr.

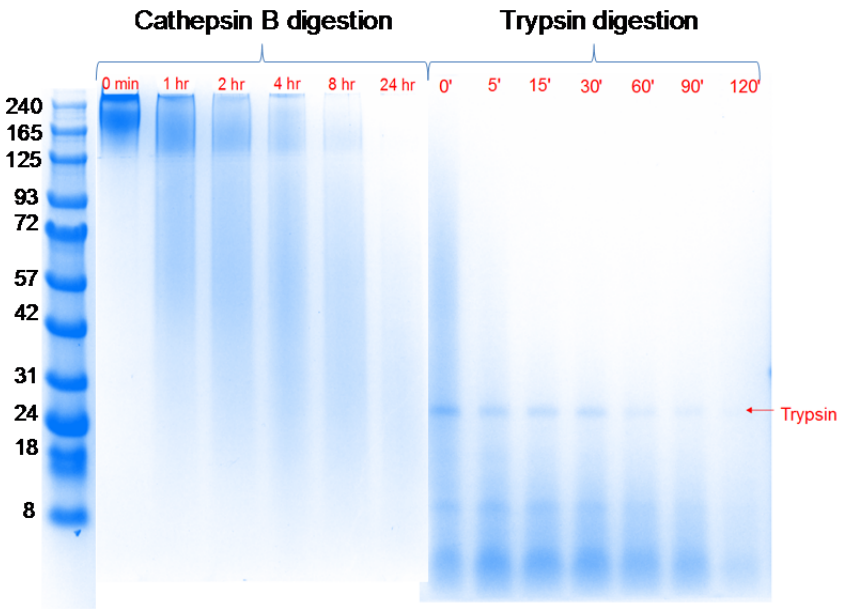

Figure 4-15. Coomassie stained SDS-PAGE of cHSA-PEO(2000)$_{16}$-DOX$_{27}$ (**2-24**) digested by Cathepsin B and Trypsin. Adapted with permission [61]. Copyright 2012, Wiley-VCH.

After proving the enzymatic degradation of the micelles, we further investigated the metabolites produced by cathepsin B. cHSA-PEO(2000)$_{16}$-DOX$_{27}$ (**2-24**) was incubated with cathepsin B at pH 5 under the previously reported conditions mimicking the lysosome [64]. Samples were taken from the reaction mixture and extracted for LC-MS analysis over 48 hr (These experiments were done in close collaboration with Dr. Seah Ling Kuan in Ulm University). As shown in **Figure 4-16b**, the active form of DOX (proved by the corresponding MS spectrum and retention time, see **Figure 4-17a**) was observed and the concentration was significantly increasing over time. Besides, we also observed a broad peak at a retention time of ~8 min in the sample after 1 hr incubation. This peak decreased in the later samples, and the corresponding MS spectrum (**Figure 4-17b**) revealed a complicated mixture which was difficult to resolve. We presume this peak was likely corresponding to large peptide fragments which were further digested into

small fragments over time. Considering the solid-phase extraction step in the sample preparation which was necessary before the LC-MS study, the hydrophilic small peptide fragments were unable to bind to the reverse phase matrix and therefore would not be analyzed by our method. Notably, the peak at a retention time of ~9 min had strong absorbance at 480 nm (**Figure 4-18**) indicating DOX-containing components, which most likely corresponded to some peptide fragment intermediates still containing DOX.

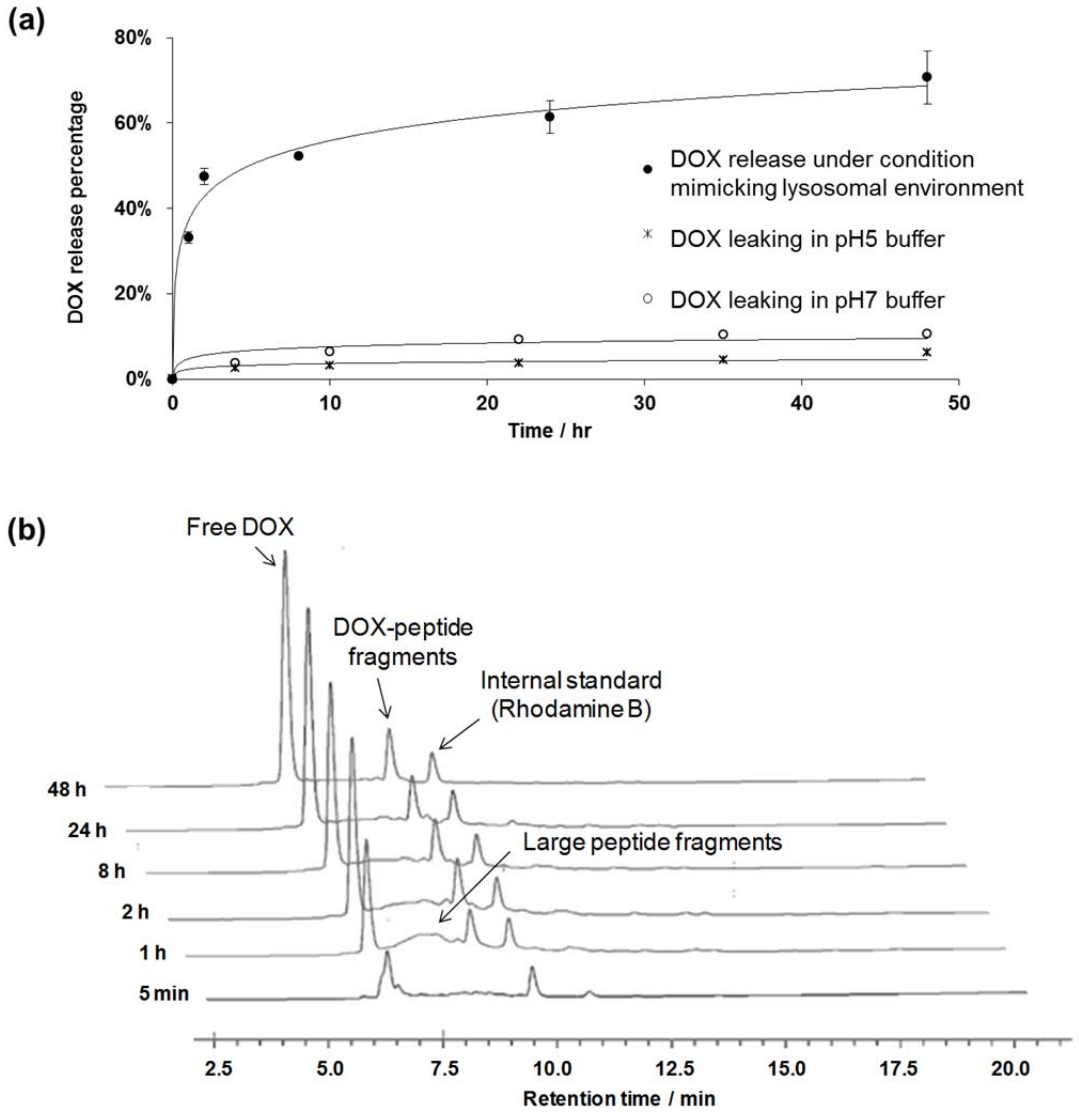

Figure 4-16. *In vitro* DOX release from cHSA-PEO(2000)$_{16}$-DOX$_{27}$ (**2-24**). (a) Drug release profile in pH 5 buffer with Cathepsin B to mimic lysosomal conditions, compared with DOX leaking in pH 5 and pH 7 buffer without

enzymatic degradation; (b) HPLC profiles monitoring DOX release and cHSA-PEO(2000)$_{16}$-DOX$_{27}$ (**2-24**) degradation in the presence of Cathepsin B at pH 5. Reproduced with permission [61]. Copyright 2012, Wiley-VCH.

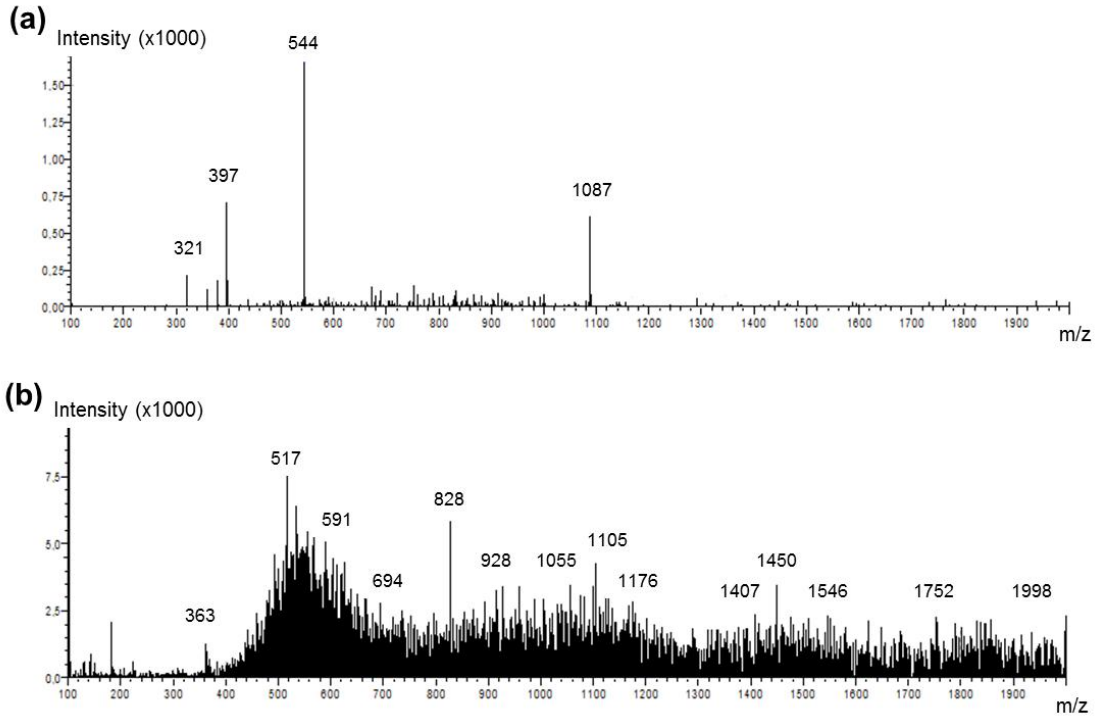

Figure 4-17. Representative ESI-MS spectrum of (a) free DOX and (b) peptide fragments after Cathepsin B digestion analyzed by LC-MS.

Rhodamine B was spiked into each sample as internal standard for quantification. According to the HPLC chromatogram monitored at 480 nm and compared with the Rhodamine B signal at 554 nm (**Figure 4-18**), we calculated the amount of DOX released over time in the presence of Cathepsin B. ~50% of active DOX was found released from cHSA-PEO(2000)$_{16}$-DOX$_{27}$ micelles within first 2 hr, and over 70% of DOX was released after 48 hr (**Figure 4-16a**). These results were in good agreement with other systems using the same hydrazone linker [65]. Interestingly, cHSA-PEO(2000)$_{16}$-DOX$_{27}$ (**2-24**) incubated in the same pH 5 buffer without Cathepsin B reveals only ~10 % DOX release (**Figure 4-19**) after 24 hr.

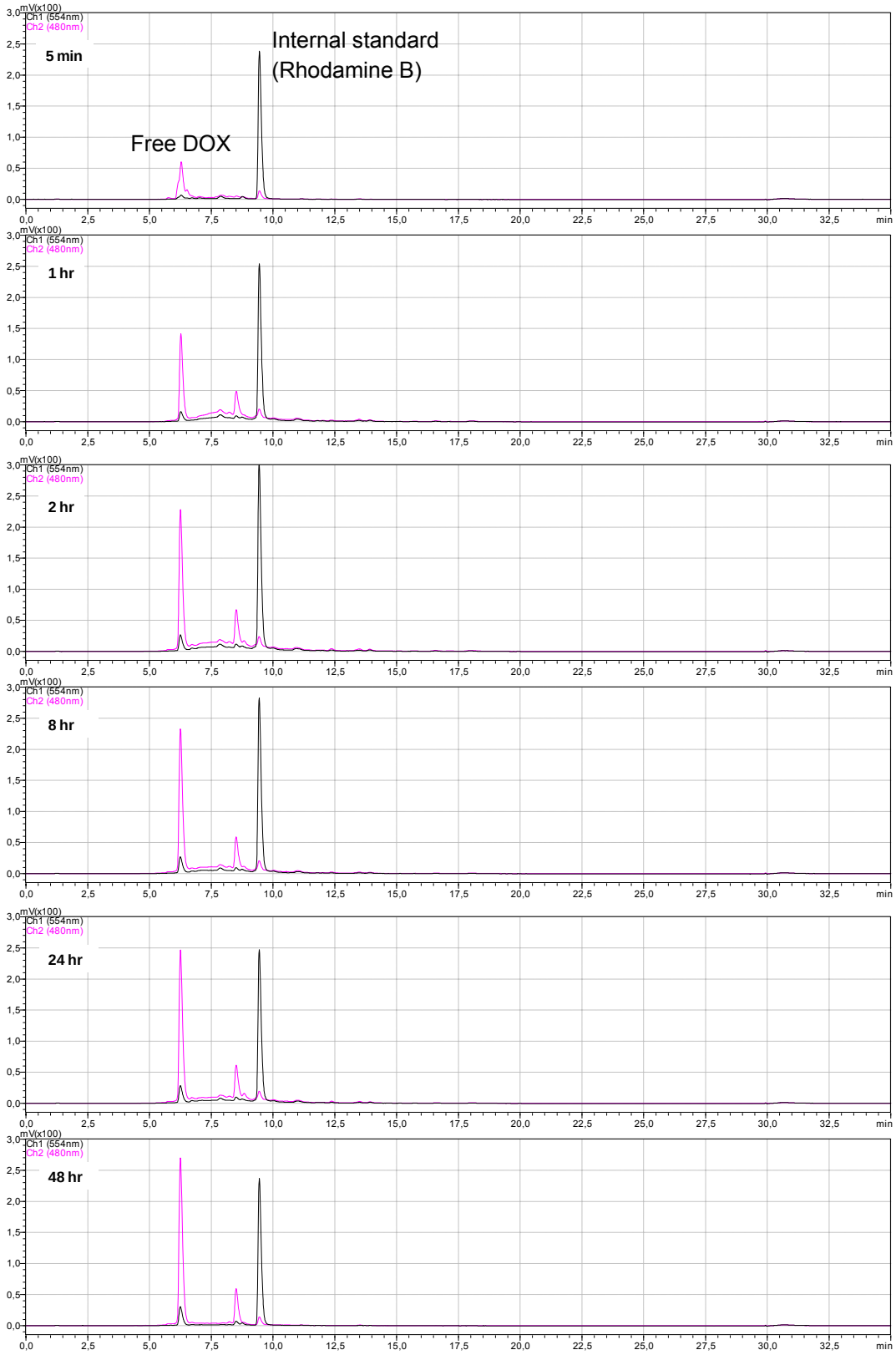

Figure 4-18. HPLC chromatogram of cHSA-PEO(2000)$_{16}$-DOX$_{27}$ (**2-24**) digestion metabolites recorded at 480 nm and 554 nm. Reproduced with permission [61]. Copyright 2012, Wiley-VCH.

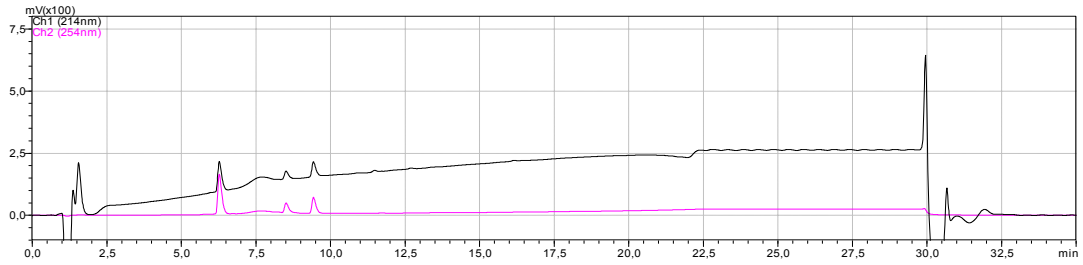

Figure 4-19. HPLC chromatogram of cHSA-PEO(2000)$_{16}$-DOX$_{27}$ (**2-24**) incubated at pH 5 buffer without enzyme for 48 hr. Reproduced with permission [61]. Copyright 2012, Wiley-VCH.

In addition to the LC-MS study, we also monitored the DOX leakage in the absence of enzymes by dialysing the micelles in pH 5 citrate buffer and pH 7.4 PBS for 48 hr. A similar result with less than 10% DOX leakage was observed in pH 5 buffer after 48 hr (**Figure 4-16a**). And even less leakage in PBS buffer was observed suggesting a significant stability of these micelles under physiological conditions (**Figure 4-16a**). The remarkable stability could be attributed to the presence of strong hydrophobic interactions between the cleaved DOX and the lipophilic interior of the albumin-derived polypeptide chain which efficiently prevented any leakage of hydrolyzed DOX before degradation of the entire micellar structure. Thus, according to these *in vitro* drug release studies, cHSA-PEO(2000)$_{16}$-DOX$_{27}$ micelles (**2-24**) revealed promising potential to ensure minimal leakage of DOX molecules during the circulation as well as efficient intracellular release of active DOX molecules.

4.3.5 Cellular uptake and intracellular localization of cHSA-PEO(2000)$_{16}$-DOX$_{27}$ (2-24)

The intracellular localization and cellular uptake efficiency of DOX loaded cHSA-PEO(2000)$_{16}$-DOX$_{27}$ (**2-24**) was evaluated by laser scanning confocal microscopy. The same amount of DOX (0.3 μg) either in the hydrochloride

form or conjugated with cHSA-PEO(2000)$_{16}$ was incubated with HeLa cells. After 24 hr, DOX was found mainly located in the cell nuclei and localized at the perinuclear region in both cases (**Figure 4-20**), but slightly stronger emission intensities of the cell nuclei were obtained with free DOX. This result is not surprising if one considers that DOX encapsulated inside the drug delivery carrier first needs to be released in order to be able to enter the cell nucleus. Therefore, in case of cHSA-PEO(2000)$_{16}$-DOX$_{27}$ (**2-24**), less DOX might be present in the cell nuclei after 24 hr due to additional time required for the release and translocation process. However, cHSA-PEO(2000)$_{16}$-DOX$_{27}$ (**2-24**) treated cells displayed higher total intensity of DOX inside the cells compared to free DOX (**Figure 4-21**), indicating an efficient cellular uptake rate of cHSA-PEO(2000)$_{16}$-DOX$_{27}$. When the cells were treated with higher concentrations of cHSA-PEO(2000)$_{16}$-DOX$_{27}$ (**2-24**), significant DOX uptake into the cytosol and cell nuclei can even be observed after 6 hr (**Figure 4-22**).

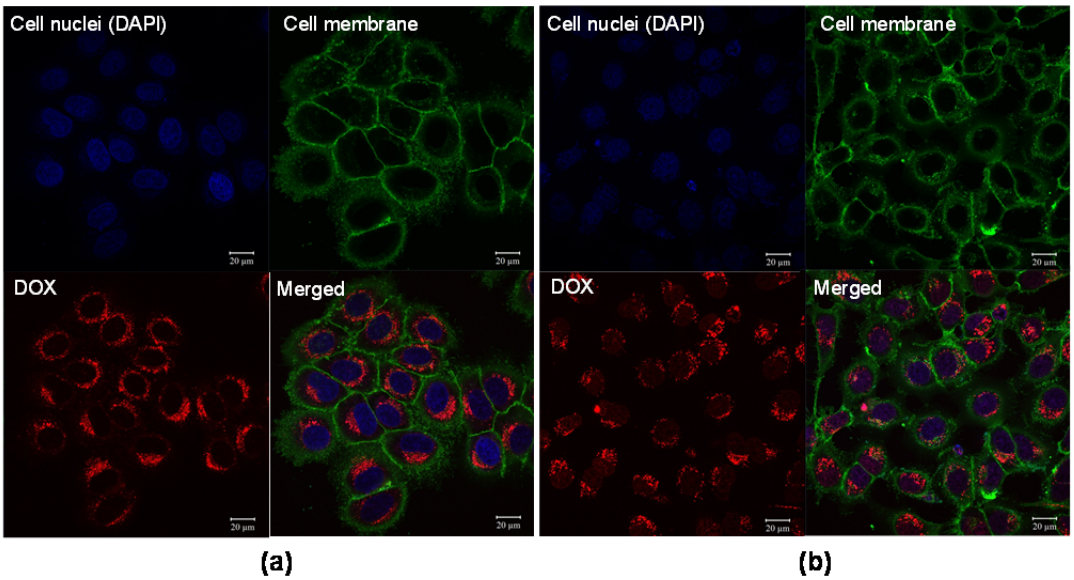

Figure 4-20. Confocal microscope imaging of HeLa cells incubated with (a) DOX loaded cHSA-PEO(2000)$_{16}$-DOX$_{27}$ (**2-24**) and (a) DOX hydrochloride for 24 hr. Reproduced with permission [61]. Copyright 2012, Wiley-VCH.

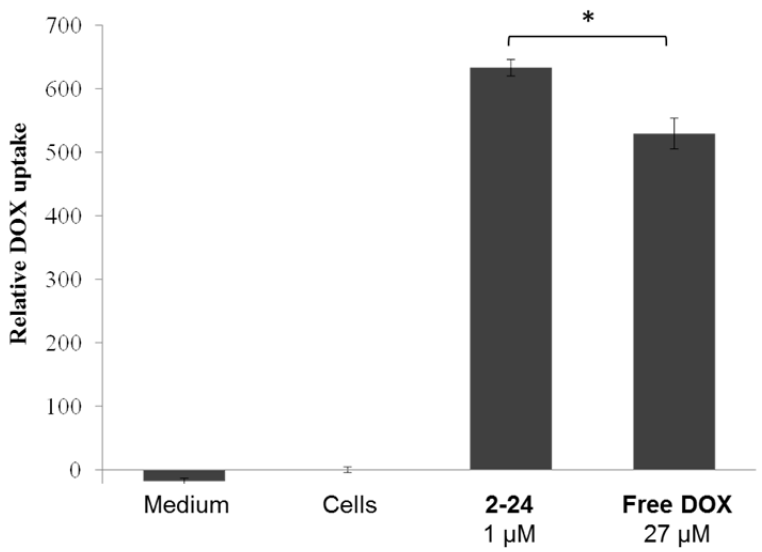

Figure 4-21. Quantification of DOX uptake based on Confocal imaging. p<0.05. Reproduced with permission [61]. Copyright 2012, Wiley-VCH.

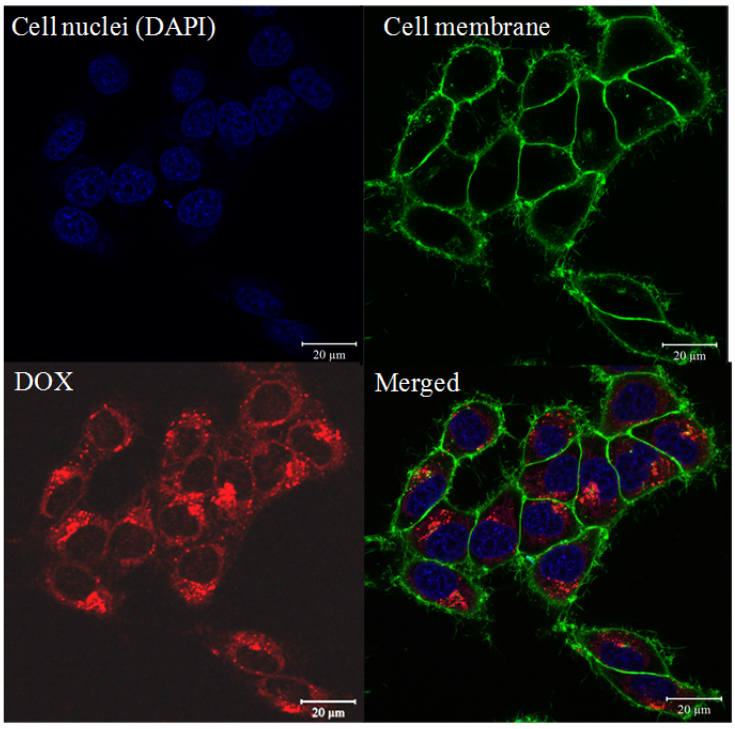

Figure 4-22. Confocal microscope image of cHSA-PEG2000$_{16}$-DOX$_{27}$ (**2-24**) uptake by HeLa cells after 6 hr. Reproduced with permission [61]. Copyright 2012, Wiley-VCH.

4.3.6 Cytotoxicity and apoptosis in HeLa cells

The cytotoxicity of cHSA-PEO(2000)$_{16}$-DOX$_{27}$ (**2-24**) was firstly investigated with HeLa cells, which represented a popular cell model for solid cancers. Upon 24 hr incubation time, cHSA-PEO(2000)$_{16}$-DOX$_{27}$ (**2-24**) micelles already displayed higher cell toxicity (IC_{50} = 129±19 nM) in comparison to DOX hydrochloride (IC_{50} = 517±108 nM) (**Figure 4-23a**). This enhanced toxicity effect could be attributed to the very high drug loading capacity and efficient cellular uptake of cHSA-PEO(2000)$_{16}$-DOX$_{27}$ micelles as discussed above. Moreover, in order to demonstrate the stability of cHSA-PEO(2000)$_{16}$-DOX$_{27}$ (**2-24**) in the blood stream, cHSA-PEO(2000)$_{16}$-DOX$_{27}$ (**2-24**) was firstly incubated with complete fetal bovine serum for 2 hr and then applied to HeLa cells. Similar cytotoxicity with IC_{50} of 170 nM was found indicating promising stability of cHSA-PEO(2000)$_{16}$-DOX$_{27}$ (**2-24**) when applied in the blood plasma (**Figure 4-23a**). The cytotoxicity of cHSA-PEO(2000)$_{16}$ nanocarriers was also evaluated. Negligible cytotoxicity was found for cHSA-PEO(2000)$_{16}$ at the tested concentration of 10 μM (**Figure 4-23b**).

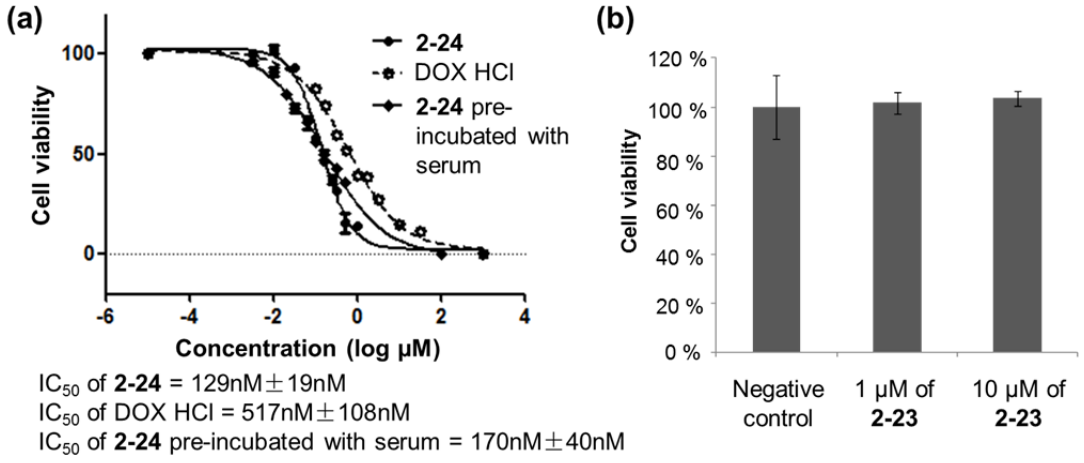

Figure 4-23. Cytotoxicity of (a) cHSA-PEO(2000)$_{16}$-DOX$_{27}$ (**2-24**) in HeLa cells (24 hr incubation) in comparison to DOX hydrochloride and (b) the free

carrier cHSA-PEO(2000)$_{16}$ (**2-23**). Adapted with permission [61]. Copyright 2012, Wiley-VCH.

It is known that DOX could cause early activation of p53 proteins in tumor cells, which is followed by Caspase-3 activation, a crucial process to induce cell apoptosis [66]. Therefore, quantification of Caspase-3 activity could give an idea of the early stage functional effects of DOX which has important implications for the mechanism of apoptosis induction. By incubating cHSA-PEO(2000)$_{16}$-DOX$_{27}$ (**2-24**) and DOX hydrochloride with HeLa cells for 16 hr, enhanced Caspase activity was found in both cases (**Figure 4-24**). However, DOX loaded cHSA-PEO(2000)$_{16}$-DOX$_{27}$ micelles revealed an approximately two-times higher Caspase-3 activity in comparison to free DOX hydrochloride, which is in good agreement with the observed cytotoxicity data. Both cytotoxicity and Caspase-3 activity results again supported that covalently loaded DOX encapsulated inside cHSA-PEO(2000)$_{16}$ polymers was efficiently released from the carrier and maintained its activity.

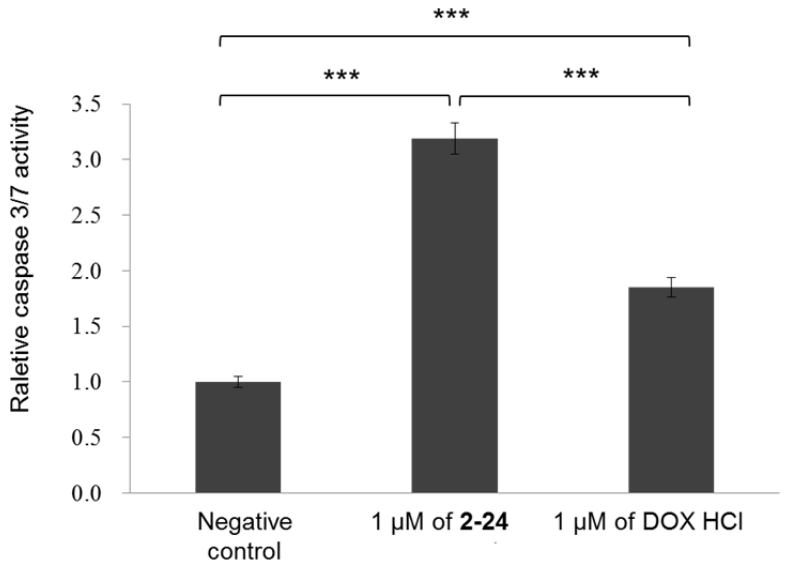

Figure 4-24. Caspase-3/7 activity of DOX loaded cHSA-PEO(2000)$_{16}$-DOX$_{27}$ (**2-24**) in comparison to DOX hydrochloride. *** p <= 0.0001. Adapted with permission [61]. Copyright 2012, Wiley-VCH.

4.3.7 cHSA-$(PEO2000)_{16}$-DOX_{27} (2-24) micelles with reduced immunogenicity

Pegylation represents a valuable post-modification technique used to improve the pharmacokinetics of therapeutic proteins and to reduce their immunogenicity [59, 60]. Polyethylene(oxide) chains form a hydrophilic shell around the protein surface to mask epitopes of protein drugs and reduce their binding to plasma proteins [60]. To demonstrate the efficient masking of human albumin epitopes on cHSA-$PEO(2000)_{16}$, the competitive ELISA immunoassay kit (from BioCat GmbH, Germany) was introduced and samples were studied according to the manufacturer protocol. Compared with native HSA that was recognized by HSA antibodies in a concentration dependent fashion (**Figure 4-25**), HSA antibodies were not able to interact with cHSA-$PEO(2000)_{16}$ anymore. This result was in good agreement with literature reports and already indicated the promising potential for *in vivo* applications. However, noteworthy this *in vitro* experiment only revealed the silencing of HSA antibodies, the actual *in vivo* immunogenicity could be more complicated and would still need to be further assessed.

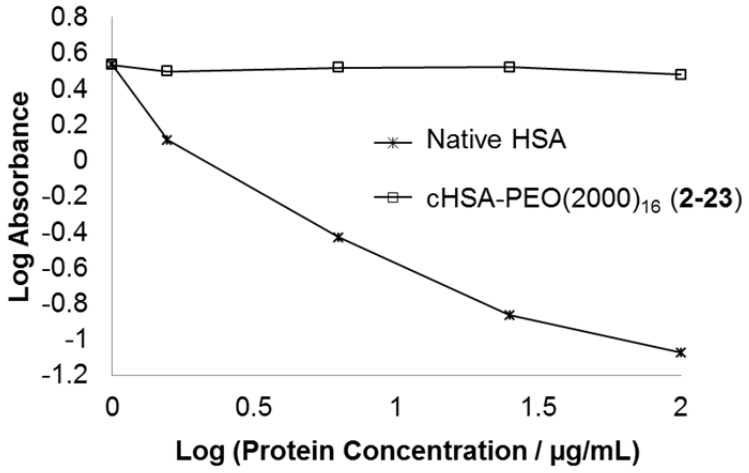

Figure 4-25. Human albumin ELISA immunoassay evaluating immunogenicity

of cHSA-PEO(2000)$_{16}$ (**2-23**). Reproduced with permission [61]. Copyright 2012, Wiley-VCH.

4.3.8 *In vitro* anti-leukemia activity

Since DOX remains one of the most effective therapeutics for the treatment of acute myeloid leukemia (AML) [25, 26], it is highly attractive to investigate the potential of cHSA-PEO(2000)$_{16}$-DOX$_{27}$ (**2-24**) as a macromolecular drug for AML chemotherapy. For this purpose, the *in vitro* cytotoxicity of cHSA-PEO(2000)$_{16}$-DOX$_{27}$ (**2-24**) was firstly tested on three different AML cell lines, representing the most frequent genotypes of primary human AML cases (MV 4-11, Kasumi-1 and OCI-AML3). cHSA-PEO(2000)$_{16}$-DOX$_{27}$ (**2-24**) displayed high cytotoxicities with IC_{50} values in the low nanomolar range toward all three leukemia cell lines, especially after 48 or 72 hr of incubation time (**Figure 4-26**, **Table 4-2**). Compared to free DOX hydrochloride, the cytotoxicity of cHSA-PEO(2000)$_{16}$-DOX$_{27}$ (**2-24**) was notably increased in most of the cases, which was similar as observed with HeLa cells. In addition, a significantly increased cytotoxicity was observed between 24 hr to 48 hr most likely reflecting the time required for DOX release from the carrier. This effect was most pronounced in the Kasumi-1 cell line, where cHSA-PEO(2000)$_{16}$-DOX$_{27}$ (**2-24**) exhibited lower cytotoxicity than DOX hydrochloride after 24 hr incubation (IC_{50} = 880±296 nM) but significantly higher potency after 48 hr (IC_{50} = 54±30 nM). The highest cytotoxicity was obtained after treating MV4-11 cells with cHSA-PEO(2000)$_{16}$-DOX$_{27}$ (**2-24**) for 72 hr, yielding an IC_{50} as low as 1.9 nM (**Table 4-2** and **Figure 4-26**). This cell line and incubation time were therefore selected for further experiments. The

highly promising cytotoxicity data suggested an attractive potential of cHSA-PEO(2000)$_{16}$-DOX$_{27}$ (**2-24**) for AML treatment.

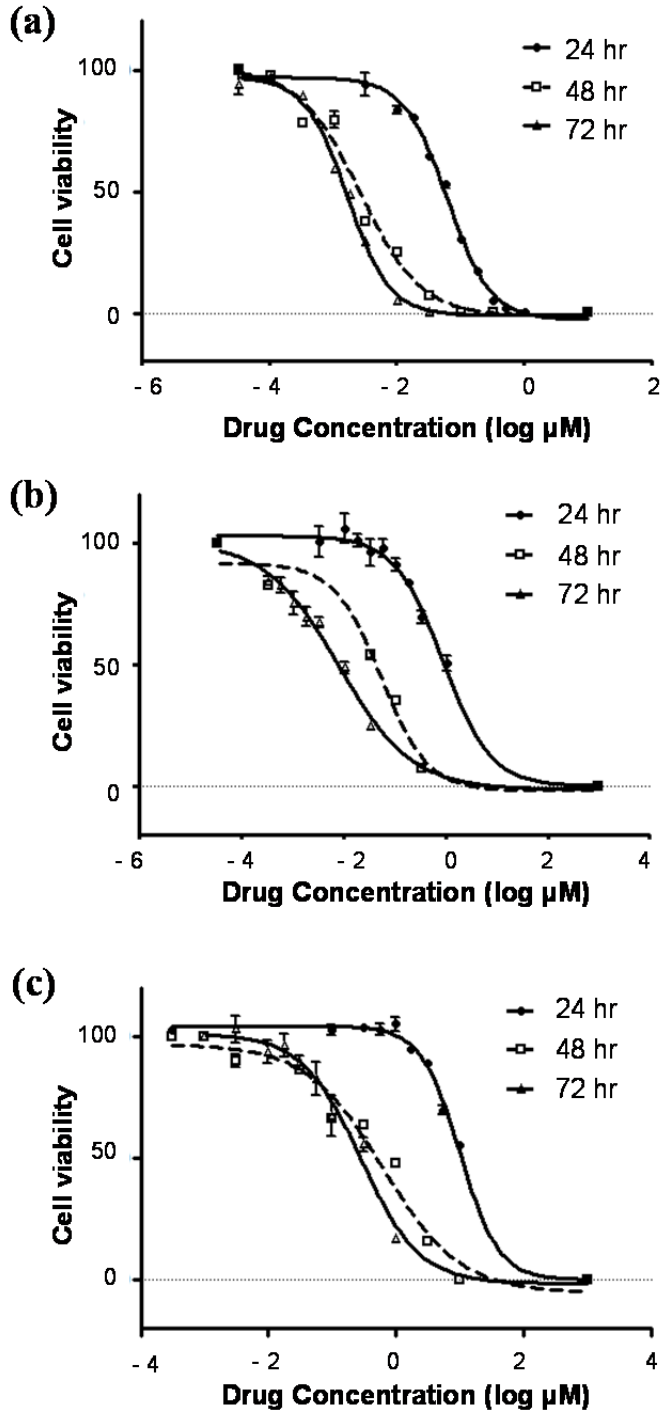

Figure 4-26. Cytotoxicity of cHSA-PEO(2000)$_{16}$-DOX$_{27}$ (**2-24**) in (a) MV4-11 cells, (b) Kasumi-1 cells and (c) Oci-AML3 cells after different incubation times.

Table 4-2. Summary of the IC_{50} of DOX loaded cHSA-PEO(2000)$_{16}$-DOX$_{27}$ (**2-24**) in different cell lines.

		HeLa	MV4-11	Kasumi-1	Oci-AML3
24hrs	**2-24**	129±19nM	64±8nM	880±296nM	335±45nM
	DOX HCl	517±108nM	123±12nM	410±75nM	559±96nM
48hrs	**2-24**	48±2nM	2.6±0.8nM	54±30M	30±16nM
	DOX HCl	97±8nM	16±5nM	234±30nM	136±32nM
72hrs	**2-24**	19±1nM	1.9±0.4nM	7.6±2.6nM	8.2±3.4nM
	DOX HCl	61±4nM	12±3nM	37±14nM	45±8nM

4.3.9 Therapeutic efficacy on leukemic engraftment*

Based on the encouraging results from *in vitro* experiments, we further investigated the anti-leukemia activity on the leukemic engraftment potential of MV4-11 cells (one of the frequent used AML cell line established from a 10-year-old boy with AML at diagnosis). MV4-11 cells were incubated *in vitro* for 72 hr with 33 nM of (a) cHSA-PEO(2000)$_{16}$-DOX$_{27}$ micelles (**2-24**), (b) DOX hydrochloride as well as (c) without any drug treatment. The normal doubling time of the MV4-11 cell line was approximately 50 hr. The cell number in the untreated control increased from $3x10^6$ on day 0 up to $9.77x10^6$ (72 hr), compared to DOX hydrochloride treated MV4-11 cells with $5.88x10^6$ (72 hr) and the cHSA-PEO(2000)$_{16}$-DOX$_{27}$ (**2-24**) micelle group with $1.98x10^6$ (72 hr) cells. Thereafter, these cells were injected to NSG mice (the most immunodeficient strains of inbred laboratory mice that allow successful

* These results were obtained in Prof. Christian Buske's laboratory (Institute of Experimental Tumour Research, Ulm University), and experiments were performed together with Ms. Susann Ihme.

engraftment of human cells) to monitor the leukemia development. After incubation for 72 hr, MV4-11 cells were injected into 3 NSG mice per arm. The mice in the control arm died by leukemic engraftment after a median for 35 days (**Figure 4-27**). These mice were sacrificed after 12 weeks at latest. After 72 hr incubation with DOX HCl, the median survival of the mice was 69 days (**Figure 4-27**). Compared with the control arm mice from the 72 hr cohort with those mice treated with DOX HCl, the median survival increased significantly from 35 days to 69 days (p=0.02). For mice treated with cHSA-PEO(2000)$_{16}$-DOX$_{27}$ (**2-24**), 100 % survival rates were observed even after 12 weeks without any engraftment of leukemia cells (**Figure 4-27**). These data suggested that cHSA-PEO(2000)$_{16}$-DOX$_{27}$ (**2-24**) could efficiently suppress the growth of leukemia cells for a long time, which might due to the prolonged blood circulation of these macromolecular drug allowing continuously release of active therapeutics. Although further *in vivo* studies were still needed to fully evaluate the therapeutic effect of this system, such preliminary data already suggested a promising potential to develop cHSA-PEO(2000)$_{16}$-DOX$_{27}$ (**2-24**) as highly potent therapeutic for AML treatment.

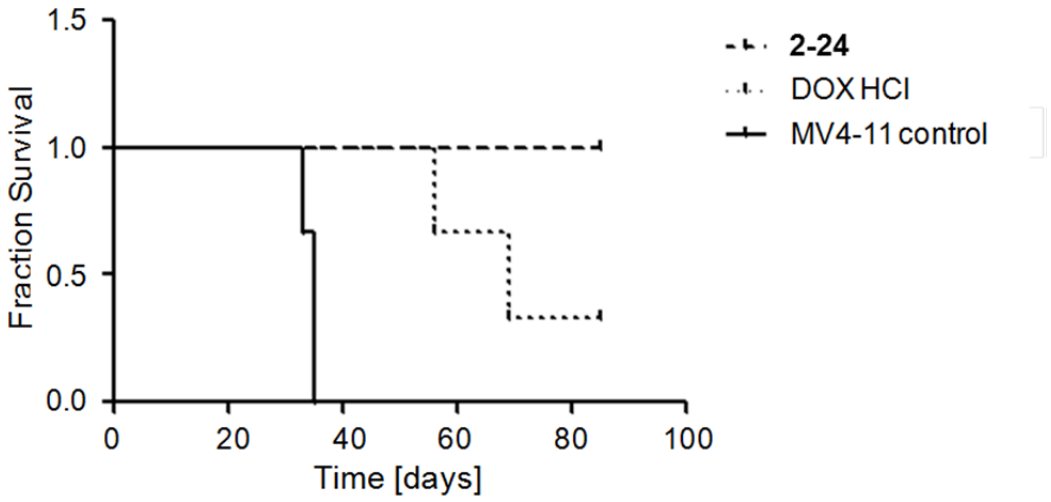

Figure 4-27. Survival curve of NSG mice injected with MV4-11 cells pre-

treated by drugs for 72 hr. Reproduced with permission [61]. Copyright 2012, Wiley-VCH.

4.4 PbPs based carriers for anticancer drug delivery and simultaneous ultrasensitive MR imaging

Although efficient cancer chemotherapy could be achieved by targeted accumulation of nanocarriers into tumor tissue and triggered drug release by specific stimuli, the accumulation processes and biodistribution inside the body could still vary among individual patients, which was crucial for determining the administration dose and targeting strategies [67, 68]. For establishment of safe and effective tumor therapy, image-guided cancer therapy and theranostic nanoplatform that evolved in recent years were expected to engender next generation of “personalized” chemotherapy. Among various diagnostic imaging techniques used in clinic, including computer tomography (CT), positron emission tomography (PET) and magnetic resonance (MR) imaging, the MR imaging technique was especially favourable due to its beneficial characteristics (e.g. deep penetration into soft tissues, high spatiotemporal resolution and facile operation) [69, 70]. For MR imaging diagnosis, the administration of contrast agents was required to enhance the contrast over background signals and improve the detection sensitivity. Based on the functional principle, contrast agents could be classified into *T1*-type (e.g. DOTA-Gd, DTPA-Gd) and *T2*-type (e.g. superparamagnetic iron oxide (SPIO) nanoparticles), which could positively and negatively enhance the contrast, respectively [70]. Compared to *T2*-type

contrast agents, the *T1*-type offered favourably positive imaging contrast enhancement and were more widely clinically applied [71].Therefore, it is highly attractive to integrate *T1*-type MR imaging contrast agents with drug delivery nanocarriers to build up theranostic nanoparticles. This is an emerging area in nanomedicine which has been only explored recently [72]. Therefore, we also developed multifunctional nanocarries from the PbPs systems capable of tumor targeted delivery of therapeutic and diagnostic agents simultaneously.

4.4.1 Preparation of PbP micelles with high loading of DOX and DOTA-Gd†

The *T1*-type MR contrast agent, DOTA-Gd, was conjugated onto cHSA-PEO(2000)$_{16}$ (**2-23**) *via* coupling to amino groups on the protein surface. The synthesis of DOTA-Gd conjugated PbP (**2-26**) was demonstrated in Chapter 2, section 2.4.3.3 and shown again in **Figure 4-28** (this material was prepared together with Ms Tao Wang). 85 DOTA-Gd could be incorporated into (**2-23**) according to MALDI-Tof MS (**Figure 2-23**). Further loading of DOX could be achieved *via* the same procedure described in section 2.4.3.2 for the preparation of cHSA-PEO(2000)$_{16}$-DOX$_{27}$ (**2-24**) (this material was prepared together with Ms Tao Wang). According to UV-Vis spectra, 27±3 DOX could be loaded into each denatured (**2-26**) backbone, which was the same as observed for (**2-24**). The resulting DOTA-Gd and DOX conjugated PbP (cHSA-PEO(2000)$_{16}$-Gd-DOX$_{27}$ (**4-2**)) self-assembled into nanosized core-

† These studies were performed in close cooperation with Ms Tao Wang and will also be included in her PhD thesis. Ms Tao Wang synthesized NHS-DOTA and performed the last step preparation of (**2-25**), (**2-26**) and (**4-2**).

shell structures in aqueous solution with the hydrophilic PEO shell outside and hydrophobic imaging and therapeutic core pointing to the inside from the protein backbone (**Figure 4-28**). This system combined the advantages of the two-step controlled release as discussed for (**2-24**) as well as ultrasensitive MR imaging due to the high number of DOTA-Gd, which could be highly attractive for imaging guided "personalized" cancer therapy.

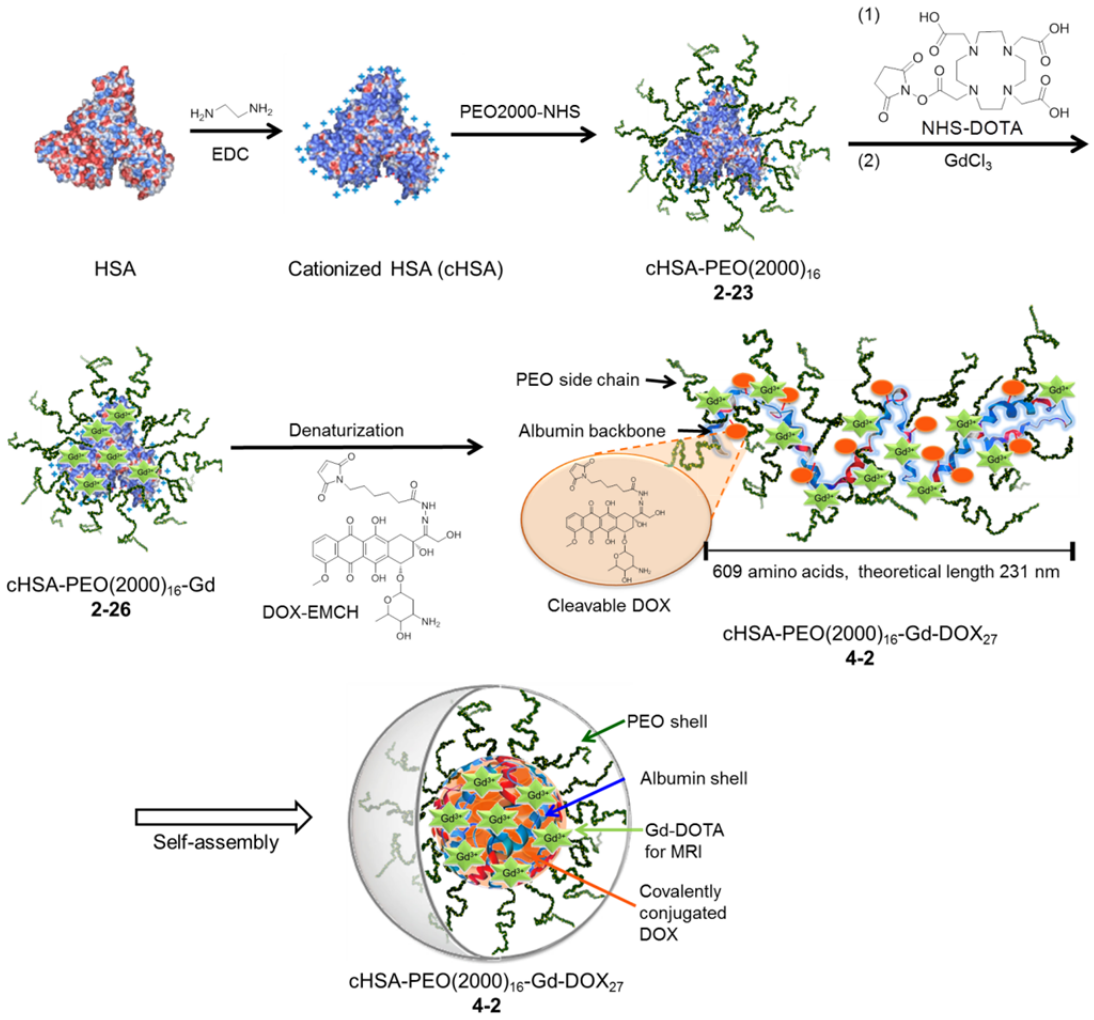

Figure 4-28. Preparation of Gd and DOX loaded PbP micelles cHSA-PEO(2000)$_{16}$-Gd-DOX$_{27}$ (**4-2**). Adapted with permission [61]. Copyright 2012, Wiley-VCH.

4.4.2 Characterization of the relaxivity of DOTA-Gd loaded PbP (2-26)‡.

Conjugation of DOTA-Gd onto nanocarriers could overcome intrinsic limits associated with small molecule Gd(III) complexes such as broad tissue distribution and the risk of Nephrogenic Systemic Fibrosis (NSF)§ [73]. In addition, the contrast enhancement using small molecular Gd^{3+} complexes was relatively low, therefore required high administration doses which increases the risk of side effects [73]. It was demonstrated that covalent and non-covalent attachments of Gd(III) complexes to slowly tumbling objects, such as nanoparticles, liposomes, polymers, etc., could significantly improve the contrast efficiency [74, 75, 76].

The effect of an MR contrast agent was assessed based on its longitudinal and transverse relaxivities, r1 and r2, which reflected the ability of the contrast agent to alter T1 (spin-lattice relaxation) and T2 (spin-spin relaxation), respectively. Relaxivities were calculated through the linear least quare fitting of 1/relaxation time (S^{-1}) versus the gadolinium concentration (mM Gd). *Via* this method, we assessed the relaxivity of DOTA-Gd loaded PbP (**2-26**) on an 3T MR imager. Since Gd(III) complexes are T1-type contrast agents, the longitudinal relaxivity r1 was calculated by plotting 1/T1 of (**2-26**) as a function of Gd^{3+} concentration. As shown in **Figure 4-29**, the linear relation between 1/T1 and Gd^{3+} concentration was observed for (**2-26**)

‡ These experiments were done together with Prof. Rasche's group (Klinik für Innere Medizin II, Experimental Cardiovascular Imaging, Ulm University).

§ Nephrogenic systemic fibrosis (NSF) is a rare but serious syndrome that involves fibrosis of skin, joints, eyes, and internal organs. The first cases were identified in 1997 and much evidence suggests that it is associated with exposure to gadolinium-based MRI contrast agents in patients with severe kidney failure.

and the r1 relaxivity per gadolinium was extracted from the slope of the line as 13.75 $mM^{-1}s^{-1}$. Compared to the r1 relaxivity of clinically used Gd(III) contrast agents of Gd-DOTA (4.3 $mM^{-1}s^{-1}$) and Gd-DTPA (4.5 $mM^{-1}s^{-1}$), the polymeric Gd(III) micelles (**2-26**) exhibited significantly improved contrast potency which was highly attractive for MR imaging. Compared to other gadolinium-based macromolecular contrast agents reported previously, the paramagnetic properties of (**2-26**) were also in a comparable level. For instance, dendrimer conjugated gadolinium, such as gadolinium-labeled PAMAM (G5) dendrimers, had a r1 relaxivity of 10.1 $mM^{-1}s^{-1}$ per gadolinium atom [74] which was slightly lower than our system, but gadolinium containing nanoparticles, such as gadolinium-DTPA-Gold nanoparticle could raise the relaxivity to ~20 $mM^{-1}s^{-1}$ per gadolinium [77].

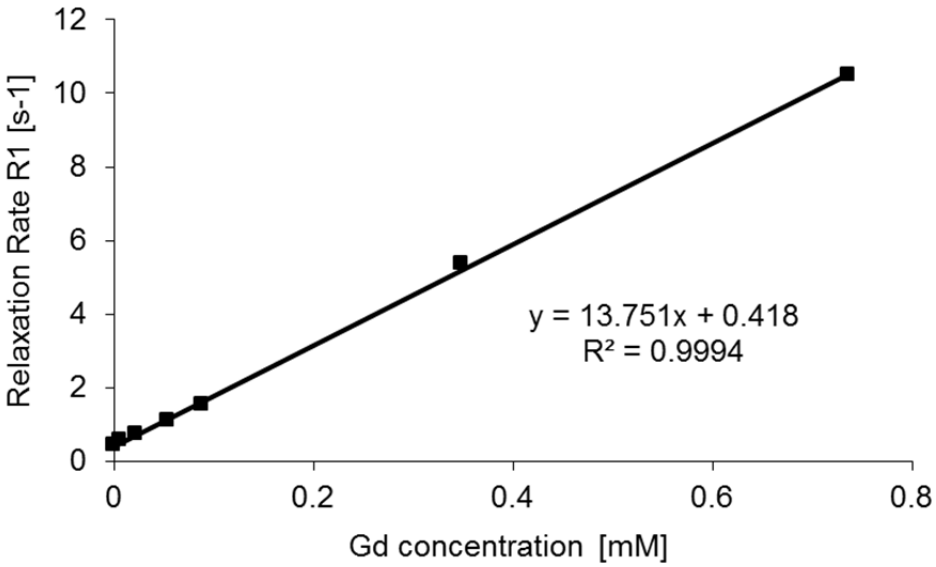

Figure 4-29. Relaxivity test of cHSA-PEG$(2000)_{16}$-Gd (**2-26**) compared with gadoteric acid.

4.4.3 *In vitro* test of cHSA-PEG(2000)$_{16}$-Gd-DOX$_{27}$ (4-2) in mammalian cells.

DOX was loaded into DOTA-Gd containing (**2-26**) backbone *via* covalently conjugation through a pH sensitive hydrazone linker. This strategy has been discussed in detail in section 4.3. In this structure, DOX molecules were tightly encapsulated into the PbP based protein shell and could be released inside the cells under lysosomal conditions. The PEO shell outside the protein core contributed to the high water solubility as well as reduced immune potential, whereas the cationized PbP backbone facilitated an efficient cell uptake of the whole construct. The cell uptake of the DOX-DOTA-Gd co-loaded PbP micelles (**4-2**) was also investigated by confocal microscopy (**Figure 4-30**). After 24 hr incubation of (**4-2**) (1 μM) with HeLa cells, the DOX signal was observed mainly at the perinuclear region, and a week DOX signal was also found in the cell nucleus. This observation is comparable as for cHSA-PEO(2000)$_{16}$-DOX$_{27}$ (**2-24**), indicating a similar cellular behavior of the MR agent and the drug co-loaded micelles (**4-2**) compared to only drug loaded micelles (**2-24**).

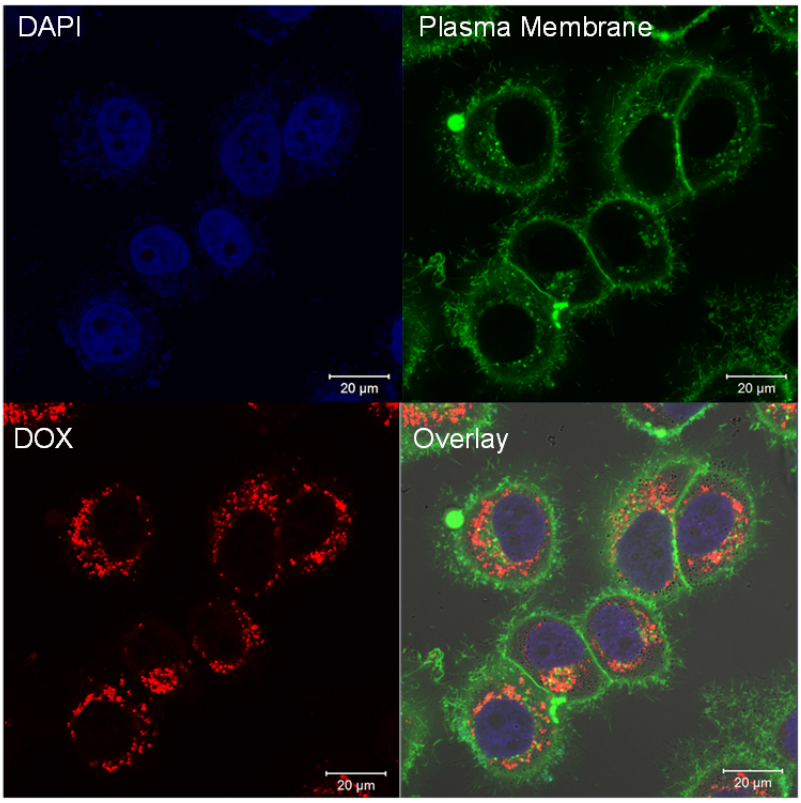

Figure 4-30. Confocal micrographs of cHSA-PEO(2000)$_{16}$-Gd-DOX$_{27}$ (**4-2**) (1 μM) incubated with HeLa cells for 24 hr.

The IC_{50} of (**4-2**) was also tested in HeLa cells (**Figure 4-31**). After 24 hr incubation, an IC_{50} of 1.4±0.2 μM was observed for (**4-2**) indicating a potent toxicity effect. However, the IC_{50} of (**4-2**) was slightly larger than both free DOX and DOX-PbP micelles (**2-24**) (**Table 4-3**). This might be due to less positive charges after the reaction with DOTA-Gd on the lysine groups, which affected the cell uptake efficiency of (**4-2**). In addition, after longer incubation time (48 hr and 72 hr), the cytotoxicity of (**4-2**) was increased, which was similar as observed for DOX micelles (**2-24**). Although the cytotoxicity of (**4-2**) was slightly less than (**2-24**) and free DOX, the highly sensitive MR imaging contrast together with the observed cytotoxicity effect suggested (**4-2**) as highly attractive theranostic agent.

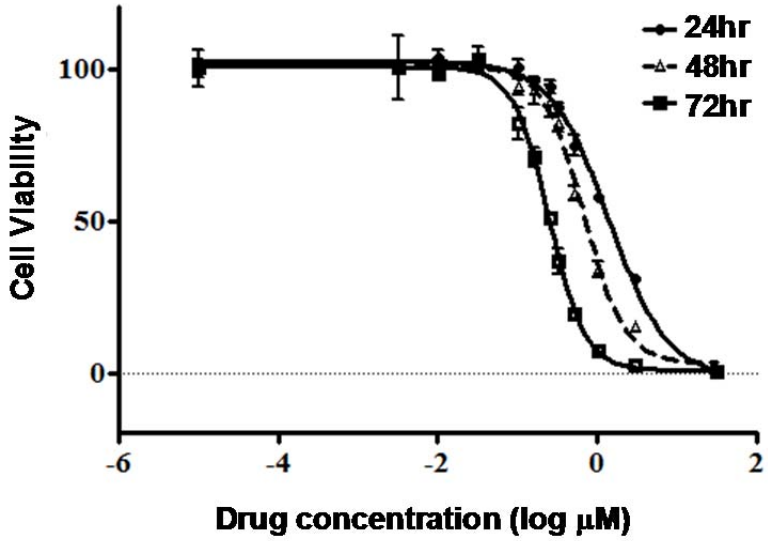

Figure 4-31. Cytotoxicity of cHSA-PEO(2000)$_{16}$-Gd-DOX$_{27}$ (**4-2**) in HeLa cells after 24 hr, 48 hr and 72 hr incubation.

Table 4-3. Summary of the IC_{50} of free DOX, DOX loaded cHSA-PEO(2000)$_{16}$-DOX$_{27}$ (**2-24**) and DOX and DOTA-Gd co-loaded cHSA-PEO(2000)$_{16}$-Gd-DOX$_{27}$ (**4-2**).

Sample Name	24hr IC_{50}	48hr IC_{50}	72hr IC_{50}
Free HCl	0.52±0.11μM	91±8 nM	61±4 nM
(**2-24**)	0.13±0.02 μM	48±2 nM	19±1 nM
(**4-2**)	1.4±0.2 μM	0.68±0.08 μM	0.25±0.03 μM

4.5 Summary

The three efficient drug delivery systems based on PbPs were prepared. The anti-cancer drug DOX was loaded into PbPs micelles *via* non-covalent encapsulation as well as covalent conjugation. The dcBSA-PEO(5000)$_{27}$-DOX micelles (**4-1**) encapsulating DOX *via* hydrophobic interactions were designed

to encompass several important features, such as (1) positive charges to facilitate cellular uptake *via* endocytosis, (2) narrowly dispersed micelle sizes of about 56 nm and high stability in different physiological buffers, cell media and a broad pH range, (3) PEO side chains along the backbone to reduce plasma protein binding, immunogenicity and to contribute to high micelle stability in solution, (4) high drug loading of about 14 lipophilic DOX molecules per micelle. Cell imaging *via* confocal microscopy revealed fast cell uptake of dcBSA-PEO(5000)$_{27}$-DOX (**4-1**) immediately after only 1hr of incubation time. DOX uptake after encapsulation into micelles was five-fold increased compared to free DOX. *In vitro* cytotoxicity experiments indicated an about five-times higher cytotoxicity of (**4-1**) compared to free DOX. Such PbPs based system could in principle be universal to a broad range of lipophilic drug molecules and might therefore be attractive for combination therapy, e.g. the application of different drugs acting *via* different modes of actions.

However, some limitations were still associated with such transporters, e.g. the number of drug molecules loaded in each micelle was less defined and difficult to control, and non-specific drug leakage was expected when interacting with other hydrophobic molecules or membranes. Therefore, more defined drug carriers with covalently conjugated drugs were desirable to further advance this approach.

The core-shell DOX delivery system cHSA-PEO(2000)$_{16}$-DOX$_{27}$ (**2-24**) based on an innovative protein denaturing-repacking strategy was further developed. DOX was covalently conjugated to the albumin hydrophobic core *via* an acid sensitive hydrazone linker. Polycationic and highly pegylated HSA formed the biocompatible and biodegradable protection shell. This

macromolecular architecture possessed a considerable DOX loading capacity for up to 27 DOX, a two-step drug release mechanism, attractive biocompatibility and narrow size distribution inherited from the monodisperse albumin backbone, as well as fast cellular uptake and reduced potential immunogenicity due to cationization and pegylation. Highly potent cytotoxicities were found *in vitro* with HeLa cells as well as with different acute leukemia cell lines, with lowest IC_{50} of 1.9 nM for the MV4-11 cell line after 72 hr. The efficacy of this delivery system was further confirmed by *in vivo* transplantation assays demonstrating that (**2-24**) significantly impaired the engraftment potential of highly aggressive AML cell lines after 72 hr incubation. These preliminary *in vivo* transplantation studies further underlined the high efficiency of (**2-24**) versus conventional application of DOX HCl and suggested an attractive potential of this nanomedicinal formulation for targeting leukemia cells under *in vivo* conditions with a promising safety profile and minimized drug leakage. However, more pharmacological studies were required to completely understand the *in vivo* pharmacokinetics of such macromolecular drug.

In addition, the denatured protein backbone provided multiple functional groups available for further chemical modifications. Therefore, PbPs were highly attractive for creating multifunctional drug delivery carriers. We have demonstrated that a “theranostic magic bullet” could be prepared by conbining contrast agents for MR imaging together with the anti-cancer drug DOX into one PbP. The resulting cHSA-PEO$(2000)_{16}$-Gd-DOX_{27} (**4-2**) revealed significantly enhanced r1 relaxivity as well as efficient cellular uptake and cytotoxicity, which makes it highly attractive as novel theranostic agent. In

principle, further decoration of PbPs drug delivery systems with additional functionalities, such as receptor targeting molecules, could also be envisaged. In this way, we have shown that PbPs represent a highly versatile and attractive platform for anticancer drug delivery and even possess great potential for developing multifunctional nanomedicines.

4.6 Materials and Methods

4.6.1 Materials

Albumins from bovine serum (BSA) (>=98%, Sigma Aldrich Chemie Gmbh, Munich, Germany), O-(2-maleimidoethyl)- O'-methyl-polyethylene glycol 5000 (PEG-5000-MI) (>90% NMR, Sigma Aldrich Chemie Gmbh, Munich, Germany), MeO-PEO2000-NHS (Iris Biotech GmbH, Germany), doxorubicin hydrochloride salt (DOX) (>=99.0%, XingCheng ChemPhar Co. LTD, Taizhou, China), cathepsin B from bovine spleen (lyophilized powder, 4.8 units/mg solid, Sigma-Aldrich Chemie Gmbh, Munich, Germany) were used as received without further purification. Bio-Gel P30 desalting column (Bio-Rad, Germany), 3.5K MWCO Slide-A-Lyzer MINI Dialysis cassettes (Pierce, Thermo Fisher Scientific, Bonn, Germany) and Vivaspin® ultrafiltration tubes (GE healthcare, Munich, Germany) were used for purification. Dulbecco's Modified Eagle Medium (DMEM) (1X) liquid (high glucose), Fetal Bovine Serum (FBS) Standard Quality (EU approved), penicillin/streptomycin solution (100X) were purchased from PAA Laboratories GmbH (Cölbe, Germany), MEM (non-essential amino acids solution 10 mM

(100X)), CellMask® Deep Red plasma membrane stain were purchased from Invitrogen Life Technologies GmbH, Darmstadt, Germany. DOX-EMCH was synthesized according to literature procedure [78]. Deionized distilled water was produced using ultra pure water system from SG water (Siemens, Berlin, Germany).

4.6.2 Preparation of dcBSA-PEO(5000)$_{27}$ micelle (4-1)

DOX hydrochloride (DOX*HCl) (4 mg, 7 mmol) was dissolved in 500 µL deionized-distilled water and mixed with 1.2 equivalents of triethylamine (1.2 µL, 8.4 mmol). The aqueous solution was extracted five times with dichloromethane. The combined organic extracts were evaporated in vacuum and 3 mg of DOX were obtained. This DOX stock solution was prepared by dissolving the obtained solid in 500 µL of DMF to achieve a total concentration of 6 mg/mL. dcBSA-PEO(5000)$_{27}$-alkyne (**2-15**) (0.5 mg, 2.8 nmol) in distilled-deionized water was combined with the desired molar ratios of DOX (1:1, 1:5, 1:10, 1:20, 1:50, 1:100) and allowed to stir overnight in the dark at RT. The reaction mixtures were transferred to 3.5K MWCO Slide-A-Lyzer MINI Dialysis cassettes and dialyzed in 1 L of distilled-deionized water for 24 hr at 4°C; during this time period, water was exchanged 3 to 5 times. The amount of entrapped DOX in each molar ratio was determined by measuring the absorbance at 488 nm using Tecan Infinite® M-1000 microplate reader.

4.6.3 Characterization of dcBSA-PEO(5000)$_{27}$ micelle (4-1)

4.6.3.1 Negative staining transmission electron microscopy (TEM)

The morphology of dcBSA-PEO(5000)$_{27}$-DOX micelles (**4-1**) was characterized *via* TEM applying the negative staining technique. A drop of 1

mg/mL (**4-1**) dissolved in an aqueous solution was deposited onto a hydrophilic copper grid with a carbon film for approximately 1 min and then blotted excess of the sample by filter paper. The grid was allowed to dry at RT for overnight and then stained with 1% Uranyl acetate solution for TEM investigations.

4.6.3.2 Dynamic light scattering (DLS)

The hydrodynamic size distribution of dcBSA-PEO(5000)$_{27}$-DOX micelles (**4-1**) was characterized by DLS using a Malvern Nanosizer (Malvern Ltd, Malvern, UK). (**4-1**) was prepared at 0.15 mg/mL concentration in aqueous solution and filtered through 0.2 μm microsyringe filtered before measurement to avoid dust contamination. Autocorrelation functions were analyzed by cumulants method and COTIN routine to estimate hydrodynamic diameter. The hydrodynamic diameter distribution was presented as number distribution.

4.6.3.3 Characterization of micelle stability in various media

100 μL aliquots of 0.1 mg dcBSA-PEO(5000)$_{27}$-DOX (**4-1**) samples were dialyzed using 3.5K MWCO Slide-A-Lyzer MINI Dialysis devices (Pierce) in 10 mM (pH 3 and 5) citrate buffer and 10 mM (pH 7 and 9) and Tris buffer, respectively, for 2 days and the absorbance spectra were recorded before and after dialysis.

4.6.4 Drug delivery efficiency of dcBSA-PEO(5000)$_{27}$ micelle (4-1) evaluated in mammalian cells.

4.6.4.1 Cell culture

HeLa cells (human cervix carcinomic cell line) and A549 cells (carcinomic human alveolar basal epithelial cell line) were obtained from DSMZ (German

Collection of Microorganisms and Cell Cultures, Braunschweig) and cultured in DMEM medium with high glucose supplemented and with 10% fetal bovine serum (FBS), 100 U/mL Penicillin, 0.1 mg/mL Streptomycin, 0.1 mM non-essential amino acids at 37°C in a humidified 5% CO_2 incubator.

4.6.4.2 Cytotoxicity assay

HeLa cells were plated into a white 96 well microplate at a density of 8000 cells per well and incubated overnight for attachment. After incubation, the media from each well were aspirated and exchanged with 100 μL of fresh DMEM medium and the desired amount of either free DOX or dcBSA-PEO(5000)$_{27}$-DOX micelles (**4-1**). All concentrations were prepared as triplicates. After further incubation with drug molecules for 12 hr, 24 hr and 48 hr, cell viability was tested by CellTiter-Glo® (Promega GmbH, Mannheim, Germany) cell viability assay kit according to manufactory's instruction. Cells that were not treated with any drug were considered as blank. The IC_{50} values and the 50% inhibitory concentrations were obtained through GraphPad Prism 3 software.

4.6.4.3 Live cell imaging of intracellular DOX in A549 cells

A549 cells were plated onto glass cover slips and incubated for 12 hr to allow cell attachment and spreading. Thereafter, 0.1 μM of either free DOX or dcBSA-PEO(5000)$_{27}$-DOX micelles (**4-1**) were added to the cells and incubated for one additional hour. The cells were then washed 3 times with PBS, replaced with fresh medium and incubated with 5 μg/ml of WGA-Alexa Fluor 594 conjugate (Cat # W11262, Invitrogen) for 10 min to label the cell membrane and imaged without further washing. Microscopy was performed

with a Zeiss LSM 710 META laser scanning microscope fitted with Argon, HeNe543 and Diode405-30 lasers. Z-sections of chosen field were acquired with a 40x oil immersion objective (Zeiss, Germany). Excitation and emission wavelengths of 535-562 nm for DOX and of 600-620 nm for WGA-Alexa Fluor 594 detection were selected. The acquired images were processed with Zen software developed by Carl Zeiss.

4.6.4.4 Quantification of DOX uptake

For the quantification of DOX cell uptake, images obtained from five different sections in each of the slides were analyzed using the public domain NIH ImageJ program with default settings (developed at the U.S. National Institutes of Health and available on the Internet at http://rsb.info.nih.gov/nih-image/). To calculate the percentage of intracellular DOX, the fluorescence intensity of DOX [green] was divided by the total fluorescence (DOX [green] and the cell membrane [red]) and multiplied by 100.

4.6.5 Preparation of DOX loaded cHSA-PEO(2000)$_{16}$-DOX$_{27}$ micelles (2-24)

10 mg (50 nmol) of cHSA-PEO(2000)$_{16}$ (**2-23**) were dissolved in degassed urea-phosphate buffer (10 ml, 50 mM phosphate buffer, pH 7.4, 5 M urea and 2 mM EDTA) and stirred at room temperature for 15 min. TCEP (0.29 mg, 1 μmol) was added as a solid and the solution was stirred for additional 30 min under argon atmosphere. Then, DOX-EMCH (15 mg, 10 μmol) was added and stirred under argon atmosphere for overnight. Thereafter, the reaction mixture was purified by ultrafiltration with urea-phosphate buffer (10 mM phosphate buffer, pH 7.4, 5 M urea and 2 mM EDTA) 3 times and with water 5

times, then lyophilized to obtain cHSA-PEO(2000)$_{16}$-DOX$_{27}$ (**2-24**) 5.4 mg as red solid, yield 45%.

4.6.6 Characterization of DOX loaded cHSA-PEO(2000)$_{16}$-DOX$_{27}$ micelles (2-24)

*4.6.6.1 Calculation of DOX loading into cHSA-PEO(2000)$_{16}$-DOX$_{27}$ micelles (**2-24**)*

The amount of DOX covalently loaded in cHSA-PEO(2000)$_{16}$-DOX$_{27}$ micelles was calculated according to the molecular weight increase characterized by MALDI-ToF mass spectrometry. The total DOX loading was measured according to the absorbance of doxorubicin at 488 nm at pH 1 in aqueous solution (calibration curve was made using DOX HCl aqueous solution). The Number of DOX molecules in each micelle was calculated as DOX loading using following equations.

$$\text{Covalent DOX loading} = \frac{\text{MW(cHSA-PEO(2000)}_{16}\text{-DOX}_{27}) - \text{MW(cHSA-PEO(2000)}_{16})}{\text{MW(DOX-EMCH)}}$$

$$\text{Total DOX loading} = \frac{\text{DOX concentration calculated by absorbance at 488nm}}{\text{cHSA-PEO(2000)}_{16}\text{-DOX}_{27}\text{ concentration}}$$

The total DOX loading calculated based on UV-Vis absorbance was used as DOX concentration in cell studies.

4.6.6.2 Characterization of size distribution

The size distribution of cHSA-PEO(2000)$_{16}$-DOX$_{27}$ micelles (**2-24**) was characterized by transmission electron microscope (TEM) and Dynamic light scattering (DLS). For TEM measurements, a drop of 1 mg/ml cHSA-

$PEO(2000)_{16}$-DOX_{27} solution was placed onto a freshly glow discharged 300 mesh size copper grid covered with a continuous carbon film. Excess solution was removed by an adsorbent paper and the sample was dried at room temperature overnight. A Jeol 1400 Transmissions electron microscope was used to obtain bright field TEM images. DLS measurements were performed using a Malvern Zetasizer ZEN3600 (Malvern Ltd, Malvern, UK). cHSA-cHSA-$PEO(2000)_{16}$-DOX_{27} micelles (**2-24**) were prepared at 0.15 mg/ml in aqueous solution and measured at 25°C with 173° angle. Autocorrelation functions were analyzed applying the cumulants method and COTIN routine to estimate the hydrodynamic diameter and polydispersity index (PDI). The hydrodynamic diameter distribution was presented as number distribution.

4.6.6.3 Characterization of the surface charge

The net surface charge of cHSA-$PEO(2000)_{16}$-DOX_{27} micelles (**2-24**) was characterized by agarose gel electrophoresis using 0.5% agarose gel in pH 7.4 TAE buffer. Positively charged species moved toward the anode whereas the negatively charged molecules moved toward the cathode. To investigate the zeta potential of (**2-24**), 0.1 mg/mL of these micelles was prepared in 1mM KCl solution and zeta potential was recorded 5 times independently using Malvern Zetasizer ZEN3600 (Malvern Ltd, Malvern, UK).

4.6.7 Study of DOX release from cHSA-$PEO(2000)_{16}$-DOX_{27} micelles (2-24)

4.5.7.1 In vitro drug release profile Mimicking lysosomal conditions[**]

** These experiments were performed in close collaboration with Dr. Seah Ling Kuan (Institute of Organic Chemistry III, Ulm University).

The DOX release profile was determined under an *in vitro* condition mimicking lysosomal environment [64]. Cathepsin B was added to activation buffer (30 mM DTT, 15 mM EDTA) to a final concentration of 1.6 U/mL cathepsin B, 20 mM DTT, 10 mM EDTA and incubated at 37 °C for 15 min. The pre-activated cathepsin B solution was added to cHSA-PEO$(2000)_{16}$-DOX_{27} micelles (**2-24**) in reaction buffer (25 mM acetate, 1 mM EDTA, pH 5, pre-warmed at 37 °C) to obtain the final concentration of 0.5 U/mL cathepsin B, 24.6 mM acetate, 1.1 mM EDTA, 0.33 mM DTT and 5.8 μM cHSA-PEO$(2000)_{16}$-DOX_{27} micelles (**2-24**). The reaction solution was incubated at 37 °C. Aliquots were removed at various time points and enzymatic activity stopped by addition of cysteine-protease inhibitor E-64 (Sigma Aldrich Chemie Gmbh, Munich, Germany) to a final concentration of 10 μM. Samples are extracted by C18 reverse phase silica gel and eluted by 60% acetonitrile with 0.1% formic acid. The eluents were concentrated to a same concentration by applying a Spin Vac Concentrator and spiked 2 ppm Rhodmine B as internal standard before LC-MS analysis. As control experiments, the same concentration of cHSA-PEO$(2000)_{16}$-DOX_{27} (**2-24**) incubated 24 hr in the same reaction buffer but without cathepsin B was prepared in parallel. And the cHSA-PEO$(2000)_{16}$ carriers without DOX were also subjected to cathepsin B digestion under the same condition and analyzed to compare with the metabolites generated from DOX loaded micelles.

LC-MS analysis was performed on a Shimadzu LC-MS 2020 equipped with an electrospray ionsation source and a SPD-20A UV-Vis detector (Shimadzu, Duisburg, Germany). Aliquots (40 μL) were injected onto a Luna

C-18 reverse phase column (50 x 4.6 mm, 5 μm) (Phenomenex, CA, Torrance). The column temperature was set at 40°C. The mobile phase consisted of 0.1% formic acid in water (A) and 0.1% formic acid in acetonitrile (B). The gradient was linearly increased from 5% to 95% A over 20 min, held at 95% for an additional 8 min, and then immediately stepped back down to 5% for re-equilibration. The mobile phase flow rate was 0.4 mL/min. Identification of free doxorubicin was performed simultaneously by UV-VIS detection at 480 nm and selective ion monitoring (SIM) of the $[M+H]^+$ at m/z = 544. Mass spectrometric parameters are optimized for detection of doxorubicin by using sample infusion and flow injection analysis (FIA).

The amount of DOX released at each time interval was determined as a ratio of free doxorubicin (integrated according to 480 nm chromatogram) to the internal standard Rhodamine (integrated according to 544 nm chromotagram). 27 eq of DOX mixed with cHSA-PEO$(2000)_{16}$ (**2-23**) was used to as the control of complete DOX release.

4.6.7.2 Monitor nonspecific DOX leaking without micelle degradation

A solution of cHSA-PEO$(2000)_{16}$-DOX_{27} (0.5 mg/ml, 50 μL) was prepared in phosphate buffer (20 mM, pH 7.4) and citrate buffer (20 mM, pH5) respectively and dialyzed in 1 mL (perfect sink conditions maintained) of phosphate buffer (20 mM, pH 7.4) and citrate buffer (20 mM, pH5) accordingly at 37 °C using Slide-A-Lyzer MINI Dialysis Devices (10K MWCO). The 1 mL of dialysis buffer was sampled at desired time point by freezing at -80oC and replaced by fresh buffer. The reaction was monitored over 48 hr. All dialysis solutions are concentrated to 100 μL in a Spin Vac Concentrator and the amount of DOX was determined by measuring absorbance at 488 nm.

4.6.8 Drug delivery efficiency of cHSA-PEO(2000)$_{16}$-DOX$_{27}$ evaluated in mammalian cells.

4.6.8.1 Cell culture

HeLa cells (human cervix carcinomic cell line) were obtained from DSMZ (German Collection of Microorganisms and Cell Cultures, Braunschweig) and cultured in DMEM medium with high glucose supplemented and with 10% fetal bovine serum (FBS), 100 U/ml Penicillin, 0.1 mg/ml Streptomycin, 0.1 mM non-essential amino acids at 37°C in a humidified 5% CO_2 incubator. Leukemia cell lines MV 4-11, Kasumi-1 and Oci-AML3 were obtained from DSMZ (German Collection of Microorganisms and Cell Cultures, Braunschweig) and cultured in RPMI medium supplemented with 10% fetal bovine serum (FBS), 100 U/ml Penicillin, 0.1 mg/ml Streptomycin, 0.1 mM non-essential amino acids at 37°C in a humidified 5% CO_2 incubator.

4.6.8.2 Cytotoxicity assay

HeLa, MV 4-11, Kasumi-1 and Oci-AML3 cells were plated into 96-well microplates at a density of 8000 cells per well, 5000 cells per well and 3000 cells per well for investigations at different time points respectively and incubated overnight for attachment. After incubation, the media from each well were aspirated and exchanged with 100 µl of fresh DMEM with the desired amount of either DOX hydrochloride or cHSA-PEO(2000)$_{16}$-DOX$_{27}$ (**2-24**). All concentrations were prepared as triplicates. After further incubation with these two drug molecules for 24 hr, 48 hr and 72 hr, cell viability was tested by the CellTiter-Glo® cell viability assay kit according to manufacturer's instructions. Cells that were not treated with any drug were considered as blank. The IC_{50}

values and the 50% inhibitory concentrations were obtained through GraphPad Prism 3 software.

4.6.8.3 Confocal laser scanning microscope (CLSM)

HeLa cells were plated in a Coverglass Lab-Tek 8-well chamber (Nunc, Denmark) at a density of 30,000 cells per well in 300 μl DMEM containing 10% FCS, 1% penicillin/streptomycin and 1% MEM. The cells were incubated overnight at 37°C in 5% CO_2 to allow adhesion. The next day, 2.5 μg of cHSA-PEO(2000)$_{16}$-DOX$_{27}$ (**2-24**) and 0.3 μg of DOX hydrochloride were added to the cell culture medium respectively to reach a final DOX concentration of 1.8 μM in the medium. The cells were then further incubated for 24 hr in the incubator. Before imaging, cells were washed with fresh complete medium 3 times. Cell nuclei were stained with 1 μl of DAPI solution (5 mg/ml) for 15 min and the cell membrane was further stained with 0.5 μl of CellMask® Deep Red plasma membrane stain solution (0.5 mg/ml) for 5 min. Imaging was then performed using a LSM 710 laser scanning confocal microscope system (Zeiss, Germany) coupled to an XL-LSM 710 S incubator and equipped with a 63× oil immersion objective. The DAPI nuclei stain and CellMask® Deep Red plasma membrane stain was excited with a Diode405-30 laser and a HeNe633 laser, respectively, and the emission was collected using 410-582 nm and 647-759 nm filters, respectively. The fluorescence of DOX was separately recorded using a 531-648 nm filter and a 488 nm Argon laser for excitation. The acquired images were processed with Zen software developed by Carl Zeiss.

4.6.8.4 Caspase activity assay

HeLa cells were plated into a white 96 well half area microplate at a density of 5000 cells per well with 50 μl DMEM and incubated overnight for attachment. After incubation, the media from each well were aspirated and exchanged with 50 μl of fresh DMEM with the desired amount of either DOX hydrochloride or cHSA-PEO(2000)$_{16}$-DOX$_{27}$ (**2-24**). All concentrations were prepared as triplicates. After further incubation with both drugs for 16 hr, caspase activity was tested by Caspase-Glo® 3/7 assay kit (Promega GmbH, Mannheim, Germany) according to manufacturer's instruction.

4.6.9 Anti-leukemia efficacy of cHSA-PEO(2000)$_{16}$-DOX$_{27}$ (2-24) evaluated in NSG mice[††].

MV4-11 (acute monocytic leukemia, FAB M5) cells were plated into 6-well suspension plates at a density of 3 million cells per well and cultured in 6 ml RPMI with 10% FBS, 100 U/ml Penicillin, 0.1 mg/ml Streptomycin (control group) or supplemented with 0.33 μM for the 48 hr or 0.033 μM for the 72 hr *in vitro* incubation of either cHSA-PEO(2000)$_{16}$-DOX$_{27}$ or DOX hydrochloride. The cells were incubated for 72 hr at 37°C in a humidified 5% CO_2 incubator. Cell numbers were determined with trypan blue stain and equal cell numbers were injected into 3 NOD.Cg-Prkdc scid Il2rg tm1Wjl /SzJ (NSG) mice per cohort after 72 hr incubation time. The leukemia development in NSG mice was proven by immunophenotyping of isolated bone marrow. NSG mice were bred in the animal care facility of the University of Ulm. 24 hr prior transplantation, 8-12 week old mice were irradiated (325 cGy) and injected

[††] The experiments were performed by Ms. Susann Ihme in Prof. Christian Buske's laboratory (Institute of Experimental Tumour Research, Ulm University).

intraperitoneally with 1mg/g IVIG (CSL Behring). Cells were injected intravenously after the 72 hr *in vitro* incubation. Bone marrow aspiration was performed in week 5 and 8 after transplantation. Mice were sacrificed 12 weeks post transplantation and human engraftment was verified by evaluating huCD45 expression using flow cytometry ananlysis.

4.6.10 MRI relaxivity test for cHSA-PEG(2000)$_{16}$-Gd (2-26)[‡‡].

All samples were measured at a 3-T clinical scanner (Intera, Philips Medical Systems) using a standard head coil. An SSFP-Look Locker technique (TE/TR/α: 1.5/12000/16°, acquisition matrix 256 x 256, field of view [FOV] 330 mm, temporal resolution 30 ms) was used to measure longitudinal relaxation times. Longitudinal relaxivities were retrieved from a dilution series containing Gd concentrations from 15 μM to 200 μM 0.9% NaCl aqueous solution. The T1 values for the samples were calculated by a three parameter exponential fit applying a Levenberg-Marquardt optimization algorithm(MatLab, MathWorks Inc.). The longitudinal relaxation rate (1/T1 in s-1) was plotted vs. the Gd concentration (mM) in PbP (**2-26**), and the slope was calculated according to give the value of r1 relaxivity.

4.6.11. Statistical analysis

The results are expressed as the mean ± standard deviation (SDV) according to 3 individual experiments if not otherwise mentioned. The differences between the groups were analyzed by a standard t-test with

[‡‡] The experiments were performed by Prof. Rascher's group (Klinik für Innere Medizin II, Experimental Cardiovascular Imaging, Ulm University).

confidence intervals of 95% using GraphPad Prism 3 software. A value of p <= 0.05 was considered significant.

4.7 Reference

[1]. Kim, D. K.; Dobson, J., Nanomedicine for targeted drug delivery. *J. Mater. Chem.* **2009,** *19* (35), 6294-6307.

[2]. Davis, M. E.; Chen, Z.; Shin, D. M., Nanoparticle therapeutics: an emerging treatment modality for cancer. *Nat. Rev. Drug Discov.* **2008,** *7* (9), 771-782.

[3]. Peer, D.; Karp, J. M.; Hong, S.; Farokhzad, O. C.; Margalit, R.; Langer, R., Nanocarriers as an emerging platform for cancer therapy. *Nat. Nanotechnol.* **2007,** *2* (12), 751-760.

[4]. Al-Jamal, W. T.; Kostarelos, K., Liposomes: From a clinically established drug delivery system to a nanoparticle platform for theranostic nanomedicine. *Acc. Chem. Res.* **2011,** *44* (10), 1094-1104.

[5]. Duncan, R., Polymer conjugates as anticancer nanomedicines. *Nat. Rev. Cancer* **2006,** *6* (9), 688-701.

[6]. Xu, Z. P.; Zeng, Q. H.; Lu, G. Q.; Yu, A. B., Inorganic nanoparticles as carriers for efficient cellular delivery. *Chem. Eng. Sci.* **2006,** *61* (3), 1027-1040.

[7]. Ren, Y.; Wong, S. M.; Lim, L.-Y., Folic acid-conjugated protein cages of a plant virus: A novel delivery platform for doxorubicin. *Bioconjug.Chem.* **2007,** *18* (3), 836-843.

[8]. Neumann, E.; Frei, E.; Funk, D.; Becker, M. D.; Schrenk, H. H.; Muller-Ladner, U.; Fiehn, C., Native albumin for targeted drug delivery. *Expert Opin. Drug Deliv.* **2011,** *7* (8), 915-925.

[9]. Maeda, H.; Wu, J.; Sawa, T.; Matsumura, Y.; Hori, K., Tumor vascular permeability and the EPR effect in macromolecular therapeutics: a review. *J. Control. Release* **2000,** *65* (1-2), 271-284.

[10]. Lammers, T.; Hennink, W. E.; Storm, G., Tumour-targeted nanomedicines: principles and practice. *Br. J. Cancer* **2008,** *99* (3), 392-397.

[11]. Della Rocca, J.; Liu, D.; Lin, W., Nanoscale metal-organic frameworks for biomedical imaging and drug delivery. *Acc. Chem. Res.* **2011,** *44* (10), 957-968.

[12]. Khemtong, C.; Kessinger, C. W.; Gao, J., Polymeric nanomedicine for cancer MR imaging and drug delivery. *Chem. Commun.* **2009,** (24), 3497-3510.

[13]. Yoo, J.-W.; Irvine, D. J.; Discher, D. E.; Mitragotri, S., Bio-inspired, bioengineered and biomimetic drug delivery carriers. *Nat. Rev. Drug Discov.* **2011,** *10* (7), 521-535.

[14]. Kratz, F.; Elsadek, B., Clinical impact of serum proteins on drug delivery. *J. Control. Release* **2012,** *161* (2), 429-445.

[15]. Kratz, F.; Muller-Driver, R.; Hofmann, I.; Drevs, J.; Unger, C., A novel macromolecular prodrug concept exploiting endogenous serum albumin as a drug carrier for cancer chemotherapy. *J. Med. Chem.* **2000,** *43* (7), 1253-1256.

[16]. Stefano, G. D.; Lanza, M.; Kratz, F.; Merina, L.; Fiume, L., A novel method for coupling doxorubicin to lactosaminated human albumin by an acid sensitive hydrazone bond: synthesis, characterization and preliminary biological properties of the conjugate. *Eur. J. Pharm. Sci.* **2004,** *23* (4-5), 393-397.

[17]. Gupta, P. K.; Hung, C. T., Albumin microspheres. I: Physico-chemical characteristics. *J. Microencapsul.* **1989,** *6* (4), 427-462.

[18]. Gupta, P. K.; Hung, C. T., Albumin microspheres. II: Applications in drug delivery. *J. Microencapsul.* **1989,** *6* (4), 463-472.

[19]. Stinchcombe, T. E., Nanoparticle albumin-bound paclitaxel: a novel Cremphor-EL-free formulation of paclitaxel. *Nanomedicine (Lond.)* **2007,** *2* (4), 415-423.

[20]. Montana, M.; Ducros, C.; Verhaeghe, P.; Terme, T.; Vanelle, P.; Rathelot, P., Albumin-bound paclitaxel: the benefit of this new formulation in the treatment of various cancers. *J. Chemother.* **2011,** *23* (2), 59-66.

[21]. Heidel, J.; Davis, M., Clinical developments in nanotechnology for cancer therapy. *Pharm. Res.* **2011,** *28* (2), 187-199.

[22]. Yoshikawa, K.; Kitaoka, H., Prolonged intra-aortic infusion therapy with anti-tumor agents for advanced cancer of the stomach, colon and rectum. *Jpn. J. Surg.* **1971,** *1* (4), 256-262.

[23]. Laginha, K. M.; Verwoert, S.; Charrois, G. J.; Allen, T. M., Determination of doxorubicin levels in whole tumor and tumor nuclei in murine breast cancer tumors. *Clin. Cancer Res.* **2005,** *11* (19 Pt 1), 6944-6949.

[24]. Blanka, R., Clinical experience with anthracycline antibiotics-HPMA copolymer-human immunoglobulin conjugates. *Adv. Drug Deliv. Rev.* **2009,** *61* (13), 1149-1158.

[25]. Bishop, J. F., Adult acute myeloid leukaemia: update on treatment. *Med. J. Aust.* **1999,** *170* (1), 39-43.

[26]. Canzoniero, J. V.; Bhatnagar, B.; Baer, M. R.; Gojo, I., Upfront therapy of acute myeloid leukemia. *Curr. Oncol. Rep.* **2011,** *13* (5), 361-370.

[27]. Minko, T.; Kopecková, P.; Pozharov, V.; Kopecek, J., HPMA copolymer bound adriamycin overcomes MDR1 gene encoded resistance in a human ovarian carcinoma cell line. *J. Control. Release* **1998,** *54* (2), 223-233.

[28]. Hershman, D. L.; McBride, R. B.; Eisenberger, A.; Tsai, W. Y.; Grann, V. R.; Jacobson, J. S., Doxorubicin, cardiac risk factors, and cardiac toxicity in elderly patients with diffuse B-cell non-Hodgkin's lymphoma. *J. Clin. Oncol.* **2008,** *26* (19), 3159-3165.

[29]. Schmitt, C. J.; Dietrich, S.; Ho, A. D.; Witzens-Harig, M., Replacement of conventional doxorubicin by pegylated liposomal doxorubicin is a safe and effective alternative in the treatment of non-Hodgkin's lymphoma patients with cardiac risk factors. *Ann. Hematol.* **2011,** *91* (3), 391-397.

[30]. Bachur, N. R.; Gee, M., Daunorubicin metabolism by rat tissue preparations. *J. Pharmacol. Exp. Ther.* **1971,** *177* (3), 567-572.

[31]. Wang, H.; Zhao, Y.; Wu, Y.; Hu, Y.-l.; Nan, K.; Nie, G.; Chen, H., Enhanced anti-tumor efficacy by co-delivery of doxorubicin and paclitaxel with

amphiphilic methoxy PEG-PLGA copolymer nanoparticles. *Biomaterials* **2011,** *32* (32), 8281-8290.

[32]. Ogawara, K.; Un, K.; Minato, K.; Tanaka, K.; Higaki, K.; Kimura, T., Determinants for *in vivo* anti-tumor effects of PEG liposomal doxorubicin: importance of vascular permeability within tumors. *Int. J. Pharm.* **2008,** *359* (1-2), 234-240.

[33]. Lee, S. M.; Ahn, R. W.; Chen, F.; Fought, A. J.; O'Halloran, T. V.; Cryns, V. L.; Nguyen, S. T., Biological evaluation of pH-responsive polymer-caged nanobins for breast cancer therapy. *ACS Nano* **2010,** *4* (9), 4971-4978.

[34]. Nagykalnai, T., Non-pegylated doxorubicin (Myocet(R)) as the less cardiotoxic alternative of free doxorubicin. *Magy. Onkol.* **2010,** *54* (4), 359-367.

[35]. Liu, S. Q.; Tong, Y. W.; Yang, Y.-Y., Incorporation and *in vitro* release of doxorubicin in thermally sensitive micelles made from poly(N-isopropylacrylamide-co-N,N-dimethylacrylamide)-b-poly(d,l-lactide-co-glycolide) with varying compositions. *Biomaterials* **2005,** *26* (24), 5064-5074.

[36]. Lu, J.; Shi, M.; Shoichet, M. S., Click chemistry functionalized polymeric nanoparticles target corneal epithelial cells through RGD-cell surface receptors. *Bioconjug. Chem.* **2008,** *20* (1), 87-94.

[37]. Khandare, J.; Minko, T., Polymer-drug conjugates: Progress in polymeric prodrugs. *Prog. Polym. Sci.* **2006,** *31* (4), 359-397.

[38]. Yoo, H. S.; Lee, E. A.; Park, T. G., Doxorubicin-conjugated biodegradable polymeric micelles having acid-cleavable linkages. *J. Control. Release* **2002,** *82* (1), 17-27.

[39]. Bae, Y.; Fukushima, S.; Harada, A.; Kataoka, K., Design of environment-sensitive supramolecular assemblies for intracellular drug delivery: Polymeric micelles that are responsive to intracellular pH change. *Angew. Chem. Int. Ed.* **2003,** *42* (38), 4640-4643.

[40]. Andresen, T. L.; Thompson, D. H.; Kaasgaard, T., Enzyme-triggered nanomedicine: Drug release strategies in cancer therapy. *Mol. Membr. Biol.* **2010,** *27* (7), 353-363.

[41]. Kurisawa, M.; Yui, N., Dual-stimuli-responsive drug release from interpenetrating polymer network-structured hydrogels of gelatin and dextran. *J. Control. Release* **1998,** *54* (2), 191-200.

[42]. Klaikherd, A.; Nagamani, C.; Thayumanavan, S., Multi-stimuli sensitive amphiphilic block copolymer assemblies. *J. Am. Chem. Soc.* **2009,** *131* (13), 4830-4838.

[43]. Shi, J.; Liu, L.; Sun, X.; Cao, S.; Mano, J. F., Biomineralized polysaccharide beads for dual-stimuli-responsive drug delivery. *Macromol. Biosci.* **2008,** *8* (3), 260-267.

[44]. Vemula, P. K.; Cruikshank, G. A.; Karp, J. M.; John, G., Self-assembled prodrugs: An enzymatically triggered drug-delivery platform. *Biomaterials* **2009,** *30* (3), 383-393.

[45]. Elliott, E.; Sloane, B., The cysteine protease cathepsin B in cancer. *Perspect. Drug Discov.* **1996,** *6* (1), 12-32.

[46]. Sloane, B. F.; Yan, S.; Podgorski, I.; Linebaugh, B. E.; Cher, M. L.; Mai, J.; Cavallo-Medved, D.; Sameni, M.; Dosescu, J.; Moin, K., Cathepsin B and tumor proteolysis: contribution of the tumor microenvironment. *Semin. Cancer Biol.* **2005,** *15* (2), 149-157.

[47]. Dong, L.; Xia, S.; Wu, K.; Huang, Z.; Chen, H.; Chen, J.; Zhang, J., A pH/Enzyme-responsive tumor-specific delivery system for doxorubicin. *Biomaterials* **2010,** *31* (24), 6309-6316.

[48]. Etrych, T.; Strohalm, J.; Chytil, P.; Černoch, P.; Starovoytova, L.; Pechar, M.; Ulbrich, K., Biodegradable star HPMA polymer conjugates of doxorubicin for passive tumor targeting. *Eur. J. Pharm. Sci.* **2011,** *42* (5), 527-539.

[49]. Wu, Y.; Er, K. S.; Ramanathan, A.; Vasudevan, S.; Weil, T., Nano-sized albumin-copolymer micelles for efficient doxorubicin delivery. *Biointerphases* **2012,** *7* (1-4), 5.

[50]. Bhattacharya, A. A.; Grune, T.; Curry, S., Crystallographic analysis reveals common modes of binding of medium and long-chain fatty acids to human serum albumin. *J. Mol. Biol.* **2000,** *303* (5), 721-732.

[51]. Kataoka, K.; Matsumoto, T.; Yokoyama, M.; Okano, T.; Sakurai, Y.; Fukushima, S.; Okamoto, K.; Kwon, G. S., Doxorubicin-loaded poly(ethylene glycol)-poly(beta-benzyl-L-aspartate) copolymer micelles: their pharmaceutical characteristics and biological significance. *J. Control. Release* **2000,** *64* (1-3), 143-153.

[52]. Yoo, H. S.; Lee, E. A.; Park, T. G., Doxorubicin-conjugated biodegradable polymeric micelles having acid-cleavable linkages. *J Control Release* **2002,** *82* (1), 17-27.

[53]. Kumagai, A. K.; Eisenberg, J. B.; Pardridge, W. M., Absorptive-mediated endocytosis of cationized albumin and a beta-endorphin-cationized albumin chimeric peptide by isolated brain capillaries. Model system of blood-brain barrier transport. *J. Biol. Chem.* **1987,** *262* (31), 15214-15219.

[54]. Smith, K. R.; Borchardt, R. T., Permeability and mechanism of albumin, cationized albumin, and glycosylated albumin transcellular transport across monolayers of cultured bovine brain capillary endothelial cells. *Pharm. Res.* **1989,** *6* (6), 466-473.

[55]. Eisele, K.; Gropeanu, R. A.; Zehendner, C. M.; Rouhanipour, A.; Ramanathan, A.; Mihov, G.; Koynov, K.; Kuhlmann, C. R. W.; Vasudevan, S. G.; Luhmann, H. J.; Weil, T., Fine-tuning DNA/albumin polyelectrolyte interactions to produce the efficient transfection agent cBSA-147. *Biomaterials* **2010,** *31* (33), 8789-8801.

[56]. Zöphel, L.; Eisele, K.; Gropeanu, R.; Rouhanipour, A.; Koynov, K.; Lieberwirth, I.; Müllen, K.; Weil, T., Preparation of defined albumin-polymer hybrids for efficient cell transfection. *Macromol. Chem. Phys.* **2010,** *211* (2), 146-153.

[57]. Belting, M.; Sandgren, S.; Wittrup, A., Nuclear delivery of macromolecules: barriers and carriers. *Adv. Drug Deliv. Rev.* **2005,** *57* (4), 505-527.

[58]. J.Gabriel, M., Cationization of protein antigens: VI. Effects of cationization on the immunoregulatory properties of a bovine serum albumin peptide, a.a. 506-589. *Cell. Immunol.* **1991,** *138* (1), 121-129.

[59]. van Hest, J. C. M., Biosynthetic-synthetic polymer conjugates. *Polym. Rev.* **2007,** *47* (1), 63-92.

[60]. Jevševar, S.; Kunstelj, M.; Porekar, V. G., PEGylation of therapeutic proteins. *Biotechnol. J.* **2010,** *5* (1), 113-128.

[61]. Wu, Y.; Ihme, S.; Feuring-Buske, M.; Kuan, S. L.; Eisele, K.; Lamla, M.; Wang, Y.; Buske, C.; Weil, T., A core-shell albumin copolymer nanotransporter for high capacity loading and two-step release of doxorubicin

with enhanced anti-leukemia activity. *Adv. Healthcare Mater.* **2013**, DOI: 10.1002/adhm.201200296.

[62]. Kratz, F.; Warnecke, A.; Scheuermann, K.; Stockmar, C.; Schwab, J.; Lazar, P.; Druckes, P.; Esser, N.; Drevs, J.; Rognan, D.; Bissantz, C.; Hinderling, C.; Folkers, G.; Fichtner, I.; Unger, C., Probing the cysteine-34 position of endogenous serum albumin with thiol-binding doxorubicin derivatives. Improved efficacy of an acid-sensitive doxorubicin derivative with specific albumin-binding properties compared to that of the parent compound. *J. Med. Chem.* **2002,** *45* (25), 5523-5533.

[63]. Unger, C.; Haring, B.; Medinger, M.; Drevs, J.; Steinbild, S.; Kratz, F.; Mross, K., Phase I and pharmacokinetic study of the (6-maleimidocaproyl)hydrazone derivative of doxorubicin. *Clin. Cancer Res.* **2007,** *13* (16), 4858-4866.

[64]. Eldar-Boock, A.; Miller, K.; Sanchis, J.; Lupu, R.; Vicent, M. J.; Satchi-Fainaro, R., Integrin-assisted drug delivery of nano-scaled polymer therapeutics bearing paclitaxel. *Biomaterials* **2011,** *32* (15), 3862-3874.

[65]. Jia, Z.; Wong, L.; Davis, T. P.; Bulmus, V., One-pot conversion of RAFT-generated multifunctional block copolymers of HPMA to doxorubicin conjugated acid- and reductant-sensitive crosslinked micelles. *Biomacromolecules* **2008,** *9* (11), 3106-3113.

[66]. Wang, S.; Konorev, E. A.; Kotamraju, S.; Joseph, J.; Kalivendi, S.; Kalyanaraman, B., Doxorubicin induces apoptosis in normal and tumor cells *via* distinctly different mechanisms. *J. Biol. Chem.* **2004,** *279* (24), 25535-25543.

[67]. Kim, J.; Lee, J. E.; Lee, S. H.; Yu, J. H.; Lee, J. H.; Park, T. G.; Hyeon, T., Designed fabrication of a multifunctional polymer nanomedical platform for simultaneous cancer- targeted imaging and magnetically guided drug delivery. *Adv. Mater.* **2008,** *20* (3), 478-483.

[68]. Kono, K.; Nakashima, S.; Kokuryo, D.; Aoki, I.; Shimomoto, H.; Aoshima, S.; Maruyama, K.; Yuba, E.; Kojima, C.; Harada, A.; Ishizaka, Y., Multi-functional liposomes having temperature-triggered release and magnetic resonance imaging for tumor-specific chemotherapy. *Biomaterials* **2011,** *32* (5), 1387-1395.

[69]. Janib, S. M.; Moses, A. S.; MacKay, J. A., Imaging and drug delivery using theranostic nanoparticles. *Adv. Dru. Deliver. Rev.* **2010,** *62* (11), 1052-1063.

[70]. L. Villaraza, A. J.; Bumb, A.; Brechbiel, M. W., Macromolecules, dendrimers, and nanomaterials in magnetic resonance imaging: The interplay between size, function, and pharmacokinetics. *Chem. Rev.* **2010,** *110* (5), 2921-2959.

[71]. Na, H. B.; Hyeon, T., Nanostructured T1 MRI contrast agents. *J. Mater. Chem.* **2009,** *19* (35), 6267-6273.

[72]. Liu, T.; Li, X.; Qian, Y.; Hu, X.; Liu, S., Multifunctional pH-Disintegrable micellar nanoparticles of asymmetrically functionalized β-cyclodextrin-Based star copolymer covalently conjugated with doxorubicin and DOTA-Gd moieties. *Biomaterials* **2012,** *33* (8), 2521-2531.

[73]. Bui, T.; Stevenson, J.; Hoekman, J.; Zhang, S.; Maravilla, K.; Ho, R. J. Y., Novel Gd nanoparticles enhance vascular contrast for high-resolution magnetic resonance imaging. *PLoS ONE* **2010,** *5* (9), e13082.

[74]. Cheng, Z.; Thorek, D. L. J.; Tsourkas, A., Gadolinium-conjugated dendrimer nanoclusters as a tumor-targeted T1 magnetic resonance imaging contrast agent. *Angew. Chem., Int. Ed.* **2010,** *49* (2), 346-350.

[75]. Moriggi, L.; Cannizzo, C.; Dumas, E.; Mayer, C. R.; Ulianov, A.; Helm, L., Gold nanoparticles functionalized with gadolinium chelates as high-relaxivity MRI contrast agents. *J. Am. Chem. Soc.* **2009,** *131* (31), 10828-10829.

[76]. Kielar, F.; Tei, L.; Terreno, E.; Botta, M., Large relaxivity enhancement of paramagnetic lipid nanoparticles by restricting the local motions of the GdIII chelates. *J. Am. Chem. Soc.* **2010,** *132* (23), 7836-7837.

[77]. Kim, H.-K.; Jung, H.-Y.; Park, J.-A.; Huh, M.-I.; Jung, J.-C.; Chang, Y.; Kim, T.-J., Gold nanoparticles coated with gadolinium-DTPA-bisamide conjugate of penicillamine (Au@GdL) as a T1-weighted blood pool contrast agent. *Journal of Materials Chemistry* **2010,** *20* (26), 5411-5417.

[78]. Willner, D.; Trail, P. A.; Hofstead, S. J.; King, H. D.; Lasch, S. J.; Braslawsky, G. R.; Greenfield, R. S.; Kaneko, T.; Firestone, R. A., (6-Maleimidocaproyl)hydrazone of doxorubicin. A new derivative for the

preparation of immunoconjugates of doxorubicin. *Bioconjug.Chem.* **1993,** *4* (6), 521-527.

Chapter 5

Conclusions and Perspectives

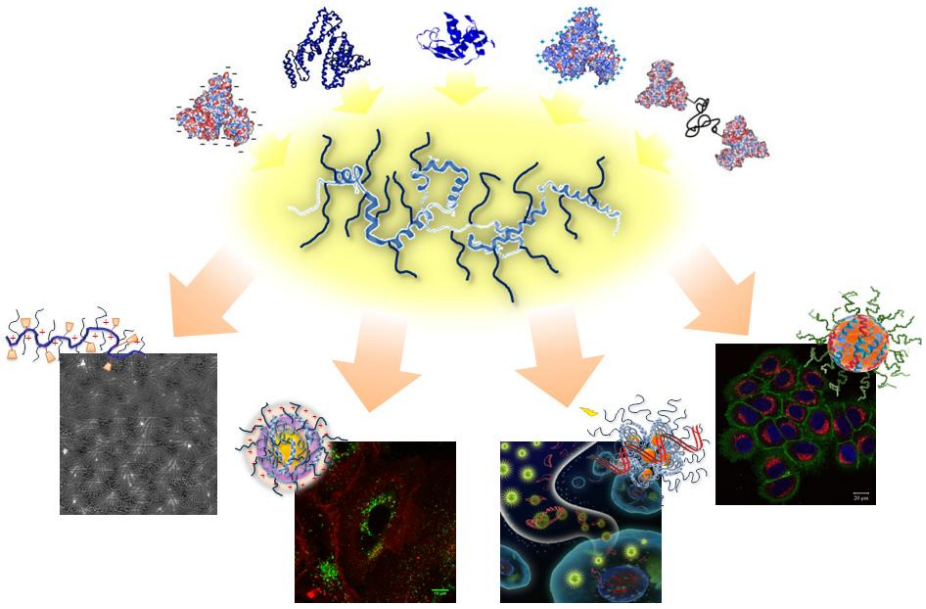

Partially adapted with permission*. Copyright 2012, American Chemical Society and Copyright 2012, Wiley-VCH.

* Pictures partially adapted from (1). Wu, Y.; Pramanik, G.; Eisele, K.; Weil, T., Convenient approach to polypeptide copolymers derived from native proteins. Biomacromolecules 2012, 13 (6), 1890-1898; (2). Wu, Y.; Eisele, K.; Doroshenko, M.; Algara-Siller, G.; Kaiser, U.; Koynov, K.; Weil, T., A quantum dot photoswitch for DNA detection, gene transfection, and live-cell imaging. Small 2012, 8 (22), 3465-3475.

5. 1 Conclusion

In this thesis, an innovative concept has been introduced makes use of the large pool of natural proteins as resource for preparing various artificial polypeptide materials. We have developed a versatile “semi-synthetic” approach to achieve protein based polypeptide copolymers (PbPs), a novel class of structurally defined and multifunctional polypeptide materials. PbPs were prepared by the controlled denaturation of the native proteins followed by an in situ stabilization with polyethylene(oxide) chains. The resulting PbPs were highly stable and well soluble in water. Their backbone lengths were precisely defined and the secondary structure elements from precursor proteins partially retained. Supramolecular architectures were formed from PbPs in solution as well as on self-assembled monolayers. These supramolecular structures could be tuned by altering the different hydrophobic and hydrophilic domains along the polypeptide main chain. As promising biomedical materials, PbPs exhibited insignificant cytotoxicity in many cell lines and they could be degraded *via* proteolysis according to *in vitro* tests. There were diverse native functional groups available at precise positions along PbPs backbone which allowed multiple orthogonal modifications. Therefore, both *a priori* and *a posteriori* modification strategies were explored to tune PbPs properties adapting to different applications. The functionalized PbPs could have variable net charges, distinct hydrophobicity as well as different self-assembling possibilities. Moreover, functional moieties, such as chromophores, anti-cancer drugs or MRI contrast agents, could also be introduced into PbPs, which demonstrated PbPs as a highly versatile platform for broad applications.

With the established preparation and functionalization strategies, we further investigated the potential of PbPs in different biomedical applications. For instance, PbPs were attached with thioctic acid groups to facilitate interactions with nanoparticles. *Via* this approach, highly stable and water soluble QDs coated with PbPs were prepared and successfully applied for bioimaging as well as gene delivery. These PbP-QDs were found non-cytotoxic and highly stable in live cells. More interestingly, unique properties, such as pH responsiveness as well as DNA sensitive optical properties were found for PbP-QDs, which make them extremely attractive as functional probes. By tune the net charge of PbPs, PbP-QDs could also be prepared with different surface charges. We showed that negatively charged QDs were not well uptaken into cells, whereas positively charged QDs facilitated efficient cell uptake and have proven even suitable for gene delivery. Since the cationic PbP-QDs exhibited significant photo-responsiveness to DNA loading, they had great potential for studying gene delivery processes which has been demonstrated in preliminary experiments by FCS studies in live cells. In addition, we have further explored the potential of using PbPs for anti-cancer drug delivery. Drug molecules were loaded into PbPs *via* both hydrophobic interactions and covalent conjugation. The hydrophobic loading strategy offers great potential to become generally applicable for hydrophobic drug molecules and in principle allowed combinational cancer therapy, whereas the covalent loading approach resulted in more controlled drug release mechanisms which minimized nonspecific drug leakage. The highly defined multi-stimuli responsive core-shell drug delivery system developed by the covalent loading approach was further tested for their pharmaceutical properties, including *in vitro* drug release kinetics, cellular toxicity and uptake studies, as well as preliminary *in vivo* anti-leukemia potential. All the results suggested that this system could efficiently deliver drug molecules offering highly controlled drug release and potent

therapeutic effects. MRI contrast agents were further introduced into this system, thus a theranostic “magic bullet” was constructed allowing highly sensitive MRI imaging and controlled anti-cancer therapy simultaneously.

In summary, the strategy for preparing PbPs provided an efficient route to access highly defined, large molecular weight polypeptides with multiple functionalities. Such innovative strategy was complementary to conventional polypeptide synthesis and revealed the bright future of developing natural polypeptides as synthetic resources. These PbPs exhibited plenty of unique features, which could not be achieved by conventional approaches. They have great potential to be further developed for various biomedical applications.

5. 2 Perspectives

Although the protocols to achieve stable and versatile PbPs were successfully established and their great application potentials were demonstrated, there are still several unexplored features that require further studies. Therefore, further directions could be proposed to enhance our understanding of PbPs system. For instance:

(1) In addition to the proteins which have been used to prepare PbPs, such as albumin and lysozyme, it will be wealth wise to investigate other proteins in order to expand the library of PbPs. Proteins with different chain lengths and characteristic secondary structures could be investigated to develop PbPs with more variety of molecular weight as well as special properties.

(2) Polyethyleneoxide (PEO) as a highly biocompatible and water soluble polymer was chosen in this thesis to stabilize PbPs and provide solubility in aqueous media. However, it is in principle also possible to use other polymers or dendrimers as stabilizing agent to replace PEO chains. The development of a broader stabilizing

strategy would allow PbPs to adapt to more diverse application requirements. For instance, using hydrophobic polymers as side chains might result in unique self-assembling properties and using dendrimers as side chains might lead to more rigid structure of PbPs.

(3) Bioengineering techniques could also be considered to contribute to PbPs development. Using bioengineering techniques to genetically modify natural proteins would allow further expansion of the available precursor proteins especially for specifically designed applications. For instance, one of the most important advantages of PbPs is the exact known location of functional groups which could be used for attaching functional moieties. However, if the desired functionalities need to be conjugated on a specific position where the natural amino acid sequence does not allow, it would need to specifically mutate this amino acid on the precursor protein *via* bioengineering techniques. Moreover, genetically engineered proteins could also provide possibilities to study PbPs in a more systematic fashion. PbPs prepared from the complete sequence of native proteins have presented many unique properties, such as secondary structures, spontaneous backfolding and self-assembling behavior. However, it is often difficult to understand the mechanism and determine critical factors to achieve a desired property. In this case, it would be valuable to systematically study the different segments of a PbP by expressing a specific domain of a protein as precursor. *Via* these studies, one might gain additional insights how the protein precursors and side chain modification methods contribute to the resultant properties of PbPs, which might ultimately allow predicting the properties of PbPs based on the protein sequence and stabilization strategy.

(4) Encouraged by the very promising applications of PbPs for bioimaging and drug delivery, it would be also interesting to further explore the potential of PbPs for a broader range of applications. For instance, PbPs might also serve as an ideal

polymer matrix for tissue engineering. Crosslinking of PbPs might form hydrogels with high biocompatibility and biodegradability and thus would be attractive as cell culture matrix for tissue regeneration. In addition, once the self-assembling behavior of PbPs could be controlled in a more designed fashion, it would be also attractive to investigate the potential of PbPs to form sophisticated architectures, such as polymersomes, artificial membranes and nanofibers/nanowires.

Erklärung

Ich versichere hiermit, daß ich die Arbeit selbständig angefertigt habe und keine anderen als die angegebenen Quellen und Hilfsmittel benutzt sowie die wörtlich oder inhaltlich übernommenen Stellen als solche kenntlich gemacht habe.

Ulm, den



.....

(Yuzhou Wu)

Declaration of Originality

I hereby declare that this thesis and the work reported herein was composed by and originated entirely from me. Information derived from the published and unpublished work of others has been acknowledged in the text and references are given in the list of sources.

Ulm, den



.....

(Yuzhou Wu)

Acknowledgments

It is my great pleasure to take this opportunity to express my acknowledgements to all the people who have helped and encouraged me throughout my PhD period. This thesis could not have been accomplished without your support.

First and foremost, my deepest appreciation and respect go to my supervisor, Prof. Tanja Weil. I wish to express my sincere gratitude for her invaluable guidance, motivation, and enthusiasm for my projects. She has believed in me every step of the way and allowed me great freedom in developing projects. I also appreciate the precious opportunities she has given me to interact and collaborate with other talent scientists, as well as her generous support not only on research but also on my future career. It is my great honor to have the opportunity to be her PhD student. What I have learned from her profound knowledge, passion of research and creative ideas has inspired me all the time during my thesis and will also have an extraordinary impact on my life.

I am indebted to all the members in Prof. Weil's group, past and present, for creating such an enjoyable research environment. Among them, I would like to especially thank Dr. Seah Ling Kuan, Dr. Klaus Eisele, Pramanik Goutam, David Y.W. Ng and Tao Wang. We have had the pleasure to work together for a long time and enjoyed invaluable friendship. I have also benefited a lot from the intellective discussions and rewarding collaborations with them. I also would like to express my great appreciation to Ms. Zimmermann, Mr. Lamla, Dr. Meier, Dr. Hoffmann-Richter, and Prof. Ziener,

who have provided important technical support and beneficial discussions during my thesis. I'm also thankful to the bachelor students Kai Shih Er and Felix Boldt worked together with me on these projects. Thanks also go to all my other colleagues, Ms. Munz, Pfisterer Anna, Wilhelmi Jörg, Mishra Archana, Xi Chen, Mr. Weber, Fekete Natalie, Enlund Eveliina, Yanran Wang, Schrade Anika, Gülcher Jochen, Stöckle Bettina, Pendi Laura, Thomas Jessica, Yangguang Dai and Eggers Berend. The group has been a source of good advice and collaboration as well as valuable friendships.

Gratitude is also extended to all our collaborators: Dr. Kaloian Koynov and his students at Max-Planck institute for polymer research; Dr. Yin Thai Chan and his students Yang Xu and Sabyasachi Chakrabortty in National University of Singapore; Prof. Christian Buske and his student Ms. Susann Ihme in Institute of Experimental Tumour Research, Ulm University; and Prof. Rascher in Klinik für Innere Medizin II, Ulm University. They all have made a tremendous contribution to these projects.

Finally, special recognition goes out to my family, for their support, encouragement and patience during my pursuit of my Doctorate degree. To my beloved husband Fangrui, who inspired and encouraged me during the entire process. To my parents, who stand behind me and believe in me all the time. I thank all my family for your constant demonstrations of love.

Curriculum Vitae

Education

06/2010-05/2013	Ph.D. Institute of Organic Chemistry III / Macromolecular Chemistry, University of Ulm (Supervisor: Prof. Tanja Weil).
08/2008-06/2010	M.Sc. Medicinal Chemistry Program, Department of Chemistry, National University of Singapore (Supervisor: Prof. Tanja Weil).
09/2004-07/2008	B.Sc. Department of Chemistry, Zhejiang University, China.
08/2006-07/2007	Exchange Student Chemistry Department, Hong Kong University, Hong Kong, China.

Research Experience

04/2012-04/2013	Research scientist under Prof. Dr. Klaus Müllen (Max-Planck Institute for Polymer Research, Mainz, Germany) and Prof. Dr. Heiko Luhmann (Institute for Physiology, Mainz University, Germany). **Topic:** Protein-polymer hybrid biomaterials for biomedical applications.
06/2010- 03/2012	Research scientist under Prof. Tanja Weil. (Institute of Organic Chemistry III, Ulm University, Germany). **Topic:** Polypeptide hybrid biomaterials developed from protein precursors - A novel strategy and biomedical applications.
01/2009-06/2010	Research assistant under Prof. Tanja Weil. (Medicinal Chemistry Program, Department of Chemistry, National University of Singapore, Singapore). **Topic:** Generation of aptamers against the ganglioside-binding proteins *via* single bead SELEX.
11/2008-01/2009	Research assistant under Prof. Chu Young Kim. (Medicinal Chemistry Program, Department of Biology, National University of Singapore, Singapore). **Topic:** Expression and crystallization of epoxide hydrolase Lsd 19.
08/2008-11/2008	Research assistant under Prof. Shao Qin Yao. (Medicinal Chemistry Program, Department of Chemistry, National University of Singapore, Singapore). **Topic:** Aspartic protease inhibitor design for fragment based screening on self-assemble monolayer.
01/2008-07/2008	Bachelor thesis under A/P. Ming Lei. (Department of Chemistry, Zhejiang University, China).

Topic: Green catalytic oxidation of alcohol in ionic liquid involving Salen complex.

08/2006-07/2007 Research assistant in Prof. Patrick Toy´s lab. (Department of Chemistry, Hong Kong University, Hong Kong).

Topic: Solid phase supported catalysts.

02/2006-08/2006 Research assistant in Prof. Xian Huang´s lab. (Department of Chemistry, Zhejiang University, China).

Topic: Preparation of polystyrene-supported organoselenium reagents and their application in organic synthesis.

List of Publications

Publications on Peer-reviewed Journals:

1. **Yuzhou Wu**, Sabyasachi Chakrabortty, Radu A. Gropeanu,Joerg Wilhelmi,Yang Xu, Kai Shih Er, Seah Ling Kuan, Kaloian Koynov, Yinthai Chan and Tanja Weil. pH-Responsive Quantum Dots via an Albumin Polymer Surface Coating. *J. Am. Chem. Soc.*, **2010**, 132(14):5012-5014.
2. **Yuzhou Wu**, Kai Shih Er, Arvind Ramanathan, Subhash Vasudevan, Tanja Weil. Nano-sized albumin-copolymer micelles for efficient doxorubicin delivery. *Biointerphases*. **2012**, 7(1-4):5.
3. **Yuzhou Wu**, Klaus Eisele, Mikheil Doroshenko, Gerardo Algara-Siller, Ute Kaiser, Kaloian Koynov, Tanja Weil, A Quantum Dot Photoswitch for DNA Detection, Gene Transfection, and Live-Cell Imaging. *Small*, **2012**, 8 (22): 3465–3475.
4. **Yuzhou Wu**, Klaus Eisele, Mikheil Doroshenko, Gerardo Algara-Siller, Ute Kaiser, Kaloian Koynov, Tanja Weil, Quantum Dots: A Quantum Dot Photoswitch for DNA Detection, Gene Transfection, and Live-Cell Imaging (Cover picture). *Small*, **2012**, 8(22): 3381.
5. **Yuzhou Wu**, Goutam Pramanik, Klaus Eisele, Tanja Weil. Convenient approach to polypeptide copolymers derived from native proteins. *Biomacromolecules*, **2012**, 13(6):1890-1898.
6. **Yuzhou Wu**, Tao Wang, David Y.W. Ng, Tanja Weil. Multifunctional Polypeptide-PEO Nanoreactors via the Hydrophobic Switch. *Macromol. Rapid Commun*., **2012**, 33(17): 1474–1481,.
7. **Yuzhou Wu**; Tanja Weil. An Efficient Approach for Preparing Giant Polypeptide Triblock Copolymers by Protein Dimerization. *Macromol. Rapid Commun.,* **2012**, 33(15): 1304–1309.
8. **Yuzhou Wu**, Susann Ihme, Michaela Feuring-Buske, Seah Ling Kuan, Klaus Eisele, Markus Lamla, Yanran Wang, Christian Buske, and Tanja Weil. A core-shell albumin copolymer nanotransporter for high capacity loading and two-step release of doxorubicin with enhanced anti-leukemia activity. *Adv. Healthcare Mater.*, **2012,** doi: 10.1002/adhm.201200296.
9. Yasar Akdogan, **Yuzhou Wu**, Klaus Eisele, Manuela Schaz, Tanja Weil and Dariush Hinderberger, Host-Guest Interactions in Polycationic Human Serum Albumin Bioconjugates, *Soft Matter*, **2012**, 8(43): 11106-11114.
10. Seah Ling Kuan, **Yuzhou Wu**, Tanja Weil, Precision Biopolymers from Protein Precursors for Biomedical Applications*. Macromol. Rapid Commun*., **2012**, DOI: 10.1002/marc.201200662*.*

11. Diego Pesce[#], **Yuzhou Wu**[#], Anke Kolbe, Tanja Weil and Andreas Herrmann, Enhancing Cellular Uptake of GFP via Unfolded Supercharged Protein Tags, *Biomaterials*, **2013**, DOI: 10.1016/j.biomaterials.2013.02.038. **([#]Shared first authorship)**.
12. Seah Ling Kuan, Bettina Stöckle, David Y.W. Ng, **Yuzhou Wu**, Mikheil Doroshenko, Jörg Reichenwallner, Kaloian Koynov, Dariush Hinderberger, Klaus Müllen and Tanja Weil, Dendronized Albumin Biohybrids as Efficient Core-Shell Doxorubicin Delivery Systems. *Biomacromolecules*, **2013**, 14 (2): 367–376.
13. Tao Wang, Anne Pfisterer, Seah Ling Kuan, **Yuzhou Wu**, Oliver Dumele, Markus Lamla, Klaus Müllen and Tanja Weil. Cross-conjugation of DNA, proteins and peptides *via* a pH switch. *Chem. Sci.*, **2013**, DOI: 10.1039/c3sc22015j.
14. David Yuen Wah Ng, Jörg Fahrer, **Yuzhou Wu**, Klaus Eisele, Seah Ling Kuan, Klaus Müllen, Holger Barth, and Tanja Weil. Efficient delivery of p53 and cytochrome C by supramolecular assembly of a dendritic multi-domain delivery system*. Adv. Healthcare Mater.,* **2013***, doi: 10.1002/adhm.201200419.*
15. Christoph Meier, **Yuzhou Wu**, Goutam Pramanik, and Tanja Weil, Self-assembly of Polypeptide Copolymers into Nanostructured Protein Coatings Christoph, *Soft Matter*, **2013**, *Submitted*.
16. Goutam Pramanik[#], **Yuzhou Wu**[#], Gerado Algara-Siller, Christoph. Meier, Paul Walter, Uta Kaiser, Tanja Weil, High Performance, Ultrasmall Near Infrared (NIR) Gold Nanoemitters for Cell Imaging Applications. *Nanoscale*, **2013**, *submitted*. **([#]Shared first authorship)**.

Conference Publications:

17. **Yuzhou Wu**, Tanja Weil. Multifunctional protein- hybrid and its applications in quantum dot coatings. *Polymer Preprints (American Chemical Society, Division of Polymer Chemistry)*, **2010**, 51(1): 786-787.
18. Tanja Weil, Goutam Pramanik, **Yuzhou Wu**. Protein-based copolymers for bioimaging and drug delivery applications. *Polymer Preprints (American Chemical Society, Division of Polymer Chemistry)*, **2011**, 52(1): no page given.

Manuscripts in Preparation:

19. **Yuzhou Wu**, Seah Ling Kuan, David Yuen Wah Ng and Tanja Weil, Responsive protein-polymer conjugates for drug delivery and

bioimaging applications, *Nanomedicine* (invited review), **2013**, *in preparation*.

20. Goutam Pramanik, Anna Ermakova, **Yuzhou Wu**, Liam McGuinness, Boris Naydenov, Rolf Reuter, Joerg Wrachtrup, Fedor Jelezko and Tanja Weil, Stabilization of fluorescent nanodiamonds for cell studies by a polypeptide polymer coating, *Chemistry of Materials*, **2013**, *in preparation*.

Presentations at International Conferences:

1. **Yuzhou Wu**, Goutam Pramanik, Klaus Eisele, Tanja Weil. *Precision Polypeptides Derived from Native Proteins for Biomedical Applications*. Oral presentation, Belgian-German (Macro) Molecular Meeting, Houffalize, Belgium, Dec. 3-4th, **2012**.
2. **Yuzhou Wu**, Goutam Pramanik, Klaus Eisele, Tanja Weil. *A Multifunctional Protein Derived Polypeptide Copolymer and Its Applications*. Poster presentation, EMBO Conference Series: Chemical Biology, Heidelberg, Germany, Sep. 26-29th, **2012**.
3. **Yuzhou Wu**, Tanja Weil. *Multifunctional Protein-hybrid and its Applications in Quantum Dot Coatings.* Abstracts of Papers (Oral presentation), 239th ACS National Meeting, San Francisco, CA, United States, March 21-25th, **2010**.
4. **Yuzhou Wu**, Tanja Weil. *A Multifunctional Denatured Protein Based Polymer Material and Its Applications in Bioimaging and Drug Delivery.* Oral presentation, Tag der Organischen Chemie (TOCUS), Stuttgart, Germany, Oct 15th, **2010**.
5. **Yuzhou Wu**, Tanja Weil. *Ph-Responsive Quantum Dots Via a Novel Protein-Polymer Coating.* Oral presentation, 6th Singapore International Chemical Conference (SICC-6), Singapore, Dec 15-18th, **2009**.
6. **Yuzhou Wu**, Tanja Weil. *Botulinum Neurotoxin: from Inhibitor Design to Drug Delivery*, Oral Presentation, 1st Singapore-Hong Kong Bilateral Graduate Student Congress in Chemical Sciences, Singapore, May 28-30th, **2009**.
7. Tanja Weil, Seah Ling Kuan, **Yuzhou Wu**, *Dendritic and Protein-based Nanocarriers.* Poster presentation, NUS-SNU Joint Symposium: Frontiers in Fundamental and Applied Chemistry, Seoul, Korea, Feb **2009.**